IAEA-TECDOC-429

REACTOR WATER CHEMISTRY RELEVANT TO COOLANT-CLADDING INTERACTION

A TECHNICAL DOCUMENT ISSUED BY THE
INTERNATIONAL ATOMIC ENERGY AGENCY, VIENNA, 1987

REACTOR WATER CHEMISTRY RELEVANT TO
COOLANT-CLADDING INTERACTION
IAEA, VIENNA, 1987
IAEA-TECDOC-429

Printed by the IAEA in Austria
September 1987

PLEASE BE AWARE THAT
ALL OF THE MISSING PAGES IN THIS DOCUMENT
WERE ORIGINALLY BLANK

The IAEA does not normally maintain stocks of reports in this series. However, microfiche copies of these reports can be obtained from

INIS Clearinghouse
International Atomic Energy Agency
Wagramerstrasse 5
P.O. Box 100
A-1400 Vienna, Austria

Orders should be accompanied by prepayment of Austrian Schillings 100,– in the form of a cheque or in the form of IAEA microfiche service coupons which may be ordered separately from the INIS Clearinghouse.

FOREWORD

The report is a summary of the work performed in a frame of a Coordinated Research Program organized by the IAEA and carried out from 1981 till 1986. It consist of a survey on our knowledge on coolant-cladding interaction: the basic phenomena, the relevant perameters, their control and the modelling techniques implemented for their assessment.

Based upon the results of this Coordinated Research Program, the following topics are reviewed on the report:

- role of water chemistry in reliable operation of nuclear power plants
- water chemistry specifications and their control
- behaviour of fuel cladding materials
- corrosion product behaviour and crud build-up in reactor circuits
- modelling of corrosion product behaviour

This report should be of interest to water chemistry supervisors at the power plants, to experts in utitility engineering departments, to fuel designers, to R&D institutes active in the field and to the consultants of these organizations.

EDITORIAL NOTE

In preparing this material for the press, staff of the International Atomic Energy Agency have mounted and paginated the original manuscripts as submitted by the authors and given some attention to the presentation.

The views expressed in the papers, the statements made and the general style adopted are the responsibility of the named authors. The views do not necessarily reflect those of the governments of the Member States or organizations under whose auspices the manuscripts were produced.

The use in this book of particular designations of countries or territories does not imply any judgement by the publisher, the IAEA, as to the legal status of such countries or territories, of their authorities and institutions or of the delimitation of their boundaries.

The mention of specific companies or of their products or brand names does not imply any endorsement or recommendation on the part of the IAEA.

Authors are themselves responsible for obtaining the necessary permission to reproduce copyright material from other sources.

CONTENTS

1. INTRODUCTION

1.1 History of the CCI Program

The CCI Program is a Coordinated Research Program which has been pursued over the period 1981 to 1986; its official title being "Investigation of Fuel Element Cladding Interaction with Water Coolant in Power Reactors". This program was not defined to satisfy a precipitant decision by technocrats: it was the response of concerned experts to the growing perception of the challenges arising from improved fuel utilization.

The IAEA initiatives are guided, in the field of Water Reactor Fuels by an advisory body, the International Working Group on Fuel Performance and Technology ("IWGFPT"). This IWGFPT is made up of experts representing an IAEA Member State or an international organization. The discussions during the IWGFPT sessions and the conferences, symposia, specialists meetings, technical committees and consultant meetings organized by the IAEA in line with IWGFPT's recommendations shed light on fuel related technical areas where a specific IAEA initiative would be welcome.

Such a sequence of events was operative in the case of the CCI Program. In the 70's, the thermal hydraulic operating conditions of the coolant were stretched in the most recent power plants to improve their efficiency. Simultaneously, the economic advantages of improving fuel utilization and the inherent margins of commercial fuel fostered a progressive increase of discharge burn-ups as well as possibilities of load following in most power plants. The resulting longer fuel residence times and the more aggressive coolant conditions highlighted life limitation features resulting from coolant-cladding interaction: corrosion (uniform and nodular) and crud deposits (capable of influencing cladding corrosion).

The awareness of these life limitation phenomena led interested members of the IWGFPT to suggest, in 1979, that the IAEA should survey the field, investigate the involved phenomenology and control

systems, and report the state of the art for the benefit of the Member States. The CCI Coordinated Research Program ("CRP") was launched in 1980, started in 1981 and was pursued until 1986. The present report is the final summary of this action.

The CCI program was sub-divided into 4 tasks implemented successively as the work progressed and the following four areas were defined:

Task 1 "Survey of fuel element cladding interaction with water coolant in power reactors" included the formulation of a survey questionnaire, the evaluation of the responses by experts, the summarization of the information into a survey report "Fuel Cladding Interaction with Water Coolant in Power Reactors" and its publication as IAEA-TECDOC-356 in 1985. The results of this Task 1 are reflected in sections 1.2, 2.1, 2.2, 2.3, 3.1, 3.2, 3.3 and 4.1 of the present report.

Task 2 "Analytical techniques for monitoring Water Chemistry in Power Reactors", was launched in 1982, as a result of the question marks appearing during the progress of Task 1. It consisted of the formulation of a questionnaire and summarizing the responses. The outcome is reflected in section 2.4 and Annex I of the present report.

Task 3 "Modelling of corrosion products and crud build-up in water-cooled reactor circuits" was launched in 1983 as it became apparent that powerful models were developed or being developed in several Member States to deal with the prediction and understanding of the phenomena. The review of PWR and BWR modelling approaches is reflected in Chapter 4 and Annexes II and III of the present report.

Task 4 "Summary of the results of the CRP" was launched in 1984, as it became apparent that the findings of this CCI should be organized in an orderly manner for the benefit of the Member States and the Institutes which have not been directly connected to the CRP. It has resulted in the present report.

Being a generic overview of the situation by the participants based on their own expertize and on technical reports published earlier (IAEA TECDOC - 356) or incorporated as Annexes 2 and 3, it was not found appropriate to repeat bibliographical references in the report itself. The reader is therefore provided in this report with a digested view on the topics and not an exhaustive technical review.

This 5 year study period of the CRP and the results thereof were only possible thanks to the collaboration of the participating Member States and the individuals who have contributed to the work, mainly:

Argentina: A J. G. Maroto
Belgium: H. Bairiot, P. Blanpain, M. Lippens and J. Van Vliet
Bulgaria: I. Dobrevsky
Czechoslovakia: J. Kysela
Finland: J. Hakala
United Kingdom: P. Campion, G. Comley, D. J. Ferrett, M. V. Polley, R. S. Rodliffe and E. W. Thornton
Hungary: A. Elek, F. Molnar, E. Szabo and J. Schunk
India: M. Das, S. H. Gadiyar, P. K. Mathur, S. V. Narasimhan, G. Venkaterswaran and K. S. Venkateswarlu
Japan: K. Ishingure, Y. Mishima, Y. Meguro
Romania: G. Semenescu
Soviet Union: Y. A. Khitrov, V. Kritsky and I. Rybalchenko
IAEA: A. Nechaev, N. Noe, V. Onufriev and I. Rybalchenko.

1.2 Role of Water Chemistry in Reliable Operation of Nuclear Power Plants

At present and for the near future nuclear power development in the world is based mainly upon water-cooled reactors. In nuclear power plants water is used as a neutron moderator and a reactor coolant, in the secondary circuit (PWRs and PHWRs) and in a number of auxiliary systems. At elevated temperatures water is an aggressive substance when in contact with structural materials. This means that the reliability of many nuclear power plant systems is dependent upon water quality which is especially critical when in

contact to fuel cladding and core materials. Normally, reliability and safety are achieved by using high integrity cladding and structural materials together with special measures to prevent excessive corrosion, erosion and other processes. Reliable water chemistry regimes have been developed for BWRs, PWRs and PHWRs. In recent years there has been a growing interest in this problem. Water-cooled power reactor experience shows that even under normal working conditions some undesirable effects on the fuel element cladding integrity can occur due to corrosion, erosion, hydriding and deposition on heat transfer surfaces of corrosion products as well as other coolant impurities.

Moreover, migration and transport of corrosion products and other impurities followed by activation in the reactor core can lead to formation of highly radioactive deposits in some out-of-core parts of the primary circuit and to radioactive contamination of the primary pipes and equipment. This causes difficulties in maintenance and repair because of the high radiation field and could require decontamination of some equipment and even of the primary circuit as a whole. More serious problems connected with the interaction between the water coolant and cladding material may occur under abnormal conditions. The need to decrease radiation doses from the primary circuit equipment and piping has led to new efforts to improve water chemistry. Development of advanced water reactor concepts to achieve higher burnups and better fuel utilization also requires additional safety measures because of longer residence time of fuel in reactors, in some cases higher coolant temperatures, with the possibility of nucleate boiling in PWRs, etc.

The main objectives of reactor coolant chemistry are:

- reduction of water agressivity towards the structural materials;

- minimization of in-core impurity ingress and out-of-core radioactivity build-up;

- prevention of fuel surface fouling with solid deposits which may result in heat transfer degradation and enhanced corrosion rates;

- prevention of parasitic neutron capture by the core deposits;

- achievement of the lowest possible occupational radiation exposure;

- prevention of radioactivity release to the environment.

The structural materials for the reactor primary circuit must withstand severe stresses imposed by intense neutron fluxes [10^{13} to 10^{15} n/(cm^2. s)] and radiation, high operating temperatures (typically 300 - 400°C) and pressures, strong corrosive attack of some coolant impurity anions such as chloride, sulphate etc.

Austenitic steels are the dominant materials for reactor internals, piping, steam generator tubing, pumps, valves, reheaters. This type of steels has excellent general corrosion resistance and mechanical strength. They can resist operating temperatures up to 500°C. Experience indicates however that in the presence of anions e.g. chlorides, they become susceptible to transgranular stress corrosion cracking.

Low alloy Ferritic steels are used for pressure vessel shells, steam generators, heat exchangers, drum separators and the like. For these materials the operating temperatures should be limited to below 500°C.

The use of mild steels is restricted to feed water line systems, heat exchanger vessels, saturated steam tubing and so on. The rated operation temperature should be limited to 350°C. Because of their low corrosion and temperature resistance they are not suitable for the primary components and equipment.

In the current water-cooled reactors zirconium alloys are the usual materials for fuel cladding and fuel channel pressure tubes. Zirconium alloys have low thermal neutron absorption cross-sections and show high temperature and corrosion resistance in demineralised water up to 350°C.

Nickel and Titanium -alloys are finding applications in steam generators, reheaters, regenerative heat exchangers and the like. Ni-alloys are especially attractive for their high temperature resistance, and a good resistance to transgranular corrosion (in the presence of chloride) but are susceptible to caustic intergranular cracking. The application of titanium alloys is restricted by cost and availability considerations.

Copper alloys are employed on the low temperature surfaces of the heat transfer systems (turbine condensers, regenerative heaters, auxiliary heat exchangers).

Nuclear power plant systems are composed of a large variety of metals and alloys. Corrosion resistance and possible corrosion product contamination of the primary system must always be taken into consideration. From the standpoint of the heat transfer flow-sheet, the coolant circuits in water-cooled nuclear reactors may be single or double.

In the single (direct cycle) circuit the nuclear boiler is coupled directly to the turbine system. The turbine condensate provides the primary contribution to the feed water flow, which continuously enters the reactor. Water chemistry control is complicated by a sophisticated circuit design and the necessity for feed water purification from impurities originating in the turbine and condensate systems. In addition, the in-core accumulation of the radioactive contaminants (on the core surfaces and in the liquid coolant) can lead to serious out-of-core activity buildup.

In the double (indirect cycle) systems, the closed primary circuit is coupled to the secondary circuit through the steam generator surfaces. These systems are characterized by high integrity and limited branching of the primary circuit. The primary circuit operates at higher pressures than the secondary circuit (to provide the necessary thermal gradients in the steam generator).

High water purity is the major requirement for proper coolant quality control. Reactor cooling water is treated with different chemicals (such as hydrogen, alkalis, boric acid) to prevent

radiolytic water decomposition, minimize corrosion of reactor structural materials and provide some reactivity control. To meet the purity requirements strict limitations are placed on water chemical composition and impurity content for primary and feed water, steam, turbine condensate, etc. (Table 1.1).

Table 1.1.
Impurities in coolant circuits

Source of impurities	Chemical composition of impurities	Measures to prevent or decrease impurity accumulation
Initial feed water for circuits and make up water	Soluble salts and gases (Na^+, K^+, Mg^{2+}, Ca^{2+}, Cl^-, NO_3^- SiO_2 SO_4^{2-}, O_2, N_2, CO_2 ...)	Efficient purification of water
Cladding materials (other than Zircaloys)	Corrosion products	Minimizing corrosion by water treatment
	Uranium and fission products due to surface contamination during fuel fabrication	Surface cleaning after fuel fabrication
Structural materials (heat exchangers, vessels, valve seats etc.)	Corrosion products:Fe, Co, Cr, Ni, Mn, Cu, Zn etc.	-Selection of low inputs materials -Minimizing corrosion by water treatment
Pressurizers (for PWR)	O_2, N_2	Use of pure helium or steam
Coolant and condensate purification systems	Ion exchange resins	Use of filters
Cooling water and air ejection in vacuum part of turbine	Salts, particulate matter, air	Improvements in sealing of turbine and condenser
Chemical additives for conservation, decontamination, etc.	Acids, alkalis, salts chelating agents etc.	Proper choice of chemicals, Efficient clean-up

Selection of coolant quality specifications depends on the mode of reactor operation and the type and composition on the structural materials. Commonly specified parameters are: conductivity, pH, hardness. dissolved oxygen, chlorides, fluorides, corrosion products and insolubles.

2. WATER CHEMISTRY SPECIFICATIONS AND THEIR CONTROL

2.1 PWR Primary Water Chemistry Specifications

A specific feature of the PWR nuclear power plants is the presence of two separate circuits - primary circuit and secondary circuit (Fig. 2.1, 2.2).

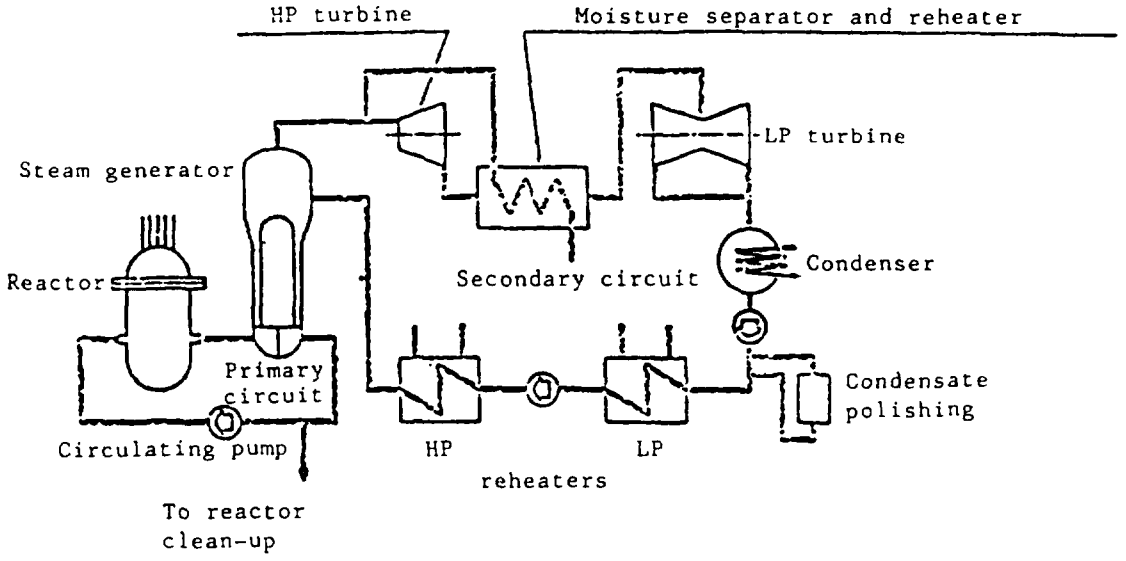

Fig. 2.1 PWR - Flow diagram

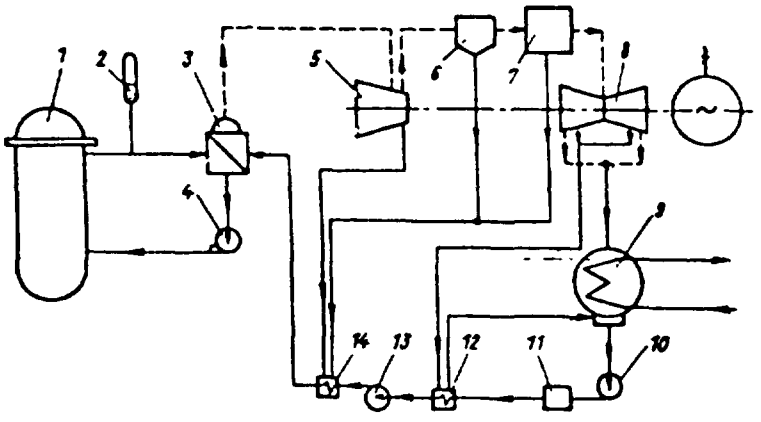

1 - reactor; 2 - pressurizer; 3 - steam generator; 4 - recirculation pump ; 5 - HP-turbine; 6 - moisture seperator; 7 - reheater; 8 - LP-turbine; 9 - condenser; 10 - condensate pump; 11 - condensate polishing; 12 - low pressure reheater; 13 - feed water pump; 14 - high pressure reheater.

Fig. 2.2 Coolant system flow diagram - WWER-440 type

The primary circuit includes a reactor (the reactor vessel houses fuel element assemblies which form a reactor core) and cooling loops with circulation pumps. The pipes of the cooling loops connect the reactor with a steam generator. In PWRs normal (light) water flowing through the core serves both as a neutron moderator and as a coolant which removes the heat generated during the reactor operation and transfers it to the heat transfer surface of the steam generator.

Bulk boiling is prevented by the use of high pressure, normally 15-16 MPa.

It is noteworthy that the cladding of the fuel elements and the walls of the assemblies are made of zirconium alloys in nearly all nuclear power plants throughout the world. The main construction material in the primary ciruit is stainless steel. The tubes of the steam generators are mostly of Inconel, Incoloy or stainless steel. Normally, the reactor vessel is manufactured of pearlite steel with internal surfaces clad with stainless steel.

Information concerning the operating parameters of these reactors is given in Table 2.1. and Figure 2.1.

Table 2.1

LIGHT-WATER PWR: OPERATING PARAMETERS OF MAIN REACTOR SYSTEM AND EQUIPMENT

Parameter	Unit	Reactor			
		Kozloduj Bulgaria	Mihama-2 Japan	Takahama-1 Japan	Ohi-1 Japan
1	2	3	4	5	6
Thermal output	MW	1 375	1 456	2 440	3 423
Electrical output	MW	440	500	826	1175
Primary Circuit					
No. of loops	-	6	2	3	4
Pressure vessel:					
Diameter	m	3.84	3.40	4.00	4.40
Height	m	11.80	11.50	12.40	12.90
Water volume in reactor circuit	m^3	256	165	260	340
Primary coolant circulation flow rate	t/h	39 000	30 000	45 000	60 000
Type of circulation		forced	forced	forced	forced
Pressure	MPa	12.5	15.4	15.4	15.4

Table 2.1 (continued)

1	2	3	4	5	6
Temperature	°C	285	300	310	310
Steam generator:		Horiz.	vertical	vertical	vertical
Diameter	m	3.2	3.1	3.3	3.3
Height (length)	m	11.9	19.3	20.6	20.6
Heat transfer area	m^2	2 500	4 100	4 800	4 800
Steam generator: Tubes	Type	I	U	U	U
No. of tubes	pcs	5 146	3 300	3 400	3 400
Fuel elements					
Type/fuel		rod/UO_2	rod/UO_2	rod/UO_2	rod/UO_2
Fuel rod diameter	mm	9.1	10.7	10.7	9.5
Fuel rod length	m	2.57	3.9	3.9	3.5
Number of fuel rods per assembly	-	126	179	204	264
Core					
Coolant inlet temperature	°C	268	289	287	289
Coolant outlet temperature	°C	301	320	322	325
Coolant velocity	m/s	3.5	4.5	4.4	4.8
Heat flux (mean)	kW/m^2	450	540	600	600
Burnup	MWd/kg	28.6	39.0	39.0	39.0
Materials in reactor circuit					
Reactor vessel		12x2MF-A	C-steel	C-steel	C-steel
Vessel inner cladding		CrNiTi.18.12*/	SS 304	SS 304	SS 304
Circuit pipes		CrNiTi.18.10	SS 306	SS 306	SS 306
Fuel element cladding		ZrNbl(H-1)	Zircaloy-4	Zirca-loy-4	Zircaloy-4
Steam generator tubes		CrNiTi.18.9	Inconel 600	Inconel 600	Inconel 600
Reactor coolant bypass purification system					
Pressure	MPa	12.5	1.4	1.4	1.4
Temperature	°C	40	53	46	46
Maximum flow rate	m^3/h	20	20.4	27.2	27.2

*/ Some PWRs of the WWER-440 type have no vessel cladding.

Data contained in Table 2.1 reflect the main differences between PWR reactors, viz:

- **The WWER-440 reactors are provided with horizontal steam generators with stainless steel straight tubing while most other PWRs have**

vertical steam generators with U-shaped tubes made of Inconel 600 or Incoloy 800,

- Fuel element cladding of the WWER-440 is made of zirconium-niobium alloy H-1 containing 1% niobium while the fuel elements of the other reactors are clad mainly with Zircaloy-4;

- temperature and pressure as well as heat load are lower in the case of the WWER-400 reactors;

- The reactor coolant by-pass purification systems of the WWER-440 reactors are operated at the reactor circuit pressures (12.5 MPa) while the purification systems in the other reactors are operated at a lower pressure (1.5 to 2.5 MPa).

A specific feature of PWR coolant water chemistry is the fact that boric acid* (H_3BO_3) is added to the reactor water. Under operating conditions, boric acid concentration varies between 0 and 1200 ppm of boron, depending on the mode of power operation an burnup conditions in the core. On the shutdown conditions, Boron concentrations up to 4000/pm can be encountered.

One of the main requirements of reactor water chemistry is sustaining the optimum range of pH values in the reactor water for the operating temperatures**. (Corrosion rates of the constructional materials and corrosion product solubility, as well as corrosion product transport in the primary circuit depend on pH at the operating temperatures). Since boric acid causes a decrease of pH of pure water this requires the use of alkalizing agents for pH control. Two models of pH control have been developed today.

---

*H_3BO_3 is added as neutron poison to control reactivity in the nuclear reactors.

**pH of water is dependent on temperature; pH can usually not be measured directly at operation temperatures (260-329°C) but must be calculated.

PWRs use lithium-7 hydroxide (^{7}LiOH) as an alkalizing agent:

- ^{7}Li has a small cross-section for the neutrons, it produces neither radioactive isotopes as observed with Na and K, nor breakdown products derived from NH_3;
- ^{7}Li is used instead of natural lithium to minimize the production of tritium in the primary coolant through the nuclear reaction $^{6}Li(n,p),^{3}H$;
- Neutron absorption results in one boron's isotope (^{10}B) producing ^{7}Li, i.e. about 5-6 Kg per fuel cycle of a 1200 MW(e) reactor. In some circumstances excess ^{7}Li must be removed from the reactor coolant.

WWER-440 type reactors use KOH and NH_3 to alkalize the reactor water(Table 2.2). The specifications of water quality of WWER- reactors allow for rather small variations of reactor water pH values, through a correlation between the concentration the alkali and boric acid in order to maintain the specified pH (see Fig. 2.3).

The Westinghouse water chemistry of PWR systems allowed for pH variation in a wider range.

The specifications for the primary coolant in KWU PWRs allow pH variations in the range pH_{25^oC} 5-10.5. Coordination of ^{7}LiOH and

Table 2.2

Specifications of reactor water quality for PWR - type WWER-440

Indicator (with reactor "on-load")	Value
pH (25°C)	> 6,0
(KOH as K^+ (depending on H_3BO_3 concentration,..) mg/kg	2.0 - 16.5
NH_3, mg/kg	5
Hydrogen, ml/kg	30 - 60
Chlorides, ug/kg	≤ 100
H_3BO_3, g/kg	0 - 8.0
Oxygen, ug/kg	≤ 10

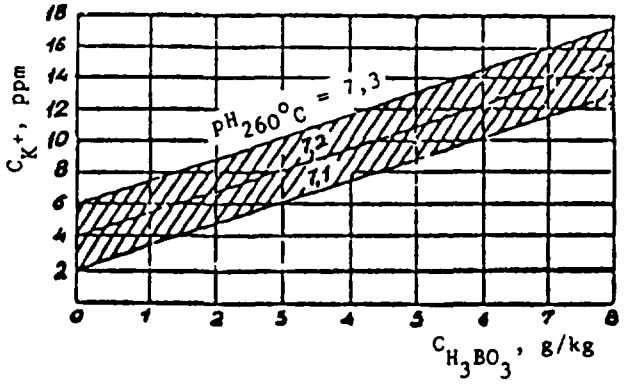

Fig. 2.3 KOH concentration change as K^+ as function of H_3BO_3 concentration in the range of pH_{260° = 7.1–7.3 .

H_3Bo_3 has also been employed since 1979 in the Biblis nuclear power station, FRG. (Fig 2.4).

More recent worldwide practice is to follow a coordinated boron to lithium ratio so as to achieve a minimum $pH_{300^\circ C}$=6.9, as believed to provide a dissolving chemistry for the corrosion products in the reactor core.

These differences in concept are also reflected in the specifications for reactor water quality (Tables 2.2 and 2.3).

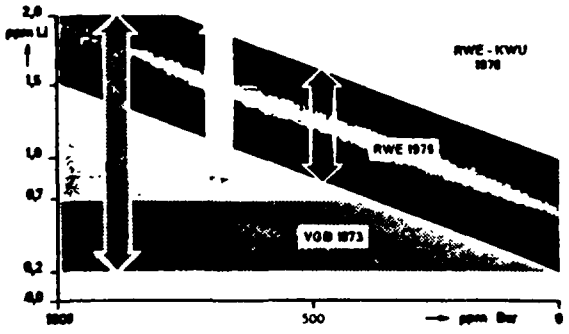

Fig. 2.4 Lithium concentration as function of boric acid concentration in the reactor water of NPP Biblis

For comparison purposes Table 2.4 contains the specified qualities of the reactor water in the Japanese, Babcock and Wilcox and German PWRs under steady state conditions.

Table 2.3

THE WESTINGHOUSE CO. REACTOR WATER QUALITY SPECIFICATIONS

Indicator	Unit	Standard values	Remarks
pH at 25°C		4.2-10.5	Depends on H_3BO_3 and ^7LiOH concentration
pH at 300°C, Fig. 9		5.4-7.6	"
Conductivity at 25°C	S/cm	1-40	As for pH 25°C
Boric acid as boron	mg/l	0-4000	
^7LiOH*/ as $^7Li^+$	mg/l	0.22-2.2**/	0.03-3.2 x 10^{-4} mol
Hydrogen	cm^3/kg	25-35	
Chlorides, max.	ppm	0.15	
Fluorides, max.	ppm	0.15	
Total suspended solids	ppm	1.0	
Oxygen, max.	ppm	0.1	For operating temperatures in excess of 250°F
Oxygen, average	ppm	0.005	During power operation when H_2 is maintained in the coolant

*/ Irrespective of H_3BO_3 concentration in coolant.

**/ The recent data are "0.7-2.2" (Private communication, 1982).

Table 2.4

CHEMISTRY SPECIFICATIONS FOR REACTOR WATER OF PWR

Indicator	Unit	Japanese PWR	Babcock & Wilcox	VGB, FRG
pH at 25°C		4.2-10.5	4.6-8.5	-
^7LiOH as $^7Li^+$	ppm	0.2-2.2	0.2-2.0	0.2-2.0
Boric acid as B	ppm	0-4000	0-2100	-
Hydrogen	cc/kg	25-35	15-40	2-4*/
Oxygen, max.	ppm	0.005	-	0.05
Chlorides, max.	ppm	0.05	0.10	0.20
Fluorides, max.	ppm	0.05	0.10	-
Total suspended solids, max.	ppm	-	0.1	-
Iron, max.	ppm	0.05	-	-
Silicates, max.	ppm	0.5	-	-
Turbidity, max.	ppm	1.0	-	-

*/ Measured results are in ppb.

Worthy of mention are the considerably lower limits of the chloride and the fluoride concentrations in the Japanese specifications for the coolant quality. This is associated with the well-known sensitivity of stainless steel even to low levels of anionic impurities.

There is a general consensus on the role of the following water coolant impurities and additives:

- Hydrogen is added, to suppress water radiolysis (oxygen formation);

- Oxygen contamination results in an increase of primary circuit corrosion rates and crud concentration in the reactor water and on the fuel cladding. The presence of both oxygen and halogens can cause stress-corrosion of stainless steel;

- pH control agents are used for corrosion protection and as a means of limiting corrosion product transport to the core and crud deposition on fuel cladding;

- The limitations for chloride and fluorides have been established to minimize the corrosion of the coolant circuit construction materials and particularly of stainless steel. The control of fluoride concentration is also linked with the fact that Zircaloy undergoes accelerated corrosion at fluoride concentrations above 2 ppm in the presence of lithium hydroxide.

Data contained in Table 2.5 indicate that the reactor water quality in a number of PWRs in Europe, Japan and the United States of America practically corresponds to the specifications. This is an indication of the realistic approach adopted when establishing the specifications and of the successful control of reactor water quality in the various nuclear power stations.

Water chemistry as applied today in PWRs does guarantee the integrity and reliability of the primary circuit including the fuel elements. The generally low level of corrosion product total activity in the primary coolant can be regarded as an indicator of acceptable operation.

However, despite this optimistic conclusion certain facts relating to more precise control should not be overlooked. In this connection the

Table 2.5

OBSERVED CONCENTRATION OF IMPURITIES AND ADDITIVES IN PWR REACTOR WATER UNDER STEADY-STATE CONDITIONS

Nuclear power station (PWR)	Chloride, ppm	Fluoride, ppm	Hydrogen, cc/kg	Oxygen, ppm	Suspended solids, ppm	Li ppm	pH
Takahama 1, Japan	0.05	0.05	30	0.005	0.1	-	6.5-7.0 (at 300°C)
Mihama 2, Japan	0.05	0.05	30	0.005	0.1	-	6.5-7.0 (at 300°C)
Kozloduj, Bulgaria	0.1	0.1	40-50	0.005	0.1	2-17 K	7.1-7.4 (at 260°C)
Obrigheim, FRG	0.06	-	-	0.03	-	1.4	-
Neckerwestheim, FRG	0.1	-	2-3 ppm	0.01	0.1	0.7-2.0	6.2-7.5
Biblis A & B, FRG	0.05	-	2-3 ppm	0.005	-	0.2-2*/	-
Stade, FRG	0.10	-	3.0 ppm	0.010	0.5	1.1-1.5	-
Ringhals, Sweden	0.10	0.05	15-50	0.005	0.1	0.5-1.0	-
Doel 1 & 2, Belgium	0.03	0.01	57-59	0.005	-	0.4-0.6	-
Tihange, France-Belgium	0.03	0.02	23-30	0.010	0.025	-	-
Beznau, Switzerland	0.15	0.05	35	0.005	0.3	1.0	-
Zorita, Spain	0.02	0.02	35	0.001	0.03	0.7	-
Novovoronezh, USSR	0.1	0.1	40	0.005	0.1	2-17K	7.1-7.4 (at 260°C)
BR-3, Belgium (1979-1980)	0.03	-	7-9	0.03	0.01-0.18	0.9-1.1	6-8 (at 25°C)
Oconee, USA	0.05	0.05	20	0.005	0.01	0.4-0.5	6 (at 300°C)

*/ K^+ and Li concentration at Kozloduj, Novovoronezh and Biblis depends on H_3BO_3 concentration

investigations conducted by Thomazet, Noe and Stora revealed that effective prevention of fuel element cladding crud deposition requires the maintenance of practically constant pH values at the operating temperature, thus requiring the continuous decrease of lithium hydroxide during the cycle.

Results obtained by Thomazet et al. correspond with the earlier practical conclusions drawn at Biblis in 1979 on the need to maintain reactor water pH within a narrow range through a suitable concentration of H_3BO_3 and LiOH, Fig 2.4.

It seems advisable therefore that the future PWR coolant chemistry specifications should be amended to allow for a practically constant and high pH value, which should be maintained throughout fuel cycles. This will involve the coordinated variation of the alkali level with the boron concentration. Data on pH changes in the reactor coolant of a Japanese PWR for the period 1975-1981 indicate that such a policy of pH control has already been achieved in the past. It is now worldwide common practice.

From the standpoint of the behaviour and reliability of the fuel element cladding it is also necessary to take into account the adverse effect of any deviations from the reactor coolant specifications. According to Lippens, Haas, Gubel, Van der Velde and Van Loon the failure of the fuel elements in the Belgian reactor BR-3 was due to the considerable amount of impurities entering the primary circuit water during decontamination operations. These impurities deposited on the fuel elements and accelerated the corrosion of the cladding.

An important circumstance influencing fuel rod failure in the BR-3 reactor was significant deviation from the reactor coolant specifications:

- "Hydrogen concentration oscillated between 7 and 9 cm^3/Kg". i.e. a lower than specified value (25 - 30 cm^3/Kg)...,

- "Oxygen content in the reactor coolant was 0.03 ppm on average, i.e. a higher than specified value (0.005 ppm)".

Evidently, the low hydrogen content is the reason for the observed higher oxygen amount (resulting from water radiolysis) on one hand, and the decrease of the dissolved iron concentration on the other. The comparatively low pH of the reactor water during the reactor campaign (pH_{25^oC} = 8) also contributed to this effect.

Under these unfavourable conditions, the comparatively moderate concentration of undissolved crud between 0.01 and 0.18 ppm had been enough to form significant crud deposits on the fuel element cladding. As a result, the process led to corrosion damage.

Pressurized heavy water reactors are presently in operation in Canada, Argentina, India and in some other countries. The high temperature - high pressure primary coolant (D_2O) system of these reactors uses an alkaline pH regime under controlled dissolved oxygen levels. The philosophy behind this primary system chemistry control is to minimize the corrosion/release rates of the major constructional materials, like carbon steel and Monel 400, and also to favour the reduction of corrosion product residence time in the core. These objectives would reduce:

(a) the deposition of corrosion products on fuel elements and the concentration of aggressive chemicals within the deposits;

(b) the radiation field build-up on out-of-core surfaces.

The specifications of water quality for the reactor coolant of NPS Atucha-1, Argentina* (1179 MW(th) and 335 MW(e)) are similar to PWRs.

The permissible concentration ranges of various ions and compounds are:

LiOH	1-2 ppm Li
D_2	6 ppm
Oxygen	0.05 ppm
Chloride	0.2 ppm
pD at 25°C	10.5-10.9
Silica	max 4 ppm SiO_2
Dissolved iron	0.5 ppm
Crud	1 ppm

The observed concentration for impurities and additives during normal operation for PWR Atucha-1 and for RAPS (PWR of Rajastan Atomic Power Station) are given in the Table. 2.6.

Table 2.6

indicators	Unit	Atucha-1	RAPS
Conductivity, 25°C	uS/cm	10-15	19-25
Chlorides	ppm	0.01	0.1-0.2
Oxygen	ppb	5-20	10
D_2	cm^3/kg	1-2	3-10
pD at 25°C		10.0-11.0	9.5-10.5
LiOH	ppm Li	0.7-1.1	-
Boron	ppm	0.5	-

*Data about Atucha-1 are taken from "Answers to IAEA Questionnaire NPS Achuta-1, Argentina (1981).

2.2 BWR Reactor and Feed Water Chemistry Specifications

In a typical light water BWR, water passes through a core acting as both the moderator and coolant removing heat from the core. (Fig 2.5) A portion of the coolant then evaporates and enters the turbine as steam. The condensed steam is collected in a hot-well located below the condenser cooling tubes. The full flow of condensate passes through a condensate polishing unit in order to remove soluble and insoluble impurities. This high-purity water is heated and is injected as feedwater into the reactor. The required reactor water quality is provided by purification of separate bleed in the reactor water polishing unit.

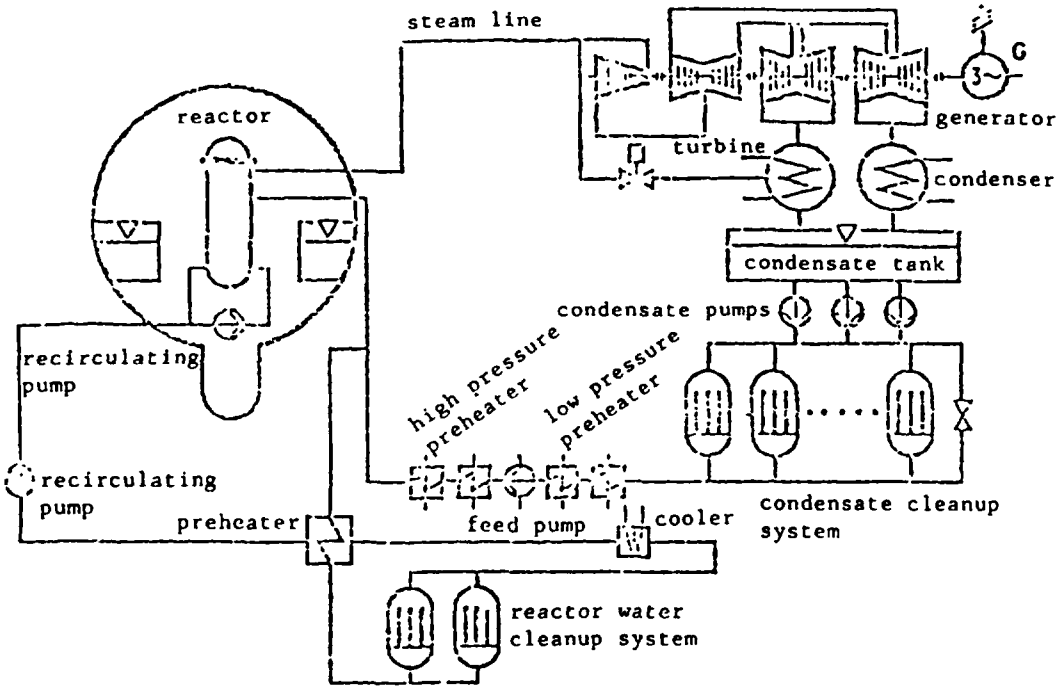

Fig. 2.5 BWR - Flow diagram

BWRs which use heavy water or graphite as the moderator and light water as the coolant and working fluid can be considered from the chemical viewpoint as a typical light-water BWR. For that reason, this chapter on the light-water BWRs will include also reference to the Steam Generating Heavy Water reactor in Winfrith and the BWR of the type RBMK-1000 in the USSR. The latter is a light-water BWR of the channel type with the graphite moderator (Fig 2.6).

Information on the main system characteristics, operational parameters and construction materials is given in Table 2.7.

A specific feature of BWR water chemistry is that water radiolysis in the core is not suppressed*. Reactor operation at a given capacity leads to water radiolysis at a constant level. In most cases the O_2 level in the recirculating coolant due to radiolysis is usually between 0.1 and 0.3 ppm, and the O_2 level in the produced steam ranges between 15 and 30 ppm.

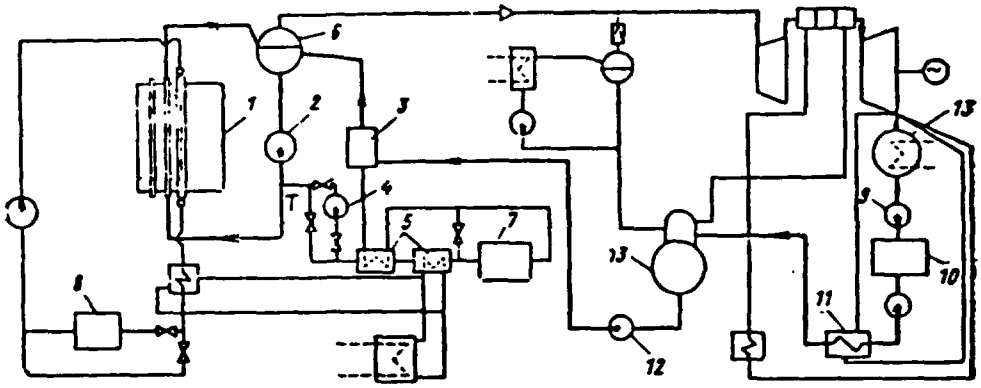

1- reactor; 2 - main recirculation pump; 3 - mixer; 4 - cooler pump; 5 - cooler; 6 - seperator; 7 - bypass cleanup; 8 - control and safety rod assembly cleanup; 9 - condensate pump ; 10 - demineralizer; 11 - low pressure heater; 12 - feedwater pump; 13 - deaerator

Fig. 2.6 Flow diagram of the coolant circuit: BWR of the RBMK-1000 type

It is known that even small amounts of oxygen in the coolant induce deleterious effects on the intergrannular corrosion of the recirculation piping. It has turned out that the addition of hydrogen reduces the oxygen level in the recirculation lines through the radiolytic recombination reaction in the downcomer. Therefore, hydrogen injection to the feed water system of BWRs has been proposed as remedy to piping corrosion. This water chemistry regime is called: "hydrogen water chemistry" and, its demonstration is now being conducted in several power plants.

The presence of radiations rules out pH control by hydrazine or ammonia because the radiolysis can produce nitric acid which is

---

* Unlike PWRs, water radiolysis suppression by maintaining certain H_2 concentrations is difficult because the hydrogen added is removed continuously with the steam from the core.

Table 2.7

LIGHT WATER BWR. MAIN REACTOR CHARACTERISTICS AND PARAMETERS. CONSTRUCTION MATERIALS

Parameters	Unit	Boiling-water reactors in nuclear power stations				
		WSGHR UW	Tarapur India	Mühleberg Switzerland	Tsuruga Japan	Hamaoka 2 Japan
1	2	3	4	5	6	7
Thermal capacity	MW	330	-	1 000	1 070	2 436
Electrical capacity	MW	100	210	320	357	840
Coolant system data						
Flow diagram						
Primary coolant circulation flow rate	t/h	7 000	10 500	14 000	17 700	34 900
Type of circulation		forced	forced	forced	forced	forced
Number of loops		2	2	2	3	2
Steam production	t/h	550	I - 875 II - 362	1 800	1 935	4 750
Pressure	MPa	6.4	5.8	7.1	6.99	7.2
Temperature	°C	280	285	276	285	286
Volume of water	m^3(t)	38	93.7	100	160	212
Fuel elements						
Type			6 x 6	8 x 8	7 x 7 8 x 8	8 x 8
Number of fuel elements in core		104	284	240	308	560
Core						
Heat flux, mean	kW/m^2	411	383	457	370	452
Heat flux, maximum	kW/m^2	1 087	1 277	1 003	1 120	1 105
Heat transfer surface	m^2	793.4	1 672	2 200	2 793	5 147
Neutron flux, mean						
thermal neutrons	$n/cm^2.s$	5.7×10^{13}	3×10^{13}		3.6×10^{13}	4.6×10^{13}
fast neutrons	$n/cm^2.s$	1.3×10^{13}	1.8×10^{9}		3.7×10^{13}	1.3×10^{14}
Coolant velocity	m/sec	5.0	2.17	0.7	2.0	
Inlet temperature	°C	274	267	190	189	
Outlet temperature	°C	280	285	276	285	286
Outlet void, mean	%	9			59	42.2
Outlet void, maximum	%	22.5			69	
Burnup, mean	MWd/t	27 500	21 600	25 000	25 000	27 500
Materials in reactor						
Reactor vessel	type		St.302	St.A508	St.302B	St.533
Vessel cladding	type		St.308	St.304	St.308	St.371
Pressure tubes		Zircaloy 2				
Fuel cladding			Zircaloy 2	Zircaloy 2	Zircaloy 2	Zircaloy 2
Reactor water clean-up system	type		St.304	St.304	St.304	St.304
Recirculation loops	type	St.321	SS316	St.304	SA106	St.304
Materials in secondary side						
Steam piping	type	St.304	St.304	St.45.8	A106	St.304
Condenser tubes	type	70/30 brass		Admiralty brass		
LP feed heater	type	90/10 brass		St.304	St.304	
HP feed heater	type	90/10 brass		AxlOCrNiTi 18/9	St.304	
Feedwater pipe	type	St.304		St.35	A.106	

corrosive. In BWR coolant pH cannot be controlled even with the non-volatile KOH or LiOH because of the danger of local concentration increase of these alkalis in the core.

Under these circumstances, the minimization of the corrosion processes in the BWR requires both the use of highly corrosion-resistant construction materials and of high-purity water throughout the cycle.

As it is can be seen from Table 2.7 reactor circuit system is made of corrosion-resistant materials, mainly stainless steel. However, in the presence of chlorides and oxygen these materials are susceptible to stress corrosion cracking. For this reason, the reactor water, and hence the feedwater of a BWR should have the lowest possible chloride and fluoride concentration.

Other parts of the plant can use less corrosion-resistant materials such as low-alloy steels. The corrosion products released from the large surface areas of these materials must be removed. Condensate demineralizer installed after the turbine condenser before the flow enters the reactor vessel are used for this purpose. However, the corrosion products released downstream of the condensate demineralizer are not removed. The oxygen concentration is very important for minimizing the corrosion products release in the feedwater system. Therefore the oxygen level must be controlled in the feedwater. In this way fuel surface deposits are minimized and flow and radioactivation problems reduced.

For that reason, corrosion product control of the water before it enters the core is essential in BWR operation. The corrosion product concentrations in the reactor and feedwater are therefore subject to strict specification limits.

Evidently, both the feedwater and the coolant in the BWRs should have a high degree of purity. This has been reflected in the specifications for feedwater and reactor water quality in BWRs. Table 2.8, 2.9 and 2.10 give the feedwater and reactor water qualities in a number of BWRs as specified by various companies and countries.

A comparison of the data in these Tables leads to the conclusion that irrespective of some differences in the specified parameters and the

Table 2.8

FEEDWATER SPECIFICATIONS FOR BWRs IN SOME NUCLEAR POWER STATIONS

Parameters	Unit	WSGHWR	Tarapur	Mühleberg	Tsuruga	Hamaoka 2
Conductivity	uS/cm	0.2	0.1	0.1	0.1	0.1
Chlorides	ppb	20	n.s.*/	n.s.*/	n.s.*/	n.s.*/
Silica	ppb	30				
Corrosion products:						
Iron	ppb	20		5	15**/	30
Copper	ppb	5(3)	2	2	2	
Cr total	ppb			15		
Ni total	ppb			15		
Oxygen	ppb		14		20-200	20-200
pH at 25°C					6.5-7.5	

*/ Not specified but should be maintained low enough to satisfy the reactor water requirements.
**/ Total metal.

Table 2.9

REACTOR WATER SPECIFICATIONS FOR BWRs IN SOME NUCLEAR POWER STATIONS

Parameters	Unit	WSGHWR	Tarapur	Mühleberg	Tsuruga	Hamaoka 2
Conductivity	us/cm	1.0	1.0	1.0	1.0	1.0
pH at 25°C			5.6-8.6	5.8-8.6	5.6-8.6	5.6-8.6
Chlorides	ppb	200	100	200	100	200
Silica	ppb	2000(1000)	1000	1000		
Iron (below 0.45um)	ppb			20		
Copper	ppb	35		50		
Boron	ppb		200			
Dissolved oxygen	ppb		400			
I-131	uCi/l	100	5000			

Table 2.10

FEEDWATER AND REACTOR WATER SPECIFICATIONS FOR BWRs

Parameters	Unit	VGB***		KWU Würgassen		General Electric		RBMK USSR	
		fw	rw	fw	rw	fw	rw	fw	rw
Conductivity	uS/cm	0.15	1.0	0.1	1.0	0.1	1.0	0.1	1.0
pH at 25°C				6.5-7.5	5.6-8.6		7.0±0.2		6.5-8.5
Chlorides	ppb	ns*/	200	10	100	ns	200	4	100**/
Silica as SiO_2	pb	ns	4000	5	ns	ns	4000	ns	1000
Iron	ppb	25	ns	ns	ns	13	ns	10	200
Copper	ppb	3	ns	2	ns	2	ns	2	50
Oxygen	ppb	ns	ns	14	ns	ns	ns	ns	ns
Insolubles,(below 0.45um)									
total crud	ppb	ns	ns	ns	ns	ns	ns	ns	200
Total activity	uCi/l	ns	ns	ns	ns	ns	ns	ns	100

*/ ns = not specified.
**/ Total chlorides and fluorides (50 ppb chlorides + 50 ppb fluorides).
***/ VGB: Vereinigung der Grosskraftwerks Betreiber.

permissible amounts of the impurities in the feedwater and the reactor water of the BWRs the specified main characteristics of reactor water and feedwater are essentially the same:

- Feedwater is highly demineralized. Specific conductivity varies between 0.1 and 0.2 uS/cm. Chloride level in the feedwater must be sufficiently low to meet the requirements for chloride concentration in the reactor water. (In a number of specifications the chloride level in the feedwater is not specified due to difficulties in the experimental determination and the extremely low chloride ion concentration.)

- The reactor water is also highly demineralized, the amount of the respective impurities being in such ranges as to guarantee the reliable operation of the fuel elements and the stainless-steel equipment and pipes as well as the sufficient purity of the produced steam. The specifications generally allow for max. 100 or 200 ppb chloride while the critical concentration is 350 ppb.

The silica concentrations are specified for two reasons - first, to avoid deposits on the heat exchange surfaces in the core, and secondly, to avoid impurities in the steam which could in turn lead to deposition in the turbine. A silica concentration of 1000 ppb is sufficiently low to avoid this. However, in the case of demineralizing make-up of water (specific conductivity about 0.1 uS/cm) the maximum silica concentration is between 20 and 30 ppb. Thus, silica from make-up water is rarely the source of high coolant levels of SiO_2. Silicious matter, e.g. lagging and dust from building materials, can however enter reactor systems at shutdown and during maintenance and this is the main cause of high levels, particularly after reactor startup.

As illustrated in Table 2.11 under normal operating conditions of the BWR the feedwater and the reactor water qualities meet the specifications, or are even better. Reactor water conductivity is 3 to 4 times lower than the specified value. The same is true for the amount of silica in the reactor water. In most BWRs, corrosion product levels present in the feedwater and the reactor water are considerably less than the specified values.

Table 2.11

OBSERVED QUALITY OF FEEDWATER AND REACTOR WATER DURING NORMAL OPERATION OF BWR (AVERAGE VALUES)

Indicator	Unit	WSGHWR		Tarapur		Mühleberg		Tsuruga		Hamaoka 2	
		fw	rw	fw	rw	fw	rw	fw	rw	fw	rw
Conductivity	µs/cm	0.07	0.3	0.07	0.3	0.1	0.1	0.07	0.16	0.06	0.24
pH at 25°C		6.9			6				6.6	6	8.0
Chlorides	ppb	2	200		20		10		20		10
Silica as SiO_2	ppb	2			200		250		10		168
Iron	ppb	8	60		50	0.1	2	1.1	6.3	6	11
Cobalt	ppb	0.008	0.1		0.4	0.005		0.001	0.1		
Copper	ppb	1	15	0.2	1	0.05	3	0.1	0.3		
Nickel	ppb	0.3	1		2	0.1	0.2	0.03	0.07		
Chromium	ppb		3		5	0.2	3	0.01	0.03		
Oxygen	ppb	40	60	20	250			40	300	29	
Purification system	type	Pow	Pow	DB	MF/DB	Pow	Pow	DB	MF/DB	DB	Pow

Remarks fw = feedwater; rw = reactor water
Pow - Powdex; DB - deep bed; MF - mechanical filtration.

Any change of operating conditions, startup or shutdown of BWRs can lead to considerable deterioration of the feed and reactor water quality. The effect of the transient conditions is best illustrated by reference to Table 2.12.

Table 2.12

METAL IMPURITY CONCENTRATION IN THE FEEDWATER AND THE COOLANT OF THE BWR AT MUHLBERG UNDER NORMAL OPERATING CONDITIONS, WHEN CHANGING THE MODE OF OPERATION AND DURING STARTUPS

Indicators	Unit	Normal operation		Startup		Change of mode	
		feedwater	coolant	feedwater	coolant	feedwater	coolant
Iron	ppb	0.1	0.3	1.5	50	10	1
Chromium	ppb	0.02	2.1	0.1	4	0.1	2.5
Nickel	ppb	0.1	0.1	0.1	0.1	0.2	0.3
Cobalt	ppb	0.005	0.06	-	-	-	-
Copper	ppb	0.05	2.0	0.1	3	0.4	3

Many results indicate that during changes of operating conditions or startup of BWRs the clean-up plant is not always able to adequately remove corrosion products and some ion impurities from the treated water. In the case of WSGHWR the situation is as follows:

"- Feedwater conductivity is higher than the specified value during the first five hours after startup of the reactor and immediately after recoating the Powdex-filters (with powdered ion-exchange resin in the plant) for simultaneous clean-up of the feedwater and the reactor water;

"- Silica levels in the feedwater are higher than the specified value during the first five hours after startup and shutdown of the reactor;

"- Considerable increase of iron concentration in the reactor water is observed for short periods after reactor perturbation but there is no increase in the feedwater."

These points emphasize the importance of the plants for maximum possible clean-up of the feedwater and some of the reactor water in BWR water chemistry.

It can be concluded therefore that the feedwater and the reactor water qualities as required by the specifications are realistic and attainable. This is every indication that under normal operating conditions the plants for condensate (feedwater) and reactor water clean-up can satisfactorily meet the requirements for impurity removal from the processed water.

2.3 Water Cleaning Control Systems

The reactor water purification is the key to adequate coolant chemistry control. Usually the coolant purification flow from the primary circuit constitutes 0.1 to several percent of the reactor steam generating flow rate (up to tens of tonnes/hour for PWRs and some tens to hundreds of tonnes/hour for BWRs.)

The normal clean-up flow in BWRs is about 2% of the feedwater flow at 100% reactor power. However, in some BWRs the amount of bypass treated coolant is larger, e.g. in Tsuruga the plant for coolant clean-up has a capacity 6.7% compared to that for feedwater.

The reactor water may be purified in by-pass equipment or by "feed and bleed" method (removal of the system water with simultaneous addition of high purity make-up water).

The selection of the purification technique is based on the following considerations:

- the primary water directed to the purification plant has the temperature 250-300^{o}C and pressure 75 to 150 bars
- the water impurity inventory consists of corrosion products (suspended and dissolved), organic species, dissolved salts and gases; (radioactive species are also unavoidably present);
- with the by-pass purification the decontamination factor (for individual components) should be about 10; a higher value is unnecessary since it does not affect the impurity balance (except if some fraction of the treated water is used for another technological aims, eg. for cooling the control rod drives).

There are three basic concepts of the reactor water purification technology:

- depressurizing (with respective water temperature decrease), cleaning-up and returning to the circuit;
- purification at nearly circuit pressure, but at a lower temperature;
- purification at the circuit pressure and temperature.

The two former concepts have been preferred.

Water may be cleaned up by filtration, ion exchange, distillation, electrodialysis, electrophoresis, etc. The former two types are proven and most widely used today.

The demineralization units are generally loaded with mixed beds of cation exchanger resin in H-form and anion exchanger resin in OH-form in ratio 1:1 to 2:1.

The ion-exchange resins used have grain size 0.3-1 mm or 0.02-0.06 mm. The first type is used in bulk while the second type forms a thin (0.2-0.8 cm) filtering layer in special pre-coated filters of (eg., Powdex filters at the winfrith WSGHWR).

In a number of clean-up plants the ion-exchanger units are preceded by mechanical filters. These are mostly pre-coated with cellulose, Solcafloc or other filtering materials. The mechanical filters are designed to remove the main portion of the suspended corrosion products. For this purpose electromagnetic filters have also been recommended.

Powdered resin filters, (and in a number of cases Monobed*/ units) act simultaneously as mechanical filters and ion-exchange demineralizers.

Typical reactor water clean-up systems (for PWRs and BWRs) are shown in Figs 2.7 and 2.8.

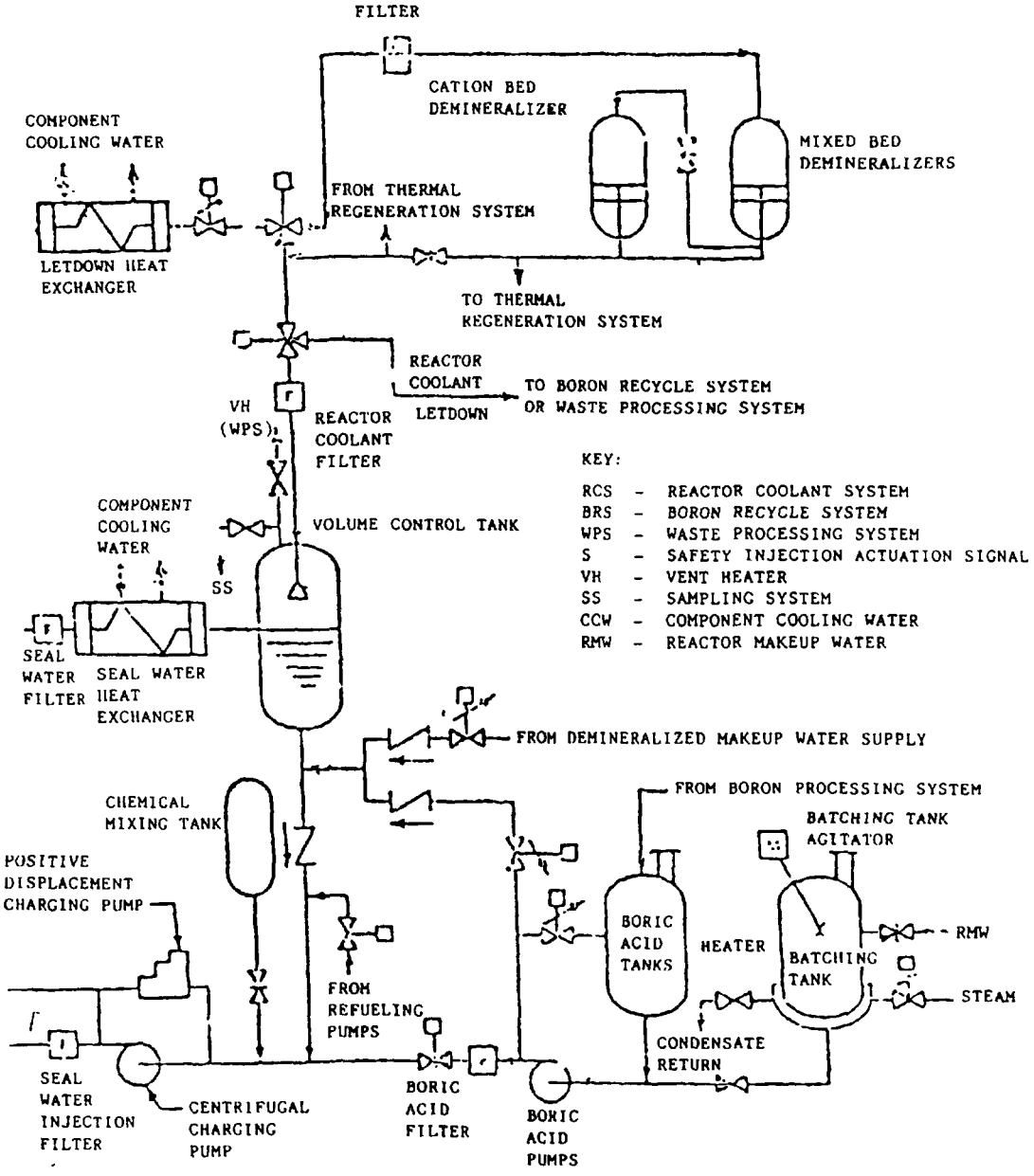

Fig. 2.7 Chemical and volume control system

* Monobed is a commercial name for single stage unit.

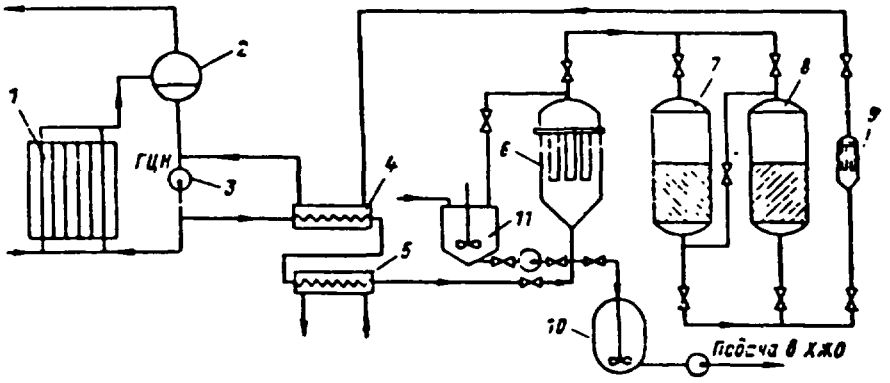

1 - reactor; 2 - drum separator; 3 - recirculation pump; 4 - regenerative heat exchanger; 5 - cooler; 6 - pre-coated filter; 7 & 8 - demineralizers; 9 - trap-filter; 10 - slurry tank; 11 - tank for powder filter precoating

Fig. 2.8 Bypass reactor water cleanup system for BWR of the RBMK-1000 type

Removal efficiency of impurities from treated coolant is about 90% when the plant comprises only ion-exchange demineralizers of the Monobed type.

The mechanical filters (pre-coat type) preceding the Monobed remove 96-99% of the particulate corrosion products (size larger than 0.45 um)

Table 2.13 illustrates the decontamination capacities of Monobed ion-exchange demineralizers (installed after the mechanical filters) in the case of Tarapur NPS.

Table 2.13

Nuclides	Decontamination factors in the ion-exchange units of the coolant clean-up plant at Tarapur	
	Initial phase of operating cycle	End of cycle*/
^{131}I	8000	16
^{132}I	3.1×10^4	2.6×10^3
^{133}I	5.2×10^3	1.3×10^3
^{239}Np	7.1×10^4	670
^{99}Tc	-	6.5×10^3
^{137}Cs	5.8×10^3	1.2×10^2
^{134}Cs	5.3×10^3	1.4×10^2
^{60}Co	over 1.5×10^2	1.7
^{103}Ru	-	5.9
^{95}Zr	-	1.52

*/ This cycle ranges between 8 and 12 months.

For comparison purposes, Table 2.14 illustrates the overall effect of decontamination at Tsuruga NPS whose coolant clean-up consists of:

- Unit for mechanical filtration: pre-coated filter with Solcafloc
- Unit for ion-exchange demineralization, Monobed type.

The usual life of the ion-exchanger is between 8 and 10 months after which it is replaced or regenerated.

Table 2.14

Impurities, nuclides	Unit	Inlet mechanical filter	Outlet mixed bed demineralizer	Removal efficiency inlet concentr. / outlet concentr.
Conductivity at 25°C	µs/cm	0.10-0.16	0.05	
Chlorides	ppb	20	20	
Iron: a/ > 0.45 µm	ppb	6.3	0.02	315
b/ < 0.45 µm	ppb	0.04	0.01	4
Copper: a/ > 0.45 µm	ppb	0.1	0.001	10
b/ < 0.45 µm	ppb	0.32	0.005	64
Nickel: a/ > 0.45 µm	ppb	0.02	0.005	4
b/ < 0.45 µm	ppb	0.05	0.007	7
Cobalt: a/ > 0.45 µm	ppb	1.0	0.1	10
b/ < 0.45 µm	ppb	8.3	1.0	8.3
I-131	µCi/ml	2.5×10^{-4}	2.7×10^{-8}	9360 = DF
I-133	µCi/ml	3.5×10^{-3}	5.2×10^{-7}	6730 = DF
Cs-137	µCi/ml	9.0×10^{-7}	1.1×10^{-7}	8.2 = DF
Co-60	µCi/ml	3.6×10^{-5}	4.6×10^{-6}	9 = DF

The efficiency of the coolant clean-up plants consisting only of Powdex-filters is usually higher than that with Monobed. The life of the Powdex-filters is normally about a month. The experience of Mühleberg NPS reveals that the coolant clean-up plant comprising only Powdex-filters treats about 220 000m^3 monthly, and powdered ion-exchange consumption is about 0.25g per 1m^3 treated water.

The condensate clean-up plants consisting only of Monobed demineralizers, when treating the whole amount of turbine condensate, guarantee an efficiency close to that illustrated in Table 2.15.

Table 2.15

Indicator	Unit	Inlet CCU concentration	Outlet CCU concentration	Removal efficiency: inlet concentr. / outlet concentr.
Conductivity at 25°C	µs/cm	0.07	0.06	-
Iron (> 0.45 µm	ppb	26.6	1.6	17
< 0.45 µm)	ppb	0.7	0.4	1.8
Copper (> 0.45 µm	ppb	1.56	0.03	52
< 0.45 µm)	ppb	0.50	0.03	17
Nickel (> 0.45 µm	ppb	0.03	0.004	7.5
< 0.45 µm)	ppb	0.05	0.007	7.1
Chromium (> 0.45 µm	ppb	0.05	0.004	13
< 0.45 µm)	ppb	0.004	0.002	2
Cobalt (> 0.45 µm	ppb	2.6	0.3	8.7
< 0.45 µm)	ppb	12.1	0.9	13
I-131	µCi/ml	8.1×10^{-6}	1.1×10^{-8}	736 = DF
I-133	µCi/ml	8.5×10^{-5}	1.3×10^{-7}	654 = DF
Co-60	µCi/ml	1.1×10^{-8}	1.3×10^{-10}	85 = DF

The efficiency of turbine condensate clean-up is usually higher in the plants with Powdex-filters. However, a disadvantage is the short life in cases when large amounts of salt enter the condensate as the result of leakage in the turbine condenser. (This disadvantage is particularly important when the turbine condensers are cooled with highly saline water, e.g. sea water).

In order to guarantee operation under condenser leak conditions in some BWRs (e.g. Ringhals, Sweden) the Powdex-filters are complemented with deep-bed demineralizers. Under normal operating conditions only the Powdex-filters are in operation. When turbine condensate salinity (conductivity) increases the Powdex-filters are bypassed, i.e. the deep beds are operated.

The use of magnetic filters for removing insoluble corrosion products remains of potential interest. This could be of importance in purifying high-temperature condensate which comes from the feedwater heaters before being mixed with the turbine condensate or the feedwater.

2.4 Monitoring Water Chemistry

Sampling and control of primary coolant is performed on a regular basis to confirm that the water chemistry is within specified values. These specifications have been selected to meet the two following objectives:

1. Keep the integrity of fuel cladding and related core materials;

2. Minimize the radiation buildup on the out-of-core surfaces, so as to reduce personal exposure.

A questionnaire was issued in 1982 to collect information on the sampling and analytical procedures and methods which are used to qualify the primary coolant and corrosion product behaviour in the primary circuits at the operating nuclear power plants. Responses were received from 42 PWR, 12 PHWR, 14 BWR reactor type units and from one WSGHWR and one RBMK-1000 type plant. The list of responding countries along with their code number is given in Annex I, which also shows the plant capacity and year of commissioning.

The responses were compiled in the form of condensed tabulations (Annex I) according to the main points of the questionnaire:

1. Code listing of nuclear power plants
2. Overview of NPPs
3. General concepts of sampling, control of sampling and parameters to be measured
4. Chemical analytical techniques
5. Radiochemical and physical measurements

The answers from the same reactor types are grouped, so as to give a comparative view. For clarity, the flow-sheets of the primary circuits provided by the plants are not included.

Chemical parameters measured in the primary circuit are different for different reactor types. Annexe I, Table 1.3) For example dissolved H_2 is measured only in PWRs, and D_2 in PHWRs. In some PWRs nitrate or NO_x which is formed under nucleate boiling conditions on the fuel element surfaces is also measured. Among halogens, chloride is measured by all the plants, while fluoride is only measured in certain PWRs. Fe and total insolubles are

measured in all plants while other corrosion products are measured only in some of them. At certain units continuous monitoring and automated control are employed. PWRs of advanced generation which can undergo some nucleate boiling conditions on the surface of the hot assemblies are submitted to stringent specifications on mineral impurities, susceptible to form zeolite type deposits (Ca, Mg, Al, Si). These specifications must be derived both from loop experiments and feedback from PIE bearing in mind practical limits on the purification systems.

The control of these chemical parameters is not an easy operation and, representative values are not always obtained; despite an increasing capability to measure levels in the ppb range. Account must be taken of the cooling of the sample and the potential pollution and/or deposition of particles in the sampling lines.

The sampling systems are, without exception, designed for low temperature sampling. At units JAPW 32-42, ASTM standards are applied, while at units FIBW 56 and 57, UNIPEDE recommendations are used.

Stainless steel is mainly used as the material of construction for the sampling system, except in UKSG 55 and in units JABW 60 and 61, where Inconel and Ti lines respectively are used.

Isokinetic sampling is carried out at units JABW 60 and 61, FIBW 56, and 57 along with capillary lines at UKSG-55. Continuous flow is maintained in sampling lines in units, CAPH 44-51 and FRPW 5 to 30. This specialized design facilitates the collection of representative samples of the coolant at the sampling point.

Filtration is used widely as a method for crud separation and preconcentration of soluble impurities. For this purpose, membrane filters (in unit JABW 60-70; FIBW 56 and 57; UKSG 55; BEPW 1; FRPW 5 to 30 except 4 and CAPH 44 to 51) and ion exchange filters (in units JABW 62-70; FIBW 56 and 57; UKSG 55; FRPW 5 to 30 except 4 and CAPH 44 to 51) are used.

In reactors where deposits sampling is undertaken (FRPW 5-30 except 4, JAPW 32-39 and 41 and 42, FIBW 56 and 57, INPH 52-54 and JABW 60-62) the surface of fuel elements is mechanically treated in a pool and the released deposits are collected by filtration.

As already mentioned, metallic impurities are preconcentrated mainly by filtration. In this way the sensitivity of 0.1 ppb is often achieved, the sensitivity of cobalt determination by UKSG 55 is 0.02 ppb.

It is known that dissolved oxygen, chloride and fluoride have deleterious corrosion effects. A sensitivity of oxygen determination of 1 to 50 ppb can now be achieved using a diaphragm type electrode.

In PWRs, oxygen pollution can generally not be detected in the primary coolant under steady state operation because of fast interactions with the circuit surfaces and eventually recombination with dissolved hydrogen under irradiation. However, oxygen levels should be carefully controled in the feedwater to avoid crud formation.

For chloride determination the mercury-thiocyanate method was mainly used and the chloride sensitivities were 5 to 50 ppb. For fluoride determination ion-selective electrodes were used (Code No. of units JAPW 32 to 40) with a sensitivity of 50 ppb.

From the analysis of the responses the following conclusions can be drawn:

- a great variety of analytical techniques have been used at the different NPPS;

- to achieve representative samples, the sampling systems in some plants are designed with continuous and isokinetic flows; sample lines being stainless steel, Inconel or titanium;

- in many plants, the material and radioactivity balance of impurities is evaluated by using membrane and ion-exchange filters;

- the filtration method is also used for the evaluation of soluble/insoluble impurity balance;

- in certain plants, parameters like pH, specific conductivity, dissolved oxygen, chloride and sodium concentration are continuously monitored by automated techniques.

3. BEHAVIOUR OF FUEL CLADDING MATERIALS

From considerations of neutron economy the suitability of materials for water-cooled thermal power reactors is restricted to metals like aluminium, beryllium, magnesium and zirconium or their alloys. While pure aluminium (25) has been used for cladding and structural components in research reactors where operational temperatures are low (100°C or less), severe blistering and accelerated corrosion has precluded its use for power reactor applications at temperatures above 150°C. Beryllium, magnesium and their alloys, although possessing a low neutron absorption cross-section, were not considered for cladding because of their failure to meet the mechanical property and corrosion requirements at water cooled reactor operating temperatures (200-300°C). The potential of zirconium alloys for use as cladding was thus recognized, and this was as early as 1946-47, when it was realized that hafnium-free zirconium absorbs only a few neutrons and has all the qualities required for cladding. The first use of pure zirconium for containing the fuel was for the MARK I PWR. Research on zirconium-based alloys has subsequently led to the general use of these alloys for cladding in water-cooled reactors.

The alloy development work was aimed primarily at: (1) overcoming the deleterious effects of impurities, (2) achieving the desired mechanical strength and (3) strengthening the oxide against cracking. The choice and the proportions of the alloying elements were dictated by the following: (1) the alloying elements should not unduly increase the absorption of thermal neutrons; (2) they should stabilize the corrosion resistance and reduce the tendency to pick-up hydrogen; (3) they should have an out-of-pile post-transition corrosion rate of 1mg/dm^2/day or less and the oxide should be adherent; (4) they should improve the mechanical properties; and (5) they should not make the metal more difficult to process.

Table 3.1 summarizes the alloys currently acceptable under reactor conditions and the experimental ones being investigated.

3.1. WATERSIDE CORROSION OF FUEL CLADDING

Experience with water reactor fuels has been reviewed extensively elsewhere. The main operational requirements for LWR fuel are summarized in

Table 3.1

ZIRCONIUM ALLOYS FOR WATER-COOLED REACTOR SERVICE
(ALLOYING ADDITIONS, WEIGHT PERCENT)

A. Commercial Alloys:

Zircaloy-2; Zircaloy-4; Nickel-free Zircaloy-2;

Zr-1Nb; Zr-2.5Nb; Zr-3Nb-1Sn.

B. Experimental Alloys;

Ozhennite-0.5 (Sn 0.2, Fe 0.1, Nb 0.1).

Scanuk-4 (Nb-0.91, Fe-0.026, Cr - 0.01, O-0.1, UTS (25°C);

[47, kg/mm^2].

Scanuk-4 (Nb-0.52, Fe-0.036, Sn-0.06, Cr-0.49, O-0.134,

[UTS 47 kg/mm^2].

Zr-1Cr-0.1Fe (Valloy)

Zr-1Cu-0.1 to 0.3Fe

Zr-1.0Sn-1-0Nb-0.5Fe

Zr-1Nb-1Cu

Zr-o.5Nb-1Cr

Table 3.2. With regard to the status of zirconium alloy corrosion, it can be stated that most of the problem areas relating to hydriding, pellet clad interaction, wear and fretting have been identified, and wherever needed, the corrective measures have been taken either during fabrication or during operation. Experience with UO_2 fuel performance has shown very low (<0.2%) failure incidence, which has demonstrated that reactor operation is not much affected by fuel failure. Good results are also reported from high-rated PHWR plants with a <0.03% bundle failure in CANDU reactors and with a $\leq$0.01% rod failure in PHWRs delivered by KWU.

It becomes apparent then that under maximum burnup conditions for current fuel generations, waterside corrosion has not been a substantial operational problem. However, delays in fuel reprocessing have motivated several programmes to demonstrate whether LWR fuel burnups can be extended, for example, to 35 000-40 000 MWD/te for BWR fuel and to 50 000-55 000 MWD/te for PWR fuel. In this context, it has been found necessary to minimize corrosion

Table 3.2

OPERATIONAL REQUIREMENTS FOR LWR FUEL (TYPICAL VALUES)

Parameter	PWR	BWR
Average linear heat generation rate (W/cm)	155-255	155-230
Residence time (years)	3	4
Hot channel factor		
Steady state	1.5-2.1	1.8-2.2
Transient	2.3-2.5	2.3-2.5
Neutron flux:		
thermal($cm^{-2}s^{-1}$)	4-6 x 10^{13}	3-5 x 10^{13}
fast (cm^{-2} s^{-1})	6-9 x 10^{13}	4-6 x 10^{13}
Burnup (assembly average) (GW.d/t(U)	28-34	22-28
Coolant pressure (bar)	145-158	72
Coolant temperature (^{o}C)	303-316	287

for the high burnup fuel. The dissolved oxygen concentration of the water has been shown to be of major importance with respect to fuel cladding corrosion during irradiation. At dissolved oxygen concentration above 15 ppb, accelerated corrosion has been observed and is often characterized as nodular corrosion. When hydrogen is added to the coolant to maintain reducing conditions in the system, corrosion is uniform and irradiation-induced accelerated corrosion is small.

Reported results with respect to influence of sub-cooled nucleate boiling are inconclusive . Although work reported from experimental CANDU-BLW irradiations suggested that corrosion may be accelerated under sub-cooled boiling conditions, examinations of higher rated German PWR cladding did not indicate that it is of major influence.

Since the PWR coolant temperatures generally exceed those of BWR coolant (by 30-50^{o}C) the PWR thermal corrosion rates are higher. However, hydrogen is maintained in the PWR coolant to suppress oxygen, and hence the radiation-enhanced corrosion of cladding is minimized. The corrosion pattern in PWRs in general follows the out-of-pile rates and is dependent on the temperature. At the temperatures above 425^{o}C, the oxide growth is quite rapid and spalling of the oxide is initiated in a relatively short time; this becomes more prevalent with further increase in temperature.

Under normal operating conditions, maximum corrosion (oxide growth) occurs over the upper third level of the fuel rods. The cladding corrosion data for PWR fuel rods at this axial position summarized by Garzarolli is presented in Fig. 3.1. The measured values were higher compared to those theoretically predicted from the out-of-pile rate constants. This deviation to higher values has been attributed to irradiation enhancement of corrosion.

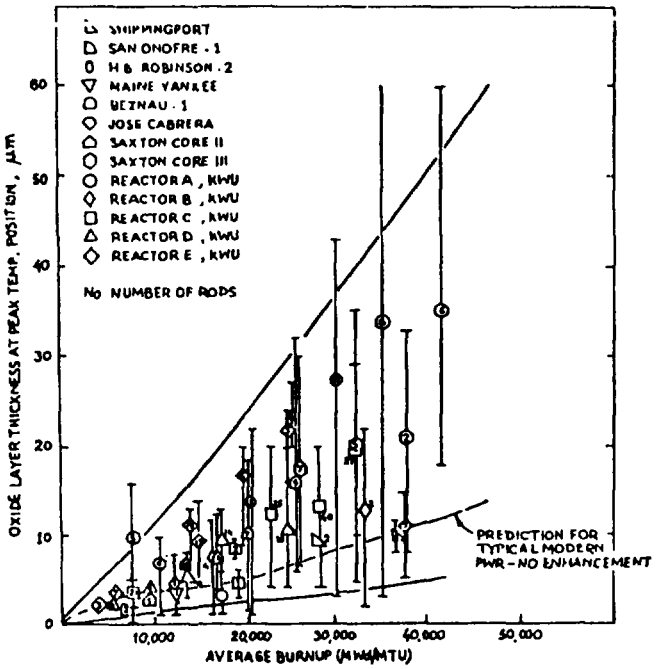

Fig. 3.1 Maximum oxide layer thickness of PWR fuel rods versus burnup

As seen on fig. 3.1 corrosion rates from reactors are usually higher than those expected from autoclave tests, and models in which the thermal barrier of the oxide to the heat transfer is calculated.

To account for these deviations, some models include an "enhancement" or fitting factor, F, introduced to account for reactor effects on the corrosion rate. Typical values of F range from 1.7 to 2.5 or according to a more recent assessment done by Garzarolli et al., 0.8 to 2.8 (data from 13 reactors, with burnups up to 44 GW/d/t). It should be noted that the fitting factor and its large scatter from reactor to reactor and from cycle to cycle could be attributed to specific physico-chemical or thermo hydraulical conditions existing in reactors, and not accurately described in the models (variations in zirconium oxide thermal conductivity, existence of additional thermal barriers due to crud, variable power histories, occurence of nucleate boiling heat transfer, and eventual irradiation effects.)

Circumferential variations in the oxide thickness, up to a factor of 2, have also been currently observed, which could probably be attributed to local variations in the thermal-hydraulic conditions at different locations of the metal-to-oxide interface.

Thus, the contribution of irradiation to corrosion remains uncertain. It was concluded that there is not a sufficient basis to extrapolate current cladding corrosion data to burnups of 50 000 MWD/te. The major uncertainty in the calculated models is the variation in oxide thermal conductivity over fuel rod life. The uncertainty could only be resolved by actual corrosion measurements on fuel rods with burnups exceeding 50 000 MWD/te.

It is worth noting that, in contrast to flux-enhanced corrosion of zircaloy, corrosion of Zr-2.5Nb coupons, has been consistently mildly suppressed in PWR-like environments, compared to unirradiated controls. The explanation appears to involve radiation-enhanced ageing of the 2.5Nb alloy, which improves the corrosion resistance by precipitating some niobium from the solid solution.

Hillner has examined Zircaloy-clad fuel irradiated in the Shippingport reactor (PWR) for 17 years (12.3 y at reactor operating conditions). Maximum fuel burnups were 41 000 MWD/te, reaching a maximum neutron fluence of 7.8×10^{21} n/cm^2, > 0.8 MeV. Corrosion films were light grey and tightly adherent. Pre-transition in-reactor corrosion rates appeared to be similar to corresponding out-of-reactor rates. However, post-transition in-reactor rates were consistently accelerated compared to the corresponding out-of-reactor rates. (The mean post-transition in-reactor corrosion rate was 0.093 mg/dm^2 d; the corresponding out-of-reactor rate was 0.024 mg/dm^{2}d. The range of the clad temperature was estimated to be 260-280^{o}C).

Two major types of flux-related corrosion have developed in the oxygenated BWR coolants: Figure 3.2 shows the uniform and local oxide growth on Zircaloy-2 cladding in BWRs. There is continuing evidence from BWR fuel cladding investigations that uniform Zircaloy corrosion is accelerated by the BWR flux. This observation correlates the earlier loop tests which demonstrated that oxygen and radiation interact to cause accelerated uniform corrosion of zirconium alloys. While nodular corrosion is suspected to have been a factor in fuel failures at one or two reactors, it has not appeared to be a substantial cause of cladding failures for the current generation of BWR

fuel. Some cases of oxide coalescence on fuel rods have been observed, leading to areas of contiguous oxide. Oxide spallation has occurred due to advanced nodular corrosion of BWR fuel channels.

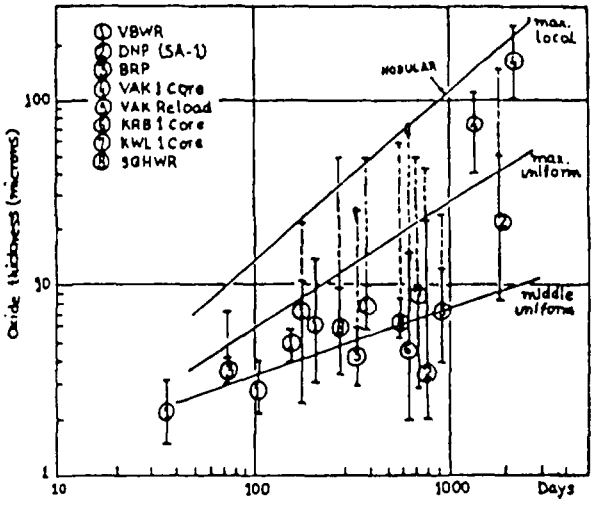

Fig. 3.2 Uniform and local oxide growth of Zircaloy-2 cladding in BWRs. Most data collected by AEG

Since heavy nodular corrosion is accompanied by considerable wall thinning, efforts are required to control this type of corrosion, particularly at higher burnups. Considerable effort has developed to mitigate the nodular corrosion of Zircaloys. It was demonstrated that anneals in the beta or alpha plus beta regions followed by rapid cooling resulted in complete elimination of nodules on subsequent autoclaving at 475-500°C in steam. Subsequently, Urguhart and Vermilyea investigated the relationship between nodule development in a selection of out-of-reactor tests and nodule development under irradiation in a BWR. They concluded that the 500°C steam test provided a reasonable simulation of BWR nodular corrosion phenomena. More recently, Swedish workers also reported that the 475-500°C autoclave treatment forecasts in-reactor resistance to nodular attack. They found that beta treatments prior to final rolling followed by an alpha anneal were almost as effective as the final beta anneal to suppress nodular corrosion of Zircaloy.

A third type of increased uniform oxide layer has been observed at (a) the contact area between the flow channel and the upper core grid, (b) at oxygen-contaminated heat-affected zones and (c) at flow channels made from poorly heat-treated samples. This oxide has shown spalling above the thickness of about 70 μm.

The corrosion rate of Zircaloy under oxygenated conditions at about 280°C as a function of fast flux is summarized in Fig. 3.3. The increase in corrosion with flux can clearly be seen.

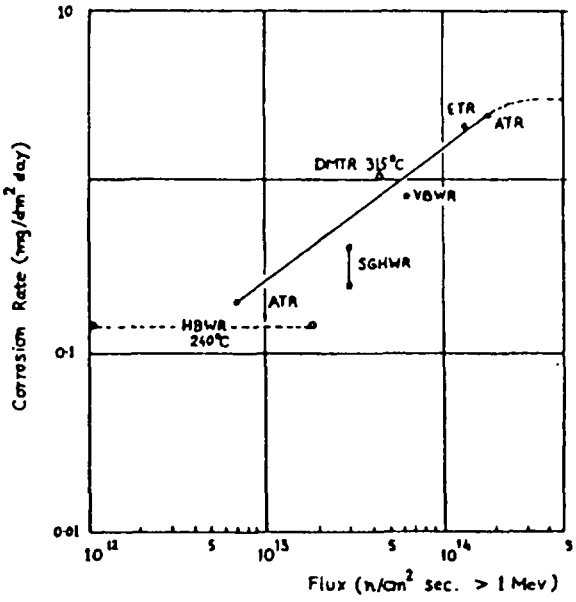

Fig. 3.3 The corrosion rate of Zircaloy under oxygenated conditions as a function of fast flux

Fretting corrosion, a type of accelerated attack caused by the relative movement of two surfaces in contact, occurs mainly at the spacer contacts. This is concerned more with design aspects rather than with corrosion, e.g. by careful spacer design, particularly with respect to construction and selection of materials, this type of attack can be prevented.

Under normal operating conditions of LWRs, the external corrosion of Zircaloys is not considered to be life-limiting, which is evident from the fact that a large number of fuel rods have been brought to full design burnup without corrosion failures. In the context of minimizing clad corrosion, in addition to water chemistry aspects, the following three options were also suggested: (i) to improve upon the current fabrication procedures for Zircaloy cladding; (ii) to modify the chemical composition of Zircaloy with respect to impurity levels; (iii) to improve surface treatment; (iv) to select an alternative zirconium-based alloy. The alloy development did not get large impetus, in the 1970s, because of fairly adequate in-reactor performance of Zircaloys. Improved clad performance was achieved in Japan on modified fabrication sequences and better control of chemical composition both with respect to alloying elements and impurities. As a result the number of failed fuel rods in Japanese LWRs was far below that assumed in the reactor design.

The advent of programmes to investigate extending fuel burnups prompted a study of alloys which might have better long-term in-reactor corrosion resistance than the Zircaloys, particularly regarding nodular corrosion. Alloys Zr-2.5Nb and Zr-1Nb-1Sn-0.5Fe resisted nodular corrosion under conditions which produce nodules on Zircaloy-2. Zr-2.5Nb was also reported to resist nodular attack in the SGHWR. To date, the corrosion performance of Zircaloy-clad fuel with higher burnups appears to be acceptable, but few detailed examinations are yet available on fuel with the highest burnups.

Early alloy development in the Soviet Union centered on alloys containing niobium. The Zr-1Nb alloy has been the principal cladding alloy in Soviet reactors, both BWRs and PWRs. its performance appears to be satisfactory.

The Zr-2.5Nb alloy has shown better corrosion resistance, at least in some environments, but the neutron economy is not as good as with Zr-1Nb. In the stress-relieved condition, the alloy can be considered for fuel cladding for prolonged high-temperature operation under normal PWR conditions. Welding may disturb the optimum structure attained by the heat treatment, but as mentioned earlier, these problems can be overcome by adopting resistance welding techniques. Valloy, scanuk and ozhenniter-alloys have merits at and above 400^{o}C, but their advantages over Zircaloys or Zr-Nb alloys have not clearly been established at the current operating temperatures.

Two factors which have been shown to be important in determining the uniform oxidation rate in LWRs are fast neutron flux and water chemistry. It is also important that one encounters post-transition regimes of oxidation during the residence time of the fuel elements. Expressions have been derived by combining the contributions due to thermal parameters, flux parameters and pre-film weight gain. At high fluxes in oxygenated coolants, linear, flux-dependent kinetics were rapidly established for zirconium and most of the alloys.

BWR environments contain 100-300 ppb of dissolved oxygen in the reactor water. Studies of oxide film grown in irradiated oxygenated water suggest an increase in porosity, and also have given evidence of enhanced porosity in the oxide which would reflect in the enhanced oxide growth in these environments. Another factor which is of importance is the creep of zirconia in the presence of oxygen and irradiation which would affect the stoechiometry of the surface layers giving rise to an increased number of pores. Thus, there is

considerable evidence that radiation nucleates local oxide breakdown and porosity, which also includes nodule nucleation and growth. Segregation of intermetallics enhances the local oxide growth, giving rise to initiation of nodular growth. Alloy composition and heat treatment modify the corrosion response possibly because of the different sites created by these factors. At elevated temperatures (400-450°C), the slow disappearance of the effect of irradiation could be as a result of slow thermal healing of the damage in the oxide.

In conclusion:

1. it becomes evident that the oxide build-up due to uniform corrosion may not be a serious problem under current operating conditions.

2. If it is found necessary to minimize corrosion for high-burnup fuel, in addition to careful control of water chemistry, the following three options have been suggested: (i) to improve the current fabrication procedures for Zircaloy cladding, (ii) to modify the chemical composition of Zircaloy with respect to impurity levels, and (iii) to select an alternative zirconium-based alloy.

3.2 Hydrogen absorption

It is known that the hydrogen formed during corrosion can either escape to the environment or can get absorbed by the metal or the alloy, forming hydride precipitates. The pick-up depends upon the nature of the oxide scale present on the metal or alloy. During the pre-transition period, the hydrogen pick-up by the metal is expected to be very low due to the protective nature of the oxide. During the post-transition, the hydrogen uptake depends upon the temperature, the environment and the alloying additions. On Zircaloy-2 for example, about 40% of corrosion hydrogen can be absorbed in PWR environments, while in oxygenated coolants of BWR this can be only as much as 5-10%. The beneficial effects of Fe, Cr and Nb as alloying additions to Zr against hydrogen pick-up have been attributed to the cathodic nature of the respective intermetallic compound particles existing in the structure. The intermetallics depolarize hydrogen and decrease the possibility of its passage into the film. The functions of Zr-Ni intermetallics are not clearly understood, but these enhance the ability of H_2 to enter the film, eventually to end up in the metal or alloy substrate.

The pick-up rates on the cladding material in the oxygenated environments encountered in BWRs, are well within the design limits. In PWRs, the hydrogen absorption rates have been relatively higher, but they still lie below the design limits. For pressure tubes and core internals, Zircaloy-4 or the Zr-2.5Nb alloy are superior materials from the hydrogen pick-up point of view. The latter alloy, after proper heat treatment, possesses superior mechanical properties compared to Zircaloys.

The more disturbing factors on cladding failures have been attributed to stress corrosion cracking by fission products (mainly iodine) and subsequent corrosion and hydriding of the defected cladding. Design and operational parameters are defined to overcome this serious phenomenon. Internal hydriding of the cladding, which is attributed to residual moisture present in the fuel, is another occurrence observed during the initial stages of reactor operation. Adopting proper moisture control in the fuel has alleviated this type of hydriding.

The resistance of the cladding to hydrogen embrittlement is not only related to the composition of the alloy, but also to the last annealing steps and the extent of cold work left in the material, which creates preferential orientations of the hydride platelets.

Several arguments have been put forward to explain the various aspects of zirconium alloys' corrosion, particularly on the transition and the behaviour under actual service conditions. It still appears that more work is to be done in fields such as the effect of microstructure, second phase and heat treatment, environmental chemistry variation, fast-neutron flux, nodular corrosion and surface effects. Quantifying the pore formation in the oxide layers in the presence of dissolved oxygen and fast flux as a function of temperature would be a contribution needed to understand more on corrosion and hydrogen pick-up under BWR environments. Though, at this stage, a lot of information is available on the zirconium alloy performance, it is yet felt that the post-irradiation evaluation data can be compiled and compared for a verification of the design codes.

3.3 Accident conditions

The behaviour of the fuel cladding during accidental transients is a key phenomenon which determines whether an actual or a design basis accident will

or will not lead to activity release to the coolant or to the environment; it determines also the extent of core damage which can possibly penalize further power plant operation.

In off-normal and accidental situations, a strong chemical interaction may arise between Zircaloy and the coolant. This results essentially from the chemical affinity of Zircaloy for oxygen, together with the thermodynamic conditions of the interaction.

Fuel rod behaviour during any accident is significantly affected by some rod design parameters and by the rod status before the accident. Most of the parameters, including CCI, are interlinked; they are therefore briefly summarized hereafter.

A necessary condition for significant interaction between cladding and the coolant is that film boiling takes place. This condition may be satisfied with most types of accidents, even with RIAs* because of the thermal time constant of the rod which is usually about 10 seconds: in case of sufficient energy deposition, boiling may take place during 10 to 20 seconds.

The temperature transient to which cladding is subject during a LOCA is a variable of reactor design and the particular form of accident under consideration. Studies on Zircaloy cladding ballooning in a LOCA situation and results of burst tests with indirectly heated fuel rod simulators are beyond the scope of this review.

Tests carried out to investigate the ballooning behaviour of Zircaloy cladding (LWR) have shown that the deformation mechanism of the cladding tubes is governed mainly by the distribution of temperature in the cladding. In the case of non-uniform temperature distributions, maximum cladding deformation is concentrated on relatively small hot zones on the cladding which prevents large circumferential and axially extended strains. The two-phase cooling during the reflooding phase enhances axial and azimuthal temperature differences on the cladding tubes and contributes in this way to a limitation of the circumferential strains and the resulting coolant channel blockage in a rod bundle.

---

* Reactivity Initiated Accidents.

In most design basis accidents, the initiation phase is followed by a transition from normal cooling to film boiling, resulting in a rapid decrease of the film heat transfer coefficient, which drops from about $2W/cm^2\ ^oC$ down to values ten or a hundred times smaller. Experiments show that, in a very short time, cladding temperatures rise until the clad either melts (severe accident simultations) or stabilizes at a given level, usually 700 to 1000^oC in PCM* or LOCA situations. In these latter cases, which are representative of power plant accident sequences, the temperature results from an equilibrium between the heat produced and the heat transferred to the coolant, which may be superheated steam with sub-cooled droplets.

Due to the low heat transfer capability, clad temperatures in that period are extremely sensitive to heat production and this explains why exothermic clad oxidation may play the dominant role in the temperature evolution. The rise in the clad temperature and also in the fuel surface temperatures quickly induces an increase of the inner gas pressure, which is important for the balance of the forces acting on the clad.

If the resultant inner pressure is less than the outer pressure, the cladding collapses onto the fuel. Its high creep rate and ductility may lead to extrusion of the cladding into pellet cracks. However, as a result of the rod pre-pressurization, the clad usually moves away from the fuel, and if conditions are fulfilled, ballooning may start. At that moment, three parameters are important:

(1) The azimuthal temperature gradient around the rod;

(2) The extent of clad oxidation;

(3) The extent of alpha-beta transformation.

These three parameters determine by which mechanism the rod might fail. The absolute value of the pressure difference across the clad is of course also important: in that respect, one has to consider fission gas release during film boiling as a possible additional contributor. Different failure modes are, with increasing clad temperature:

---

* Power Coolant Mismatch

- Stress-corrosion cracking due to PCI;

- Stress-corrosion cracking due to gas pressure;

- Ductility exhaustion of oxidized material;

- Clad melt-through.

Other possibilities for clad failures may arise from the contact between neighbouring rods. One important point is that at high temperature, brittle failure is difficult due to the intrinsic material behaviour, and also due to the follwoing fact: as the heat transfer capability from the clad is very low, the thermal time constant of the rod is significantly higher than the 10 seconds previously mentioned; the temperature variations are therefore comparatively slow.

In the case of ballooning, failure depends on many parameters which have been previously examined, i.e. oxidation rate, oxygen diffusion rate, mechanical properties of the oxidized layer, phase changes; the azimuthal temperature gradient determines whether the overall rod failure strain will be high or low, and this is the key parameter controlling sub-channel cross-section reduction and potential blockage inside the bundle.

Once failure has taken place, eliminating the pressure difference across the cladding, steam is brougt into contact with the fuel and with the still unoxidized (or only weakly oxidized) cladding inner surface. The processes that may take place are, for example, the following:

- Fuel oxidation;

- Gross fuel swelling;

- Fission product release;

- Failure propagation.

Fuel oxidation results in an extensive modification of the internal fuel rod chemistry and an enhancement of all the diffusion processes.

Gross fuel swelling is mainly observed in RIA tested fuel at high burnup. The high temperatures experienced in such a situation lead to an increase of fission product inventory on grain boundaries; fission gases or volatile fission products precipitate into intergranular bubbles which can induce significant swelling of the fuel; the latter is most important when fuel, pre-irradiated at low temperatures, is brought up to the melting point.

High temperatures and high diffusion properties of the fuel lead to an enhancement of fission product release: grain growth is accompanied by grain boundary sweeping, and simultaneously, fission products diffuse more easily out of the grain. This results in a fission product release from the fuel which is large with respect to the release under normal operating conditions.

Clad failure propagation may affect the release, if it takes place along one single rod, or if the propagation takes place between neighbouring rods. Such a propagation has not yet been clearly demonstrated, and it remains an open question.

Accidents terminate by the return to normal cooling conditions, with decay heat as the only power production. The key phenomenon at this stage is the quenching of the fuel rod.

The temperature decrease at the end of the accident results in the beta-alpha transformation of oxidized Zircaloy if it has been into the beta phase. Depending on the velocity of the quench front, the quenching may result in two main phenomena:

- Fragmentation of the oxide, i.e. "chunk" break-up, with liberation of the gases present in the affected grain boundaries; in extreme cases, this may completely destroy the pellet stack geometry;
- Fragmentation of the oxygen-embrittled cladding under the thermal shock.

These phenomena are extremely important because they lead to fuel dispersal into the core.

We shall not discuss here all licensing aspects of clad-coolant interaction during accidents. The main questions connected directly to fuel element licensing are clad temperatures, clad oxidation, deposited energy failure threshold, together with the basic demand for core coolability.

According to the US-NRC licensing rules, the clad temperature limit for LOCA situations is 2200°F (1204°C), and the fraction of oxidized clad is limited to 17%. The US licensing procedure has to demonstrate that these regulatory limits are never exceeded. The discussion of these figures is beyond the scope of this paper. However, one can remark that these limits are to be supported by an adequate experimental data base.

Experimental evidence supporting the RIA-related deposited energy failure threshold has been recently gained through tests in PBF* and NSRR**. The results of the previous SPERT*** tests were generally confirmed, with however a trend to reduce the failure threshold from 280 cal/g UO_2 down to 265 cal/g UO_2.

Coolability of a partially blocked bundle appears to be better than is conservatively assumed in licensing calculations, i.e. clad temperatures do not appear to be significantly increased by local ballooning.

It is clear that coolant-cladding interation plays a dominant role in accident situations; and determines to a large extent the failure mode of the rods and the subsequent activity release and ultimately the loss of geometry with dispersion of fuel within the primary circuit.

The clad-coolant interaction arises mainly from Zircaloy oxidation through reaction with superheated steam. This oxidation reduces the Zircaloy creep rate and induces embrittlement. Furthermore, the exothermic character of the reaction, together with the reduced heat transfer capability of a dried-out rod bundle, shows that, in accident situations, CCI must be considered in the global frame of core thermal-chemical-hydraulic behaviour.

---

* Power Burst Facility

** Nuclear Safety Research Reactor (Japan)

*** Idaho site facility

4. CORROSION PRODUCT BEHAVIOUR AND CRUD BUILD-UP IN REACTOR CIRCUITS

4.1 Migration and Deposition of Corrosion Products and Impurities

Reactor experience with the migration and deposition of corrosion products and impurities is considered in detail in chapter 3 of IAEA TECDOC 356(1985). The following is a brief summary of the key-points:

4.1.1 Transport Processes and Mechanisms

In the foregoing sections a background has been given to the source of corrosion products in water reactor coolants, the chemical environment into which they are released and the major forms of metal species present. It is useful to put the transport process into quantitative perspective. After about a year's steady operation the coolant circuit inventory of released corrosion products is likely to be several tens of kilogrammes. It is also clear from considerable operating experience that under steady-state conditions only a few tens of ppbs of corrosion products are carried by WR coolants. This means that less than 20g or < 0.1% of corrosion product inventory is being transported at any instant in time. In non-radioactive environment, e.g. a conventional boiler, this might be acceptable and not give rise to plant problems but in WRs the situation is entirely different. Because of the large fuel surface area and the internal reactor neutron flux, even slight deposition there produces radioactivation products which become a significant problem to station personnel when they are in turn transported to out-of-core surfaces. In general fuel surface crud deposition is heavier in BWRs than in PWRs by up to an order of magnitude and in PWRs it is more irregular. Even if the lower PWR crudding (e.g. 0.05mg cm^{-2}) levels are taken as applying to entire cores this can account for over 3 kg in-flux after a year's operation in a 1000 MW(e) plant. Swedish BWRs have perhaps the lowest level of fuel surface fouling (< 1mg cm^{-2}) but in other BWRs fuel deposits of up to 5mg cm^{-2} are typical, indicating in-core deposition involving several tens of kilogrammes. Fortunately the open-textured iron-based deposit in BWRs rarely leads to heat transfer problems and in fact it can assist the free boiling of coolant. In PWRs the incidence of fuel cladding fouling is also rare but deposits of up to 9mg cm^{-2} have been reported. In the worst cases this can lead to increases in the shear stress and pressure drop across the core resulting in a power reduction due to the

Doppler effect. It is possible for over a thousand curies (>3.7 x 10^4 GBq) of radioactivation products to be present in fuel deposits when current WRs shut down for refuelling and overhauls.

The above data illustrate the basic problem brought about by a complex series of transport processes occurring in the coolant circuit. As well as being detached from corroding surfaces, corrosion products are also released from deposits on in-core and out-of-core surfaces. Both particulate and soluble species are involved. In PWRs differential solubility effects are important because of the range of temperature and chemistry changes involved and in BWRs evaporative effects and metal oxide transformations can lead to migration of corrosion products. The overall scheme is best appreciated by diagramatic representation as shown in Fig. 4.1 which is widely used as the basis for transport process modelling in water-cooled reactors. The figure does not attempt to differentiate between soluble, insoluble and colloidal material transport. As well as chemical and thermodynamic effects, hydrodynamic processes are also involved because of the high fluid flow rates throughout the coolant circuits. In the first cycle of reactor operation, high corrosion product release are generally observed, in both PWRs and BWRs. After several months of steady operation, the in-core situation can tend towards a steady state. During the initial period of operation protective films are still in the process of stabilizing to the physicochemical

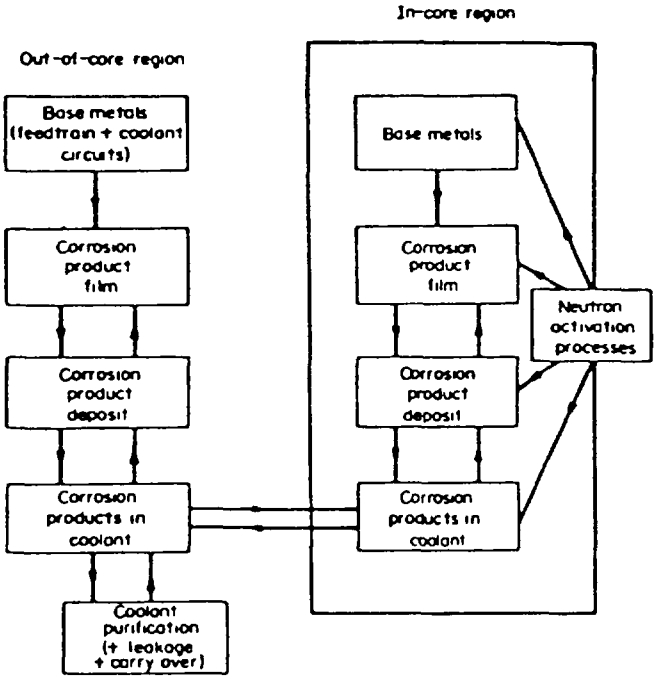

FIGURE 4.1 SCHEMATIC DIAGRAM FOR CORROSION PRODUCT TRANSPORT IN WR's

conditions of the operating regime. The preconditioning of system surfaces is therefore important in relation to initial crud input rates especially in direct cycle systems where large areas of ferrous material outside the coolant circuit are involved.

In order to more fully understand or mathematically model the overall process of corrosion product (and activity) migration in coolant circuits it is necessary to define the component stages and superimpose upon these the physical parameters for a specific reactor design. The stages or phenomena of the transport process have been defined for BWRs and PWRs following extensive laboratory investigations and field studies on operating reactors during the 1970s. Their prime aim is the forward prediction of activity formation and deposition, and isolation of key variables for future design purposes. It is clear that ^{60}Co is the major cause of dose to operators of all WRs and that in PWRs ^{58}Co is important in the first few years of operation. While some of the models developed are semi-empirical, being based partly on hypothesis and observation, they are all ultimately concerned with the fate of activity produced by activation of corrosion products more specifically with respect to the cobalt isotopes. It should be stressed that while cobalt is only a minor impurity (<0.1 w/o) of most coolant circuit materials and is thus a small contributor to corrosion product inventory, it nevertheless plays a disproportionate role in activity transport. ^{60}Co is usually the nuclide resposible for most dose in WRs in the longer term of reactor operation.

Detailed description of the phenomena involved in the formation, transport and deposition of radioactive corrosion products are included in IAEA-TECDOC-356 and Annexes 2 and 3.

4.1.2 Corrosion Products in Operating Reactors

Recent data from operating BWRs have illustrated the significant improvements that have been achieved in the last decade. In this case the problem can readily be monitored by measuring final feedwater corrosion product levels. In older reactors (e.g. WSGHWR and early operation of Tsuruga) levels in feedwater reached and exceeded 10 ppb on occasions. Before remedial actions were taken at Tsuruga iron input into the coolant circuit had reached several hundred kilogrammes per cycle. The improvements adopted included improved condensate purification as well as oxygen injection to the feedwater system at 40 ppb during normal operation and dry storage under

shutdown conditions. Very large reductions in iron transport, especially of particulate material in the feedsystem, resulted in subsequent improvements in activated corrosion product transport and some reduction and stabilization of out-of-core radiation fields. It should be noted, however, that there was little change in the "soluble"* ^{60}Co level of about 0.05 uCi/l^{-1} in the coolant. Similar improvements were brought about at the Shimane BWR which now operates with less than 1 ppb of total iron (75% insoluble) in feedwater dosed with 15 to 25 ppb of oxygen.

Good corrosion product transport performance is reported from the Swiss Mühleberg BWR, where figures for feedwater and coolant are similar to those reported for Swedish BWRs. It might therefore be predicted that average fuel element deposition values would be similarly low. The reported "normal" ranges for the minor constituents in Mühleberg fuel crud are, however, very similar to those found on WSGHWR fuel. It is important in such comparisons that the feedwater, coolant and fuel element deposition data represent the same operational periods. This is uncertain for the Mühleberg data.

The complexity of the transport picture is emphasized by the different time dependences of ^{60}Co deposition on out-of-core surfaces in the RAPS-1 (CANDU-PHW) and in the WSGHWR (BWR). In RAPS-1 the relative increase of ^{60}Co on two identical boiler banks differed by a factor of 6 over 360 EFPDs. In WSGHWR, feeder pipe contamination levels in the two identical coolant circuits differed by a factor of 2 to 3 after 1200 EFPDs. In both cases the circuits were exposed to the same chemistries. This illustration suggests that pre-operational plant history or some early operational feature could be responsible for the different behaviour. We cannot therefore assume that design, materials or chemistry are the only governing variables in the retention of activated corrosion species.

In the PWRs and PWPWRs reported upon recently, the total corrosion product concentration in coolants under steady operational conditions is variable but rarely exceeds a few tens of ppbs. For example, in French PWRs iron is the major component, generally at 10 to 30 ppb, with smaller contributions from nickel (< 10 ppb), Cu, Mn and Co (< 2 ppb). Somewhat higher iron levels at Kozodluj (50-80 ppb Fe) may be due to the stainless steel steam generators or

---

* This term is commonly utilized to denote the fraction not retained by filters (see Section 4.2.3).

the chemistry regime. The Japanese data shows that most of the corrosion products are present as dissolved species (i.e. 98% of 21 ppb). Enhanced corrosion product release is apparent at shutdown. It is significant that the estimate of total annual crud production (13-27 kg) in the 275 MW(e) Atucha (PHWR) reactor is similar to that estimated for other water reactors of comparable size. The operational level of corrosion products in bulk PWR and similar reactor coolants therefore corresponds to about 10 to 20g in circulation at any time, a very small fraction of the corrosion product inventory.

4.1.3 Reactor Transient Effects

It is an established fact that coolant transients which occur under abnormal operating conditions give rise to changes in coolant-borne corrosion and activation products. In general, because of solubility considerations, these transients are accompanied by significant increases in particulate species in the coolant. The initiating factor is a variation in thermal, chemical, physicochemical or hydrodynamic properties of the bulk coolant.

Thermal transients accompany power changes, reactor startup, controlled shutdown or trip situations. The thermal gradient is highest at the fuel surface, hence the crud release will favour in-core deposits. Coolant temperature reduction is also accompanied by an increase in the viscosity of water with consequential increase in the forces of erosion and entrainment. Under reactor trip conditions suspended crud levels in WSGHWR, for example, have increased by over two orders of magnitude from tens of ppb to several ppm. In PWRs some redissolution of soluble compounds also occurs during cooling due to the increased acidity of the borated coolant. Reactor evidence also confirms that such transport transients are reversed on reheating or return to power when rapid redeposition occurs. Observations at WSGHWR, suggest that activity levels on out-of-core pipework are not largely affected by such "crud bursts". It is possible, however, for insoluble species released in transients to be retained preferentially in low-velocity zones of coolant circuits or in dead-legs. The time taken to restore normal operating conditions is important in this respect.

Chemical transients can occur due to short-term coolant contamination. In direct cycle systems (BWRs) this can follow failure of feedwater purification systems or the transport of ion-exchange resins to the coolant

circuit. Coolant contamination from IX purifiers in PWR systems has also occurred. Release of activity also follows the addition of boric acid in PWRs producing a similar effect to that of reduced coolant temperature. Oxygenation of PWR coolant, either deliberately by addition of hydrogen peroxide, or by air under cool shutdown conditions causes a more pronounced release and transport of radioactive species. This possible redox effect is associated with the preferential solubilization or precipitation of some species. Again the materials released in this way originate mainly from in-core deposits where short-lived radiolytic species will also assist by bringing about chemical changes in the absence of excess hydrogen.

The separate effects of reducing temperature (240 - 100^{o}C) and the addition of hydrogen peroxide in PWR circuits have been studied. Nuclides such as ^{54}Mn, ^{58}Co, ^{60}Co and ^{59}Fe, transported mainly in soluble cationic forms , were found to be released to a greater extent by cooling than as a result of adding 200 ppm of H_2O_2. The opposite effect was noted in the case of ^{51}Cr, ^{99}Mo and ^{124}Sb, which tend to be present in insoluble or anionic form. The peroxide therefore promotes the formation of soluble species from nuclides capable of anionic combinations, e.g. Cr. The shutdown option of deliberately adding H_2O_2 in order to achieve a partial decontamination of the PWR coolant circuit (or fuel surfaces) is still practised by some stations and rejected by others as having only a short-term effect. More recent investigations at Doel PWR have indicated that H_2O_2 has only limited influence on activity released at shutdown.

4.1.4 Water Reactor Fuel Surface Crudding Levels

The thickness and composition of the deposited crud layer contribute not only to the problem of radioactivation but also to the extent of interference with core heat transfer and pressure drop. Porous magnetite deposits on simulated fuel rods do not cause large increases in cladding temperature. Laboratory tests on open-textured magnetite of less than 100 microns thick at a heat flux of 100 W cm^{-2} showed less than a 10^{o}C alteration of cladding temperature under BWR conditions; a similar deposit but impregnated with the salts normally associated with hard water showed a cladding temperature increase of up to 92^{o}C. The surface friction factor of a crudded rod in these tests exceeded that of a clean rod by a factor of 3.3.

Both of these observations have parallels in early BWR experience when crudding levels on fuel surfaces were high. In the first year of WSGHWR

experience, for example, copper infilling of the Fe_2O_3-based deposit occurred leading in some cases to fuel cladding failures due to steam blanketing and overheating. Subsequent operation of WSGHWR with considerably reduced Cu and Ni levels in feedwater and lower overall crud input rates have led to no further fuel cladding failures, although the fuel crud thickness peaks at about 25 um corresponding to 1.5 to 2.0 mg cm^{-2} of deposit. The porous deposits now formed have been found to assist heat transfer by what has been termed "the wick boiling mechanism".

In second-generation BWRs with reduced iron levels in feedwater (< 10 ppb) and with little or no use of non-ferrous alloys, few fuel defects have occurred due to crudding. Deposition levels still vary considerably depending on design, materials and operating factors, e.g. the type of feedwater purification plant and its location or the addition of oxygen to the feedwater. An indication of the improvement in deposition levels in the more recently commissioned BWRs is illustrated by comparing data from WSGHWR and the Swedish reactors. A summary of fuel crud deposition levels for various BWRs is given below:

BW Reactor	Typical Fuel Crud Deposition Levels, mg cm-2
WSGHWR	1 to 2
Swedish BWRs	0.1 to 0.5
Nine Mile Point	< 1 to 10
German BWRs:	
VAK (Kahl)	0.5 to 1.0
KWL (Lingen)	0.2 to 0.4
KRB (Gundremmingen)	3.3 to 7.6
Garigliano	1 to 4
Tsuruga	0.5 to 3

In general, fuel deposition in PWR and CANDU-PHWR cores is less than in BWRs by up to an order of magnitude and is explained by differences in the sources of crud, its chemical composition, the non-boiling coolant and the coolant chemistry itself.

It is evident from the available data and from recent discussions convened by the IAEA leading to this review that no fuel failures have occured in commercial PWRs which have been attributed to fuel surface crudding. There are currently no reports of fluid dynamics problems related to core crudding.

There is, however, some recent concern in Europe that localized hard crud formation due to elements other than associated with dominant corrosion products (e.g. Si, Al, Ca, Mg) could be a problem.

A summary of fuel crud deposition levels for various PWRs is given below:

PW Reactor	Typical Fuel Crud Deposition Level, mg cm-2	
Beznau	0.5 to 4.7	(1st cycle)
Beznau	< 0.01 to 0.48	(3rd cycle)
Point Beach	< 0.01 to 0.46	(1st cycle)
Saxton	0.5 to 0.8	(1st cycle)
Yankee Rowe	0.7 to 1.5	(1st cycle)
Yankee Rowe	10 to 14	(2nd/3rd cycle)
Obrigheim	max 8	(1st cycle)
Stade	negligible	
Douglas Point	0.1 to 0.5	(1st cycle)
Douglas Point	0.05 to 0.07	(subsequently)
Pickering	negligible	

Crud thicknesses associated with the above deposition levels vary from < 0.5 μm with minimum deposits of < 0.05mg cm^{-2} to 100 um for peak levels of 10mg cm^{-2}.

4.1.5 Radio Nuclides Formed From Corrosion Products

Despite the variations in system chemistries the general nature and composition of the corrosion products are essentially the same. They are transported to the core where following deposition and residence for a finite time in flux they become activated either by thermal, epithermal or fast neutrons. The activation nuclides generally encountered in order of half-life are ^{51}Cr, ^{59}Fe, ^{58}Co, ^{65}Zn, ^{54}Mn and ^{60}Co. Other activation products found regularly in water reactor coolants include ^{95}Zr and ^{95}Nb (which are also fission products), ^{124}Sb, ^{110}Ag and ^{99}Tc, but these are not responsible for a significant proportion of dose around the circuit, except in some plants.

A summary of the principal nuclides formed from water reactor corrosion products under neutron flux is given in Table 4.1.

Table 4.1

PRINCIPAL GAMMA-EMITTING NUCLIDES FORMED FROM CORROSION PRODUCTS IN WATER REACTORS

Radio-nuclide	Parent nuclide	Formation mechanism	Half-life	Gamma emission(s) energy MeV	Main source of parent nuclide	Abundance of parent nuclides in natural Metal
^{51}Cr	^{50}Cr	n, γ	28 d	0.3	Stainless iron; stainless steels; Inconel-600; Incoloy-800	4.3% ^{50}Cr in chromium
^{59}Fe	^{58}Fe	n, γ	45 d	1.1 1.3	All steels; Inconel-600; Incoloy-800	0.33% ^{58}Fe in iron
^{58}Co	^{58}Ni	n, p	71 d	0.8	Stainless steels; Monel; Inconel-600; Incoloy-800; Cupro nickel alloys	68% ^{58}Ni in nickel
^{65}Zn	^{64}Zn	n, γ	244 d	1.1	Brass (direct cycle condensers)	49% ^{64}Zn in zinc
^{54}Mn	^{54}Fe	n, p	313 d	0.8	Most steels	5.8% ^{54}Fe in iron
^{60}Co	^{59}Co	n, γ	5.28 y	1.2 1.3	Cobalt impurity levels in carbon steel, stainless steels, nickel alloys (0.02-0.3%) Hard-facing alloys - cobalt-based (50-70%)	100% ^{59}Co in cobalt

4.1.6 Transport of Coolant Impurities other than Corrosion Products

While much R and D effort has been allocated to the problems associated with corrosion product transport, little published information exists on the role of other elements capable of fuel-surface deposition in water reactors. The elements referred to in this context are normally associated with the main station water supply, water treatment plant materials or as impurities in chemicals used for water conditioning. They include calcium, magnesium, aluminium silicon and possibly carbon and barium which are capable of forming

compounds of low solubility in combination with each other or with the metal oxides considered in previous sections. Silicon is also present in some steels and alloys but generally in small proportion.

There are non-documented, recent reports of fuel integrity problems relating to fouling by hard crud based on mineral elements in European PWRs. Such a problem could be aggravated by newer PWR designs in which localized boiling is intended to occur. This is believed to be the reason behind recent changes to PWR coolant chemistry specifications to include new limits for silica (e.g.< 0.2 ppm), aluminium (< 0.05 ppm), calcium (< 0.05 ppm) and magnesium (< 0.05 ppm).

A full review of operating experience with those impurities is in IAEA TEC-DOC 356.

4.2. Modelling of Corrosion Product Behaviour and Crud Build-up in PWR and BWR Circuits

The behaviour of corrosion products in the primary heat transfer circuits of all water reactors is governed by the same general principles. However, there are distinctions between reactors of the PWR and BWR types which result in different emphasis are reflected in the reviews for PWR ad BWR systems incorporated in this report as Annexes II and III respectively. This chapter will draw together the two reviews, identifying those features which are common and those which are specific to each reactor type.

Firstly a brief description will be given of those characteristics of PWR and BWR systems which underline the differences in corrosion product behaviour. Then individual corrosion product mechanisms and their modelling will be considered under headings which correspond broadly to the stages in the construction of a comprehensive model:

i) Corrosion of alloys;
ii) Nature of circulating material;
iii) Transfer to and from surfaces;
iv) Interactions with surfaces;
v) Performance of purification plant.

Finally, mechanistic models and computer codes intended to provide complete descriptions of corrosion product behaviour will be surveyed.

4.2.1 Characteristics of PWR and BWR Systems

The major differences in corrosion and corrosion product behaviour are attributable, directly or indirectly, to the natures of the primary coolant circuits and their heat transfer processes. In a PWR, heat is transferred from the core to the boiler via a recirculating flow of predominantly single-phase water and steam is generated in a secondary circuit. Sub-cooled boiling may occur locally on the surfaces of highly rated fuel in some advanced reactors. In a BWR, heat is transferred from the fuel to the coolant predominantly by boiling processes; steam is separated and is passed to the turbine while the water is recirculated to the core. Condensed steam from the turbine is returned to the recirculating primary flow via a feedwater system. The direct consequences of these distinctions are thus:

i) The release of corrosion products into the recirculating coolant in BWRs generally has a major, if not dominant, contribution from the relatively low temperature surfaces in the turbine condenser and feedwater plant.

ii) Transfer of corrosion products in a BWR occurs in two-phase as well as single-phase water environments. This distinction is particularly critical in respect of the influence of boiling heat transfer on deposition on fuel surfaces.

The thermal-hydraulic environments also affect corrosion and corrosion product behaviour indirectly since they have a strong influence on the coolant chemistry regimes which may be sustained. The chemistries differ in two key respects:

i) Dissolved hydrogen, typically 10 to 30 or 30 to 60 NTP cm^3/kg (see Section 2.1), is generally added to the coolant of a PWR in order to promote the recombination of oxygen produced by the radiolysis of water and thus to maintain a reducing, essentially oxygen-free environment.

In a BWR, the hydrogen and oxygen produced by radiolysis of water are stripped efficiently during steam separation and are subsequently removed by the condenser off-gas system. The effectiveness of hydrogen addition is therefore limited. Oxygen is usually present in the recirculating coolant at

levels between about 100 and 300 ppb, although somewhat lower values are achieved in those BWR in which hydrogen is injected to the feedstream to prevent stress corrosion cracking

ii) Corrosion of the alloys in the oxygen-free environment of a PWR is generally minimized by the adoption of an alkaline regime. The alkalising agent can be lithium, potassium or ammonium hydroxides singly or in combination. Boric acid may also be added to the coolant as a neutron absorber to control reactivity; its concentration is varied throughout a cycle in order to compensate for fuel burn-up. The concentration of the alkalising agent may also be varied, for example to maintain a constant pH.

A low-conductivity, neutral regime has generally proved satisfactory in BWRs. Chemicals are not added to the primary coolant or feedwater, paticularly to avoid the possible generation of aggressive chemical environments in the boiling regions on fuel surfaces.

4.2.2 Corrosion of Alloys

The corrosion product input to the recirculating coolant in most modern BWRs is dominated by iron which arises primarily from the uniform corrosion of stainless and carbon steels in the feedwater systems. Corrosion of these materials (considered in Annex III, Section 1.2) is strongly dpendent on the concentration of dissolved oxygen and on the flow conditions. The corrosion films which form on carbon and low alloy ferritic steels between 200 and 300 C generally exhibit a two-layered structure whose formation is most often described in terms of the model originally proposed by Potter and Mann. The inner layer is composed of magnetite which is produced at the metal/oxide interface by the reaction of metal with the oxygen bearing species diffusing inwards. Half of the ferrous ions produced by the metal reaction are assumed to diffuse outward to the oxide/water interface where they may either go into solution or deposit to form the outer layer.

The corrosion mechanisms for stainless steels and higher nickel alloys under PWR conditions are not so well understood but there is evidence to suggest that a two-layer description may be appropriate with an outer layer consisting of accumulations of crystals (Annex II, Section 2.1). Unfortunately it is not clear whether corrosion ions are transported through

the inner layer by solid state diffusion or by aqueous phase diffusion through pores. There are consequently major uncertainties in the descriptions not only of corrosion ion release but also of contamination of growing films by soluble radioactivity.

Wear, erosion or erosion-corrosion of hard facing alloys such as Stellites can be significant contributors to cobalt inputs in both PWRs and BWRs. Data on these processes are sparse (Annex II, Section 2.2; Annex III, Section 1.2).

4.2.3 Nature of Circulating Matertial

It is shown in Annex II (Sections 5 and 6) that it is valuable to distinguish between colloidal (< 1um) and inertial (> 1um) particles since not only their transport to and from surfaces but also their interactions with surfaces are governed by distinctly different mechanisms. However, it is conventionally assumed that coolant-borne corrosion products may be characterised as "particulate" or "soluble" depending on their retention or otherwise on 0.45um microporous filters. Thus some of the material which would be conventionally described as "soluble" should be more appropriately described as colloidal particulate. This distinction is crucial for modelling since truly soluble and colloidal material exhibit distinctly different behaviours.

The characterisation of circulating corrosion products from filter samples is also complicated. Firstly, it is necessary to ensure that the sample line obtains and delivers a representative sample. In practice, the sample will be modified during its passage down the line. Secondly, as noted in Annexe III (Section I.3.(1), the mechanism of particle filtration is not simply the effect of sieving. There is also an effect of the electrokinetic interactions between colloidal particles and the filter surface; this influence is strongly dependent on the coolant pH and ionic strength. consequently there are circumstances in which particles with diameters much smaller than the filter medium's nominal pore size may be collected efficiently. For example, haematite particles of 0.15µm diameter in suspension at neutral pH are readily collected on a Millipore filter with normal 8 µm pores.

It is apparent, therefore, that adequate modelling of corrosion product behaviour may require the definition of at least three types of material:

i) Truly soluble;

ii) Colloidal particulate (< 1 μm);

iii) Inertial particulate (> 1 μm).

A complete description will require that the detailed size distributions of the latter two categories should be known. It is also clear that considerable care needs to be exercised when attempting to distinguish between these forms using filtration techniques.

The physico-chemical forms and elemental compositions of circulating corrosion products vary from one system to another reflecting differences in coolant chemistry and materials of construction. Thus, the majority of coolant-borne crud in the reducing environment of a PWR is present as magnetite or combined oxides of the ferrite type whereas haematite is the predominant form in the oxidising environment of a BWR. Evidence on the size distribution of this material is generally sparse but there are indications that significant fractions of mass and radioactivity in both systems may be associated with particles smaller than 1 μm.

Soluble species may arise directly from the corrosion process or from the dissolution of solid oxides. They are believed to play a particularly important role in the transport of the major elements, iron and nickel, in PWR (Annex II, Section 3.1.1). For example, the dependence of solubility on pH generally has a dominant influence on the choice of optimal strategies for coolant chemistry control. Solubilities for model systems, such as magnetite and nickel ferrite, have, therefore, been widely studied both theoretically and experimentally under PWR conditions although there are as yet no data for real corrosion products. Thermodynamic calculations for magnetite solubility are well-founded and generally account for both ferrous and ferric species. The resulting solubilities are expected to depend on coolant pH and temperature and, to a lesser extent, on the partial pressure of hydrogen. Agreement with experimental data is generally good. Thermodynamic calculations for mixed oxides, such as nickel ferrite, are less well-founded due to uncertainties in the most appropriate values for the activities of the respective solid phases. It is, therefore, generally assumed that the solubilities of these oxides may be adequately represented by that of magnetite. The available experimental data suport this assumption in respect of iron species, other elements, such as nickel are accommodated by references either to the oxide stoichiometry or to experimentally observed solubilities.

Cobalt is chemically a minor component although it is of great radiological significance as the precursor of cobalt-60. Its presence in soluble form is likely to be controlled by equilibria with the solid oxides of major species. Adsorption of cobalt ions on oxide particles plays a major role in BWRs (Annex III, Section I.4.(1)), although it is not clear whether the transfer occurs predominantly to the particles in suspension or following their deposition. Sorption processes are considered in the section on interactions with surfaces. Transfer of soluble species from the coolant bulk to the surface of a particle may be described by a mass transfer coefficient determined from an appropriate correlation.

The sources of particulate corrosion products are very uncertain (Annex II, Section 3.2) but in principle they may originate from three types of process:

i) Erosion of deposits or outer layer crystals by hydrodynamic interactions and/or transients in coolant chemistry.
ii) Spalling of oxide films as a result of thermal transients.
iii) Nucleation in the coolant bulk.

The first two processes may be significant but their contributions are difficult to quantify. Classical theories of nucleation are currently adequate to draw preliminary conclusions about the importance of this process in the bulk coolant; the surface energies of corrosion product oxides and hydroxides are not known with sufficient precision to warrant more sophisticated descriptions. Calculations show that it is possible to dismiss homogeneous nucleation in the coolant bulk as a major source due to the relatively high surface energies of oxides and hydroxides. However, heterogeneous nucleation cannot be dismissed without a careful consideration of the possible sources of particulate impurity which could act as nucleation sites.

The importance of particle interactions in the coolant bulk, including dissolution and growth (Annex II, Section 3.3) and agglomerate formation and break-up (Annex II, Section 3.4), remains unclear.

4.2.4 Transfer to and from Surfaces

Transfer between surfaces and the coolant bulk in single-phase water can be considered in predominantly mechanistic terms. Mass transfer coefficients

for soluble species and colloidal particles may be readily derived from empirical correlations with very little extrapolation (Annex II, Sections 4.1 and 5.1.1 respectively). Thermophoresis may exert a significant influence on 0.1 to 1.0 μm diameter colloidal particles to heat transfer surfaces but its description requires validation under appropriate conditions (Annex II, Section 5.1.2). The transport of inertial particles is well understood but theories have only been validated for aerosol systems (Annex II, Section 5.1.3).

Particle deposition on boiling surfaces is a key process in BWRs. In view of its complexity it is generally dealt with empirically (Annex III, Section 1.3.(3). As a consequence, a clear distinction cannot be drawn between transfer in the coolant and the interaction with the surface. First order rate constants are considered adequate to define the deposition and release processes. Little is known about the latter. However, there is experimental evidence showing how the deposition rate constant depends on:

i) The nature of the boiling process, i.e. whether it is sub-cooled or nucleate.
ii) The coolant pH. This influences interfacial interactions via the surface electrical properties of the particle, deposition substrate and vapour bubble.
iii) Particle size.
iv) Hydrodynamics.

Plant data show that deposits on fuel surfaces exhibit inner and outer layers. It is inferred that the latter is transformed into the former but nothing is known about the rate constant.

4.2.5 Interactions with Surfaces

Precipitation and dissolution of the major soluble species iron and nickel are important mechanisms in PWRs (Annex II, Sections 4.2 and 6.4). A surface film may be precipitated or dissolved depending on whether or not the concentration of soluble species in the bulk coolant over the surface exceeds the saturation solubility at the surface. The kinetics may be adequately described as a first order rate process providing boundary layer mass transfer is limiting; higher order rate processes may be more appropriate if the kinetics of surface reactions are limiting.

It has already been noted that uptake of cobalt ions by oxide plays an important role in BWRs (Annex III, Section I.4.(1)). At room temperature it is essentially a surface phenomenon and may therefore be described by an appropriate form of adsorption isotherm e.g. Langmuir or Freundlich. At high temperatures it is possible that adsorption may be followed by absorption, in which the absorbed species penetrates the interface and diffuses into the oxide bulk. Under such circumstances it is also necessary to include a description of this diffusion process which may become limiting at long times. Experimental investigations have concentrated on adsorption equilibrium and its dependence and pH. However, there have been few studies of this mechanism at high temperature and there are very limited data on the kinetics of the adsorption and desorption processes.

A minor element such as cobalt may also be incorporated in both the outer precipitated and inner grown-on oxides (Annex II, Section 4.3). The former process is effectively co-precipitation and will occur at a rate governed by the precipitation rate of the major species and the relative concentration of the cobalt. The latter process requires the cobalt to diffuse through the inner and outer oxide layers to be incorporated in the growing oxide at the metal-oxide interface. It has already been noted that the present knowledge of film growth is inadequate to enable a confident description of this mechanism.

The initial interactions of particles with each other and with surfaces will be governed by gravity, van der Waals, magnetic, electrical double layer and hydrodynamic forces. Well validated theoretical descriptions are available in all cases for simple ideal systems (Annex II, Section 5.2). Their application to real systems is limited in two respects. Firstly, it is necessary to account for the influences of surface asperities and interfacial deformation. Secondly, there are inadequate data for the bulk and surface properties of corrosion product oxides. The Hamaker constant can be estimated with a fair degree of confidence. However, surface electrical properties are very uncertain, particularly with respect to the influences of operating temperature, radiation, and specific ion adsorption. Haematite is not spontaneously magnetised so that in the absence of an externally applied magnetic field there is no significant magnetic interaction with an oxide surface. Magnetite and nickel ferrite are spontaneously magnetised and particles may exist as single domains up to 0.1 to 1.0μm in size. it is, therefore, the domain structure of a particle which introduces the greatest uncertainty rather than the saturation magnetisation.

In the longer term, the adhesion of particles to a substrate may be affected by processes such as sintering and ion bonding.

The surface reactions during deposition and resuspension of colloidal particles may both be described by first order rate processes (Annex II, Sections 5.4 and 6.3) using theories which have been validated for model systems. The interactions are dominated by van der Waals, magnetic and surface electrical forces. Resuspension is influenced strongly by changes in coolant chemistry and temperature via the electrical double layer interaction.

The interactions of inertial particles with surfaces during deposition and resuspension are strongly influenced by hydrodynamic forces (Annex II, Sections 5.3 and 6.1). A sticking probability is generally defined for the deposition process by comparing observed deposits and predicted arrival rates in model experiments. Erosion, or resuspension, is also described as a first order rate process with values for the rate constant derived from limited experimental correlations. Mechanistic descriptions of both processes have so far involved arbitrary normalisation to experimental data. However, a promising approach has been developed recently which enables sticking and entrainment to be described from first principles in terms of the turbulent motions of the fluid adjacent to the surface and the interaction potential between the particles and the surface.

4.2.6 Performance of Purification System

It was noted above that the release of corrosion products into the recirculating coolant of a BWR has a major contribution from the turbine condenser and feedwater plant. The majority of this material is crud which penetrates through the condensate treatment systems. The performance of condensate demineralisers, deep bed ion-exchange resin columns and/or powdered resin filters is therefore crucial to the control of corrosion product levels in the final feedwater. Theories for filtration of particles in deep beds are considered in Annex III (Section I.3.(2)). The removal efficiency is observed to depend on the size of the suspended particles and the pH and ionic strength of the coolant. The main features of the process can be satisfactorily explained in terms of double layer interactions providing allowance is made for the modification of the surface electrical potential of the resin beads as coverage by crud particles increases.

The primary coolant of PWRs is generally purified through a by-pass flow treating up to 1% of the total flow rate. The by-pass flow rate is usually more important than the filtration efficiency so that a full description of the filtration process is not essential. However, the principles are identical to those described for BWRs.

4.2.7 Mechanistic Models and Codes

Comprehensively documented codes descibing the formation, transport and deposition of radioactive corrosion products in BWRs are surveyed in Annex III (Section II). Annex II did not include a similar survey for PWRs; fully documented models and codes are, therefore, briefly described in the following paragraphs.

- PACTOLE

i) Corrosion of the base metal (stainless steel and Inconel) leads both to the formation of an oxide layer in situ and to the release of ions into the fluid. The release rate is governed by the solubility gradient between the bulk coolant and the pores of the oxide.

ii) If the concentration of a given element in solution in the coolant is less than its thermodynamic solubility in the immediate vicinity of a surface, then deposits are dissolved. The dissolution rate is proportional to the difference between the solubility and the actual concentration of soluble species. The equilibrium solubility is calculated from thermodynamic equilibria using the POTHY code module.

iii) If the concentration of soluble species in the coolant exceeds the solubility in the vicinity of a surface then precipitation may occur.

iv) Particles may nucleate in the coolant, agglomerate to a size limited by turbulent shear (generally less than 1 or 2um), and are subsequently deposited on coolant circuit surfaces.

v) The deposits formed in this way are subject to erosion and possibly dissolution.

vi) The ions and particles deposited on in-flux surfaces undergo neutron activation.

vii) Account is taken of removal and possible sources in the by-pass clean-up plant.

- CORA II. It is based on available theory but is keyed to operating plant data and observations such that it is basically a semi-empirical model. The major features are:

i) Corrosion of materials such as stainless steel and Inconel releases products in soluble forms at a rate proportional to solubility.

ii) The oxide films on circuit surfaces are multi-layered. Corrosion of the base metal produces an oxidised region over which a protective film grows. The outer layers are formed by corrosion product deposition; there is a permanent layer adjacent to the protective film and an outermost transient layer.

iii) Transport in the coolant is via both soluble and particulate forms. Particles may deposit on all circuit surfaces. Deposition and dissolution of soluble species are controlled by the relative magnitudes of the concentration in the coolant bulk and the local saturation solubility.

iv) Transient deposits may be eroded or converted to a permanent form. This erosion process is the dominant source of coolant-borne particles.

v) In-core structural alloys and permanent and transient deposits undergo neutron activation.

vi) Removal of circulating corrosion products in the purification is accounted for.

- BURRILL's mechanistic model was developed to describe the behaviour of corrosion products in the CANDU Pressurised Heavy Water-Reactor (PHWR). This system is a pressure tube reactor whose operation is characterised by an essentially constant coolant chemistry: no boron addition, lithium hydroxide dosing, pD about 11 at 25 C. The hypothesis is that:

i) Corrosion products from the out-core materials appear both as particles and as solute in the coolant.

ii) The high coolant pD inhibits precipitation of soluble species on in-core surfaces. However, particles of corrosion products deposit on all circuit surfaces including the fuel sheath and pressure tube surfaces in-core.

iii) Particles deposited in-core are irradiated in the neutron flux.

iv) Dissolution is the only release process from in-core surfaces.

v) Dissolved radionuclides are carried by the coolant to out-core surfaces and are incorporated into the corrosion layer being formed there.

- BABCOCK and WILCOX a mechanistic model was developed following success with a phenomenological description of dynamic crud behaviour in Oconee Unit 1. The key features of this model are:

i) Most of the crud transport, both non-radioactive and radioactive, takes place by mechanisms involving particulate removal, transport and redeposition.

ii) The corrosion of stainless steel and Inconel surfaces releases soluble species which are subsequently converted into particulate material in the coolant bulk.

iii) Particles deposit on all primary circuit surfaces. The deposits on in-core surfaces are converted from an initially loosely deposited layer to a more tightly adherent form by a sintering process.

iv) The loosely adherent deposits on all surfaces are released by erosion.

It is apparent that complete mechanistic descriptions of the formation, transport and deposition of radioactive corrosion products in both PWR and BWR systems require a diversity of complex phenomena to be modelled. Unfortunately, it is not yet possible to identify with certainty all those

mechanisms which are crucial to an adequate description and those which may be omitted. Thus, models are developed from a simplified network of routes, each of which may be described either mechanistically or phenomenologically according to the state of understanding. It must be expected, therefore, that all models will require some refinement as the detailed understanding of mechanisms improves.

5. CONCLUSIONS

This Coordinated Research Programme has provided a survey on the state of the art of all aspects related to CCI. It is therefore a comprehensive picture of the relevant phenomena and their impact on fuel behaviour, of the techniques used to monitor and control the key parameters and of the development of modelling approaches. No conclusions are drawn at this stage is to what actions and constraints are involved in improving the CCI behaviour of the fuel and operation of the power plant. In fact, it is a survey, not a manual of good practice: it provides an exhaustive documentation on the lessons learned in this field and on basis for each organization to guide decisions on practices. Amongst the conclusions on each different improved aspect, the following can be mentioned.

- On water chemistry specifications and their control, the observed trend to increase simultaneously: the coolant enthalpy (exit temperature on PWRs, void fraction in BWRs), the fuel rod surface heat flux, the operational flexibility (load following with transient coolant conditions) and the fuel residence time in the reactor core, leads to reductions in the failure margins of fuel by CCI. It results in a need for improved water chemistry specifications and controls.

- On behaviour of fuel cladding materials, optimized thermohydraulic design of fuel assemblies and improved cladding varieties are gaining importance to restore CCI margins in both operating and accidental conditions.

- On corrosion product behaviour and crud build-up in reactor circuits, the collection of an experimental data base and the assessments by modelling approaches should be pursued to improve the understanding of the parametric interplay and guide the modifications or adaptions to be implemented.

At this stage, it is useful for the international nuclear community to launch a continuation of the work initiated through this CCI program and to attempt, under the IAEA auspices, to produce a guidebook which could constitute a "Manual of good practice on reactor water chemistry in nuclear power plants".

Annex I

ANALYTICAL TECHNIQUES FOR MONITORING WATER CHEMISTRY

A. ELEK
Central Research Institute for Physics,
Budapest, Hungary

K.S. VENKATESWARLU
Bhabha Atomic Research Centre,
Bombay, India

Table I.1

Code Listing of Nuclear Power Plants

Reactor Type	Country	Code No.
PWR	Belgium	BE PW 01,
PWR	Czechoslovakia	CZ PW 02, 03.
PWR	France	FR PW 04 to 30.
PWR	Hungary	HU PW 31.
PWR	Japan	JA PW 32 to 42.
PHWR	Argentina	AR PH 43.
PHWR	Canada	CA PH 44 to 51.
PHWR	India	IN PH 52 to 54.
SGHWR	United Kingdom	UK SG 55.
BWR	Finland	FI BW 56, 57.
BWR	India	IN BW 58, 59.
BWR	Japan	JA BW 60 to 70.
RBWK - 1000	Soviet Union	SU RB 71, 72, 73, 74.

In all the subsequent tables, the Code No. is employed to identify the power reactor.

This Annex is based on the responses recieved by the end of 1983 on the IAEA questionnaire sent in the frame of the CCI Coordinated Research Programme.

Table I.2

Overview of NPPs answering the questionnaire by end 1983

Code No.	Title of NPP	Country	Place	Reactor Type	Effective Fullpower in MW_e	Start up
BE PW 01	D -3	Belgium	Doel	PWR	950	1982
CZ PW 02	Bohunice-1	Czechoslo-vakia	Jaslowske Bohunice	PWR WWER-440	2x440	1980
CZ PW 03	Bohunice-2	"	"	"	2x440	1985
FR PW 04	SENA	France	Ardennes a Chooz	PWR	320	1965
FR PW 05	Blayais-1	"		"	910	1981
FR PW 06	Blayais-2	"		"	910	1982
FR PW 07	Blayais-3	"		"	910	1983
FR PW 03	Blayais-4	"		"	910	1983
FR PW 09	Bugey-2	"		"	920	1978
FR PW 10	Bugey-3	"		"	920	1978
FR PW 11	Bugey-4	"		"	900	1979
FR PW 12	Bugey-5	"		"	900	1979
FR PW 13	Chinon B-1	"		"	870	1982
FR PW 14	Cruas-1	"		"	880	1983
FR PW 15	Dampierre-1	"		"	890	1980
FR PW 16	Dampierre-2	"		"	890	1980
FR PW 17	Dampierre-3	"		"	890	1981
FR PW 18	Dampierre-4	"		"	890	1981
FR PW 19	Fessenheim-1	"		"	880	1977
FR PW 20	Fessenheim-2	"		"	880	1977
FR PW 21	Gravelines-B1	"		"	910	1980
FR PW 22	Gravelines-B2	"		"	910	1980
FR PW 23	Gravelines-B3	"		"	910	1980
FR PW 24	Gravelines-B4	"		"	910	1981
FR PW 25	St.Laurent-B1	"		"	880	1981
FR PW 26	St.Laurent-B2	"		"	880	1981
FR PW 27	Tricastin-1	"		"	915	1980
FR PW 28	Tricastin-2	"		"	915	1980
FR PW 29	Tricastin-3	"		"	915	1981
FR PW 30	Tricastin-4	"		"	915	1981

Table I.2 (continued)

Code No.	Title of NPP	Country	Place	Reactor type	Effective fullpower in MW_e	Start up
HU PW 31	Paks-1	Hungary	Paks	PWR WWER-440	440	1982
JA PW 52	Mihama-1	Japan	Fukui Prefecture	PWR	340	1970
JA PW 33	Mihama-2	"	"	"	500	1972
JA PW 34	Mihama-3	"	"	"	826	1976
JA PW 35	Takahama-1	"	"	"	826	1977
JA PW 36	Takahama-2	"	"	"	826	1975
JA PW 37	Ohi-1	"	"	"	1175	1979
JA PW 38	Ohi-2	"	"	"	1175	1979
JA PW 59	Ikata-1	" Ehime	" Prefecture	"	538	1977
JA PW 40	Ikata-2	"	"	"	566	1982
JA PW 41	Genkai-1	"	Saga Prefecture		559	1975
JA PW 42	Genkai-2	"	"	"	559	1981
AR PH 43	Atueha-1	Argentina	Buenos Aires	PHWR	335	
CA PH 44	Pickering-1	Canada	Ontario	PHWR,CANDU	500	1971
CA PH 45	Pickering-2	"	"	"	500	1971
CA PH 46	Pickering-3	"	"	"	500	1972
CA PH 47	Pickering-4	"	"	"	500	1973
CA PH 48	Bruce-1	"	"	"	750	1977
CA PH 49	Bruce-2	"	"	"	750	1977
CA PH 50	Bruce-3	"	"	"	750	1978
CA PH 51	Bruce-4	"	"	"	750	1979
IN PH 52	RAPS-1	India	Anushakti	PHWR	210	1972
IN PH 53	RAPS-2	"	"	"	210	1980
IN PH 54	MAPS-1	"	Kalpakkam	PHWR	235	1983
UK SG 55	Winfrith	United Kingdom	Dorches-ter	SGHWR	100	1967

Table I.2 (continued)

Code No.	Title of NPP	Country	Place	Reactor type	Effective fullpower in MW_e	Start up
FI BW 56	TVO - I	Finland	Olkiluoto	BWR	660	1968
FI BW 57	TVO - II	"	"	"	660	1979
IN BW 58	TAPS - 1	India	Tarapur	"	200	1969
IN BW 59	TAPS - 2	"	"	"	200	1969
JA BW 60	Tsuruga-1	Japan	Tsuruga, Fukui	"	357	1970
JA BW 61	Tokai - 2	"	Tokai, Ibaraki	"	1100	1978
JA BW 62	Shimane	"	Kashima, Shimane	"	460	1974
JA BW 63	Hamaoka-1	"	Shizuoka Prefecture	"	540	1976
JA BW 64	Hamaoka-2	"	"	"	840	1978
JA BW 65	Fukushima-1	"	Fukushima Prefecture	"	460	1971
JA BW 66	Fukushima-2	"	"	"	784	1977
JA BW 67	Fukushima-3	"	"	"	784	1976
JA BW 68	Fukushima-4	"	"	"	784	1978
JA BW 69	Fukushima-5	"	"	"	784	1978
JA BW 70	Fukushima-6	"	"	"	1100	1978
SU RB 71	Leningrad-1	Soviet Union	Sosnovij Bor	RBMK-1000	1000	1974
SU RB 72	Leningrad-2	"	"	"	1000	1976
SU RB 73	Leningrad-3	"	"	"	1000	1981
SU RB 74	Leningrad-4	"	"	"	1000	1981

Table I.3

GENERAL CONCEPTS OF SAMPLING AND CONTROL

POINTS OF SAMPLING AND PARAMETERS TO BE MEASURED

Unit Code No.	Concepts	Sampling Points	Parameters
1	2	3	4
BEPW 01	Control of boron, lithium and disolved hydrogen concentration. Performance evaluation of filter, demineraliser & fuel cladding integrity.	From primary loops at the cold legs, Chemical Volume Control system.	Boron, Lithium, Calcium, Magnesium, Aluminium, Silica, pH, conductivity, Crud, dis H_2, fission products.
CZPW 02 CZPW 03 (WWER)	Control of boron, potassium and ammonia concentrations. Evaluation of fuel performance. There are 163 sampling points, 4 sampling boxes and 11 sampling channels. Coolant flow 6500 m^3/hr. Purification flow 20 m^3/hr.	Inlet and outlet of mixed filters of the continuous purification plant of the primary coolant, pressurisers, impure condensate tank, outlets of mechanical filters, emergency boric acid injection tank and boron concentrate tank, primary coolant makeup and cooling circuits of safety and control assemblies.	pH, conductivity, hardness, turbidity, organics boric acid, chloride, oxygen, hydrogen, ammonia, potassium, sodium, lithium, iron, copper, calcium, silica, phosphate, nitrate, radioactive Na, K, Kr, Sr, I, Xe, Cs, Ba, corrosion products and tritium.
FRPW 04	The primary circuit has 4 loops, with isolation facility, inlet temp. 284°C and 138 bars and flow 4700 m^3/hr. Sampling concepts are same as in BEPW 01.	Vapour and liquid phases of pressurisers at cold legs of loops.	pH, B, H_2, NH_4, Li, Na, Ca, Fe, Cr, Na, Zp, CU, gross β and γ-activities, tritium, radio-iodine and crud.
FRPW 05 to FRPW 30	Same as above pH control by Li Inlet temp: 286°C and Outlet: 324°C and pressure 155 bars.	Sampling is from the cold main line of the primary circuit and after the Chemical Volume Control System.	Same as above

Table I.3 (continued)

1	2	3	4
HUPW 31 (WWER)	Sampling philosophy is to get necessary confirmation to add chemicals to the primary coolant. Control of boric acid and hydrogen in the coolant is maintained. Fuel element integrity, corrosion and radioactivation in the primary circuit is monitored. Performance of demineralizers & filters is evaluated.	Coolant samples are taken from the primary loops and reactor auxilliary system: purification systems, reagent vessels and pressuriser.	Boric acid, fission & corrosion product activity, dissolved O_2, H_2, noble gases, chloride, pH, conductivity, hardness, Li, Na, K, NH_3, silica, total Fe.
JAPW 32 to JAPW 42	Same as above.	Either the primary loop or the reactor auxiliary system, residual heat removal system and Chemical Volume Control System.	Same as above except K & NH_3
ARPH 43	Sampling philosophy is to ensure isotopic purity of heavy water and chemical control to minimise corrosion & radioactivation of the primary circuit.	Sampling points are in primary D_2O coolant loop, in both moderator D_2O loops and pressuriser.	Li, D_2, O_2: chloride, pD, conductivity, silica, dissolved Fe and Crud.
CAPH 44 to CAPH 51 (CANDU)	Same as above.	At least one sampling point per reactor loop.	pD, conductivity, dissolved D_2 and O_2, chloride, fission produts and crud.
INPH 52 to INPH 54	Same as above.	Reactor outlet header, after crud filter and after purification demineralizer.	Same as above plus Cu, Ni, and tritium.
UKSG 55 (SGHWR)	Same as above Integrated sample analysis over 2 or 3 days in addition to spot sampling.	Moderator and Coolant loops along the feed train. For cobalt level integrated sampling over several weeks feed.	Chloride, silica, metallic impurities and radioactivation & fission products and specially ^{60}Co.

Table I.3 (continued)

1	2	3	4
FIBW 56 FIBW 57	Control of specifications Control of performance and cleaning system. Control of corrosion product concentrations.	In the primary circuit, condensate, heater and reheater drains, feedwater & reactor water. Makeup water.	Ionic impurities, corrosion products, oxygen, conductivity pH, Na and fission products.
INBW 58 INBW 59	To ensure fuel cladding integrity and to minimize corrosion and radioactivation of the primary circuit.	Before filter in the clean-up system and after ion exchange purification in the same and off gases.	pH, conductivity, chloride, SiO_2 , crud, Fe, Cr, Li, Ca, fission and corrosion products.
JABW 60 to JABW 70	The philosophy is for improvement of fuel cladding integrity and piping and equipment, for reduction of radiation field build-up and confirmation of water quality and evaluation of material balance of impurities.	Condensate, condensate demineralizer effluent, feedwater, reactor water and reactor water clean-up demineralizer effluent & fission gas release.	Same as above.
SURB 71 to SURB 74	Insuring fuel clad integrity and chemical control within technical requirements.	Sampling from all main process fluid lines.	pH, conductivity, hardness, Na, Fe, Ca and chloride.

1. Continuous monitoring of boron only : BEPW 01
2. Continuous monitoring of dis O_2 only : ARPH 43
3. Continuous Multipore/dultipore sampling : UKSG 55
4. Continuous sampling and monitoring of conductivity and pH. : JABW 60, 61
5. Same as above plus dis O_2 : JABW 62 to 70

Table I.4

CHEMICAL ANALYTICAL TECHNIQUES

Row number Type of units	Item to be measured	Concentration method, equipment, factor	Method and Instruments used	Analytical procedure Standardisation procedure	Lower detectable level/accuracy of the method	Remark
1	2	3	4	5	6	7
BEPW 1	Chloride, boron iron etc.		ion selective elctrode ICP, titrator	Comparison	ppb range	
CZPW 2-3	Boric acid		Titration by NaOH, addition of Uranite or glycerine on phenolpthalein,		50 µg H_3BO_3/Kg	
			Colorimetry, carminic acid method in strongly acid sulphate medium at 610nm for 2 - 22g B/kg. range.		2 µg B/Kg	
	Chloride		Mercurimmetric method for more than 5 µg Cl/kg. Turbidimetry on silver chloride for less than 5 µg Cl/kg. at 450nm.			
	Ammonium		Colorimetry, Nessler's method 400 - 410 nm			
	Iron	Evaporation	Colorimetry, Orthophenanthroline method, 490 - 520 nm		2 µg	
	Copper	Evaporation	Colorimetry, Kuprizon/bis cyclohexano - Oxaly-dihydrazine method, 590-610 nm		3 µg/kg	
	Silicate		colorimetry, molybdate-hydro fluoric acid method, 625-750 nm		4 µg/kg	
	Nitrate		Colorimetry, sodium salicylate method, 410 nm			

Table I.4 (continued)

1	2	3	4	5	6	7
FRPW 4	Chloride		ion selective electrode		5ppb	
	Fluoride		- do -		10ppm	
	Boron		potentiography; colorimetry		10ppm; 0.1ppm	
	Nitrate		ion-selective electrode		5ppb	
	Silicate		colorimetry		5ppb	
	Metal / Li, Na, Ca, Fe, Cr, Ni, Zn, CH, Al/ Crud	Yes	*atomic absorption*		5ppb	
FRPW 5 to 30	B, Cl, Na, Li, corrosion pro ducts: Fe, Ni, Cr, Co, Mn.	For corrosion products, soluble ion exchange paper insoluble: filter paper.	UV, Visible spectrophotometry atomic absorption, ion selective electrode, X-ray fluorescence.		0.1 g/kg for corrosion products	
HUPW 31	Water hardness		tritration or spectrophotometer	Standard Solut.	0.001 mg equiv./kg	
	Nitrate		spectrophotometer/reduction to nitrite	- do -	20ppb	
	Silicate		spectrophotometer/Silico-molybdo-blue/	- do -	2-5ppb	
	Hydrazine		titration, PADAB/Spectrophoto-meter	- do -	0.1ppm 10ppb	
	pH		pH meter	- do -	± 0.01	
	Conductivity		conductivity meter	KCl solution	± 0.01 µS/cm	
	Chloride		spectrophotometer	Standard solution	0.05 ppm	
	Amonia		Nessler-reagent titration	- do -	0.02 ppm	

Table 1.4 (continued)

1	2	3	4	5	6	7
HUPW 31	Boric Acid		Titration	Standard solution	0.1-0.2g/dm^3	
contd.	Dissolved oxygen		leukomethylen blue	- do -	2-5ppb	
	Dissolved hydrogen		gas chromatography	- do -	1cm^3/kg	
	Sodium		flame photometry	- do -	1ppm	
	Potassium		flame photometry	- do -	1ppm	
	Lithium		flame photometry	- do -	1ppm	
	Iron		spectrophotometer	- do -	2-5ppb	
	Oil		extraction, spectrophotometer	- do -	10ppb	
JAPW	pH		pH meter	Standard solution	(0.01 pH)	
32-38	Conductivity		conductivity meter	KCl solution	(0.1) μS/cm	
	Boron		titration	Hydrogen potassium phthalate	2ppm (0.2%)	
	Chloride		spectrophotometer	Standard solution	0.05ppm (5%)	
	Fluoride		ion-electrode	- do -	0.05ppm (5%)	
	Lithium		atomic absorption	- do -	0.1ppm (5%)	
	Dissolved oxygen		Indigo carmine method		0.005ppm(5%)	
	Dissolved hydrogen		gas chromatography		1cm^3/kg STP (5%)	
	Absolute turbidity		turbidity meter	Standard solution	0.1ppm (10%)	
	Iron		spectrophotometer	- do -	0.002ppm(10%)	
	Silica		spectrophotometer	- do -	0.002ppm(10%)	

Table I.4 (continued)

1	2	3	4	5	6	7
JAPW 39-40	pH		pH meter	Standard solution	(0.01)	
	Conductivity		conductivity meter	KCl solution	(0.01)μS/cm	
	Boron		titration	Potassium hydrogen phtalate	1ppm (0.2%)	
	Chloride		spectrophotometer	Standard solution	0.05ppm (5%)	
	Fluoride		ion electrode	- do -	0.05ppm (5%)	
	Lithium		atomic absorption	- do -	0.1 ppm (5%)	
	Dissolved oxygen		Indigo carmine method	- do -	0.005ppm (50%)	
	Dissolved hydrogen		gas chromatograph	Standard gas	$1cm^3/kg$ STP(5%)	
	Turbidity		turbidity meter	Standard solution	0.1ppm (10%)	
	Iron		atomic absorption	- do -	0.005ppm (5%)	
	Nickel		- do -	- do -	0.01ppm (5%)	
	Cobalt		- do -	- do -	0.01ppm (5%)	
	Silica		spectrophotometer	- do -	0.015ppm (10%)	
JAPW 41-42	pH		pH meter	Standard solution	(0.01)pH	
	Conductivity		conductivity meter	KCl solution	(0.01μS/cm	
	Boron		titration, spectrophotometer	Standard acid Potassium phtalate	2ppm (0.2%)	
	Chloride		spectrophotometer	Standard solution	0.05ppm (5%)	
	Fluoride		ion electrode	- do -	0.05ppm (5%)	
	Lithium		atomic absorption	- do -	0.1 ppm (5%)	
	Dissolved oxygen		Indigo carmine method			
	Dissolved hydrogen		gas chromatograph		$1cm^3/Kg$ STP(5%)	
	Absolute turbidity		turbidity meter	Standard solution	0.05ppm (10%)	
	Iron		spectrophotometer	- do -	0.002ppm (10%)	
	Silica		- do -	- do -	0.02ppm (10%)	

Table I.4 (continued)

1	2	3	4	5	6	7
ARPH 43	Nickel		Spectrophotometry dimethylglyoxime			
	Boron		Carminic acid or Curcumin			
	D_2O		Spectrophotometer			
	Tritium		Liquid scintilator			
	CRUD	filtration	weighing			
	pD		pH meter			
	Conductivity		conductivity meter			
	Lithium		flame photometer			
	Sodium		flame photometer			
	Silica		spectrophotometry and ammonium molybdate			
	Chloride		spectrophotometry nitrate mixture			
	Iron		spectrophotometry thioglycollic acid			
	Chromium		spectrophotometry diphenylcarbazide			
CAPH 44-51	pD, Lithium		ASTM methods are generally used.			
	Conductivity,					
	Dissolved oxygen,					
	Dissolved deuterium					
	Chloride, Crud,					
	Radio-iodines					

Table I.4 (continued)

1	2	3	4	5	6	7
INPH 52-54	Copper	Evaporation, concentration factors, 10-100	spectrophotometer, neocuproine method	linear calibration	10ppb(20%)	
	Nickel	- do -	spectrophotometer, dimethyl glyoxime method.	- do -	10ppb(20%)	
	pH					
	Conductivity					
	Chloride		mercurichthiocyanate method, UV-Visible spectrophotometer	- do -	20ppb(20%)	
	Dissolved oxygen		Indigo carmine method	color comparator, fixed color charts	5ppb(20%)	
	Ammonia		Nessler's reagent, colorimetric method	- do -	0.1ppm(10%)	
	Iron	Evaporation, concentration factors	spectrophotometer, ortho-phenanthroline	linear calibration fixed color charts	30ppb(20%)	
		10 to 100	method			
UKSG 55	Routine: Chloride	Continuous-on-line	by ferric-thiocyanate method, using auto-Analyser	ICPES, atomic absorption and spectrophotometry is standardised by multipoint calibrations over the		Integrated sample is passed through a single microporous filter membrane, 0.45 m.pore size and pack of three cation and three anion exchange membranes contained in aluminium filter holder on iso-kinetic lines, fitted with floating balls integrated flow meters. Iron and Copper routine determinations is done 3 times weekly using 100 dm^3.
	Dissolved oxygen	Weekly	redox potential measurement		5ppb	
	Off gas hydrogen	Daily on-line	Katharometer and discrete/Cambridge Ltd. Instrument	Using diluted commercially available and checked. Standard solutions, conductivity of diluent water is less than 0.1 S/cm.	1% in air/	

Table I.4 (continued)

1	2	3	4	5	6	7
UKSG 55 contd.	Iron	3 times weekly from integrated sample collected by 0.45 um filter membrane and ion exchange membranes, fitted in filter holders on the isokinetic lines, concentration from primary water in (3-8). 10^3, from feed water (1-3). 10^4	mercapto-acetic acid method spectrophotometer		0-5ppb	integrated samples prefilter is dissolved in $5cm^3$ concentrated hydrochloric acid on boiling water bath. After 10 minutes, $0.5cm^3$ concentrated nitric acid is added, heated for further 20 minutes, cooled and diluted to $25cm^3$ Cation membranes are eluted with 25 cc 1M H Cl. In special cases filtered material is prepared above, with prolonged digestion, separation of any acid insolubles by micro filtration and fusing with 20mg recrystallized sodium fluoborate. Fused extract and acid solubles are combined and diluted to 25 cm^3 and reducing it to molybdenum blue by adding 1 amino - 2 naphthol - 4 salphonic acid followed by colorimetry.
	Copper	see iron	zinc dibenzyldithio-carbonate spectro-photometer		0.1ppb	
	"Reactive Silicon"	Continuous-on-line	ammonium molybdate and 1 amino-2 napthol-4 sulphonic acid, reduced B molybdate silicic acid measured continuously, in-line using Technicon Monitor IV	SiO_2 fused with sodium carbonate in platinum melt dissolved in water	20ppb	
	Chloride	Also daily from grab sample		NaCl dried at 150°C for two hours, dissolved in water the same for routine chloride	20ppb	
	Silicon	- do -	by the method of reactive silicon using Autoanalyser-1		20ppb	

Table I.4 (continued)

1	2	3	4	5	6	7
UKSG 55 contd.	Special -Iron and -Cobalt, Sol./Insol.	From integrated sampler at start up, mid-run and shutdown	ICPES. Cobalt checked regularly by flame and flameless atomic absorption.		1ppb 0.02ppb	
	Multielement analyses	quarterly grab sample	ICPES for Al, Cd, Ca, Cr, Cu, Fe, Mg, Mn, Ni, Zn		Zn 0.2ppb others 0.1ppb	
	Sulphate	grab sample during transients/high conductivity.	ion chromatography /Dionex/		0.1ppb	
FIBW 56-57	Conductivity				0.01 μS/cm	
	Chloride	evaporation	spectrophotometer		5ppb	
	Metallic Impurities	filteration plus membranes	atomic absorption		0.05-0.1ppb	
	Silica	none	spectrophotometer		5ppb	
INPW 58-59	Chloride		No pretreatment, Mercuric thiocyanate methods, UV Visible spectrometer.	Linear calibration	20ppb (20%)	
	Fe, Cu, Ni, Cr.		No pretreatment, atomic absorption UV, Visible spectrophotometry	Linear calibration and standard addition.	10ppb (20%)	
	Iron		bipyridyl method		5ppb (20%)	
	Copper		neocuproine method		5ppb (20%)	
	Nickel		dimethyl glyoxime method		5ppb (20%)	
	Chromium		S-diphenylcarbazide method		5ppb (20%)	
	Silica		molybdenun blue method		5ppb (20%)	

Table I.4 (continued)

1	2	3	4	5	6	7
JABW 60	pH		glass electrode		/0.01pH	
	Conductivity		flow type cell		-	
	Boron				1ppm	
	Chloride		mercuric thlocyanate method		2ppb (1%)	
	Dissolved oxygen		Winkler Kinetics Kit		10ppb	
	Metallic impurities (Sol/Insol.) like:	filtration, ion exchange evaporation	X-ray fluorescence		1 g/ 0.1%	Concentration equipment 0.45 m millipore membrane filter and ion exchange paper in filter holder/in-line sampler/; for other ionic species: resin column ion chromatograph, for colloidal cobalt rotary quartz evaporator, concentration factors are 1000-10,000 100,1000 and 10,000 respectively. Metallic impurities are dissolved in 1:3HCl solution for determination by AAS
	- Iron		atomic absorption flame method		0.05ppm(5%)	
	- Copper		- do -		0.03ppm(5%)	
	- Cromium		- do -		0.05ppm(5%)	
	- Nickel		- do -		0.07ppm(5%)	
	- Zinc		- do -		0.08ppm(5%)	
	- Cobalt		- do -		0.05ppm(5%)	
JABW 61	pH		glass electrode		0.01	
	Conductivity		flow type cell		(2%) FS	
	Boron		atomic absorption		50ppb(5%)	
	Chloride		mercuric thiocyanate method		20ppb(1%)	
	Dissolved oxygen		diaphragm type electrode		1ppb(1%)	

Table I.4 (continued)

1	2	3	4	5	6	7
JABW 61 contd.	Metallic impurities Sol/Insol.like:	filtration, ion exchange and evaporation	X-ray fluorescence		1 m(0.1%)	Concentration equipment 0.45 m Millipore membrane filter and ion exchange
	- Iron		atomic absorption flame method		0.04ppm (5%)	paper in filter holder/ in-line sampler/, for other ionic species: resin column/
	- Copper		- do -		0.04ppm (5%)	ion chromatography/for colloidal Cobalt rotary
	- Chromium		- do -		0.04ppm (5%)	quartz evaporation. Concentration factors are 1000 -
	- Nickel		- do -		0.05ppm (5%)	10,000, 100 - 1000 and 10,000 respectively.
	- Zinc		- do -		0.02ppm (5%)	Metallic impurities are dissolved in 1:3HCl
	- Cobalt		atomic absorption flameless method		1ppb (5%)	solution for determination by AAS.
	Other ionic species like:					
	- Sodium		ion chromatograph		(0.01-0.005)ppb	
	- Chloride		- do -		(0.01-0.005)ppb	
	- Silica		Molybdenum blue method		20ppb (1%)	
JABW 62				Standardisation based on JIS		
	Conductivity			- do -		
	Boron	Solvent extraction	absorption photometry 1,2 - $C_2H_2Cl_2$, HF methylen blue	- do -	10^{-4}--10^{-3}mg (10-30%)	

Table I.4 (continued)

1	2	3	4	5	6	7
JABW 62 contd.	Chloride		absorption photometry	Standardization based on JIS	0.02-0.5mg (10 - 2%)	
	Metallic impurities	Ion exchange paper for Sol., Millipore paper	atomic absorption	- do -		
	Sol/Insol like:	for Insol Concentration factors are				
	- Iron	$20 - 2.10^5$, Insol.			1 - 10 ppb	
	- Copper	elutriated from filter			"	
	- Chromium	and dissolved in HCl			"	
	- Cobalt	and HNO_3			"	
	- Manganese				"	
	- Nickel				"	
	- Silica		absorption photometry	Standardization based on JIS	2.5-15 g (10-20%)	
JABW 63-64	pH	in-line monitor			(0.02pH)[x]	[x]Error of reading; the error of sampling is 5%
	conductivity	in-line monitor			(0.01µS/cm	
	Boron		spectrophotometer methylen blue		50ppb	
	Chloride	Silver nitrate	turbiditymeter		10ppb	
	Dissolved oxygen	in-line monitor			0.05ppm	
	Metallic impurities	$300dm^3$ grab sampling, ion exchange	atomic absorption		10ppb	
	Silica		molybdenum blue method		10ppb	

Table I.4 (continued)

1	2	3	4	5	6	7
JABW 65-70	pH Conductivity					
	Boron		Spectrophotometer methylene blue method		50ppb	Boron is converted into BF_4 in sulphuric acid,
	Chloride	precipitation of chloride as silver-chloride	tyrbidimeter	Chlorimetric scale	20ppb	and with addition of HF colored with methylene blue and extracted with
	Metallic Impurities Sol./Insol like: - Iron	filtering the sample through Millipore and ion exchachange papers is the method for Sol/Insoluble distinction. Concentration factor is 1000	X-ray fluorescent analysis of filters		0.1ppb	1,2-dichlorocthane. The concentration is calculated from optical density. Metallic impurities are filtered on by Millipore, cation and anion exchange filters. Filters are dried out and analysed by X-ray
	- Copper					fluorescence. Silica
	- Chromium					is determined by adjusting
	- Nickel					pH of the sample to 1.2-1.5,
	- Silica		colorimeter			then adding ammonium molybdate for molybdenum yellow reaction.
SURB 71-74	pH Conductivity hardness					
	Chloride	evaporation & ion-exchange				
	Sodium	- do -				
	Iron	- do -				
	Copper	- do -				

Table I.5 RADIOCHEMICAL AND PHYSICAL MEASUREMENT

Code number/ Type of Units	Radiochemical: a) dose rate measurements b) isotopic contribution to the dose rate c) gamma - spectrometry d) Möbsbauer measurements	Physical: a) crud thickness, crystal form b) crud density, thermoconductivity c) diameters of particles, etc. d) observation methods of fuel surfaces
1	2	3
BEPW 1	a) Babyline Teletector Automates	
FRPW 4	a) Canberra Jupiter b) Ge Hp semiconductor, TNU Tracor Northern	a-c) The only physical measurement is weighing of crud collected from 100-200dm^3 coolant on 0.45μm membrane. Particle sizing in with different pore size membranes.
FRPW 5 - 30	a) Babyline or total gamma dose rate b) Isotopic contribution to dose rate is calculated from the isotope content measured in the vessel. c) Ge or Ge/Li detectors	d) Scraping of deposits by a special FRAGEMA device and collecting on Millipore filter, followed by chemical and radiochemical analysis.
HUPW 31	c) Ge/Li semiconductor, camberra series 30 d) No experiment	
JAPW 32 - 38	a) Ionization monitor c) Ge/Li semiconductor	a) From amount of crud and form it's specific amount, mg/dm^2, X-ray diffraction c) SEM d) TV Camera and periscope

Table I.5 (continued)

1	2	3
JAPW 39 - 40	a) Ionisation monitor	
	c) Ce/Li/Semiconductor	d) TV camera and periscope
JAPW 41 - 42	The same as for 1-7	The same as for 1-7
ARPW 43	a) As usual	a) By X-ray diffraction and Mössbauer spectroscopy
	b) External: 15% ^{3}H, 45% ^{60}Co, 40% other gamma emitters Internal: negligible	d) Telescopic
	c) Canberra series 80	
	d) Occasionally, in aELRON Mössbauer Spectrometer ina constant acceleration mode with an Ar/CO2 filled Reuter Stokes R.S.G.-61- M2 proportional counter, with a multichannel analyser operated in the time mode. Source used ^{57}Co in Pd matrix, samples are collected on filters piled up between thin acrylic disks.	
CAPH 44-51	a) Gamma survey meters used to measure predetermined positions during shut-downs	a-c)The isothermal corrosion coupons give data on corrosion rates, both general and localized
	b) shut down surveys	

Table I.5 (continued)

1	2	3
INPH 52 -54	a) Boiler cabinet radiation fields are measured at predetermined locations 24 hours after each reactor shut-down, employing gun monitors b) The main contributor to the dose rate is ^{3}H which is monitored by liquid scintilation counter. ^{131}I, ^{137}Cs and dissolved activated corrosion products are also measured by a high resolution Ge/Li - gamma - spectometer and quantified. On-line gamma-spectrometry-carried-out at fixed locations during long shut-downs has shown ^{60}Co and ^{58}Co to be the major deposited activity on the coolant system piping surfaces. c) Measurements made on filterable crud from the coolant system.	a) About 1 /m thick magnetite coating was formed during hot conditioning in the comissioning phase.
UKSG 55	c) Routine weekly iodine balance on circuit samples, determination of ^{131}I and ^{133}I. Daily ^{131}I, ^{133}I and ^{239}Np. Examination of solutions prepared from integrated samples for ^{60}Co, ^{59}Fe, ^{65}Zn, ^{54}Mn, ^{58}Co and ^{51}Cr. Examination of grab samples, taken quarterly for short-lived nuclides and nuclides detected in the energy range 100 to 1800 keV/about 40 isotopes/. ^{64}Cu is separated by ion-exchange.	a) Cross-section and profiles of crudded pipework, measured by SEM; elemental distribution determined by energy dispersive X-ray analysis. Resolution 10 nm c) Particle diameter of surface deposited materials determined by SEM that of water born insolubles by Royco particle size analyzer. d) Scanning electron microscope autoradiography employed for the identification of radioactive particles, generally in range 1 to 10 μm diameter, in crystalline and some amorphous deposits.

Table I.5 (continued)

1	2	3
FIBW 56 -57	a) Regular program during shutdown b) Calculated Ci/m^2 - mrem/h c) One system in laboratory, one mobile	d) Visual
INBW 58 - 59	a) By gun monitor at different locations of priamary circuit b) Mainly ^{60}Co during shutdown c) Gamma-ray spectrometry for fission product iodines and cesiums and for activation products like: ^{58}Co, ^{60}Co, ^{64}Cu, etc.	a) Occasionally measured d) Boroscopic examination
JABW 60	a) Ion chamber type gamma survey meter	a) Direct measurement at fuel surface during post irradiation examination (PIE). Estimation based on crystal form, chemical composition and sampling area. Crystal form analysis is done by X-ray diffraction
JABW 61	a) Direct proportional gamma survey meter	
JABW 60-61	b) Calculated from the gamma-spectrometric measurement and gamma-emission constant of isotopes c) Using Ge/Li - semiconductor detector and PHA	b) Crud density is estimated on above data c) Screening by various pore size filters automatic particle size counting and SEM is applied d) TV camera, periscope, PIE

Table I.5 (continued)

1	2	3
JABW 62	a) TLD b) ^{60}Co, ^{58}Co, ^{54}Mn c) Ge/Li Semiconductor detector	
JABW 63 - 64	c) Gross Gamma activity is measured using NaI/Tl - detector, ^{131}I on silver iodide precipitate and radioactivity balance is measured using Ge/Li - semiconductor detector.	
JABW 65 - 70	a) Gamma Survey meter b) ^{58}Co, ^{60}Co, ^{54}Mn c) Extracting radioactive isotopes of iodine in presence of inactive carrier from the coolant and precipitating them as silver iodide, their activity in measured by Ge/Li/ semiconductor detector. Using the same detector radioactive isotopes retained on Millipore, cation and anion-exchange filters from 5dm^3 sample are measured in the reactor water.	

Annex II

MODELLING THE BEHAVIOUR OF CORROSION PRODUCTS IN THE PRIMARY HEAT TRANSFER CIRCUITS OF PRESSURIZED WATER REACTORS — A REVIEW OF PRINCIPLES

R.S. RODLIFFE, M.V. POLLEY, E.W. THORNTON
Berkeley Nuclear Laboratories,
Central Electricity Generating Board,
Berkeley, Gloucester, United Kingdom

NOMENCLATURE

A	Hamaker constant (J).
a	First order surface reaction rate constant (m s^{-1}).
B	Rate constant defining oxide dissolution (kg m^{-2} s^{-1}).
b_p	First order constant for escape of colloidal particles from a surface (s^{-1}).
C	Number concentration of particles in coolant (m^{-3})
C_b	Concentration of soluble species in bulk coolant (kg m^{-3}).
C_d	Drag coefficient for particle in still fluid.
C_h	Number concentration of particles in bulk coolant (m^{-3}).
C_p	Specific heat at constant pressure (J $mole^{-1}$ K^{-1}).
C_s	Solubility (kg m^{-3}).
C_{si}, C_{so}	Corrosion product solubility at metal-inner oxide and outer oxide-coolant interfaces respectively (kg m^{-3}).
C_w	Concentration of soluble species in coolant adjacent to surface (kg m^{-3}).
$CRYST_i$	Resistance to incorporation of trace corrosion ion at metal-oxide interface (s m^{-1}).
$CRYST_o$	Resistance to incorporation of trace corrosion ion in precipitation on outer oxide (s m^{-1}).
c_b	Concentration of trace soluble species in bulk coolant (kg m^{-3}).
c_{mi}, c_{io}, c_{ow}	Aqueous concentrations of trace soluble species in oxide film at metal-inner oxide, inner oxide-outer oxide and outer oxide-water interfaces respectively (kg m^{-3}).
c_w	Concentration of trace soluble species in coolant adjacent to surface (kg m^{-3}).

D	Ionic or molecular diffusion coefficient ($m^2\ s^{-1}$).
D_B	Particle Brownian diffusion coefficient ($m^2\ s^{-1}$).
D_i	Corrosion ion diffusion coefficient in oxide film ($m^2\ s^{-1}$).
D_l	Aqueous diffusion coefficient for trace corrosion ion ($m^2\ s^{-1}$).
$DIFF_i$	Resistance to diffusion of trace corrosion ion in inner oxide layer ($s\ m^{-1}$).
$DIFF_o$	Resistance to diffusion of trace corrosion ion in outer oxide layer ($s\ m^{-1}$).
d	Characteristic dimension of a flow system (m).
d_p	Particle or agglomerate diameter (m).
d_r	Mean height of surface roughness elements above mean surface level (m).
E	First order resuspension or erosion rate constant (s^{-1}).
e	Electronic charge (C).
F	Faraday number ($C\ mole^{-1}$).
F_a	Nett force of adhesion (N).
F_d	Tangential drag force (N).
F_e^{ψ}, F_e^{σ}	Electrical double layer forces for constant potential and constant charge interactions respectively (N).
F_g	Gravitational force (N).
F_l	Lift force (N).
F_m	Magnetic force (N).
F_r	Reaction force on deposited particle (N).
F_v	van der Waals force (N).
f	Factor modifying diffusion coefficient in oxide film, incorporating porosity and tortuosity.
f_d	Factor to allow for proximity of surface and velocity distribution normal to surface.
f_p	Particle sticking probability.
G	Free energy ($J\ mole^{-1}$).
g	Gravitational acceleration ($m\ s^{-2}$).
H	Separation between spherical particle and plane surface (m).
I	Surface reaction rate constant describing the incorporation of trace species into a growing oxide film ($m\ s^{-1}$).
J_h	Flux of particles towards surface ($m^{-2}\ s^{-1}$).
J_i	Corrosion ion flux across inner oxide layer ($kg\ m^{-2}\ s^{-1}$).
J_n	Rate of formation of critical nuclei ($m^{-3}\ s^{-1}$).

J_w	Flux of trace corrosion ion towards corroding surface ($kg\ m^{-2}\ s^{-1}$).
K_p, K_a	Thermal conductivity of particle and water respectively ($J\ K^{-1}\ m^{-1}\ s^{-1}$).
$K_{z,b}$	Solubility constants for dissolved species, $Fe(OH)_b^{(z-b)+}$
K_1, K_2, K_3	Hydrolysis constants for dissolved species.
K_w	H_2O ionization (or dissociation) equilibrium constant.
k	Boundary layer mass transfer coefficient ($m\ s^{-1}$).
k_B	Boltzmann constant ($J\ K^{-1}$).
k_i	Deposition velocity for inertial particles ($m\ s^{-1}$).
k_i^+	$= \frac{k_i}{u_\tau}$, dimensionless deposition velocity for inertial particles.
k_p	Boundary layer mass transfer coefficient for colloidal particles ($m\ s^{-1}$).
k'_p	k_p modified to account for the effects of thermophoresis or electrophoresis ($m\ s^{-1}$).
M	Deposit mass ($kg\ m^{-2}$).
M_l	Magnetisation ($A\ m^{-1}$).
m_i, m_o	Masses of inner and outer oxide layers respectively ($kg\ m^{-2}$).
N	Number concentration of those ions or molecules in solution which are capable of participating in the nucleation process (m^{-3}).
N_*	Number concentration of critical embryos (m^{-3}).
$N(\infty)$	Number concentration of anions or cations remote from a surface (m^{-3}).
n	Particle number concentration (m^{-3}).
P_i, P_o	Partition coefficients for trace corrosion ions at metal-inner oxide and outer oxide-coolant interfaces respectively.
Q	Number density of particles in deposit (m^{-2}).
R	Universal gas constant ($J\ mole^{-1}\ K^{-1}$).
Re	$= \frac{ud}{\nu}$, Reynolds number.
Re_p	$= \frac{u'd_p}{\nu}$, particle Reynolds number.
r_*	Radius of critical embryo (m).
S	Entropy ($J\ mole^{-1}\ K^{-1}$)
Sc	$= \frac{\nu}{D}$, Schmidt number.

Sh	$= \frac{kd}{D}$, Sherwood number.
Sh_p	$= \frac{kd_p}{D}$, Sherwood number for mass transfer to a particle.
s	Supersaturation, defined as the ratio of the concentration of ions or molecules in solution to the solubility.
T	Absolute temperature (K).
T_o	Reference absolute temperature (K).
t	Time (s).
t^+	$= \frac{tu_\tau^2}{\nu}$
U_a, U_c	Absolute mobilities of anion and cation respectively, defined as drift velocity established by application of unit potential gradient ($m^2\ s^{-1}\ V^{-1}$).
U_p	Mobility of colloidal particle ($m^2\ s^{-1}\ V^{-1}$).
u	Characteristic velocity of a flow system ($m\ s^{-1}$).
u'	Velocity of particle relative to fluid ($m\ s^{-1}$).
$\bar{u}$	Fluid velocity averaged over particle projected area ($m\ s^{-1}$).
u_e	Electrophoretic velocity ($m\ s^{-1}$).
u_r	Particle relative velocity due to turbulence ($m\ s^{-1}$).
u_T	Thermophoretic velocity ($m\ s^{-1}$).
u_τ	Friction velocity ($m\ s^{-1}$).
u^+	Instantaneous dimensionless fluid velocity in neighbourhood of particle: fluid velocity/u_τ.
v	Volume of a molecule in solid oxide or hydroxide (m^3).
v^+	Instantaneous dimensionless particle velocity: particle velocity/u_τ.
X_i	Thickness of inner oxide film (m).
y	Distance normal to surface (m).
y_o	Separation at minimum of potential (m).
y_1	Separation at maximum of potential (m).
z_a, z_c	Valence of anion and cation respectively.
z_1	Valence.
α_1	Surface proximity drag correction factor.
α_m	α_1 at maximum of potential.
α_2	Coefficient of static friction.
β	Kinetic coefficient defining the rate at which ions or molecules encounter and adhere to a critical embryo ($m\ s^{-1}$).

β^+ $= \dfrac{3\,\rho_f}{2\rho_p+\rho_f}$.

Γ Velocity gradient in fluid (s^{-1}).

γ $= -\dfrac{d^2\phi}{dH^2}$, at maximum of potential (J m^{-2}).

γ_q Activity coefficient of species with charge q.

ΔC_i Corrosion ion concentration difference across inner oxide film (kg m^{-3}).

ΔG_* Free energy of formation of a critical embryo for homogeneous nucleation (J).

$\Delta G'_*$ Free energy of formation of a critical embryo for heterogeneous nucleation (J).

$\Delta\phi$ Height of potential energy barrier (J).

δ Maximum extent of surface interaction potential (m).

ε_t Eddy diffusivity ($m^2\ s^{-1}$).

ε_o Permittivity of free space (F m^{-1}).

ε_1 Dielectric constant.

θ Parameter analogous to the contact angle for a liquid-solid-gas interface.

θ_1 Angle between normal to surface and line joining particle centre to pivot.

κ $= \left(\dfrac{2z_1^2e^2N(\infty)}{\varepsilon_1\varepsilon_o k_B T}\right)^{1/2}$, inverse diffuse layer thickness (m^{-1}).

μ Fluid viscosity (kg $m^{-1}\ s^{-1}$).

μ_I Ionic strength.

μ_o Permeability of free space (H m^{-1}).

μ_1 Relative permeability.

ν Kinematic viscosity of fluid ($m^2\ s^{-1}$).

ρ_f, ρ_p Fluid and particle densities respectively (kg m^{-3}).

ρ_i, ρ_o Densities of inner and outer oxide layers respectively (kg m^{-3}).

σ Interfacial energy of the oxide- or hydroxide-water interface (J m^{-2}).

σ_i^+ Component of dimensionless r.m.s. velocity of particles on projection into boundary layer normal to the wall.

τ^+ Dimensionless particle relaxation time.

τ_i, τ_o Tortuosities of inner and outer oxide layers respectively.

Φ Particle volume fraction in suspension.

ϕ_1 Factor relating critical free energy for heterogeneous nucleation to that for homogeneous nucleation.

ϕ_i, ϕ_o	Porosities of inner and outer oxide layers respectively.
ϕ	Surface interaction potential (J).
ϕ^{max}	Maximum surface interaction potential (J).
ϕ_E	Electrical double layer interaction potential (J).
ϕ_M	Magnetic interaction potential (J).
ϕ_W	van der Waals interaction potential (J).
$\psi(o)$	Surface electrical potential (V).

1. INTRODUCTION

The corrosion of the surfaces composing the primary heat transfer and auxiliary circuits of water reactors is minimised by the selection of construction materials and the rigorous control of coolant quality. Despite these precautions corrosion products are inevitably released from surfaces, are transferred in the coolant and are subsequently deposited on primary circuit surfaces unless they are removed by the clean-up plant. This transfer can potentially cause several problems in reactor operation (e.g. Berry and Diegle, 1979):

(1) Deposits may reduce flow areas and increase roughness, leading to increased flow resistance and reduced coolant flow rates.

(2) It is possible for fuel failure to be induced if the cladding environment is substantially modified. The thermal conductivity of deposits on fuel element surfaces is relatively low so that increased thermal resistance leads to raised cladding and fuel temperatures. If the fuel rating is sufficiently high local boiling may be experienced and, if porous deposits are present, concentration of chemicals may occur. The resulting enhancement of corrosion may then induce cladding failure.

(3) Radioactive corrosion products may contaminate out-of-flux surfaces, contributing to shutdown radiation fields and thus to the radiation exposure of workers during inspection, maintenance and repair operations.

Corrosion is generally sufficiently well controlled to ensure that the influences of deposits on system thermal-hydraulics are not limiting. However, the trends to higher fuel rating and higher coolant temperature in advanced reactor designs result in a significant fraction of the fuel surface experiencing boiling with the potential for concentration of chemicals in any porous deposits which may form. The resulting environment may also be aggravated if it is considered desirable to increase the concentration of alkalising agents in order to operate with higher coolant pH_T.

It is well established that radioactive corrosion products are dominant or major contributors to shutdown radiation fields on all water reactors (e.g. Hinson and Murphy, 1979; Beslu, Frejaville and Jeanson, 1979; Mishima, 1983; Varovin, Eperin, Konstantinov, Sedov, Senin and Filippov, 1983; Barber and Lister, 1982; Jarnstrom, 1982). In this case the impetus to understand corrosion product behaviour results from the ICRP recommendation that plants should be designed and operated to ensure that the radiation exposure of personnel involved in tasks such as maintenance, inspection and repair should be as low as reasonably achievable (ALARA) (ICRP, 1977).

This review covers all reactors in which the primary heat transfer medium is predominantly single-phase water and in which steam is generated in a secondary circuit, i.e. including CANDU pressurised heavy water reactors (CANDU PHWR), Soviet VVERs, etc. These systems will be denoted as pressurised water reactors (PWR) throughout the text. A full appreciation of the effects of boiling and two-phase flow is necessary to extend this work to direct cycle reactors.

Reviews of the formation, transport and deposition of radioactive corrosion products in PWR have been presented by several authors (Berry and Diegle, 1979; Darras, 1980; Vanbrabant and de Regge, 1982; Gautsch, Lanza and Weisgerber, 1979). More general reviews of relevance to corrosion product fouling have also been published: fouling in heat exchangers (Epstein, 1978); corrosion products in power generating systems (Lister, 1979a); particulate fouling (Gudmundsson, 1979); and precipitation fouling (Hasson, 1979). This review focusses attention on the principles which must form the basis for any mechanistic model for predicting the contamination of PWR primary circuit surfaces by radioactive corrosion products.

There are two noteworthy exceptions from this review. Firstly, neutron activation. In the simplest terms, the production rate of an isotope by a given reaction may be determined from a knowledge of the parent abundance in the target material, the cross-section for the reaction and the relevant neutron flux. It is implicit that a complete description of this process will include appropriate allowances for the neutron flux spectrum, its variation from one component to another within the reactor vessel and its temporal variation. A detailed discussion of this topic would be lengthy and is considered to be beyond the scope of this review. Secondly, the effects of boiling. There have been numerous studies on corrosion product behaviour in boiling conditions, principally of relevance to direct cycle reactors. This topic is the subject of a separate review (K. Ishigure, private communication) whose implications for the boiling conditions encountered in advanced designs of PWR will need to be considered at a later date.

Radioactive corrosion products may be generated either directly or indirectly. In the former case, corrosion may result in the release of neutron radioactivation products from in-flux structural materials. In the latter case, corrosion products from out-of-flux surfaces may be released into the coolant, may deposit on in-flux surfaces and undergo neutron activation, and may subsequently be resuspended into the coolant.

The radioactive corrosion products dominating shutdown radiation fields are generally ^{60}Co and ^{58}Co with lesser contributions from nuclides

such as ^{59}Fe, ^{51}Cr and ^{54}Mn (Berry and Diegle, 1979). ^{58}Co is generated by fast neutron activation of ^{58}Ni, which is 70% abundant in nickel. ^{60}Co is generated by thermal neutron activation of ^{59}Co, which is 100% abundant in cobalt. ^{59}Fe and ^{54}Mn are generated from ^{58}Fe and ^{54}Fe respectively; ^{51}Cr is generated from ^{50}Cr. Although cobalt is typically present in primary circuit stainless steel and alloys such as Inconel-600 and Incoloy-800 at levels from 100 to 1000 ppm it produces a potentially greater hazard than nickel because of its much higher (approximately x200) neutron activation cross-section. Also, since cobalt is present in the majority of primary circuit materials at such low levels, it is possible for high cobalt materials, such as Stellites (approximately 55% cobalt), to contribute significantly to cobalt corrosion product input despite being used in relatively few locations and, therefore, being associated with relatively low exposed surface areas.

Radioactive and non-radioactive corrosion products may be transported in the coolant both as true soluble species and as inertial (> 1 μm) or colloidal (< 1 μm) particulate species as defined by Ponting and Rodliffe (1983). Particulate material is conventionally classified by its retention on a 0.45 μm microporous filter membrane; material which is not retained, i.e. non-filterable, is often classed as 'soluble'. The non-filterable fraction, therefore, inevitably contains some colloidal particulate material. Indeed, Blesa, Larotonda, Maroto and Regazzoni (1982) have suggested that most if not all of the non-filterable ^{60}Co circulating in the coolant of the Atucha I Nuclear Power Station is in the form of particulate material. On the other hand some workers (e.g. Lister, 1978; Lister, Kushneriuk and Campbell, 1983) regard true soluble transport as dominant when coolant crud levels are low. Practical difficulties are experienced in sampling at high temperatures and in identifying and analysing particles smaller than 0.1 μm diameter so that reliable data may not be available to substantiate models.

It is often assumed, for the purpose of simplifying calculations, that iron, nickel, chromium and cobalt species exhibit identical behaviour, e.g. with respect to solubility, nucleation and precipitation, so that the elemental composition of deposited and circulating corrosion products would be predicted to be uniform around a circuit. In practice this is not observed. The Ni:Fe ratio in deposits on Zircaloy fuel may vary considerably along a channel, between channels, between the loosely and tightly adherent layers, and between different cycles of the same reactor (e.g. Oldenkamp, Paulson and Solomon, 1961; Riess, 1976; Solomon and Roesmer, 1976; Neeb and Riess, 1977). Such variations are generally postulated to be due either to varying contributions from particulate

deposition and precipitation of soluble species or to differences in the solubilities of nickel and iron. Materials such as stainless steel and higher nickel alloys exhibit an inner corrosion layer which is enriched in chromium relative to the precipitated outer layer (Michael and Plog, 1977; McIntyre, Zetaruk and Owen, 1979; Bergmann, Roesmer and Perone, 1983; Pick, 1983). Obviously all these variations must be accommodated in any complete description of corrosion product behaviour.

There is some international debate on the relative importance of steady operation and transient conditions for the transfer of activity from in-flux to out-of-flux surfaces. Direct evidence is available for transfer of activity during refuelling shutdown. For example, the radioactivity liberated and finally retained in the clean-up system during the first refuelling shutdowns at Fessenheim I and II was comparable to or greater than that deposited on out-of-core surfaces (Beslu, Frejaville, Brissaud, Nunse and Ridoux, 1982). In this case in-situ gamma spectrometry showed that there was little or no change in out-of-core deposited radioactivity. This observation has been confirmed by measurements on US PWRs (Kormuth and Barkich, 1983). The role of less major transients remains to be resolved but the indications are that the contamination of out-of-flux surfaces is dominated by transfer during steady operation. However, it is worth noting that the observation of such transients stimulated investigations of thermal and chemical cycling techniques for decontamination in Douglas Point CANDU PHWR (Montford, 1973) and Atucha I (Blesa, Baumgartner and Maroto, 1983).

A simplified diagram of the processes governing corrosion product behaviour is shown in Fig. 1. Each of these mechanisms and their analytical descriptions will be considered in the following sections.

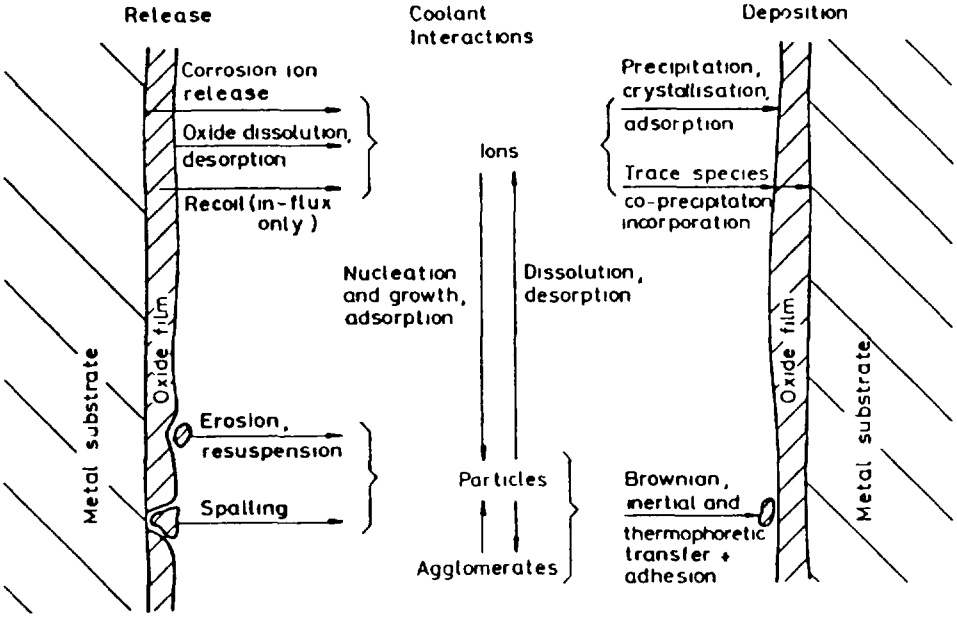

FIG 1. PWR Corrosion Product Formation, Transport and Deposition Mechanisms

2. CORROSION AND CORROSION ION RELEASE

A detailed description of the mechanisms of corrosion film formation is fundamental to any model for radioactive corrosion product behaviour. However, it is particularly necessary in order to define (i) the quantities of non-radioactive material released from out-of-flux surfaces and thus to establish the potential for deposition on in-flux surfaces; (ii) the quantities of radioactive material available for release by corrosion of in-flux structural materials; and (iii) the interaction of soluble radioactive species with the corrosion films on out-of-flux surfaces.

2.1 Uniform Corrosion

The uniform corrosion of stainless steels and higher nickel alloys in autoclaves and loops under conditions appropriate to PWR primary coolants has been comprehensively reviewed by Cohen (1969), Berry and Diegle (1979) and most recently by Lister, McAlpine and Hocking (1984). Studies of uniform corrosion of Stellite hard facing alloys have been reported by McIntyre, Zetaruk and Murphy (1979), Taylor and Armson (1983) and Lister et al (1984). Corrosion rates for all these materials are generally observed to decrease with time and display approximately parabolic kinetics. Corrosion release rates also decrease with time but may exhibit different kinetics. For example, McAlpine, Lister and Ocken (1984) observed a t^{-n} dependence for corrosion release rates from Inconel-600 and Inconel-690 after about 100 days, where n = 0.6-0.86. Unfortunately, most studies are limited to relatively short exposure times (generally less than 1 year) and there have been very few systematic investigations of the effects of variables such as surface finish and heat treatment, water chemistry and flow rate. Thus, caution is necessary when extrapolating the results of such studies to typical reactor conditions and operating times. Particular care should be exercised when interpreting data from static autoclaves since the mass transfer environment is so different from a coolant circuit.

The corrosion mechanisms for stainless steels and higher nickel alloys under PWR conditions are not well understood but there is evidence to suggest that a two-layer description may be appropriate with an outer layer consisting of accumulations of crystals (Francis and Whitlow, 1966; Warzee, Sonnen and Berge, 1967; Michael and Plog, 1977; Ensling, Fleisch, Grimm, Gruber and Gutlich, 1978; McIntyre, Zetaruk and Owen, 1979; Tachikawa, Hoshi, Sagawa, Yonezawa and Nakashima, 1984; Lister et al, 1984). Such observations inevitably invite comparison with the classical two-layered structure observed by Potter and Mann (1962; 1964; 1965) during the high temperature, high pH, aqueous oxidation of mild steel in the absence of oxygen.

One possible set of mechanisms for the formation of such films on carbon and low alloy ferritic steels between 200 and 300 ^{0}C has been briefly described by Garnsey, Hearn and Mann (1972) and more fully reviewed by Mann (1976). For these systems it has been proposed that the rate of reaction (total corrosion rate) is controlled by the diffusion of water soluble iron species through pores in the oxide layer (Castle and Masterson, 1966). Approximately half of the oxidised iron is incorporated in the magnetite formed at the metal surface (inner layer) and the remainder is transported in solution to the outer side of the oxide where it may precipitate (outer layer) or be released into the bulk solution to precipitate elsewhere (Castle and Mann, 1966). The inner layer is microcrystalline (porosity about 10%) and contains those alloying elements, such as chromium, in the parent material which form oxides of low solubility; the outer layer exhibits larger magnetite crystals (~ 1 μm) which contain some manganese or nickel. The corrosion rate depends on the dissolved iron flux, which is defined by the concentration gradient of dissolved iron, the length of the diffusion path, and an appropriate diffusion coefficient. The corrosion rate decreases with increased film thickness and is closely related to the solubility of magnetite in the solution generated at the corrosion surface (Potter and Mann, 1962; 1964; Bignold, Garnsey and Mann, 1972). However, the diffusion of ions through the inner layer of magnetite without precipitation in the pores requires some explanation. Bignold et al (1972) proposed that the solubility of magnetite varies through the layer because of a change in stoichiometry of the magnetite. A possible explanation in some conditions (of less relevance to PWR) is that a hydrogen concentration gradient across the oxide layer can be associated with a diffusion gradient of soluble iron in equilibrium with the pore walls (Berge and Saint Paul, 1973; Berge, Ribon and Saint Paul, 1977). The need to resolve blocking of pores is eliminated if ions transfer through the inner oxide layer by solid state diffusion as proposed by Effertz (1972): O_2^- diffuses inwards along grain boundaries and other short circuit paths in the inner oxide and Fe^{2+} diffuses outwards along similar routes. This mechanism has been further developed by Tomlinson (1981) in order to account for the fraction of hydrogen which is observed to be generated at the metal-oxide interface. Garnsey (1979) has suggested that aqueous diffusion through a porous inner layer governs mild steel corrosion in strongly alkaline conditions whereas solid state diffusion is more appropriate in neutral solutions.

Indirect support for the two-layer structure and aqueous phase diffusion through a porous inner film comes from interpretations of loop studies of cobalt ion contamination of growing oxide films on type 304 stainless steel (Lister, 1975; 1976a; 1976b; Richardson, Castle, Large and

Tench, 1983), carbon steel (Lister, 1976a; 1976b) and Inconel 600 (Lister, 1979b). However, the fundamental corrosion process for structural materials under PWR conditions remains uncertain.

The flux of corrosion ions across the inner layer may be written:

$$J_i = - f D_i \frac{\Delta C_i}{X_i} \qquad (1)$$

The value of the diffusion coefficient, D_i, is that appropriate either to aqueous phase diffusion through the pores or to solid state diffusion depending on the nature of the corrosion process being described. In the former case the parameter f is a constant incorporating such factors as the porosity and tortuosity of the film. In the latter case f is some complex constant depending on parameters relevant to grain boundary, lattice and probably dislocation diffusion. The concentration difference, ΔC_i, depends on the electrochemical equilibria in the oxide. The total corrosion rate will depend on the relationship between the corrosion ion flux through the inner layer and the rate of incorporation at the metal-oxide interface.

2.2 Other Forms of Corrosion and Wear

Localised corrosion of major circuit materials is not a significant source of corrosion products compared with uniform corrosion. However, wear, erosion or erosion-corrosion of hard facing alloys such as Stellites may be significant contributors to ^{59}Co input (Bergmann, 1982) . Data on these processes are sparse (e.g. Dufrane and Naughton, 1983; Ocken, 1985).

2.3 Solid Corrosion Product Stability

It is convenient to discuss the stability of solid corrosion products under the general heading of corrosion but it should be noted that the following comments apply not only to corrosion films but also to circulating particulate corrosion products and corrosion product deposits.

Rummery and Macdonald (1975) performed thermodynamic calculations for the stability of solid corrosion products in aqueous systems containing hydrogen and oxygen at temperatures up to 300^{0}C. They showed that Fe_3O_4, $NiFe_2O_4$, NiO, CoO and $CoFe_2O_4$ should be stable at 300^{0}C for dissolved hydrogen concentrations within the range of typical PWR specifications, i.e. 10 to 50 STP cm^3 H_2 kg^{-1}. Thus the description of corrosion product solubility during operation at power (see Section 3.1.1) should not be complicated by variations in stability. Rummery and Macdonald (1975) also showed that these oxides should exhibit varying degrees of stability at lower temperatures. For example at 10 STP cm^3 H_2 kg^{-1} it is predicted that: Fe_3O_4 and $CoFe_2O_4$ should be stable over the temperature range 25 to 300 ^{0}C; CoO and NiO should be unstable below 235 and 290 ^{0}C respectively; and

$NiFe_2O_4$ should be unstable with respect to Ni and Fe_3O_4 below 200 °C. These predictions formed the basis for an interpretation by Bishop, Cunnane, Kennedy, Schmotzer and Stagg (1983) of circulating corrosion product levels in a PWR during the cooldown and oxygenation stages of shutdown. However, the transfer of activity to or release from out-of-flux surfaces during refuelling shutdown is not significant (see Section 1) so that corrosion product stability is unlikely to be a major feature of models for the formation, transport and deposition of radioactive corrosion products.

There have been some studies of the kinetics of relevant solid reactions under oxidising conditions. For example, surface oxidation of magnetite to haematite or maghemite has been investigated by Feitknecht and Lehmann (1959), Colombo, Fagherazzi, Gazzarrini, Lanzavecchia and Sironi (1964), Sidhu, Gilkes and Posner (1977), and Blesa, Maroto, Passaggio, Labenski and Saragovi-Badler (1978). Studies of kinetics under reducing conditions have emphasised the formation and subsequent decomposition of ferrous hydroxide to form magnetite, the Schikorr reaction (Schikorr, 1929; Evans and Wanklyn, 1948; Shipko and Douglas, 1956; Keston and Lasher, 1959). Hazell and Irving (1966) have considered the thermal decomposition of ferrous, nickel II and cobalt II hydroxides. Unfortunately, the understanding of corrosion film formation under PWR conditions is insufficient to establish the role of oxide transformations.

3. COOLANT-BORNE CORROSION PRODUCTS

3.1 Soluble Species

Soluble species may arise directly from the corrosion process or from the dissolution of solid oxides. The behaviours of the major soluble species, such as iron and nickel, are considered in the context of corrosion product solubility in Section 3.1.1. Cobalt is of major radiological significance although it is generally present at relatively low concentrations in the coolant. Its equilibrium with solid oxides and its tendency to precipitate on or to dissolve from solid oxides will be strongly dependent on the behaviour of the major soluble species. However, phenomena such as adsorption or ion exchange depend on the cobalt species in solution and this aspect is considered briefly in Section 3.1.2.

3.1.1 Solubilities of Major Species

Thermodynamic calculations (McDonald and Rummery, 1973) show that Fe_3O_4, CoO and Ni or NiO are the stable species in aqueous solutions containing dissolved hydrogen (0.1 MN m^{-2}) at temperatures $\gtrsim$ 280 °C in contact with pure Fe, Co and Ni, respectively.

Sandler (1979) found that fuel pin crud from six US PWRs consisted essentially of the spinel $Ni_xFe_{3-x}O_4$ containing some chromium. Neither nickel metal nor NiO was definitely identified as a separate phase. $Ni_xFe_{3-x}O_4$ may be regarded as a magnetite structure with some Ni^{++} substituted for Fe^{++} or as non-stoichiometric nickel ferrite $NiFe_2O_4$. (Values of x greater than 1 would imply the presence of nickel in a form other than nickel ferrite.) Values of x were in the range from 0.45 to 0.75. In Beznau I, one of the six reactors studied (Solomon and Roesmer, 1976) data are consistent with $x = 1.3 \pm 0.4$ for high power sub-assemblies (cycle 3). Data are also reported for Point Beach 1 which are consistent with $x = 0.9 \pm 0.3$ (cycle 1). Vanbrabant and de Regge (1980) found that particles in the coolants of Doel I and Doel II were of spinel structure containing mainly Fe, Ni and Cr in varying proportions. Superficial particles on out-of-flux surfaces have been observed with a wide range of compositions consistent with $0.3 < x < 2$ (Johnson, Griggs and Kustas, 1980; Pick, 1983). Similar ranges of compositions are observed in deposited and circulating corrosion products in Kraftwerk Union PWRs (Riess, 1976).

Corrosion product elemental compositions will obviously differ between circuits constructed of different materials. For example, values of x in the range 0.1 to 0.5 have been reported for out-of-flux deposits and circulating crud in the all stainless steel Chooz reactor (Frejaville, Marchal, Beslu and Lalet, 1974). A similar range of values was observed for fuel deposits and circulating crud in the Yankee reactor (Picone and Taylor, 1966). Deposits on the fuel cladding in the CANDU PHWRs at Douglas Point and Pickering 'A', which have Monel-400 SGUs and carbon steel piping (feeders and headers), exhibit values of x in the range 0.1 to 1.5 (Urbanic, Gray and Lister, 1979). Circulating crud and out-of-flux deposits in these reactors have values of x towards the upper end of this range (Montford and Rummery, 1975; Tomlinson, 1976a). Deposits on fuel cladding at ~ 100 EFPD in Bruce 'A', which has Inconel-600 SGUs, exhibit values of x in the range 0.1 to 0.3 (Urbanic et al., 1979).

Studies of the solubility of crud have therefore centred on the 'model' systems: magnetite, nickel ferrite and 'non-stochiometric' nickel ferrite.

Thermodynamic calculations of magnetite solubility (Tremaine, von Massow and Shierman, 1977; Macdonald, Shierman and Butler, 1972a) and fits to solubility data (Sweeton and Baes, 1970; Tremaine and LeBlanc, 1980) assume a reaction scheme for soluble ferrous species $Fe(OH)_b^{(2-b)+}$, of the form:

$$1/3\ Fe_3O_4 + (2-b).H^+ + 1/3\ H_2 = Fe(OH)_b^{(2-b)+} + (4/3-b).H_2O \quad (2)$$

Tremaine and LeBlanc (1980) assume that soluble ferric species $Fe(OH)_b^{(3-b)+}$ may also be present via:

$$1/3\ Fe_3O_4 + (3-b).H^+ = Fe(OH)_b^{(3-b)+} + (4/3-b).H_2O + 1/6\ H_2 \quad (3)$$

The equilibria of equations (2) and (3) for soluble ferrous (z=2) and ferric (z=3) species may be combined into:

$$1/3\ Fe_3O_4 + (z-b).H^+ + (4/3-z/2)H_2 = Fe(OH)_b^{(z-b)+} + (4/3-b)H_2O \quad (4)$$

The total iron solubility depends on the solubility constants $K_{z,b}$ thus,

$$C_s = \sum^{z,b} [Fe(OH)_b^{(z-b)+}] = \sum^{z,b} K_{z,b}[H^+]^{z-b}.\gamma_1^{z-b}.p(H_2)^{4/3-z/2}/\gamma_{z-b} \quad (5)$$

where γ_q are the activity coefficients of species with charge q and $p(H_2)$ is the hydrogen partial pressure. For H_2O equilibrium:

$$K_w = [H^+][OH^-]\gamma_1^2 \quad (6)$$

$[H^+]$ is obtained from the charge balance equation:

$$[H^+] - \frac{k_w}{[H^+]\gamma_1^2} + (z-b) \sum^{z,b} [Fe(OH)_b^{(z-b)+}] + [Me^+] = 0 \quad (7)$$

where $[Me^+]$ is the base ion molality, or the negative of the acid molality in a solution of a strong acid. In a solution of a weak acid, equilibrium constants are required for the acid dissociation reactions at the relevant temperatures, further terms must be added to equation (7) and a conservation equation must be introduced for the weak acid. See, for example, Appendix A of Solomon and Roesmer (1978) for pH calculations in boric acid.

Each solubility constant $K_{z,b}$ is given by:

$$-RT\ \ln K_{z,b} = \Delta G(T)$$

$$= \Delta G(T_o) - \Delta S(T_o).\{T-T_o\} - \Delta C_p.T.\ln(T/T_o) + \Delta C_p(T-T_o) \quad (8)$$

where T_o is usually taken as 298^0K.
Solubilities are therefore expected to depend on pH_T, temperature and the partial pressure of dissolved hydrogen, $p(H_2)$. Dependence on the latter is fairly weak since for ferrous species $C_s \propto p(H_2)^{1/3}$ and for ferric species $C_s \propto p(H_2)^{-1/6}$. The dependence on pH_T is complex; solubilities are

generally assumed to be independent of the pH-determining additive (boric acid, LiOH, KOH etc).

There have been numerous experimental studies of magnetite solubility in the temperature range 200 to 300 ^{0}C with hydrogen typically 10-20 STP $cm^{3}kg^{-1}$, and with a variety of alkalising reagents, occasionally in the presence of boric acid, yielding pH_{300} in the range 6 to 8 (Sweeton and Baes, 1970; Tremaine and LeBlanc, 1980; Lambert, Montel and Courvoisier, 1980; Styrikovich, Martynova, Kobyakov, Men'shikova and Reznikov, 1972; Balakrishnan, 1977; Kanert, Gray and Baldwin, 1976). An example of the variation of solubility with pH_{300} is illustrated in Fig. 2 which is reproduced from the work of Tremaine and LeBlanc (1980).

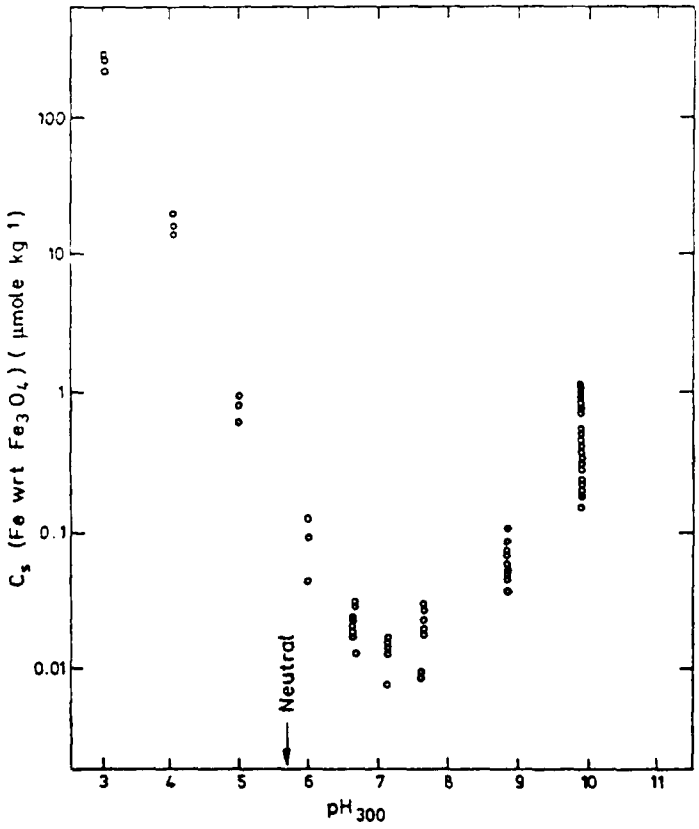

FIG. 2. Solubility of Fe_3O_4 at 300° C (from Tremaine and LeBlanc, 1980)

Thermodynamic calculations of nickel ferrite solubility must take account of the equilibrium between $NiFe_2O_4$, Fe_3O_4 and Ni (Macdonald, Rummery and Tomlinson, 1975; von Massow, Sullivan and Waugh, 1975):

$$3NiFe_2O_4 + 4H_2 \rightleftharpoons 2Fe_3O_4 + 3Ni + 4H_2O \qquad (9)$$

It is also necessary to account for the possible formation of non-stoichiometric nickel ferrite (Lambert, Montel and Courvoisier, 1983):

$$xNiFe_2O_4 + (1-x)Fe_3O_4 \rightarrow Ni_xFe_{3-x}O_4 \quad (10)$$

The solubilisation reactions are described by:

$$NiFe_2O_4 + H_2 + 6H^+ \rightleftharpoons Ni^{2+} + 2Fe^{2+} + 4H_2O \quad (11)$$

$$Ni^{2+} + mOH^- \rightleftharpoons Ni(OH)_m^{(m-2)-} \quad (12)$$

$$Fe^{2+} + nOH^- \rightleftharpoons Fe(OH)_n^{(n-2)-} \quad (13)$$

The application of these thermodynamic equilibria to the calculation of the solubility of magnetite and nickel ferrite at high temperature using the POTHY code is described by Beslu, Lalet, Joyer, Noe and Frejaville (1983).

Sandler and Kunig (1977; 1981) have measured the solubilities of a variety of synthetic non-stiochiometric nickel ferrites from room temperature to 350 ^{0}C with hydrogen typically 10-20 STP cm^{3}kg^{-1} and pH_{300} in the range 5.0 to 8.5.

These solubility studies show that at normal PWR operating temperatures (~ 300 ^{0}C) there is a negative temperature dependence of the solubility of iron in acidic solutions, a zero temperature dependence in some weakly alkaline solutions and a positive dependence in more strongly alkaline solutions. Solubilities of species other than iron with respect to mixed ferrites have been less well characterised. Solubilities in solutions containing boric acid generally increase at low temperatures ($\lesssim$ 100 ^{0}C).

3.1.2 Cobalt

Co(II) hydrolysis has been studied experimentally by several workers and some of the results are reviewed by Lambert (1975); however, more recent data (Giasson and Tewari, 1978) have been obtained for cobalt concentrations in the range 0.01-0.1 mole kg^{-1}, pH (25 ^{0}C) 4-9.5 and at 25-200 ^{0}C. The results over this limited pH range were adequately accounted for by a single hydrolysis equilibrium:

$$Co^{2+} + H_2O \overset{K_1}{\rightleftharpoons} Co(OH)^+ + H^+ \quad (14)$$

Values of pK_1 for two different standard states are listed in Table 1.

More comprehensive values have been extrapolated from thermodynamic data (Macdonald, Shierman and Butler, 1972b) using two solution equilibria in addition to (14) above:

$$Co^{2+} + 2H_2O \overset{K_2}{\rightleftharpoons} HCoO_2^- + 3H^+ \quad (15)$$

and

$$Co(OH)^+ + H_2O \overset{K_3}{\rightleftharpoons} HCoO_2^- + 2H^+ \quad (16)$$

TABLE 1

Co(II) Hydrolysis Constants

	Temperature, ^0C						Reference
	25	100	150	200	250	300	
pK_1 (μ_I=1)*	9.82	7.62	6.59	6.02			Giasson and Tewari (1978)
pK_1 (μ_I=0)	10.02	7.79	6.86	6.10			" " " "
pK_1	9.82	8.57	7.92	7.31	6.75	6.27	Macdonald, Shierman & Butler (1972b)
pK_2	31.83	25.71	23.23	21.41	20.11	18.86	" " "
pK_3	22.01	17.14	15.31	14.10	13.36	12.59	" " "

* μ_I= ionic strength

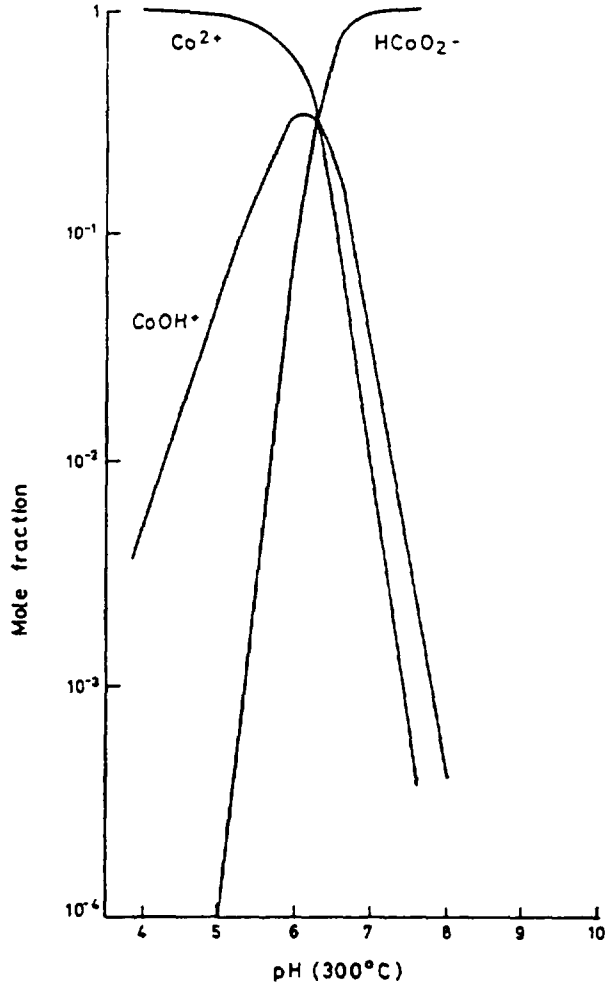

FIG 3. Thermodynamic Calculations of the Mole Fractions of Cobalt Solution Species at 300° C. Data from Macdonald, Shierman and Butler (1972b).

Values calculated for pK_1, pK_2 and pK_3 are listed in Table 1 and Fig. 3 shows plots of the mole fractions of the three Co(II) solution species against pH at 300 ^{0}C. This thermodynamic description is not complete since $Co(OH)_2$ has been neglected as a solution species and equilibrium with solid oxides is not considered. However, the available evidence suggests that the Co(II) solution species may be expected to be very strongly dependent on pH and temperature in the conditions encountered in PWR coolant.

3.2 Sources of Particulate Material

The sources of coolant-borne corrosion product particles are difficult to quantify. It is very likely that particulate material is released from precipitated outer layers or inner corrosion films by processes such as erosion or spalling, considered in Sections 6.1 and 6.2 respectively. Formation of particles by homogeneous or heterogeneous nucleation in the bulk coolant to relieve supersaturation is considered in this section. The review of spontaneous precipitation from electrolytic solutions by Furedi-Milhofer (1981) provides an interesting background to this section and Section 3.3.

3.2.1 Classical Theory for Homogeneous Nucleation

Several textbooks on precipitation and crystallisation (Nielsen, 1964; Walton, 1967; Mullin, 1972) present derivations of the rate of formation of critical nuclei based on classical theories (Volmer and Flood, 1934; Frenkel, 1955). The present work will follow the terminology of Nielsen (1964) in which: particles smaller than the critical size are called embryos; particles bigger than the critical size are called nuclei; and particles of critical size are critical embryos or critical nuclei.

After Twomey (1977), the rate of formation of spherical critical nuclei may be written:

$$J_n = 4\pi r_*^2 \beta N N_* \tag{17}$$

The radius, concentration and free energy of formation of the critical embryos are given by:

$$r_* = \frac{2v\sigma}{k_B T \log_e s} \tag{18}$$

$$N_* = N \exp\left(-\frac{\Delta G_*}{k_B T}\right) \tag{19}$$

$$\Delta G_* = \frac{16\pi}{3} \frac{v^2 \sigma^3}{(k_B T \log_e s)^2} \tag{20}$$

The expressions for r_* and ΔG_* need to be modified for non-spherical embryos; for example, the factor $\frac{16\pi}{3}$ in equation (20) for ΔG_* would become

32 for a cube. Factors for other geometric shapes are given by Nielsen (1964). The mass transfer coefficient for ions or molecules diffusing to a spherical particle of radius r_* (which is typically 10 to 100 Å) establishes an upper limit to the rate at which nucleation is predicted to occur and may be written (Treybal, 1968):

$$\beta = \frac{D}{r_*} \qquad (21)$$

The classical theory has been used successfully in many studies of nucleation in aqueous solutions (e.g Nielsen and Sohnel, 1971; Makrides, Turner and Slaughter, 1980). However, it should be remembered that in crystallisation the interfacial energy is not necessarily independent of embryo size (Frenkel, 1955) and that extra thermodynamic terms involving rotation, vibration and translation of the embryos become rather important for small embryos (Walton, 1967).

It is immediately apparent from equations (17), (19) and (20) that the nucleation rate is strongly dependent on the interfacial energy since the cube of this parameter appears in the exponent of the expression describing the concentration of the critical embryos. An indicaton of the appropriate value for interfacial energy may be obtained from the studies of hydrolysis-precipitation in iron solutions by Dousma and de Bruyn (1979). They derived values in the range 100 to 200 mJ m^{-2} for α-FeOOH at pH_{25}=2, temperature 25 °C and high ionic strength. Extrapolation to PWR conditions by making an appropriate allowance for the contribution of the electrical double layer to the interfacial energy (e.g. Kruyt, 1952) yields values between 250 and 650 mJ m^{-2}. It may be readily concluded that homogeneous nucleation in the bulk coolant is unlikely to be a significant source of coolant-borne particles.

3.2.2 Heterogeneous Nucleation

Volmer (1939) developed the classical nucleation theory for a spherical cap of crystalline deposit growing from solution on a solid surface. The situation is illustrated schematically in Fig. 4. It was shown that the critical free energy for heterogeneous nucleation ($\Delta G'_*$) could be written in terms of the critical free energy for homogeneous nucleation:

$$\Delta G'_* = \phi_1 \, \Delta G_* \qquad (22)$$

where $\phi_1 = \frac{(2+\cos\theta)(1-\cos\theta)^2}{4}$

$$\cos\theta = \frac{\sigma_{sl} - \sigma_{cs}}{\sigma_{cl}}$$

$$\sigma_{SL} = \sigma_{CS} + \sigma_{CL} \cos\theta$$

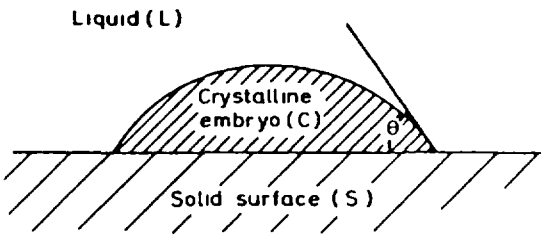

FIG 4 Nucleation on a Solid Surface

and the subscripts sl, cs and cl refer to the solid-liquid, crystal-solid and crystal-liquid interfaces respectively. Fig. 5 shows the dependence of ϕ_1 on θ. It can be seen that the critical free energy for nucleation can be significantly reduced for values of θ less than $\sim 90^0$. In particular, for complete affinity $\theta = 0$, $\phi_1 = 0$ and therefore $\Delta G^1_* = 0$.

Thus, at least in principle, heterogeneous nucleation may be a significant source of coolant-borne corrosion product particles if there is a sufficient supply of suitable impurity particles in the charging or make-up flows. It may also contribute to the relief of supersaturation; particulate impurity initially providing nucleation sites for the soluble species and subsequently growing by precipitation. The significance of this contribution must be determined by comparison with the relief of supersaturation by precipitation on circuit surfaces.

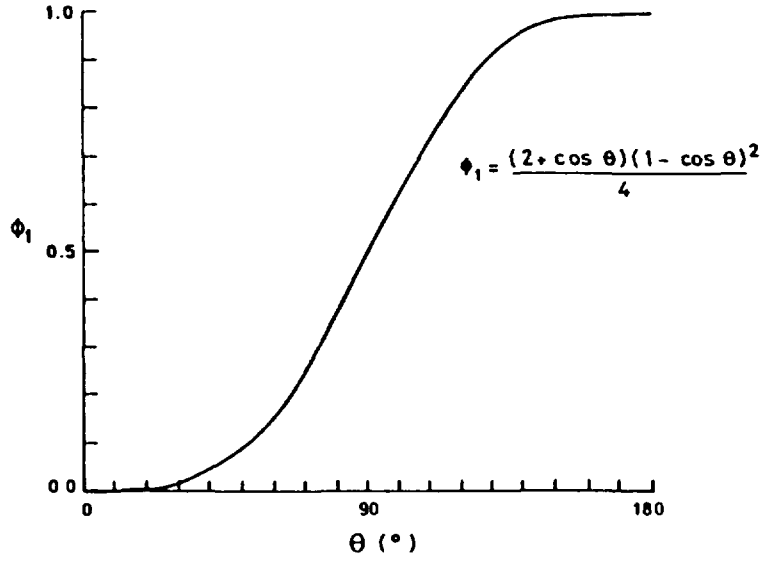

FIG. 5. Modification of Critical Free Energy for Heterogeneous or Secondary Nucleation. $\Delta G^1_* = \phi_1 \Delta G$

3.3 Dissolution and Growth of Particles

The mechanisms which govern the deposition of soluble species on circuit surfaces (Section 4) and dissolution of deposits or corrosion films from circuit surfaces (Section 6.4) also govern the growth from solution and dissolution of particles in suspension. Theories for the growth of precipitate particles (Ostwald ripening) have been reviewed by Kahlweit (1975). The tendency to precipitation or dissolution may be defined in terms of the relative magnitudes of the saturation solubility at the particle surface and the concentration of soluble species in the bulk solution over the surface; this is described in detail in Sections 4.2 and 6.4. It should be noted that the saturation solubility at the surface of a particle depends on particle size and will be increased relative to that for a plane surface by a factor which is given by equation (18) for a spherical particle with a homogeneous surface (Kelvin effect). Adsorption and desorption are described in Section 4.4. In any case the rate of transfer of soluble species to or from the surfaces of particles in suspension is described by a mass transfer coefficient and is considered in this section.

Mass transfer to particles in turbulent dispersion has been investigated by Kuboi, Komasawa, Otake and Iwasa (1974) who correlated their own and other available data by:

$$Sh_p = 2 + 0.49\,(Re_p Sc)^{1/2} \qquad \begin{matrix} 250 < Sc < 1100 \\ 0.2 < Re_p < 1000 \end{matrix} \qquad (23)$$

The particle Reynolds number, Re_p, depends on the velocity of the particles relative to the fluid due to turbulence and gravitational settling. Kuboi, Komasawa and Otake (1974) have presented a method for the derivation of this velocity.

3.4 Formation and Break-up of Agglomerates

3.4.1 Agglomeration

Agglomeration may be considered as a two stage process; transport of the particles relative to each other resulting in particle-particle collisions followed by the interaction of the colliding particles leading to the formation of agglomerates. In the absence of external body forces particle transport may occur as the result of Brownian motion, shear flow or turbulent motion. The treatment of agglomeration due to these various mechanisms is generally simplified by making the following assumptions:

(a) The agglomerating particles are spherical and monodisperse. In practice the particle size distribution will not be monodisperse and indeed as agglomeration proceeds even an originally monodisperse distribution will become polydisperse. Swift and Friedlander (1964) discuss the nature of the

particle size distribution in agglomeration by Brownian motion and shear flow.

(b) The particle volume fraction occupied by particles is sufficiently small that only binary collisions need be considered. This requires that the volume fraction is less than about 1%, a condition easily satisfied in water reactor circuits.

Smoluchowski (1917) showed that when agglomeration is controlled by Brownian diffusion the kinetics for the decay of total particle concentration may be written:

$$\frac{dn}{dt} = - \frac{4 k_B T}{3\mu} n^2 \qquad (24)$$

It is implicit in this formulation that each particle-particle collision results in agglomeration. Fuchs (1934) derived a modification of equation (24) to account for the effect of van der Waals and electrical double layer interactions between particles. An additional correction for the viscous interaction between particles has been derived by Spielman (1970) and Honig, Roebersen and Wiersema (1971).

When agglomeration is controlled by shear flow the rate of change of concentration for a system of particles of uniform size is given by (Swift and Friedlander, 1964):

$$\frac{dn}{dt} = - \frac{4\Gamma\Phi}{\pi} n \qquad (25)$$

The agglomeration of particles in turbulent flow may be described using simple mean free path concepts (e.g. Delichatsios and Probstein, 1975). The rate of decrease of particle number density is then given by:

$$\frac{dn}{dt} = - \frac{\pi}{2} d_p^2 u_r n^2 \qquad (26)$$

The relative velocity, u_r, depends on the turbulence scale and may be estimated from the work of Rotta (1972).

Means (1978) showed that the rate of agglomeration in PWR conditions is likely to be dominated by turbulent motion for particles bigger than about 1 μm and by Brownian motion for smaller particles.

3.4.2 Agglomerate Stability

An agglomerate will break-up in a turbulent flow unless the force of attraction between its constituent particles is sufficient to withstand the turbulent pressure fluctuations across its diameter and the shear forces associated with its motion relative to the fluid (Hinze, 1955; Levich, 1962).

The former is dominant for particles in water (Delichatsios, 1975; Delichatsios and Probstein, 1975). Thus, in principle, a maximum stable agglomerate size may be defined for given flow conditions and agglomerate strength; in practice, Means (1978) encountered difficulty in establishing the agglomerate strength under PWR conditions. Parker, Kaufman and Jenkins (1972) have developed a theory for the kinetics of floc break-up in turbulent flows.

4. DEPOSITION OF SOLUBLE SPECIES

4.1 Mass Transfer in the Coolant

Transfer of soluble species from the coolant bulk to the vicinity of a surface, or vice versa, will be limited by Brownian diffusion through a boundary layer. Under these conditions it is appropriate to describe transfer in terms of a coefficient, having the dimensions of a velocity, which may be determined from empirical correlations for the relevant geometry and flow conditions (e.g. Treybal, 1968). Correlations are of the following form:

$$Sh = f\ (Re,\ Sc) \tag{27}$$

In a dilute, ideal solution, i.e. one in which the diffusion of the non-dissociating solvent is not significant, the diffusion coefficient of a binary electrolyte is given by the Nernst equation (e.g. Reid and Sherwood, 1966; Erdey-Gruz, 1974).

$$D = \frac{U_c U_a}{U_c + U_a} \left(\frac{|z_c| + |z_a|}{|z_c|\,|z_a|} \right) \frac{RT}{F} \tag{28}$$

At low temperatures, $\sim 20\,^{0}C$, measured diffusion coefficients are in good agreement with predictions from equation (28) based on measured mobilities. At higher temperatures values of mobility are less readily available and the extrapolation from measurements at low temperature must consider changes in the size, and possibly ionic form, of the kinetic units. A detailed examination of extrapolation to temperatures up to $300\,^{0}C$ has been presented by Lindsay (1981) in the context of SGU secondary water chemistry. An estimate of the diffusion coefficient at temperature may be obtained from (e.g. Reid and Sherwood, 1966):

$$D_T = D_{298}\, \frac{T}{298}\, \frac{\mu_{298}}{\mu_T} \tag{29}$$

where subscripts T and 298 refer to the respective absolute temperatures.

The Schmidt number for corrosion ions varies from about 100 at 25 ^{0}C to about 1 at 300 ^{0}C.

The flow conditions encountered in reactor primary and auxiliary coolant circuits are well approximated by fully developed turbulent flow in a circular pipe providing a suitable allowance is made for the effective diameter of non-circular flow passages. Measurements of mass transfer under these conditions have been made by many workers (e.g. Harriott and Hamilton, 1965; Mizushina, Ogino, Oka and Fukuda, 1971). Berger and Hau (1977) used data from these studies and their own to derive the following correlation:

$$Sh = 2 + c\, Re^{a}\, Sc^{0.33} \qquad 0.6 < Sc < 10^4 \qquad 10^4 < Re < 10^6 \qquad (30)$$

where $c = 0.0165 + 0.011\, Sc\, e^{-Sc}$

and $a = 0.86 - \frac{10}{(4.7+Sc)^3}$

An indication of the effect of rough surfaces may be obtained from the work of Dipprey and Sabersky (1963). A factor of about 3 enhancement of the mass transfer coefficient may be estimated for soluble species under PWR conditions for 'fully rough' pipes at Reynolds numbers in the range 10^4 to 10^6.

Mass transfer of ionic species in aqueous systems under other flow conditions and geometries has been comprehensively reviewed by Poulson (1983).

4.2 Precipitation

Precipitation may occur on a surface if the concentration of soluble corrosion products in the bulk coolant over a surface exceeds the saturation solubility at the surface. The precipitation rate has been treated in several reviews (Mullin, 1972; Nancollas, 1979; Hasson, 1979; Furedi-Milhofer, 1981). At steady state (see Fig. 6) it must be equated to the rate of mass transfer through the boundary layer and may be written:

$$\frac{dM}{dt} = k(C_b - C_w) \qquad (31)$$

The kinetics of surface reaction may be most simply accommodated if first order processes are postulated so that:

$$\frac{dM}{dt} = aC_w - B \qquad (32)$$

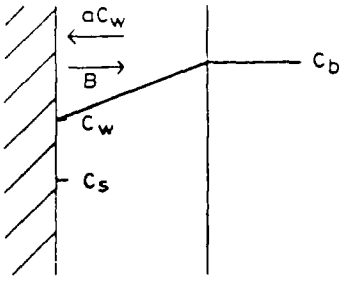

FIG 6 Precipitation on a Surface with First Order Surface Reaction

At equilibrium ($C_w = C_b = C_s$) the saturation solubility is therefore given by:

$$C_s = \frac{B}{a} \tag{33}$$

Thus the precipitation rate may be written:

$$\frac{dM}{dt} = \frac{ak}{a+k} (C_b - C_s) \tag{34}$$

The above is strictly applicable to a single dissolved species in contact with the pure solid. For one component of a mixed system the description is identical except that the solubility, C_s, is interpreted as that which is appropriate to the concentration of the species of relevance in the solid.

Theories resulting in higher order dependences on $(C_b - C_s)$ have been reviewed by Nancollas (1979), Nielsen (1981) and Furedi-Milhofer (1981).

4.3 Incorporation

Incorporation of soluble radioactive corrosion products, such as ^{60}Co, may occur in either the inner grown-on oxide or the outer precipitated oxide. A description of the processes requires a detailed understanding of the mechanisms controlling film growth which were discussed in Section 2. In particular, it must be emphasised that it is necessary to decide whether transport through the inner layer is more appropriately described by aqueous diffusion through pores or by solid state diffusion. The theoretical analysis which follows assumes the former mechanism and is essentially based on the model developed by Lister (1975; 1976a; 1976b; 1978; 1979b) to interpret his measurements of ^{60}Co incorporation into the oxide films on carbon steel, stainless steel, Inconel-600, Incoloy-800 and Monel-400 surfaces under conditions appropriate to CANDU-PHWR.

Lister's fundamental assumption is that the corrosion film develops on the metal surfaces in two layers as shown in Fig. 7. An inner layer grows due to corrosion of the base metal and activity is incorporated in this layer

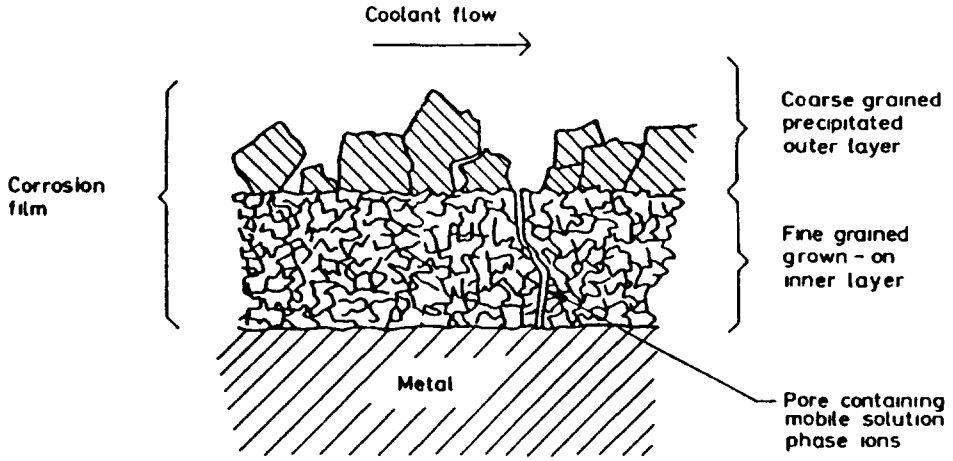

FIG 7 Two Layer Oxide Film Activity is Incorporated in the Outer Layer During Precipitation and in the Inner Layer after Diffusion Through the Porous Oxide Layers to the Oxide / Metal Interface

by diffusion of radioactive ions through pores in the material and incorporation into the oxide lattice as it grows at the metal/oxide interface. The outer layer grows by precipitation from solution and radioactive ions are incorporated in the oxide lattice during the growth process. A fraction (assumed by Lister to be one half) of the ions produced by the metal corrosion reaction are incorporated into the inner layer oxide at the oxide/metal interface; the remainder pass through the oxide layer and may be precipitated at the oxide/solution interface to form the outer layer or may be released into the bulk coolant to deposit elsewhere. It is also assumed that all soluble metal species behave identically and that the chemically insignificant quantity of radioactivity simply follows the behaviour of the major corrosion products, which can be adequately described by the solubility of magnetite or non-stoichiometric nickel ferrite as appropriate.

It must be remembered that the model as formulated describes only the activation process. It is implicit that there is no change in coolant chemistry which might cause dissolution of previously formed deposits or provide a tendency for solid state diffusion into or out of the oxide crystals.

The incorporation of a trace corrosion ion into the oxide films on a corroding surface is illustrated schematically in Fig. 8. The transfer from the coolant bulk may be described by:

$$J_w = \frac{kI}{k+I} c_b \qquad (35)$$

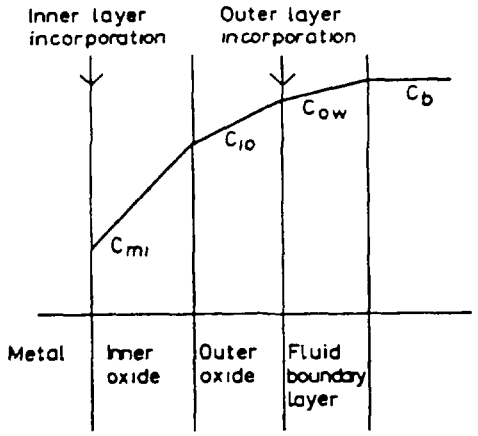

FIG. 8. Incorporation of Trace Species into Inner and Outer Layers of Growing Oxide.

The reaction rate constant for the incorporation mechanisms, I, may be written in terms of the resistances of the individual crystallisation and diffusion processes:

$$I = \frac{1}{CRYST_o} + \frac{1}{CRYST_i + DIFF_i + DIFF_o} \qquad (36)$$

The individual components may be written:

Incorporation in precipitation on the outer layer surface:

$$CRYST_o = \frac{1.5\, C_{so}}{\frac{dm_o}{dt} P_o} \qquad (37)$$

Diffusion through the outer layer:

$$DIFF_o = \frac{\tau_o m_o}{D_\ell \rho_o \phi_o (1-\phi_o)} \qquad (38)$$

Diffusion through the inner layer:

$$DIFF_i = \frac{\tau_i m_i}{D_\ell \rho_i \phi_i (1-\phi_i)} \qquad (39)$$

Incorporation at the metal-oxide interface:

$$CRYST_i = \frac{1.5\, C_{si}}{\frac{dm_i}{dt} P_i} \qquad (40)$$

The term $DIFF_o$ was not considered by Lister but has been included in the present work for the sake of completeness. The masses of the inner and outer layer oxides (m_i and m_o) and their rates of growth $\frac{dm_i}{dt}$ and $\frac{dm_o}{dt}$ must be determined from a model for base metal corrosion and duplex layer formation (Section 2). $\frac{dm_o}{dt}$ and m_o will also depend on the manner in which such a model is coupled with precipitation of material from the coolant bulk (Section 4.2).

4.4 Adsorption

While uptake of ions by oxides from aqueous solutions at room temperature is essentially a surface phenomenon (i.e. ignoring penetration into fine pores or lattice cavities as in zeolites), at high temperatures the possibility exists that adsorption will be followed by absorption, in which the adsorbed species penetrates the interface and diffuses into the oxide bulk. If the oxide crystallite is growing by precipitation this may be a particularly favourable situation for the uptake of hetero-ions, provided chemical properties are similar (e.g. crystal ionic radius), since the surface is continuously being renewed and hetero-ions become incorporated into the bulk by the crystal growth process (co-precipitation or co-crystallisation).

Adsorption of Co(II), which may in general be expected to be present as both positively and negatively charged solution species (Section 3.1.2), has been studied by a number of workers at temperatures up to 300 ^{0}C on a variety of oxide substrates under idealised conditions (Tewari, Campbell and Lee, 1972; Tewari and Lee, 1975; Tewari and McIntyre, 1975; Rommel, 1978; Bosholm, Glasel, Junge and Reinhard, 1978; Rommel, Sachse, Schlenkrich and Mittag, 1980; 1982; Blesa, Larotonda, Maroto and Regazzoni, 1982; Tamura, Matijevic and Meites, 1983; Rommel, 1983). The observed behaviour is generally describable in terms of Langmuir or Freundlich adsorption isotherms. The application of these data to reactor conditions is inhibited by the simultaneous occurrence of other phenomena such as modification of the substrate by corrosion, absorption and co-precipitation or co-crystallisation.

Lister, Kushneriuk and Campbell (1983) have studied the contribution of adsorption/desorption to the deposition of ^{60}Co on continuously changing surfaces of Zircaloy oxide at 300 ^{0}C.

5. PARTICULATE DEPOSITION

5.1 Transport to Surfaces

It is convenient to distinguish between colloidal ($\lesssim$ 1 μm) and inertial ($\gtrsim$ 1 μm) coolant-borne particulate material since their transport to circuit surfaces is controlled by distinctly different mechanisms (Ponting and Rodliffe, 1983). Transfer of colloidal material will be limited by Brownian diffusion through a boundary layer and may be determined from empirical mass transfer correlations (Section 5.1.1); transfer of inertial material will be limited by inertial projection through a boundary layer and may be estimated from modification of aerosol theory (Section 5.1.3). In addition both colloidal and inertial material will be subjected to the

influence of thermophoresis on heat transfer surfaces, tending to inhibit their deposition on fuel can surfaces whilst promoting it on steam generator tubes. Thermophoresis is only significant for larger colloidal material, about 0.1 to 1.0 μm diameter, and is considered in Section 5.1.2.

5.1.1 Brownian Diffusion

Transfer of colloidal particulate from the coolant bulk to the vicinity of a surface, or vice versa, will be limited by Brownian diffusion through a boundary layer and may be described in terms of a mass transfer coefficient identical in concept to that for ionic species (Section 4.1). Thus the diffusion coefficient may be written (Einstein, 1905):

$$D_B = \frac{k_B T}{3\pi\mu d_p} \qquad (41)$$

For non-spherical particles the diameter, d_p, must be replaced by an appropriate effective diameter determined by the shape. If the particle surface is charged (see Section 5.2.4) the diffusion coefficient will need to be modified (Bruins, 1931a; 1931b; 1931c; 1932). This effect is potentially significant for particles smaller than 0.1 μm but detailed calculations are presently unwarranted in view of the uncertainties in surface electrical properties.

The Schmidt number for a 1 μm diameter particle in water at 300 ^{0}C is about 10^4. Thus the correlation of Berger and Hau (1977) for fully developed turbulent pipe flow (Section 4.1, equation (30)) will be directly applicable to all colloidal particulate material in coolant at operating temperature. The Schmidt number is greater at lower temperatures and below about 200 ^{0}C some extrapolation will be required outside the range of experimental data. An indication of the effect of rough surfaces may be obtained from the work of Dipprey and Sabersky (1963). For example, Rodliffe (1980) calculated a factor of about 10 enhancement of the mass transfer coefficient for 55 nm particles in water at about 300 ^{0}C in a 'fully rough' pipe at Reynolds numbers in the range 4×10^4 to 2×10^5.

5.1.2 Thermophoresis

The phenomenon of thermophoresis arises when particles suspended in a fluid are subject to a temperature gradient and as a result experience a force. This force acts in the opposite direction to the temperature gradient and arises from the unequal velocity distributions of molecules in the hotter and cooler regions of the fluid, resulting in unequal transfer of momentum tangential to the particle surface. When the particle system is in equilibrium the particles exhibit a constant velocity known as the thermophoretic velocity.

Much work has been done to derive equations suitable for all conditions in gas systems (Talbot, Cheng, Scheter and Willis, 1980). However, the application of these equations to liquid systems is open to criticism. The existence of thermophoresis in liquid systems has been demonstrated experimentally by McNab and Meisen (1973) who determined the following equation for the thermophoretic velocity which should be valid for corrosion product particles in PWR coolant:

$$u_T = -0.26 \frac{K_a}{2K_a + K_p} \frac{\nu}{T} \frac{dT}{dy} \qquad (42)$$

It can be shown that thermophoresis may be considered to contribute an additional convection term to the diffusion equation of colloidal particles such that:

$$J_h = -D_B \frac{dC}{dy} + u_T C \qquad (43)$$

Then at equilibrium the boundary layer transfer coefficient, k_p, can be shown to be modified by thermophoresis to a value k_p' given by:

$$k_p' = \frac{u_T}{\exp(u_T/k_p) - 1} \qquad (44)$$

The thermophoretic velocity may be calculated from a knowledge of the temperature gradient in the boundary layer.

The effect is likely to be significant only in the size range 0.1 to 1.0 μm (Ponting and Rodliffe, 1983). It should be noted that the effect of thermophoresis will vary along the length of a fuel pin since the temperature difference between the fuel can surface and the bulk coolant varies significantly.

5.1.3 Inertial Deposition

The inertial character of a particle in a fluid is generally defined by a parameter known as the relaxation time (Fuchs, 1964), which is a measure of the time taken by the particle to respond to changes in the velocity of the surrounding fluid defined in the equation of particle motion (dimensionless form) as follows:

$$\frac{dv^+}{dt^+} + \frac{(v^+ - u^+)}{\tau^+} = \beta^+ \frac{du^+}{dt^+} \qquad (45)$$

where the Bassett history term has been omitted for simplicity.

It may be shown that the dimensionless relaxation time is given by (Ponting, 1982):

$$\tau^+ = \frac{1}{18}\left(\frac{d_p u_\tau}{\nu}\right)^2 \left(\frac{\rho_p}{\rho_f} + 0.5\right) \qquad \frac{d_p u_\tau}{\nu} < 2 \qquad (46)$$

Inertial behaviour becomes important in deposition from turbulent pipe flows when the dimensionless relaxation time is greater than about 0.3, since it is then possible for some of the particles projected across the laminar layer to reach the wall before their velocities have been reduced to those of Brownian proportions.

The theories of Friedlander and Johnstone (1957), Beal (1970), Liu and Ilori (1974) and Reeks and Skyrme (1976) give good agreement with data for inertial deposition of aerosols on perfectly sticky surfaces over relatively wide ranges of dimensionless relaxation time. Comparable data are not available for water systems where it appears to be difficult to achieve perfect sticking. The present poor knowledge of the magnitudes of the physical quantities defining the sticking process (Section 5.3) precludes an unambiguous validation of any theory for water systems.

The flux of particles to a surface may be described in the simplest terms by a Fick's law expression incorporating a coefficient for turbulent diffusion:

$$J_h = -(D_B + \varepsilon_t) \frac{dC_h}{dy} \qquad (47)$$

This equation may be solved given an expression for the eddy diffusivity, ε_t, and a suitable boundary condition. In some cases (Friedlander and Johnstone, 1957; Beal, 1970) it is assumed that particles need only diffuse to within one stopping distance from the wall and thereafter travel to the wall by virtue of their momentum. The stopping distance is defined as the distance travelled by a particle with a given initial velocity in a stagnant fluid under the influence of drag forces alone. The initial velocity is generally considered to be approximately equal to the friction velocity for the flow. Several authors (Browne, 1974; El-Shobokshy and Ismail, 1980; Wood, 1981) have extended this type of treatment to rough surfaces.

Reeks and Skyrme (1976) followed a fundamentally different approach to the formulation of the boundary condition. They assumed a two-stage process in which:

(i) Particles transfer by eddy diffusion from the fluid bulk to the interface with the laminar sub-layer.

(ii) Particles at the interface exhibit a distribution of velocities and thus a distribution of stopping distances so that only a fraction of the particles may penetrate to the surface.

This method provides a better mechanistic description of the process and since it allows finite velocities for particles reaching the surface it has the advantage that phenomena such as imperfect sticking due to bouncing may be amenable to analysis.

Ponting (1982) has considered the extension of the Reeks and Skyrme theory to aqueous systems. The dimensionless deposition velocity, ignoring effects due to the Basset history term in the particle equation of motion, may be written:

$$k_i^+ = 0.7\ \sigma_i^+ \operatorname{erfc}\left[\frac{5-(3\beta^+\tau^+)^{1/2} - \frac{d_r}{d_p}(12\beta^+\tau^+)^{1/2}}{\sqrt{2}\ \sigma_i^+\tau^+}\right] \quad (48)$$

The component of the dimensionless r.m.s. velocity of the particles on projection into the laminar sub-layer normal to the wall, σ_i^+, may be determined from the structure of turbulence normal to and close to the pipe wall (Reeks and Skyrme, 1976). It should be noted that the means of incorporating the effect of surface roughness, i.e. the term containing d_r, is valid only for hydraulically smooth surfaces, i.e. $\frac{u_\tau d_r}{\nu} < 5$, a condition which should be satisfied in PWR coolant circuits under most circumstances.

The theories of Beal (1970) and Ponting (1982) predict deposition velocities within a factor of 2 for values of τ^+ greater than 10. However, for $1 < \tau^+ < 10$ Ponting predicts that failure to allow for the effects of particle size and surface roughness cause Beal to underestimate deposition velocities by up to an order of magnitude. Values of τ^+ in the range 1 to 10 correspond approximately to particles of diameter 1 to 3 μm under PWR conditions.

5.2 Interaction with Surfaces

As in Section 5.1 it is convenient to distinguish between colloidal ($\lesssim$ 1 μm) and inertial ($\gtrsim$ 1 μm) particulate material. The general characteristics of colloidal and inertial particulate material are summarised in Table 2 (Ponting and Rodliffe, 1983).

Most of the forces which will be considered in this review have been quantified theoretically only for simple ideal systems. Consequently the following considerations will be based on an ideal system defined by a spherical homogeneous particle interacting with the surface of a semi-infinite slab of similar material with water as the intervening medium. Real system effects, such as those due to surface asperities and interfacial deformation, have been reviewed by Krupp (1967) and Visser (1973) but a detailed consideration in this note is unwarranted in view of the major uncertainties in the ideal systems.

5.2.1 Gravity

The gravitational force on a spherical particle resting on top of a horizontal surface is given by:

$$F_g = \frac{\pi}{6} d_p^3 (\rho_p - \rho_f) g \qquad (49)$$

The particle therefore experiences an effectively attractive force. A particle on the underside of a horizontal surface will of course experience an effectively repulsive force of magnitude defined by equation (49).

5.2.2 van der Waals Force

The van der Waals force of adhesion between a perfect sphere and a flat plate at small separations may be written (Hamaker, 1937):

$$F_v = \frac{Ad_p}{12H^2} \qquad (d_p >> H) \qquad (50)$$

The Hamaker constant, A, may be determined theoretically either from a microscopic approximation involving a simple summation over the individual contributions from the London interactions between the constituent atoms or molecules (Hamaker, 1937) or from a macroscopic approximation requiring a knowledge of the optical properties of the materials with respect to the whole electromagnetic spectrum (Lifshitz, 1956). In the latter case it is shown that the interaction is dominated by the ultra-violet region of the absorption spectrum and consequently equation (50) is only valid if the separation, H, is much less than about 1000 Å, in which case the force is termed unretarded.

Hamaker constants calculated by both methods have been compared with measurements of van der Waals forces for a very wide range of materials and have exhibited reasonable agreement (Krupp, 1967; Gregory, 1970; Visser, 1972; 1973; Coakley and Tabor, 1978). A significant error in the calculation of van der Waals forces in aqueous systems is likely to be introduced by the value estimated for the particle-surface separation (H). Krupp (1967) considers that a lower limit to the separation may be estimated from the interatomic spacing of the materials under consideration and is typically about 4 Å. For sub-micron carbon-black particles on cellulose film in water Visser (1970) determined a separation of 16 Å at the zero point of charge (i.e. in the absence of electrical double layer interaction). In a later study (Visser, 1976) of sub-micron polystyrene particles on cellophane in water a separation of about 20 Å was estimated at the zero point of charge. In both studies it was suggested that the separation is defined by the water structure in intimate contact with the surfaces. Some uncertainty is also

likely to be introduced by the particle-surface geometry of real systems although the magnitude of the uncertainty should be readily quantifiable using simple approximations. Krupp (1967) gives an account of a statistical approach to the geometry of the particle-substrate interface which allows for a distribution of the size of asperities. Simple correction factors have been proposed (van Bree, Poulis, Verhaar and Schram, 1974; Czarnecki and Dabros, 1980) to estimate the influence of surface roughness on the van der Waals attraction energy. Dahneke (1972) and Derjaguin, Muller and Toporov (1975) have considered the effects of contact deformations.

5.2.3 Magnetic Force

The force of adhesion for a uniformly magnetized sphere in contact with the surface of a semi-infinite magnetizable medium is (Rodliffe and Means, 1979):

$$F_m \approx \frac{1}{5} \mu_o \frac{(\mu_1 - 1)}{(\mu_1 + 1)} M_1^2 d_p^2 \qquad (51)$$

The magnitude of the force is approximately independent of separation providing $H \ll d_p$.

Haematite is not spontaneously magnetized so that in the absence of an externally applied magnetic field there is no significant magnetic interaction with an oxide surface. However, both magnetite and nickel ferrite are spontaneously magnetised and particles may exist as single domains up to 0.1 or 1 μm in size (e.g. Kittel, 1956). For particles much greater than about 1 μm the spontaneous magnetization will be less than that at saturation, because many domains will be present, so that the magnetic force will drop off rapidly with increasing size.

5.2.4 Surface Electrical Force

There are several possible contributions to the surface electrical potential of a deposition substrate. Firstly, the oxide film on the deposition substrate may undergo hydration followed by dissociation or ion adsorption. The interaction under these conditions is considered in this section. Secondly, a potential gradient may be established by some process such as substrate corrosion as considered in the first part of Section 5.4.

The surface charge of solid oxides and hydroxides may be qualitatively explained in terms of a two step process: surface hydration followed by either the adsorption of H_3O^+ and OH^- ions or the dissociation of the surface 'hydroxide' (Parks, 1965). The ion adsorption or surface dissociation may be described by:

$$H_3O^+ + MOH_s \rightleftharpoons M(H_2O)_s^+ + H_2O \qquad (52)$$

$$OH^- + MOH_s \rightleftharpoons MO_s^- + H_2O \qquad (53)$$

where the subscript s refers to surface species.

In the absence of specific adsorption, which will be considered later, the ions H_3O^+ and OH^- define the surface charge, and thus the surface potential, and are known as the potential determining ions (pdi) of the system. The sign and magnitude of the nett charge on the surface will thus depend on the pH of the solution and the affinities of the surface for the potential determining ions.

In the absence of specific adsorption the electrical potential of the surface relative to the bulk solution may be determined by considering a potential determining ion and equating the chemical potential difference between surface and bulk solution to the electrical work required to bring the ion from the bulk to the surface. The surface potential may then be written (Parks and de Bruyn, 1962) in terms of the pH of the bulk solution and the point of zero charge (pzc), which is the solution pH at which the surface carries zero nett charge:

$$\psi(o) = 2.3 \frac{RT}{F} (pzc - pH) \qquad (54)$$

It is recognised that the simple Nernst equation (equation 54) is inaccurate for oxide-aqueous electrolyte interfaces in general (Furlong, Yates and Healy, 1981) although de Bruyn (1978) states that no major objection can be raised to its application to metal hydroxides and oxyhydroxides (e.g. FeOOH). A study on authentic corrosion products at temperatures up to 300^0C is obviously desirable to resolve this issue.

The theory for the interaction between two double layers, each described by Gouy-Chapman theory (Gouy, 1910; Chapman, 1913), was given by Derjaguin and Landau (1941) and Verwey and Overbeek (1948). The case of two dissimilar particles with $\kappa d_p >> 1$ has been analysed by Hogg, Healy and Fuerstenau (1966) and Wiese and Healy (1970) for assumptions of constant potential and constant charge interaction respectively. For a spherical particle interacting with a plane surface of dissimilar surface chemistry, i.e. different surface electrical potentials $\psi(o)_1$ and $\psi(o)_2$, the electrical double layer force may be written for interaction at constant potential, if $H < d_p$:

$$F_e^{\psi} = \pi\varepsilon_1\varepsilon_o d_p(\psi(o)_1^2 + \psi(o)_2^2) \frac{\kappa exp(-\kappa H)}{1-exp(-2\kappa H)} \left[\frac{2\psi(o)_1\psi(o)_2}{(\psi(o)_1^2 + \psi(o)_2^2)} - exp\ (-\kappa H) \right] \qquad (55)$$

For constant charge interaction, if $H < d_p$:

$$F_e^{\sigma} = \pi\varepsilon_1\varepsilon_o d_p\ (\psi(o)_1^2 + \psi(o)_2^2)\ \frac{\kappa exp(-\kappa H)}{1-exp(-2\kappa H)} \left[\frac{2\psi(o)_1\psi(o)_2}{(\psi(o)_1^2 + \psi(o)_2^2)} + exp\ (-\kappa H) \right] \qquad (56)$$

The interaction potentials from which the forces in equations (55) and (56) were derived are strictly applicable to situations in which $\left|z_1 e\psi(o)\right|$ is less than $k_B T$ but should be good approximations up to about 200 mV in water at 300°C.

The assumption of a planar interface, i.e. $\kappa d_p > 10$, limits the application of the expressions in equations (55) and (56) to particles which are defined as inertial ($d_p \gtrsim 1$ μm) in this work. The electrical double layer interaction for colloidal particles ($d_p \lesssim 1$ μm) is considered in Section 5.4.

The two assumptions for the interaction, i.e. constant potential and constant charge, represent extremes in possible behaviour. When two surfaces are brought together the ion populations at the surface and in the intervening solution will tend to adjust for the effectively different solution chemistry. The time constant for the response of the ion populations must therefore be compared with the time constant for the process bringing the surfaces together. The latter would have very different values for particle-particle collisions in turbulent flow and for particles settling onto a horizontal surface. If the time constant for ion response is small compared with that for surface interaction, so that equilibrium is maintained, then the constant potential assumption is relevant. If the time constant for ion response is large compared with that for surface interaction, so that equilibrium is not achieved, then the constant charge interaction is relevant. The general situation has been considered by Chan, Perram, White and Healy (1975). Lyklema (1980) has considered the rates of adjustment of ion populations in the diffuse layer and on the surfaces in the context of a Brownian encounter.

The point of zero charge may be equated to the iso-electric point in the absence of specific adsorption. There are some measurements of the points of zero charge of oxides similar to those encountered in PWR but there are very few data on temperature dependences with which to extrapolate to 300°C. The theory of the temperature dependence of the point of zero charge of metal oxides has been discussed by Bérubé and de Bruyn (1968).

The electrophoretic mobilities of ZrO_2 particles in aqueous dispersion in the temperature range 25 to 80°C have been studied by Maroto, Blesa, Passaggio and Regazzoni (1981). The resulting iso-electric point at 25°C was 6.5 and the temperature dependence followed $\frac{1}{2}\,pK_w$. Thus a pzc of about 5.2 was predicted by extrapolating the dependence on pK_w to 300°C. However, these values are not consistent with the streaming currents measured by Tewari and Campbell (1972) on freshly machined Zircaloy capillary at 25 and 200°C.

Tewari and McLean (1972) and Tewari and Campbell (1976) reported pzc in the temperature range 25 to 90^{0}C for a number of oxides and hydroxides of iron, nickel and cobalt. Potentiometric titration and electrophoretic mobility measurements on NiO, $Ni(OH)_2$, $Co(OH)_2$ and Co_3O_4 revealed a similar behaviour to ZrO_2, i.e. (pzc - $\frac{1}{2}$ pK_w) was independent of temperature, and may be extrapolated to values of pzc in the range 9-10 at 300^{0}C. A third method based on the measurement of the pH for the primary equilibrium distribution of H^+ and OH^- ions yielded somewhat lower values of pzc. The pzc of magnetite showed a change greater than $\frac{1}{2}$ pK_w and may be extrapolated to a value of 4.1 at 300^{0}C if an Arrhenius temperature dependence is assumed. The temperature dependence of magnetite pzc has been confirmed by Blesa, Figliolia, Maroto and Regazzoni (1984) but their interpretation of the corresponding enthalpy and entropy changes attending ionization suggests that an Arrhenius extrapolation up to 300^{0}C may not be valid. Room temperature measurements of the points of zero charge or iso-electric points of iron and chromium oxides and hydroxides (Parks, 1965) and nickel ferrite (Tomlinson, 1976b) exhibit a wide scatter and are very dependent on the methods of preparation but are generally in the range 4 to 7. Kittaka and Morimoto (1980) have studied the iso-electric point of binary metal oxides having spinel structure and reported values in the range 4 to 7 for $NiO-Fe_2O_3$ with nickel compositions between 5 and 50%. For oxides dominated by iron and chromium (i.e. Ni $\leq$ 50%) extrapolation of all these data to 300^{0}C, based on either $\frac{1}{2}$ pK_w or the Arrhenius dependence for magnetite, yields values which are less than 6. Martynova, Gromoglasov, Mikhailov and Nasyrov (1977) measured the electrophoretic mobilities of particulate corrosion products of indeterminate composition from the condensate of the Russian MEI heat and power station at pH_{25} = 8.8 and temperatures up to 180^{0}C. The pzc estimated from these data at 25^{0}C is 8.5, which is higher than that observed by Tewari and McLean (1972) for magnetite although it exhibits a similar temperature dependence. Martynova et al (1977) also report similar measurements, at pH_{25} = 4.4 and temperatures up to 235^{0}C, on corrosion products obtained by electrolysis with austenitic steel. The pzc of this material may be estimated as 4.8 throughout the observed temperature range. Extrapolation of both sets of data to 300^{0}C, based on Arrhenius temperature dependences, gives values of about 5.

It should be noted that specific adsorption might be sufficient in some circumstances to reverse the surface charge when the pH is greater than the pzc. This effect has been observed for cobalt adsorption on the oxides of interest (Tewari, Campbell and Lee, 1972; Tewari and Lee, 1975; Tewari and McIntyre, 1975), although the cobalt solution concentrations were much higher

than those in a typical operating PWR. Surface flocculation following adsorption of ions released by substrate corrosion has been postulated (Rodliffe, 1980) as an explanation of auto-retardation in the deposition of colloidal magnetite particles on a steel surface (Thomas and Grigull, 1974). It should also be noted that adsorption of boric acid on magnetite and zirconium dioxide in aqueous suspensions has been shown to shift both the points of zero charge and the iso-electric points to lower pH values (Blesa, Maroto and Regazzoni, 1984). These major uncertainties in oxide surface electrical properties will only be resolved by measurements on representative samples, preferably from operating reactors, at temperatures up to 300 ^{0}C. It may also be necessary to consider the possible in-flux modification of surface properties by interaction with the products of radiolysis (Sellers, 1976).

5.2.5 Hydrodynamic Resuspension Forces

Corn (1966) outlines the calculation of tangential drag forces acting on a particle resting on a surface. For a spherical particle the force may be written:

$$F_d = f_d C_d(Re_p) \frac{1}{2} \rho_f \bar{u}^2 \frac{\pi d_p^2}{4} \qquad (57)$$

The particle drag coefficient and appropriate methods for averaging the fluid velocity have also been considered by Corn (1966). The factor f_d has been evaluated by O'Neill (1968) for a sphere in contact with a plane wall in a slow linear shear flow (i.e. $Re_p < 2$) and has the value 1.7.

The lift force on a spherical particle in a slow linear shear flow (i.e. $Re_p < 2$) may be estimated from the theory of Saffman (1965) and may be shown to be insignificant in magnitude compared with the tangential drag. The lift force is similarly insignificant in other circumstances (Corn, 1966).

5.2.6 Other Factors

The adhesion of particles may be affected in the longer term by processes such as sintering and ion bonding (Krupp, 1967; Visser, 1968; 1973). For example, Hopkins (1973) and Hopkins and Epstein (1974) have postulated that the products of substrate corrosion may bind deposited particulate material more firmly in order to explain their observations of the thermal fouling of stainless steel tubes by flowing ferric oxide suspensions. These effects have not been systematically investigated for corrosion products in high temperature aqueous systems.

5.3 Inertial Particle Sticking

The interaction of inertial particles with circuit surfaces may be significantly modified by hydrodynamic forces (Rodliffe and Means, 1979).

Sticking requires that a particle should (i) have sufficient energy to overcome any barrier due to electrical double layer repulsion, (ii) should lose sufficient energy to be retained within the potential well produced by attractive forces (Dahneke, 1971), and (iii) should be stable against short term resuspension, i.e. the adhesion force should exceed the hydrodynamic force of resuspension. The sticking probability will thus depend on the availability of suitable sites, the geometries and mechanical properties of the particle and the substrate, and the nature of the interaction potential. Theories to describe sticking have not been sufficiently developed to enable reliable predictions or interpretations of experimental data. The deposition rate may be written:

$$J_h = f_p k_i C_h \tag{58}$$

Beal (1978) used data from laboratory experiments to determine a correlation between sticking probability, f_p, and the dimensionless particle relaxation time, τ^+, (a function of particle size and flow conditions). Means, Rodliffe and Harding (1980) measured deposition rate constants as a function of particle size in the Winfrith Steam Generating Heavy Water Reactor from which a sticking probability of $\sim 10^{-3}$ was inferred for particles bigger than 2 μm. In both cases the evaluation of sticking probability relies on the prediction of arrival rates using theories which have not been validated for water systems (see Section 5.1.3).

5.4 Surface Reaction Rate for Colloidal Particles

The interaction of a corrosion product particle with an electrical potential gradient of thermal or galvanic origin at a circuit surface has been considered by Brusakov (1971) and Brusakov, Sedov, Khitrov and Rybalchenko (1983). An electrophoretic velocity may be defined:

$$u_e = -U_p \frac{d\psi}{dy} \tag{59}$$

The effect of electrophoresis on transfer through a boundary layer in the presence of a uniform electric field may then be described by analogy with the expression for thermophoresis in equation (44):

$$k_p' = \frac{u_e}{\exp(u_e/k_p)-1} \tag{60}$$

The mobility of colloidal corrosion product particles may be determined from experimental measurements (Brusakov et al., 1983) and approximate analytic expressions (Ohshima, Healy and White, 1972b).

In certain circumstances the electrical double layer interaction may produce a potential barrier of the general form shown in Fig. 9 which

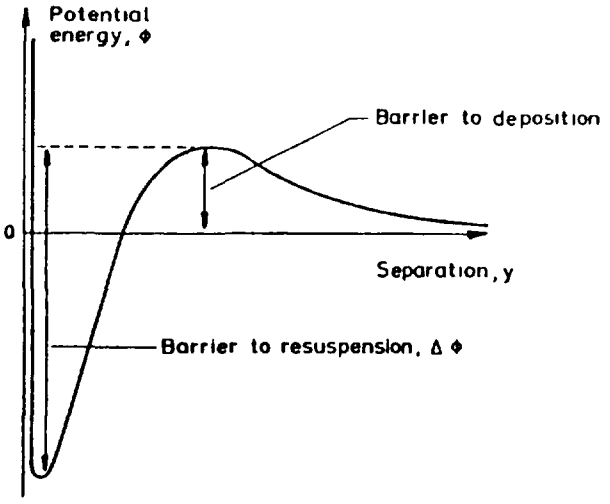

FIG 9. Interaction Potential for Combination of Attractive van der Waals and Repulsive Electrical Double Layer Forces.

must be overcome if deposition is to occur. Various authors (Ruckenstein and Prieve, 1973; Spielman and Friedlander, 1974; Dahneke, 1974; Bowen, Levine and Epstein, 1976; Prieve and Ruckenstein, 1976; 1977; 1978; Adamczyk and Dabros, 1978) have shown that deposition in such circumstances may be described by a first order surface reaction rate constant imposed as a boundary condition on the particle diffusion equation. Such a description is valid provided the interaction with the surface is confined to a region which is smaller than the boundary layer, a condition which is satisfied in the PWR circuit. The deposition rate is given by:

$$\frac{dQ}{dt} = \frac{a\, k_p}{a + k_p} C_h \tag{61}$$

where the apparent surface reaction rate constant is:

$$a = \frac{D_B}{\int_o^\delta (\alpha_1 \exp(\phi/k_B T) - 1)\, dH} \tag{62}$$

The surface proximity drag factor, α_1, is generally determined from an analytical approximation (Dahneke, 1974). For large values of the interaction potential (i.e. $\phi > 10\ k_B T$) equation (62) may be accurately approximated by (Bowen and Epstein, 1979):

$$a = \frac{D_B}{\alpha_m} \left(\frac{\gamma}{2\pi k_B T} \right)^{1/2} \exp\ (-\phi^{max}/k_B T) \tag{63}$$

Clearly in order to evaluate this surface reaction rate constant it is necessary to determine explicitly the form and magnitude of the potential for the interactions identified in Table 2.

TABLE 2

Properties of Colloidal and Inertial Particles
(Ponting and Rodliffe, 1983)

Particle Diameter	Colloidal Particles	Inertial Particles
	< 1 μm	> 1 μm
Boundary layer mass transfer mechanism	(i) Brownian diffusion (ii) Thermophoresis (0.1-1.0 μm) at heat transfer surfaces	(i) Inertial projection (ii) Gravitational settling (> 100 μm)
Dominant forces acting on particles	(i) van der Waals (ii) Electrical double layer (iii) Magnetic (0.1-1.0 μm) if substrate is magnetisable	(i) van der Waals (ii) Electrical double layer (iii) Gravity (> 100 μm) (iv) Hydrodynamic drag
Surface interaction parameter	Surface reaction rate constant	Sticking probability

In PWR the maximum in the interaction potential occurs at sufficiently small particle-surface separations such that only the unretarded van der Waals interaction need be considered. Between a sphere and a flat plate the potential may be written (Hamaker, 1937):

$$\phi_W = A\left[\frac{1}{6}\ln\left(\frac{H+d_p}{H}\right) - \frac{1}{12}\frac{d_p}{H}\frac{2H+d_p}{H+d_p}\right] \qquad (64)$$

The Hamaker constants for the oxides in a PWR may be estimated from data at 20^0C (Visser, 1972) and are likely to be in the range 2 to 8 x 10^{-20} J (Rodliffe and Means, 1979).

The magnetic interaction potential between a uniformly magnetised sphere and a semi-infinite magnetizable medium may be evaluated from the analysis of Rodliffe and Means (1979):

$$\phi_M \cong -\frac{\pi}{96} M_1^2 \mu_o \frac{d_p^6}{(2H+d_p)^3} \qquad (65)$$

The electrical double layer interaction may be repulsive or attractive, depending on the similarity or otherwise of the signs of the surface electrical potentials, and will vary significantly with pH and ionic strength. The inverse diffuse layer thickness (κ) is about 2 x 10^7 m^{-1} in

PWR (in range 10^7 to 5×10^7 m^{-1} for pH_{300} 6.2 to 7.6 respectively) so that the assumption of a planar interface (strictly $\kappa d_p > 10$) used by Hogg, Healy and Fuerstenau (1966) in their derivation of the interaction potential is not generally valid for the particles defined as colloidal (i.e. $d_p < 1$ μm, $\kappa d_p < 20$). The expression of Verwey and Overbeek (1948), for the interaction of two similar particles when $\kappa d_p < 1$, can be modified by analogy with the expressions of Hogg et al to describe the interaction of a spherical particle with a dissimilar plane surface. For either constant potential or constant charge assumptions the electrical double layer potential may be approximated by:

$$\phi_E \cong 0.6\ \pi\ \varepsilon_1 \varepsilon_o\ d_p^{\,2}\ \frac{\psi(o)_1 \psi(o)_2}{(H+d_p)}\ e^{-\kappa H} \qquad (66)$$

More rigorous methods for calculating this potential are available (Bell, Levine and McCartney, 1970; Barouch, Matijevic, Ring and Finlan, 1978; Ring, 1982; Oshima, Healy and White, 1982a).

The methods outlined in this section have been used by Ponting and Rodliffe (1983) to investigate the ways in which the deposition of colloidal corrosion products on fuel clad surfaces might be minimised.

6. RELEASE MECHANISMS

The distinction between colloidal and inertial particles (see Table 2) is also useful when considering resuspension. Hydrodynamic forces tend to dominate the resuspension or erosion of inertial particles (Rodliffe and Means, 1979) whereas Brownian motion dominates the resuspension of colloidal particles.

6.1 Particle Entrainment by Hydrodynamic Forces

Force balance approaches may be used to develop models for particle entrainment which are in good agreement with experimental data and correlations (Halow, 1973; Phillips, 1980). Consider the two simple particle-surface systems illustrated in Fig. 10. The perfect sphere-flat plate geometry is not considered because the application of a tangential force inevitably produces movement irrespective of the nett adhesion force. The criterion for lift-off may be written:

$$F_l > F_a \qquad (67)$$

The criterion for rolling (Fig. 10 a or b) may be written:

$$F_d > (F_a - F_l) \tan \theta_1 \qquad (68)$$

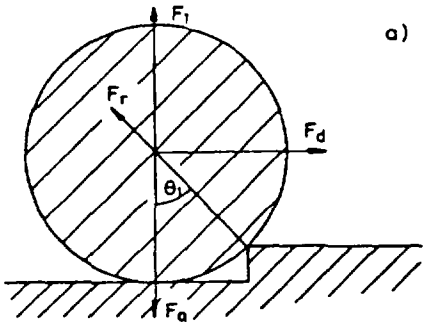

a) Perfect sphere-stepped surface Particle about to roll

$F_d \geq (F_a - F_l) \tan \theta_1$

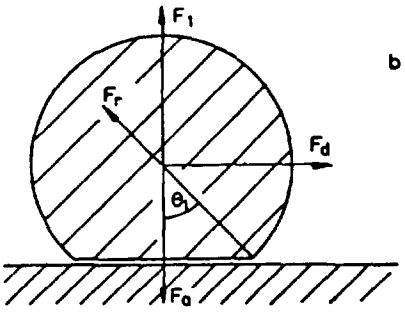

b) Flattened sphere-flat surface Particle about to roll.

$F_d \geq (F_a - F_l) \tan \theta_1$

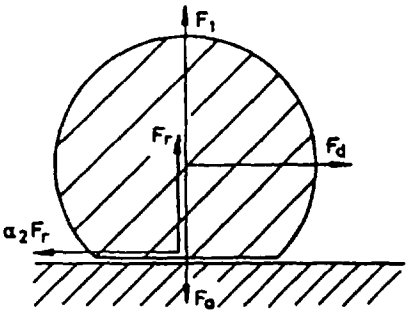

c) Flattened sphere - flat surface. Particle about to slide.

$F_d \geq \alpha_2 (F_a - F_l)$

FIG.10. Forces Acting on a Particle at Rest on a Surface.

The criterion for sliding (Fig. 10c) may be written:

$$F_d > \alpha_2 (F_a - F_l) \tag{69}$$

As considered in Section 5.2.5 the tangential drag is generally greater than the lift so that if the angle θ_1 is less than 45^0 it is more likely that particles in the system under consideration will slide or roll in preference to lifting-off. Whether the particle slides or rolls will then depend on the relative magnitude of tan θ_1 and the coefficient of friction, α_2. A simple description of this type has been used to develop empirical

correlations between the force of adhesion and the removal of submicron particles from various substrates in aqueous solutions (Visser, 1970). Under steady flow conditions it is more usual to describe re-entrainment by a first order rate constant (Epstein, 1978) so that the resuspension rate is given by:

$$\frac{dQ}{dt} = -EQ \qquad (70)$$

In studies of particulate fouling the resuspension rate constant, E, is generally correlated with the fluid shear stress at the wall. However, Beal (1978) derived a correlation with the drag force on a deposited particle using measurements on sand grains (Watkinson, 1968) and naturally occurring corrosion products (Pattison and Walton, 1961) in water. The correlation is not claimed to have any theoretical basis and is subject to considerable uncertainty due to ignorance of the particle size distribution in the latter study. A mechanistic derivation of the resuspension rate constant has been presented by Cleaver and Yates (1973) who described the interaction between deposited particles and the turbulent bursting process in the viscous sublayer. However, absolute predictions with this model require normalisation to experimental data.

During transient flow conditions it is possible that resuspension may be enhanced. For example, Punjrath and Heldman (1972) postulated that the maximum probability of re-entrainment could be at the location where the boundary layer changes from laminar to turbulent. Thus a change in flow conditions would change the location of the transition and could result in the resuspension of previously stably deposited particles.

Finally, it should be noted that particulate deposits may undergo sintering or some form of chemical bonding (see Section 5.2.6) so that they become too tightly bound to the surface to be resuspended by hydrodynamic forces. Beal (1973) describes this conversion from 'loose' to 'adherent' forms in terms of a first order rate constant.

6.2 Spalling

In the present work spalling will be defined as the release of particulate material as a result of the inability of an otherwise adherent film to withstand the strains imposed by various operational procedures. Armitt, Holmes, Manning, Meadowcroft and Metcalfe (1978) have comprehensively reviewed models for the strain-tolerance of duplex oxide layers specifically for austenitic and ferritic steels in steam environments. They presented expressions for strains, including those due to cooling, heat flux transients and oxide transformation, and outlined the options for stress relief which could lead to spalling.

6.3 Release of Colloidal Particles

A deposited colloidal particle may be considered to sit in a potential well as illustrated in Fig. 9. Such a particle may occasionally overcome the potential barrier because of random Brownian motion and may be carried away by diffusion or hydrodynamic forces. The kinetics of detachment of particles have been considered by several authors (Dahneke, 1975a; 1975b; Zimmer and Dahneke, 1976; Nelligan, Kallay and Matijevic, 1982) and may be described by a first order rate constant:

$$\frac{dQ}{dt} = -b_p Q \tag{71}$$

A simple analytical expression may be derived for the rate constant where the potential barrier is relatively large ($\Delta\phi/k_BT \gtrsim 10$) so that diffusion over the barrier is slow and the process may be considered as quasi-stationary (Dahneke, 1975b):

$$b_p = D_B \left[\int_{y=y_o}^{y_1} \left[\int_{v=y}^{\infty} \alpha_1 \exp\left(\frac{\phi(v)}{k_BT}\right) dv \right] \exp\left(-\frac{\phi(y)}{k_BT}\right) dy \right]^{-1} \tag{72}$$

If the quasi-stationary approximation is not valid. i.e. $\Delta\phi/k_BT < 10$, then numerical or series solutions of the governing equations are necessary (Zimmer and Dahneke, 1976; Nelligan, Kallay and Matijevic, 1982).

The surface interaction potential may have van der Waals, electrical double layer and magnetic components as discussed in Section 5.4. Matijevic and his co-workers have published several encouraging comparisons of theory and experiment for model systems (Kolakowski and Matijevic, 1979; Kuo and Matijevic, 1979; 1980; Kallay and Matijevic, 1981; 1983).

6.4 Dissolution

Dissolution of a deposit may occur if the concentration of soluble species in the bulk coolant over a surface is less than the saturation solubility at the surface. For a pure substance and first order kinetics the rate of dissolution may be described in an exactly similar way to the rate of precipitation (see equation 34) and may be written:

$$\frac{dM}{dt} = -\frac{ak}{a+k}(C_s - C_b) \tag{73}$$

However, it should be noted that the driving forces for release of the different species from a mixed system will, in general, differ from each other, (e.g. due to differences in redox potentials of the ions) and will therefore lead to non-congruent release. It is also possible that aged material may exhibit different solubilities than freshly deposited material.

6.5 Recoil

^{58}Co and ^{54}Mn are formed by fast neutron reactions, $^{58}Ni(n,p)^{58}Co$ and $^{54}Fe(n,p)^{54}Mn$, with neutron threshold energies of approximately 1.5 MeV. These nuclei recoil with appreciable energy so that direct recoil into the coolant may be a source of release. Cohen (1969) demonstrated the possible significance of this mechanism using simple approaches to the calculation of recoil energies and ranges. However, his calculations may be significantly in error due to the use of inappropriate range-energy correlations.

7. CONCLUSIONS

7.1 A complete mechanistic description of the formation, transport and deposition of radioactive corrosion products in PWR requires a diversity of complex phenomena to be modelled. Unfortunately, it is not yet possible to identify with certainty all those mechanisms which are crucial to an adequate description and those which may be omitted.

7.2 There is evidence that the corrosion films on stainless steel and higher nickel alloys under PWR conditions have a two-layer structure with the outer layer consisting of accumulations of crystals. However, the detailed mechanisms of film growth are not well known; in particular, it is not clear whether corrosion ions are transported through the inner layer by solid state diffusion or by aqueous phase diffusion through pores. Consequently, there are major uncertainties in the descriptions of corrosion ion release and contamination of growing films by soluble radioactivity.

7.3 It is valuable to distinguish between colloidal (< 1 μm) and inertial (> 1 μm) particles since not only their transport to and from surfaces but also their interactions with surfaces are governed by distinctly different mechanisms. It is also necessary to reconsider the traditional distinction between circulating 'particulate' and 'soluble' material according to retention or otherwise on 0.45 μm microporous filter membranes; some material which would presently be described as 'soluble' may be more appropriately described as colloidal particulate and will, of course, exhibit very different behaviour from truly soluble material.

7.4 The sources of circulating particulate corrosion products are very uncertain. Erosion of deposits or outer layer crystals and spalling may be significant but their contribution is difficult to quantify. However, it is possible to dismiss homogeneous nucleation in the coolant bulk as a source although heterogeneous nucleation cannot be dismissed without a consideration of the supply of suitable particulate impurity in the charging or make-up flows which could act as nucleation sites. This uncertainty is fundamental since it influences predictions of the relative rates of transfer by particulate and soluble routes.

7.5 Transport of soluble species and colloidal particles between surfaces and the coolant bulk is well understood and is adequately described by empirical correlations with very little extrapolation. Transfer of inertial particles from the coolant bulk to surfaces is also well understood but theories have only been validated for aerosol systems. Thermophoresis may exert a significant influence on the transport of 0.1 to 1.0 μm particles to heat transfer surfaces but its description requires validation under appropriate conditions.

7.6 Precipitation and dissolution are controlled by the local solubility of corrosion products. Solubilities for model systems, such as Fe_3O_4 and $NiFe_2O_4$, have been widely studied although there are no data for real corrosion products. These processes may be adequately described by a first order rate process providing boundary layer mass transfer is limiting; higher order rate processes may be more appropriate if the kinetics of surface reactions are limiting.

7.7 Corrosion products within a reactor circuit do not exhibit a uniform elemental composition. Thus, it is unjustified to assume that cobalt, iron, nickel and chromium species exhibit identical behaviour, for example with respect to solubility, nucleation and precipitation. However, it is not clear that the available data on thermodynamic equilibria, adsorption on oxides, etc. are sufficient to accommodate observed variations in elemental compositions.

7.8 The interactions of colloidal particles with surfaces during deposition and resuspension are adequately described by theories which have been validated for model systems. The major uncertainty in the application of these theories is introduced by the imperfect knowledge of the surface electrical properties of corrosion product particles and films at reactor operating temperatures.

7.9 The interactions of inertial particles with surfaces during deposition and resuspension are not well described. Determinations of sticking probability from experimental deposition data are inhibited by the uncertain validity of theories for predicting arrival rates at surfaces. The description of resuspension in terms of simple force balances is difficult to reconcile with observations of first order kinetics. In both cases the imperfect knowledge of surface electrical properties introduces a major uncertainty.

7.10 The importance of some processes remains to be demonstrated although relatively satisfactory theories are available to describe them. For example, the recoil of nuclei into the coolant as a direct result of the neutron activation reaction is a potentially significant contributor to the release of ^{54}Mn and ^{58}Co from fuel crud. However, the significance of

particle interactions in the coolant bulk, including dissolution and growth and agglomerate formation and break-up, is less clear.

REFERENCES

Adamczyk, Z. and Dabros, T., 1978, J. Colloid Interface Sci., 64, 580-583.

Armitt, J., Holmes, R., Manning, M. I., Meadowcroft, D. B. and Metcalfe, E., 1978, EPRI Report No. EPRI-FP-686.

Balakrishnan, P. V., 1977, Can. J. Chem. Eng., 55, 357-360.

Barber, D. and Lister, D. H., 1982, IAEA Int. Symp. on 'Water Chemistry and Corrosion Problems of Nuclear Reactor Systems and Components', Vienna, 22-26 November 1982, IAEA-SM-264/15.

Barouch, E., Matijevic, E., Ring, T. A. and Finlan, J. M., 1978, J. Colloid and Interface Sci., 67, 1-9.

Beal, S. K., 1970, Nucl. Sci. Eng., 40, 1-11.

Beal, S. K., 1973, Trans. Am. Nucl. Soc., 17, 163.

Beal, S. K., 1978, J. Aerosol Sci., 9, 455-461.

Bell, G. M., Levine, S. and McCartney, L. N., 1970, J. Colloid Interface Sci., 33, 335-359.

Berge, P. and Saint Paul, P., 1973, Comptes Rendus, Ser. C, 276, 1747.

Berge, P., Ribon, C. and Saint Paul, P., 1977, Corrosion, 33, 173.

Berger, F. P. and Hau, K.-F.F.-L., 1977, Int. J. Heat Mass Transfer, 20, 1185-1194.

Bergmann, C. A., 1982, EPRI Report No. EPRI-NP-2681.

Bergmann, C. A., Roesmer, J. and Perone, D. W., 1983, EPRI Report No. EPRI NP-2968.

Berry, W. E. and Diegle, R. B., 1979, EPRI Report No. EPRI NP-522.

Bérubé, Y. G. and de Bruyn, P. L., 1968, J. Colloid Interface Sci., 27, 305-318.

Beslu, P. M., Frejaville, G., Brissaud, A., Nunge, R. and Ridoux, P., 1982, Paper 5, IAEA Symposium on Water Chemistry and Corrosion Problems of Nuclear Reactor Systems and Components, Vienna, 22-26 November, 1982.

Beslu, P., Frejaville, G. and Jeanson, P., 1979, Nucl. Technol. 44, 84-90.

Beslu, P., Lalet, A., Joyer, F., Noe, G. and Frejaville, G., 1983, Procs. Int. Conf. 'Water Chemistry of Nuclear Reactor Systems 3', Bournemouth, 17-21 October 1983, BNES, London.

Bignold, G. J., Garnsey, R. and Mann, G. M. W., 1972, Corros. Sci., 12, 325-332.

Bishop, W. N., Cunnane, J. C., Kennedy, A. J., Schmotzer, J. K. and Stagg, W. R. (editor), 1983, EPRI Report No. EPRI NP-3280.

Blesa, M. A., Baumgartner, E. C. and Maroto, A. J. G., 1983, IAEA Specialists' Meeting on 'Influence of Water Chemistry on Fuel Element Cladding Behaviour in Water Cooled Power Reactors', Leningrad, 6-10 June 1983, IWGFPT/17, pp 150-158, IAEA, Vienna.

Blesa, M. A., Figliolia, N. M., Maroto, A. J. G. and Regazzoni, A. E., 1984, J. Colloid Interface Sci., 101, 410-418.

Blesa, M. A., Maroto, A. J. G., Passaggio, S. I., Labenski, F. and Saragovi-Badler, C., 1978, Radiat. Phys. Chem., 11, 321-326.

Blesa, M. A., Larotonda, R. M., Maroto, A. J. G. and Regazzoni, A. E., 1982, Colloids and Surfaces, 5, 197-208.

Blesa, M. A., Maroto, A. J. G. and Regazzoni, A. E., 1984, J. Colloid Interface Sci., 99, 32-40.

Bosholm, J., Glâsel, H., Junge, O. and Reinhard, G., 1978, Kernenergie, 21, 84-89.

Bowen, B. D. and Epstein, N., 1979, J. Colloid Interface Sci., 72, 81-97.

Bowen, B. D., Levine, S. and Epstein, N., 1976, J. Colloid Interface Sci., 54, 375-390.

Browne, L. W. B., 1974, Atmos. Env., 8, 801-806.

Bruins, von H. R., 1931a, Kolloid Zeitschrift, 54, 265-272.

Bruins, von H. R., 1931b, Kolloid Zeitschrift, 54, 272-278.

Bruins, von H. R., 1931c, Kolloid Zeitschrift, 57, 152-166.

Bruins, von H. R., 1932, Kolloid Zeitschrift, 59, 263-266.

Brusakov, V. P., 1971, Atomnaya Energiya, 30, 10-14.

Brusakov, V. P., Sedov, V. M., Khitrov, Y. A. and Rybalchenko, I. L., 1983, IAEA Specialists Meeting on 'Influence of Water Chemistry on Fuel Element Cladding Behaviour in Water Cooled Power Reactors', Leningrad, 6-10 June 1983, pp 35-49, IWGFPT/17.

Castle, J. E. and Mann, G. M. W., 1966, Corros. Sci., 6, 253-262.

Castle, J. E. and Masterson, H. G., 1966, Corros. Sci., 6, 93-104.

Chan, D., Perram, J. W., White, L. R. and Healy, T. W., 1975, J. Chem. Soc. Faraday Trans. I, 71, 1046.

Chapman, D. L., 1913, Phil. Mag., 25, 475.

Cleaver, J. W. and Yates, B., 1973, J. Colloid Interface Sci., 44, 464-474.

Coakley, C. J. and Tabor, D., 1978, J. Phys. D: Appl. Phys., 11, L77-L82.

Cohen, P., 1969, 'Water Coolant Technology of Power Reactors', Ch. 8, Gordon and Breach Science Publishers, London.

Colombo, U., Fagherazzi, G., Gazzarrini, F., Lanzavecchia, G. and Sironi, G., 1964, Nature, 202, 175-176.

Corn, M., 1966, 'Aerosol Science' ed. C. N. Davies, Ch. 11, Academic Press, London.

Czarnecki, J. and Dabros, T., 1980, J. Colloid Interface Sci., 78, 25-30.

Dahneke, B., 1971, J. Colloid Interface Sci., 37, 342-353.

Dahneke, B., 1972, J. Colloid Interface Sci., 40, 1-13.

Dahneke, B., 1974, J. Colloid Interface Sci., 48, 520-522.

Dahneke, B., 1975a, J. Colloid Interface Sci., 50, 89-107.

Dahneke, B., 1975b, J. Colloid Interface Sci., 50, 194-196.

Darras, R., 1980, CEA Report CEA-R-5072.

de Bruyn, P. L., 1978, Phys. Chem. Liq., 7, 181-200.

Delichatsios, M. A., 1975, Phys. Fluids, 18, 622-623.

Delichatsios, M. A. and Probstein, R. F., 1975, J. Colloid Interface Sci., 51, 394-405.

Derjaguin, B. V. and Landau, L., 1941, Acta Phys.-Chim. URSS, 14, 633.

Derjaguin, B. V. Muller, V. M. and Toporov, Y. P., 1975, J. Colloid Interface Sci., 53, 314-326.

Dipprey, D. F. and Sabersky, R. H., 1963, Int. J. Heat Mass Transfer, 6, 329-353.

Dousma, J. and de Bruyn, P. L., 1979, J. Colloid Interface Sci., 72, 314-320.

Dufrane, K. F. and Naughton, M. D., 1983, Nucl. Technol., 13, 102-109.

Effertz, P. H., 1972, Procs. 5th Int. Cong. on Metallic Corros., Tokyo, paper D26.

Einstein, A., 1905, Ann. Physik, 17, 549.

El-Shobokshy, M. S. and Ismail, I. A., 1980, J. Eng. Sci, 5, 147-157.

Ensling, J., Fleisch, J., Grimm, R., Gruber, J. and Gutlich, P., 1978, Corrosion Science, 18, 797-808.

Epstein, N., 1978, Heat Transfer 1978, pp 235-253, Hemisphere Publishing Corp., Washington.

Erdey-Gruz, T., 1974, 'Transport Phenomena in Aqueous Solutions', Ch. 3, Adam Hilger, London.

Evans, U. R. and Wanklyn, J. N., 1948, Nature, 162, 27.

Feitknecht, von W. and Lehmann, H. W., 1959, Helvetica Chimica Acta, 42, 2035-2039.

Francis, J. M. and Whitlow, W. H., 1966, J. Nuclear Materials, 20, 1-10.

Frejaville, G., Marchal, A., Beslu, P. and Lalet, A., 1974, Procs. Symp. 'Experience from Operating and Fuelling Nuclear Power Plants', Vienna, 1973, pp 401-417, IAEA-SM-178/31.

Frenkel, J., 1955, 'Kinetic Theory of Liquids', Ch. 7, Dover Publications Inc., New York.

Friedlander, S. K. and Johnstone, H. F., 1957, Ind. Eng. Chem., 49, 1151-1156.

Fuchs, N. A., 1934, Z. Phys., 89, 736.

Fuchs, N. A., 1964, 'The Mechanics of Aerosols', Pergamon Press, Oxford.

Furedi-Milhofer, H., 1981, Pure Appl. Chem., 53, 2041-2055.

Furlong, D. N., Yates, D. E. and Healy, T. W., 1981, Stud. Phys. Theor. Chem., Ch. 8, 11, 367-432.

Garnsey, R., 1979, CEGB Research, No. 9, 12-23.

Garnsey, R., Hearn, B. and Mann, G. M. W., 1972, J. British Nuclear Energy Society, 11, 65-70.

Gautsch, O., Lanza, F. and Weisgerber, P., 1979, European Appl. Res. Rept.-Nucl. Sci., Technol., 1, 1225-1314.

Giasson, G. and Tewari, P. H., 1978, Can. J. Chem., 57, 435-440.

Gouy, G., 1910, J. Phys., 9, 457.

Gregory, J., 1970, Advan. Colloid Interface Sci., 2, 396-417.

Gudmundsson, J. S., 1979, Int. Conf. Fouling of Heat Transfer Equipment, Troy, New York, 13-17 August 1979.

Halow, J. S., 1973, Chem. Eng. Sci., 28, 1-12.

Hamaker, H. C., 1937, Physica, 4, 1058-1072.

Harriott, P. and Hamilton, R. M., 1965, Chem. Eng. Sci., 20, 1073-1078.

Hasson, D., 1979, Int. Conf. Fouling of Heat Transfer Equipment, Troy, New York, 13-17 August 1979.

Hazell, I. F. and Irving, R. J., 1966, J. Chem. Soc. (A), 669-673.

Hinson, C. S. and Murphy, T. D., 1979, 'Decontamination and Decommissioning of Nuclear Facilities', pp 595-608, Plenum Press, New York.

Hinze, J. O., 1955, A.I.Ch.E. Journal, 1, 289-295.

Hogg, R., Healy, T. W. and Fuerstenau, D. W., 1966, Trans. Faraday Soc., 62, 1638-1651.

Honig, E. P., Roebersen, G. J. and Wiersema, P. H., 1971, J. Colloid Interface Sci., 36, 97-109.

Hopkins, R. M., 1973, 'Fouling of Heated Stainless Steel Tubes with Ferric Oxide from Flowing Water Suspensions', PhD Dissertation, University of British Columbia.

Hopkins, R. M. and Epstein, N., 1974, Procs. 5th Int. Heat Transfer Conf., Tokyo, 3-7 September 1974, Vol. 5, pp 180-184, The Japan Society of Mechanical Engineers/The Society of Chemical Engineers, Japan, Tokyo.

ICRP, 1977, 'Recommendations of the International Commission on Radiological Protection', Publication 26, Pergamon Press, New York.

Jarnstrom, R. T., 1982, IAEA Int. Symp. on 'Water Chemistry and Corrosion Problems of Nuclear Reactor Systems and Components', Vienna 22-26 November 1982, IAEA-SM-264/8.

Johnson, A. B., Griggs, B. and Kustas, F. M., 1980, Proc. 2nd Conf. on 'Water Chemistry of Nuclear Reactor Systems', Bournemouth, pp 273-278, BNES, London.

Kahlweit, M., 1975, Adv. Colloid Interface Sci., 5, 1-35.

Kallay, N. and Matijevic, E., 1981, J. Colloid Interface Sci., 83, 289-300.

Kallay, N. and Matijevic, E., 1983, Corrosion-NACE, 39, 15-19.

Kanert, G. A., Gray, G. W. and Baldwin, W. G., 1976, AECL Report No. AECL-5528.

Keston, A. S. and Lasher, L. S., 1959, USAEC Report No. WAPD-BT-16.

Kittaka, S. and Morimoto, T., 1980, J. Colloid Interface Sci., 75, 398-403.

Kittel, C., 1956, 'Introduction to Solid State Physics', 2nd ed., Ch. 15, Wiley, New York.

Kolakowski, J. and Matijevic E., 1979, J. Chem. Soc. Faraday Trans. I, 75, 65-78.

Kormuth, J. W. and Barkich, J. L., 1983, EPRI Report No. EPRI NP-3245.

Krupp, H., 1967, Advan. Colloid Interface Sci., 1, 111-239.

Kruyt, H. R., 1952, 'Colloid Science', Vol. 1, Ch. 4, Elsevier Publishing Company, Amsterdam.

Kuboi, R., Komasawa, I., Otake, T. and Iwasa, M., 1974, Chem. Eng. Sci., 29, 659-668.

Kuboi, R., Komasawa, I. and Otake, T., 1974, Chem. Eng. Sci., 29, 651-657.

Kuo, R. J. and Matijevic, E., 1979, J. Chem. Soc. Faraday Trans. I, 75, 2014-2026.

Kuo, R. J. and Matijevic, E., 1980, J. Colloid Interface Sci., 78, 407-421.

Lambert, I., 1975, CEA-BIB-217.

Lambert, I., Montel, J. and Courvoisier, P., 1980, Proc. 2nd Conf. on Water Chemistry of Nuclear Reactor Systems, Bournemouth, pp 31-35, BNES, London.

Lambert, I., Montel, J. and Courvoisier, P., 1983, Procs. Int. Conf. 'Water Chemistry of Nuclear Reactor Systems 3', Bournemouth, 17-21 October 1983, pp 37-41, BNES, London.

Levich, V. G., 1962, 'Physicochemical Hydrodynamics', Prentice-Hall Inc., Englewood Cliffs, N.J.

Lifshitz, E. M., 1956, Soviet Phys., 2, 73-83.

Lindsay, W. T., 1981, EPRI Report No. EPRI NP-1963.

Lister, D. H., 1975, Nucl. Sci. Eng., 58, 239-251.

Lister, D. H., 1976a, Nucl. Sci. Eng., 59, 406-426.

Lister, D. H., 1976b, Nucl. Sci. Eng., 61, 107-118.

Lister, D. H., 1978, Procs. 2nd Conf. 'Water Chemistry of Nuclear Reactor Systems', Bournemouth, pp 207-214, BNES, London.

Lister, D. H., 1979a, Int. Conf. Fouling of Heat Transfer Equipment, Troy, New York, 13-17 August 1979.

Lister, D. H., 1979b, Corrosion, 35, 219-226.

Lister, D. H., Kushneriuk, S. A. and Campbell, R. H., 1983, Nucl. Sci. Eng., 85, 221-232.

Lister, D. H., McAlpine, E. and Hocking, W. H., 1984, EPRI Report No. EPRI NP-3460.

Liu, B. Y. H. and Ilori, T. A., 1974, Environmental Science and Technology, 8, 351-356.

Lyklema, J., 1980, Pure and Appl. Chem., 52, 1221-1227.

Macdonald, D. D. and Rummery, T. E., 1973, AECL Report No. AECL-4140.

Macdonald, D. D., Rummery, T. E. and Tomlinson, M., 1975, IAEA-SM-190/19.

Macdonald, D. D., Shierman, G. R. and Butler, P., 1972a, AECL Report No. AECL-4137.

Macdonald, D. D., Shierman, G. R. and Butler, P., 1972b, AECL Report No. AECL-4138.

Makrides, A. C., Turner, M. and Slaughter, J., 1980, J. Colloid Interface Sci., 73, 345-367.

Mann, G. M. W., 1976, Procs. Conf. 'High Temperature High Pressure Electrochemistry in Aqueous Solutions', University of Surrey, England, 7-12 January 1973, NACE, Houston, Texas.

Maroto, A. J. C., Blesa, M. A., Passaggio, S. I. and Regazzoni, A. E., 1981, Procs. 2nd Int. Conf. 'Water Chemistry of Nuclear Reactor Systems', Bournemouth, 14-17 October 1980, pp 247-250, British Nuclear Energy Society, London.

Martynova, O. I., Gromoglasov, A. A., Mikhailov, A. Yu and Nasyrov, M. L., 1977, Teploenergetika, 24, 70-71.

McAlpine, E., Lister, D. H. and Ocken, H., 1984, NACE 'Corrosion 84', New Orleans, 2-6 April 1984, Paper 193.

McIntyre, N. S., Zetaruk, D. G. and Murphy, E. V., 1979, Surface and Interface Analysis, 1, 105-110.

McIntyre, W. S., Zetaruk, D. G. and Owen, D., 1979, J. Electrochem. Soc., 126, 750-760.

McNab, G. S. and Meisen, A., 1973, J. Colloid Interface Sci., 44, 339-346.

Means, F. A., 1978, CEGB Report No. RD/B/N4268.

Means, F. A., Rodliffe, R. S. and Harding, K., 1980, Nucl. Technol., 47, 385-396.

Michael, I. and Plog. C., 1977, Metallwissenschaft und Technik, 3, 252-256.

Mishima, Y., 1983, IAEA Specialists' Meeting on 'Influence of Water Chemistry on Fuel Element Cladding Behaviour in Water Cooled Power Reactors', Leningrad, 6-10 June 1983, Paper 2.

Mizushina, T., Ogino, F., Oka, Y. and Fukuda, U., 1971, Int. J. Heat Mass Transfer, 14, 1705-1716.

Montford, B., 1973, AECL Report No. AECL-4223.

Montford, B. and Rummery, T. E., 1975, AECL Report No. AECL-4444.

Mullin, J. W., 1972, 'Crystallisation', 2nd Edition, Chs. 5 and 6, Butterworths, London.

Nancollas, G. H., 1979, Advan. Colloid and Interface Sci., 10, 215-252.

Neeb, K. H. and Riess, R., 1977, BMFT FB K 77-12.

Nelligan, J. D., Kallay, N. and Matijevic, E., 1982, J. Colloid Interface Sci., 89, 9-15.

Nielsen, A. E., 1964, 'Kinetics of Precipitation', Chs. 1 and 2, Pergamon Press, Oxford.

Nielsen, A. E., 1981, Pure Appl. Chem., 53, 2025-2039.

Nielsen, A. E. and Sohnel, O., 1971, J. Crystal Growth, 11, 233-242.

Ocken, H., 1985, Nucl. Technol., 68, 18-28.

Ohshima, H., Healy, T. W. and White, L. R., 1982a, J. Colloid Interface Sci., 89, 484-493.

Ohshima, H., Healy, T. W. and White, L. R., 1982b, J. Chem. Soc. Faraday Trans. 2, 79, 1613-1628.

Oldenkamp, R. D., Paulson, C. F. and Solomon, Y., 1961, Westinghouse Reort WAPD-TM-261.

O'Neill, M. E., 1968, Chem. Eng. Sci., 23, 1293-1298.

Parker, D. S., Kaufman, W. J. and Jenkins, D., 1972, J. Sanitary Engineering Division ASCE, 98, 79-99.

Parks, G. A., 1965, Chem. Rev., 65, 177-198.

Parks, G. A. and de Bruyn, P. L., 1962, J. Phys. Chem., 66, 967-972.

Pattison, J. and Walton, G. N., 1961, UKAEA Report No. AERE-R-3661.

Phillips, M., 1980, J. Phys. D : Appl. Phys., 13, 221-233.

Pick, M. E., 1983, Procs. Int. Conf. 'Water Chemistry of Nuclear Reactor Systems 3', Bournemouth, 17-21 October 1983, pp 61-69, BNES, London.

Picone, L. F. and Taylor, G. R., 1966, USAEC Report No. WCAP-6072.

Ponting, A. C., 1982, CEGB Report No. RD/B/5232N82.

Ponting, A. C. and Rodliffe, R. S., 1983, Procs. 3rd Int. Conf. Water Chemistry of Nuclear Reactor Systems, Bournemouth, 17-21 October 1983, Vol. 1, pp 43-51, BNES, London.

Potter, E. C. and Mann, G. M. W., 1962, Procs. 1st Int. Cong. Metallic Corros. London, 1961, pp 417-426, Butterworths, London.

Potter, E. C. and Mann, G. M. W., 1964, Procs. 2nd Int. Cong. Metallic Corros., New York, 1963, pp 827-829, NACE, Houston.

Potter, E. C. and Mann, G. M. W., 1965, Brit. Corros. J., 1, 26-35.

Poulson, B., 1983, Corrosion Science, 23, 391-430.

Prieve, D. C. and Ruckenstein, E., 1976, J. Colloid Interface Sci., 57, 547-550.

Prieve, D. C. and Ruckenstein, E., 1977, J. Colloid Interface Sci., 60, 337-348.

Prieve, D. C. and Ruckenstein, E., 1978, J. Colloid Interface Sci., 63, 317-329.

Punjrath, J. S. and Heldman, D. R., 1972, Aerosol Sci., 3, 429-440.

Reeks, M. W. and Skyrme, G., 1976, J. Aerosol Sci., 7, 485-495.

Reid, R. C. and Sherwood, T. K., 1966, 'The Properties of Gases and Liquids', Ch. 11, McGraw-Hill, New York.

Richardson, S. A., Castle, J. E., Large, N. R. and Tench, A. J., 1983, Procs. Int. Conf. on 'Water Chemistry of Nuclear Reactor Systems 3', Bournemouth, 17-21 October 1983, pp 53-60, BNES, London.

Riess, R., 1976, Nucl. Technol., 29, 153-159.

Ring, T. A., 1982, J. Chem. Soc. Faraday Trans. 2, 78, 1513-1528.

Rodliffe, R. S., 1980, J. Colloid Interface Sci., 76, 157-165.

Rodliffe, R. S. and Means, F. A., 1979, CEGB Report No. RD/B/N4525.

Rommel, H., 1978, Kernenergie, 21, 49-53.

Rommel, H., 1983, Kernenergie, 26, 23-27.

Rommel, H., Sachse, G., Schlenkrich, H. and Mittag, I., 1980, J. Radioanal. Chem., 58, 153-160.

Rommel, H., Sachse, G., Schlenkrich, H. and Mittag, I., 1982, ZfK-470.

Rotta, J. C., 1972, 'Turbulente Stromungen', B.G. Teubner, Stuttgart.

Ruckenstein, E. and Prieve, D. C., 1973, J. Chem. Soc. Faraday Trans. II, 69, 1522-1536.

Rummery, T. E. and Macdonald, D. D., 1975, J. Nuclear Materials, 55, 23-32.

Saffman, P. Q., 1965, J. Fluid Mech., 22, 385-400.

Sandler, Y. L., 1979, Corrosion, 35, 205-208.

Sandler, Y. L. and Kunig, R. H., 1977, Nucl. Sci. Eng., 64, 866-874.

Sandler, Y. L. and Kunig, R. H., 1981, Nucl. Sci. Eng., 77, 211-218.

Schikorr, von G., 1929, Zeitschrift fur Electrochemie, 35, 65-70.

Sellers, R. M., 1976, CEGB Report No. RD/B/N3707.

Sidhu, P. S., Gilkes, R. J. and Posner, A. M., 1977, J. Inorg. Nucl. Chem., 39, 1953-1958.

Shipko, F. J. and Douglas, D. L., 1956, J. Phys. Chem., 60, 1519-1523.

Smoluchowski, M., 1917, Z. Phys. Chem., 92, 151.

Solomon, Y. and Roesmer, J., 1976, Nucl. Technol., 29, 166-173.

Solomon, Y. and Roesmer, J., 1978, Westinghouse Report No. WCAP-9407.

Spielman, L. A., 1970, J. Colloid Interface Sci., 33, 562-571.

Spielman, L. A. and Friedlander, S. K., 1974, J. Colloid Interface Sci., 46, 22-31.

Styrikovich, M. A., Martynova, O. I., Kobyakov, I. F., Men'shikova, V. L. and Reznikov, M. I., 1972, Thermal Engineering, 19, 127-130.

Sweeton, F. C. and Baes, C. F., 1970, J. Chem. Thermodynamics, 2, 479-500.

Swift, D. L. and Friedlander, S. K., 1964, J. Colloid Sci., 19, 621-647.

Tachikawa, E., Hoshi, M., Sagawa, C., Yonezawa, C. and Nakashima, M., 1984, Nucl. Technol., 65, 138-145.

Talbot, L., Cheng, R. K., Scheter, R. W. and Willis, D. R., 1980, J. Fluid Mech., 101, 737-758.

Tamura, H., Matijevic, E. and Meites, L., 1983, J. Colloid and Interface Sci., 92, 303-314.

Taylor, N. K. and Armson, I., 1983, Procs. Int. Conf. on 'Water Chemistry of Nuclear Reactor Systems 3', Bournemouth, 17-21 October, 1983, pp 141-151, BNES, London.

Tewari, P. H. and Campbell, A. B., 1972, Procs. Symp. 'Oxide-Electrolyte Interfaces', Miami Beach, Florida, 8-13 October 1972, Electrochemical Society, pp 102-111.

Tewari, P. H. and Campbell, A. B., 1976, J. Colloid Interface Sci., 55, 531-539.

Tewari, P. H., Campbell, A. B. and Lee, W., 1972, Can. J. Chem., 50, 1642-1648.

Tewari, P. H. and Lee, W., 1975, J. Colloid and Interface Sci., 52, 77-88.

Tewari, P. H. and McLean, A. W., 1972, J. Colloid Interface Sci., 40, 267-272.

Tewari, P. H. and McIntyre, N. S., 1975, A.I.Ch.E. Symposium Series, 71, 134-137.

Thomas, D. and Grigull, U., 1974, Brennst.-Warme-Kraft, 26, 109-115.

Tomlinson, M., 1976a, AECL Report No. AECL-4569.

Tomlinson, M., 1976b, Procs. Conf. on 'High Temperature, High Pressure Electrochemistry in Aqueous Solution', Guildford, U.K., NACE, pp 221-234.

Tomlinson, L., 1981, Corrosion, 37, 591-596.

Tremaine, P. R. and LeBlanc, J. C., 1980, J. Solution Chem., 9, 415-442.

Tremaine, P. R., von Massow, R. and Shierman, G. R., 1977, Thermochimica Acta, 19, 287-300.

Treybal, R. E., 1968, 'Mass Transfer Operations', 2nd Edition, Ch. 3, McGraw-Hill, New York.

Twomey, S., 1977, 'Atmospheric Aerosols', Ch. 2, Elsevier Scientific Publishing Company, Amsterdam.

Urbanic, V. F., Gray, R. and Lister, D. H., 1979, EPRI Report No. EPRI NP-1254.

Vanbrabant, R. and de Regge, P., 1980, Proc. 2nd Conf. 'Water Chemistry of Nuclear Reactor Systems', Bournemouth, pp 209-214, BNES, London.

Vanbrabant, R. and de Regge, P., 1982, SCK Report BLG-552.

van Bree, J. L. M. J., Poulis, J. A., Verhaar, B. J. and Schram, K., 1974, Physica, 78, 187-190.

Varovin, J. A., Eperin, A. P., Konstantinov, Y. A., Sedov, V. M., Senin, Y. V. and Filippov, Y. M., 1983, IAEA Specialists' Meeting on 'Influence of Water Chemistry on Fuel Element Cladding Behaviour in Water Cooled Power Reactors', Leningrad, 6-10 June 1983, Paper 23.

Verwey, E. J. W. and Overbeek, J. T. G., 1948, Theory of the Stability of Lyophobic Colloids, Ch. 10, Elsevier, Amsterdam.

Visser, J., 1968, Reports Prog. Appl. Chem., 53, 714-729.

Visser, J., 1970, J. Colloid Interface Sci., 34, 26-31.

Visser, J., 1972, Advan. Colloid Interface Sci., 3, 331-363.

Visser, J., 1973, Unilever Research Report No. N74 - 25977.

Visser, J., 1976, J. Colloid Interface Sci., 55, 664-677.

Volmer, M., 1939, 'Kinetik der Phasenbildung', Ch. 3; Sternkopff, Dresden and Leipzig.

Volmer, M. and Flood, H., 1934, Z. Phys. Chem., Abt. A, 170, 273-285.

von Massow, R. E., Sullivan, G. R. and Waugh, G. N., 1975, AECL Report No. AECL-4582.

Warzee, M., Sonnen, C. and Berge, Ph., 1967, European Atomic Energy Commission Report No. EURAEC-1896.

Walton, A. G., 1967, 'The Formation and Properties of Precipitates', Ch. 1, Interscience Publishers, New York.

Watkinson, A. P., 1968, 'Particulate Fouling of Sensible Heat Exchangers', PhD Dissertation, University of British Columbia.

Wiese, G. R. and Healy, T. W., 1970, Trans. Faraday Soc., 66, 490-499.

Wood, N. B., 1981, J. Aerosol Sci., 12, 275-290.

Zimmer, S. L. and Dahneke, B., 1976, J. Colloid Interface Sci., 54, 329-338.

Annex III

A REVIEW OF MODELS DESCRIBING THE BEHAVIOUR OF CORROSION PRODUCTS IN PRIMARY HEAT TRANSFER CIRCUITS OF BWRs

K. ISHIGURE
Faculty of Engineering,
University of Tokyo,
Tokyo, Japan

General Introduction

The behavior of corrosion products in the primary coolant circuits is one of the main concerns in relation to the operation and maintenance of BWR power stations. It is related to two aspects of reactor systems : one is an operational problem resulting in an increase in the core pressure drop[1] or overheating[2] of the fuel pins induced by the deposited corrosion products on the surfaces of the fuel cladding, and the other is related to occupational radiation exposures arising from the radioactivity transport through the activation of corrosion products in the reactor core.

Early operational experiences in some of the first generation BWR plants showed that the release of non-ferrous metals to feed water took place at rather high rates from the copper based alloys used in the feed water heater tubes. The high input rates of copper or nickel led to tenacious deposits of metal oxides including these metals on the boiling surfaces of the fuel pins, inducing an increase in the core pressure drop owing to the restriction in coolant flow,and in some cases, the overheating of the fuel cladding as a result of crud cracking and steam blanketting. The replacement of copper based alloy tubes of feed water heaters with stainless steel, which was carried out in many BWR plants, significantly reduced the input of the non-ferrous corrosion products into the core of early reactors, and consequently, brought about the reduction of this types of deposit, especially, the copper containing deposit, on the surfaces of the fuel cladding.

After the reduction of the problem with the copper based alloys, the current concern is mainly concentrated on the radioactivity build-up on the surfaces of out-of-core pipes, which is closely related to the occupational radiation exposures. It is well established that shut-down dose rates on the surfaces of the out-of-core pipes mainly come from corrosion products[4)-6)] activated by neutron irradiation on the surfaces of the fuel cladding. A large number of reports have appeared in the literature on the investigation of corrosion product transport in the primary circuits of BWRs in relation to radioactivity build-up. On the basis of these reports, we now have a better understanding than before of the mechanism of radioactivity transport and build-up in the primary systems of BWR, although the phenomenon is too complicated for full understanding with many problems still remaining unsolved.

In Part I of this annex a brief review of the behavior of the corrosion products under BWR conditions is described. Some of the corrosion product phenomena are already described in the annex II, and the common phenomena are not repeated.

The description is more or less phenomenological in most part of this chapter, and theoretical modeling of the phenomena is given only when it is reasonably applicable to present systems or appropriate to explain general phenomena.

The general basic concepts and mathematical formulations employed in the computer codes which are developed to describe the behaviors of corrosion products and the radioactivity build-up in BWRs are given in Part II.

References

1) R.Gasparini and E.Ioannilli, Proc. Am. Power Conf., 33, 776, 1971.

2) A.Garlick, R.Sumerling and G.L.Shires, J. Br. Nucl. Energy Soc., 16, 77, 1977.

3) G.C.W.Comley, Prog. Nucl. Energy, 2, 153, 1978.

4) R.A.Shaw, Nucl Tech., 44, 97, 1979.

5) R.Riess, Nucl. Tech., 29, 153, 1976.

6) J.E.LeSurf, J. Br. Energy Soc., 16, 53, 1977.

1. Introduction

The specification of the primary coolant in BWR is somewhat different from that in PWR, since the direct cycle is adopted in BWR with boiling of the coolant in core of the reactor. A flow diagram of the primary coolant system in a typical BWR is given in Fig.1.[1] The steam produced in core goes directly to turbines, and is condensed in the condenser. All of the condensed water is polished with a condensate demineralizer consisting of ion-exchange resins. Two type of ion-exchange resins can be used in the condensate demineralizers : one is deep-bed type resins and the other powdered resins. Some new plants have installed dual type, that is, both of the two types are arranged in series. Originally, the major function of the condensate demineralizer was the removal of the impurities arising from condenser leakage. Recently, the removal of the corrosion products generated up-stream of the condenser has grown in importance with increasing improvement of the condenser integrity. The corrosion products in the primary circuits of BWR are considered to exist in two forms, soluble species and insoluble oxide particles. The discrimination between these two forms is conventionally made by filtration using 0.45 μm millipore filters. In general, however, "the soluble" fraction

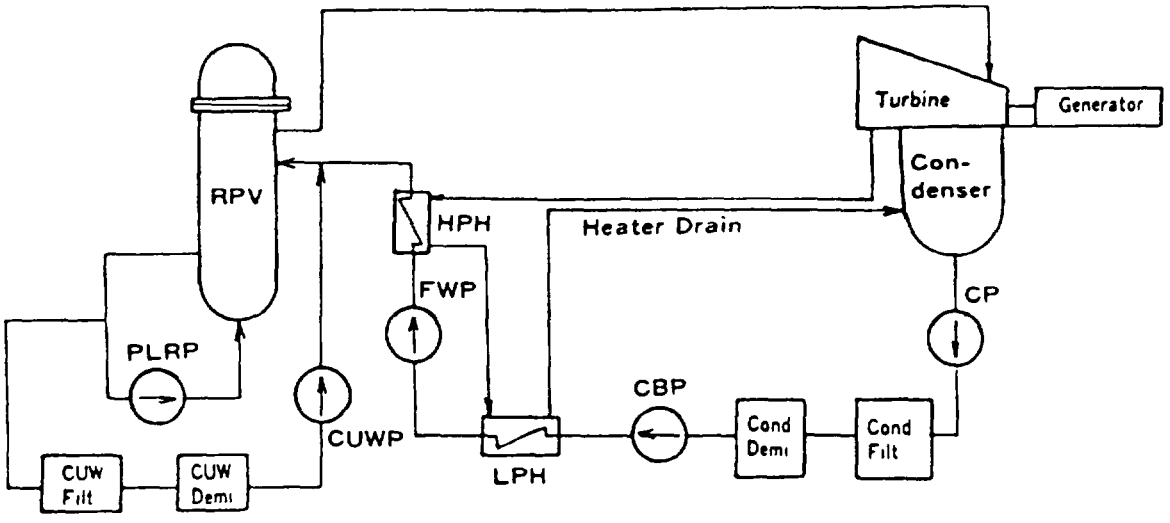

Fig.1. Flow diagram of a typical BWR.[1]

contains both truely soluble species and small particles. Corrosion products which pass through the millipore filters are called filtrates and assumed to be the soluble ions, while those collected by filters are called crud, which are insoluble oxide particles. This discrimination between crud and ions by millipore filters results in some ambiguity to the actual forms of the nominal "ions".

It is widely accepted that powdered resins are more suited to remove crud particles compared with deep-bed resins, although the ion exchange capacity of the former is lower than that of the latter.

After purification in the condensate demineralizer, feed water is heated to 180 to 200°C in a series of feed water heaters through heat exchange with steam bled from the turbine system, and then fed to the reactor core.

It has been recognized from operational experiences in BWRs that the dissolved oxygen level of the feed water is a very important factor in relation to the control of corrosion product releases from the materials consituting the feed water system. It should be noted that all the corrosion products released into feed water are fed directly into the core of the reactor.

After heat exchange in the feed water heaters, the steam condensate is usually returned to the condenser, and then polished in the condensate demineralizer. Some BWR plants, however, have the forward pumped drain systems where the bled steam condensate is added to the feed water after the condensate demineralizer.

The cooled water is recirculated through the core, and the bypass clean-up blow is taken from the recirculation system.
The reactor purification system was intended to control soluble impurities and to remove soluble fission products which are released to the reactor water through small defects in the fuel cladding. Progressive improvement in the fuel cladding integrity has uprated the importance of removing activated corrosion products from BWR coolant. It is now accepted that activated corrosion products are responsible for most of the surface dose rates from the piping which in turn dominates the radiation exposure to personnel during reactor shut down.

The capacity of the reactor water clean-up system has been 7 per cent of the feed water in the early plants, but this has decreased to one or 2 per cent in more recent BWRs.

The radiation build-up on the corroding surfaces of the out-of-core piping has become a major concern in relation to the control of BWR water chemistry. In contrast to PWR, addition of conditioning chemicals to the primary coolant systems is not possible in BWRs because of the boiling coolant in the reactor core. Therefore, the only mean for controlling coolant water chemistry are to keep impurity levels in the feed water as low as possible by purification and to minimize the input of corrosion products from the feed water system to the reactor core.

The mechanism of the radiation build-up on th primary piping of BWRs is roughly understood as follows. The corrosion products are fed into the reactor core from the feed water line, a major component of these products being iron. This is considered to play an important role in the radiation build-up process in BWRs, by providing sites for the deposition and activation of cobalt which is the element of the most concern, making the greatest contribution to the dose rate of the piping from ^{60}Co. There has been some controversy on the sources of cobalt. It is now generally accepted that the cobalt contribution by release from the core materials is not negligible, which is not the case with iron.

The corrosion products fed into the core are mostly deposited on the surfaces of the fuel cladding, and this process is markedly enhanced by boiling on the fuel surfaces in BWRs. The deposited corrosion products are activated by neutron irradiation, and re-released to the reactor water after some period of residence on the fuel surface. The radioactive nuclides, including ^{60}Co, in the reactor water are transferred by the coolant to the out-of-core circuits, and taken up on the corroding surfaces of the out-of-core pipes.

The above description is a very rough summary of the mechanism of radioactivity build-up in BWRs on which general understanding has been obtained on the basis of the model experiments and from the operational experiences in power reactors. The detailed mechanism of the process is very complicated with many ambiguous points remaining. In

the following sections a detailed description is given to the several important phenomena comprising the overall process of corrosion product transport in BWRs.

2. Release of Corrosion Products

The main component of corrosion products in the reactor water of BWR is iron which mostly comes from the feed water systems. The iron levels in the feed water immediately after the high pressure heater arise primarily from the corrosion of stainless steel and carbon steel in the feed water systems. It is recognized that significant contribution to the iron input to the reactor core is made by the passage of corrosion products, in particular crud through the condensate demineralizers especially if their efficient operation can not be maintained.

Some experimental results and in-plant tests show that the corrosion rates and the release levels of corrosion products from carbon steel and stainless steel are strongly affected by the concentration of dissolved oxygen.[2),3)] As shown in Fig.2, the corrosion rates of carbon steel decrease sharply in high purity water with increasing oxygen concentration in the range of 10 to 100 ppb.[4)] The flow rate

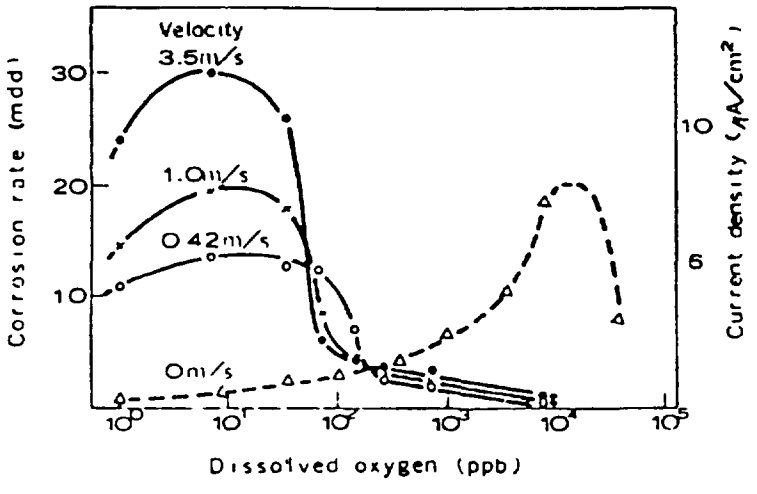

Fig. 2. Corrosion rates of carbon steel (SB 46) as function of dissolved oxygen.[3)]
33 ± 2°C, specific conductivity < 0.5μ /cm, immersion period 500 hours.

of water also has a significant influence on the corrosion control by oxygen concentration, a higher concentration of oxygen being necessary to suppress the corrosion at the lower flow rate.

This effect of oxygen has been found to be very marked in the feed water systems of BWRs ; when 30 to 50 ppb of dissolved oxygen was injected into the feed water immediately after the condensate demineralizer, the iron concentration after the high pressure heater was reduced to the level of a few ppb in comparison with the levels of approximately 50ppb before oxygen injection.[1)]

On the basis of these experiments and tests oxygen of 30 to 50 ppb level is now injected to the feed water in all Japanese BWR plants. In BWRs in other countries, oxygen injection has not been practiced so far, but it is recommended that the oxygen level in the feed water be controlled to be 20 to 50 ppb.[5)]

The above effect of dissolved oxygen is explained by the assumption that some optimum concentration of oxygen is necessary to maintain the passive oxide films on the metal surface, but a model has yet to be developed to explain the mechanism of the oxygen effect in more detail. Several models have been proposed to explain the corrosion process and the oxide structures of corroding surface of carbon steel at high temperature, most being based principally on the original Potter-Mann model.[6)] In these models the double oxide layers are assumed, an inner and outer layers being recognized. One such model is schematically shown in Fig.3.[7)] The inner layer is composed of magnetite, which is produced at the metal/oxide interface by the direct reaction of metal with the oxygen bearing species diffusing through the inner oxide layer. Ferrous(Fe^{2+}) ions produced by the corrosion reaction at the metal/oxide interface diffuse outwards through the inner oxide layer, and go into solution at the inner oxide/water interface. At the outer oxide/water interface ferrous ions in solution deposit as a result of the reactions with water molecules and form the outer layer.

$$3(Fe^{2+})\text{solution} + 4H_2O \longrightarrow Fe_3O_4 + 6H^+ + 2H \qquad (1)$$

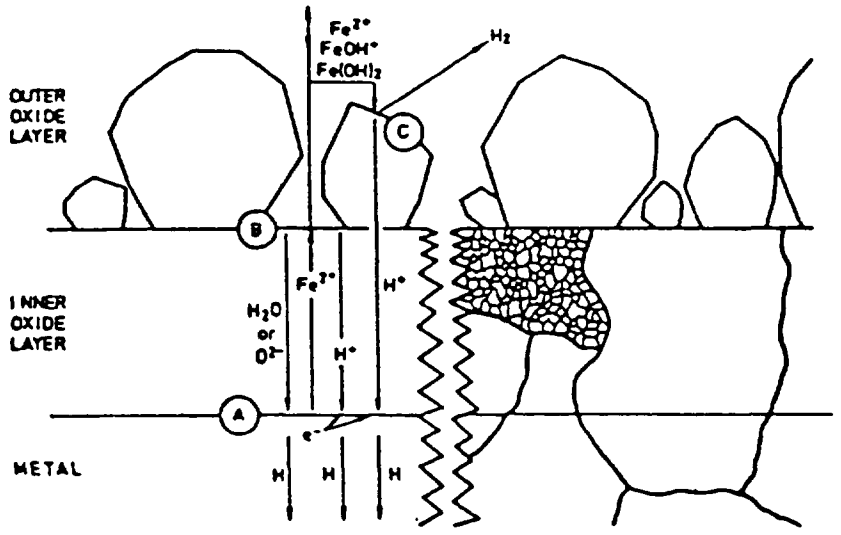

Fig. 3. Model of steel corrosion in high temperature water. (pH $\leq$ 11) [7]

In this model it is assumed that a half of the ferrous ions produced by the corrosion reactions diffuse outwards from the metal to the inner oxide/water interface and there enter solution. The ferrous ions which escape deposition at the outer oxide/water interface are released as soluble corrosion products. One possible explanation [8,9,10] of the effect of oxygen present in the solution according to this model is that ferrous ions react with oxygen in solution and also at the inner oxide/water interface, precipitating as ferric oxide and, thereby, reducing the release level of ferrous ions.

The details of this process are unknown, but another possibility for the reduction of ferrous iron level is the reduction with already existing ferric oxides.

In the BWR core the intense radiation produces an oxidizing environment owing to the radiolysis of water. This situation may have some influence on the release or behavior of the corrosion products in the coolant circuit. The results of laboratory experiments have shown that radiation enhances the release of insoluble iron but not soluble iron from carbon steel and stainless steel in pure water at high temperature.[11] The chemical form of the released insoluble iron was mainly hematite under the experimental condition. This

result was explained qualitatively as follows : the radiolysis of water gives several chemical species as shown by equation (2).

$$H_2O \rightsquigarrow H,\ OH,\ e^-_{aq},\ H_2O_2.\ H_2,\ H_3O^+ \qquad (2)$$

Among these chemical species, OH and H_2O_2 are strong oxidizing agents, while e^-_{aq} and H are reducing. As already mentioned in the previous section, ferrous iron is released from carbon steel or stainless steel by the corrosion process. The ferrous ions released react with oxidizing species to yield ferric ions as shown by equations (3)~(5). Some of ferric ions thus produced may have a chance to react with e^-_{aq}

$$Fe^{2+} + OH \longrightarrow Fe^{3+} + OH^- \qquad (3)$$

$$Fe^{2+} + H_2O_2 \longrightarrow Fe^{3+} + OH^- + OH \qquad (4)$$

$$Fe^{2+} + H + H^+ \longrightarrow Fe^{3+} + H_2 \qquad (5)$$

and be reduced to ferrous ions, but the total sum of G values for oxidizing species is larger than G values for e^-_{aq}. Ferric ions readily react with water molecules to yield ferric hydroxide as shown below. Ferric hydroxide precipitates and is dehydrated to yield hematite.

$$Fe^{3+} + 3H_2O \longrightarrow Fe(OH)_3 + 3H^+ \qquad (6)$$

$$2Fe(OH)_3 \longrightarrow Fe_2O_3 + 3H_2O \qquad (7)$$

The above result and its explanation seem to be very consistent with the fact that the corrosion products in reactor water of BWRs are mostly crud or insoluble particles mainly composed of hematite with a very small proportion of soluble iron.

Another species which is also important from the view point of the radioactivity transport is cobalt, providing the main source of ^{60}Co responsible generally for the highest contribution to circuit dose rates.

There has been some controversy on the predominant sources of ^{59}Co released by the corrosion and wear processes in BWR primary systems.[12] In one assessment of cobalt sources it was estimated that approximately 90% of the cobalt input originates from cobalt based alloys as shown in Fig.4,[13] though they are less than 0.1% of the plant's surface area. In another estimation, however, it is reported that approximately 50% of cobalt comes from stainless steel used in the feed water heaters.[14] It is known that the cobalt release rate from stainless steel and cobalt based alloys depends on the duration of the release experiment and usually decreases with increasing duration of the release test . Thus, available release data is inadequate for a general quantitative estimation of cobalt sources.

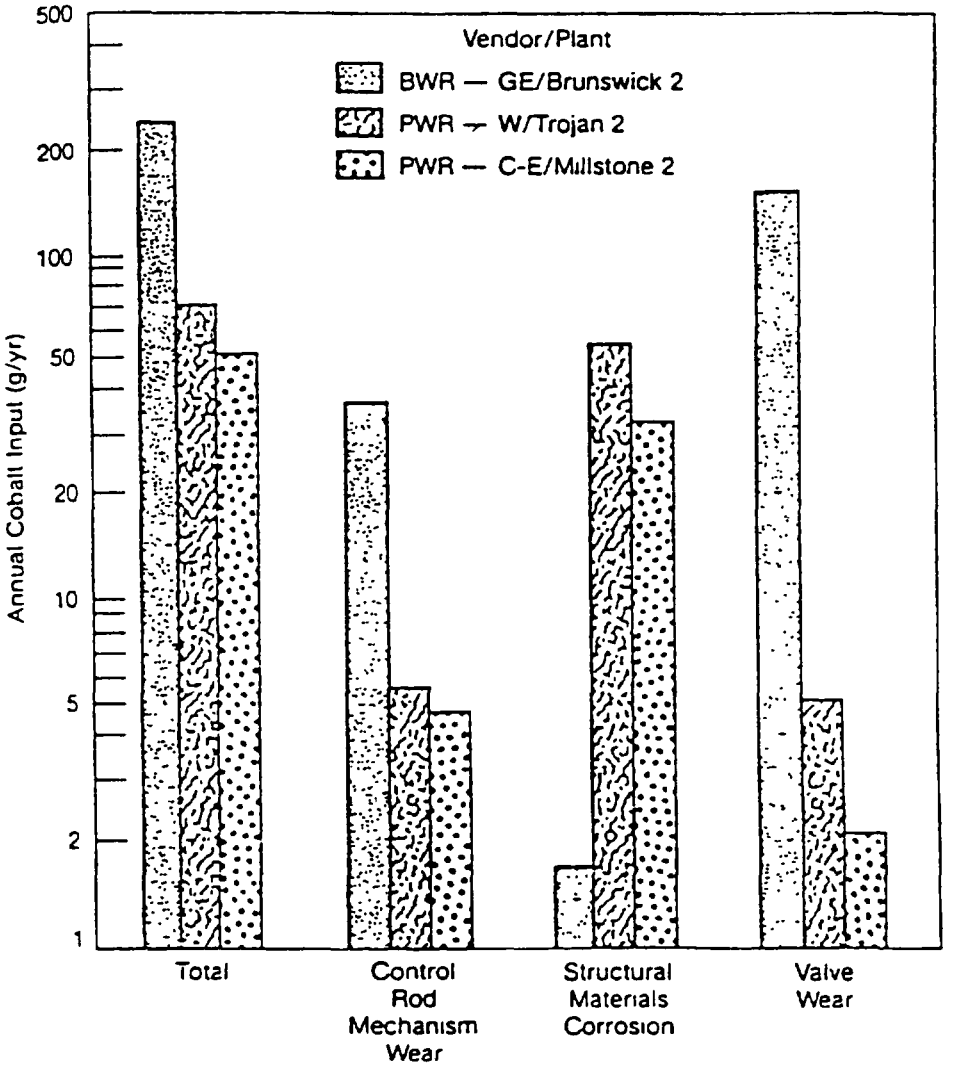

Fig. 4. Main cobalt sources in BWR and PWR plants.[13]

Cobalt is released mainly as soluble ions from stainless steel by the corrosion process, and the release rate is also dependent on the concentration of the dissolved oxygen. It is reported that high levels of dissolved oxygen such as 8ppm[15] or 40ppm[16] enhance the release of cobalt but not of iron. Hence, oxygen injection in the feed water of BWR is not so effective in suppressing the release of cobalt compared with iron.

3. Behavior of Insoluble Species.

(1) Properties and size of crud particles.

Insoluble corrosion products or crud particles play an important role in the radioactivity build-up in BWRs primary systems. Crud particles dispersed in the reactor water of BWRs are known to be predominantly hematite, unlike the PWR situation where nickel ferrite and magnetite are the main components. This difference arises both from the difference in the component materials and the corrosion environments in PWRs and BWRs. Reactor water in BWRs, usually, contains approximately 200ppb of oxygen arising from the radiolysis of water in the reactor core. Therefore, the environment in the core is more oxidizing than in PWRs where hydrogen is added in the primary sytems.

In BWR feed water hematite is considered to be the main component of crud with significant contribution of magnetite. It is believed by some people that there is also some contribution of "amorphous" corrosion products to crud in the feed water system, especially, in the lower temperature part,[17] though the actual properties of the "amorphous" crud have not been well defined. This amorphous iron based crud may be related to the leakage of corrosion products through the condensate demineralizers.

When the behavior of crud particles is considered in the modeling of corrosion products, the size distribution of the particles is one of the most important properties of crud. However, data from actual plants on the diameter of crud particles is sparse. One of the possible reasons for the scarcity of data is that experimental techniques for the particle measurements are not well developed. For instance,

scanning electron microscopy (SEM) is often used for the measurement of the particle sizes,but there is always the possibility of the particle coagulation during the preparation of the samples. One particle counter, the Coulter counter, can be used to measure the diameter of crud particles in the dispersed state, but usually has a limiting value for the measurable diameter and can not be applied to the measurement of the small particles with a diameter less than 0.5μm.

In one of the Japanese BWR plants, particle sizes were measured with crud in reactor water and feed water by SEM and values of 5～7μm were found for average diameters of the particles in both systems. [18] Relatively large average diameters(2～20μm) were also observed[19), 20] in the reactor water of SGHWR at Winfrith, which is a boiling water type reactor with pressure tubes. On the other hand, rather small diameters were observed with the crud particles in the feed water of another BWR by means of SEM[21], as shown in Fig.5.

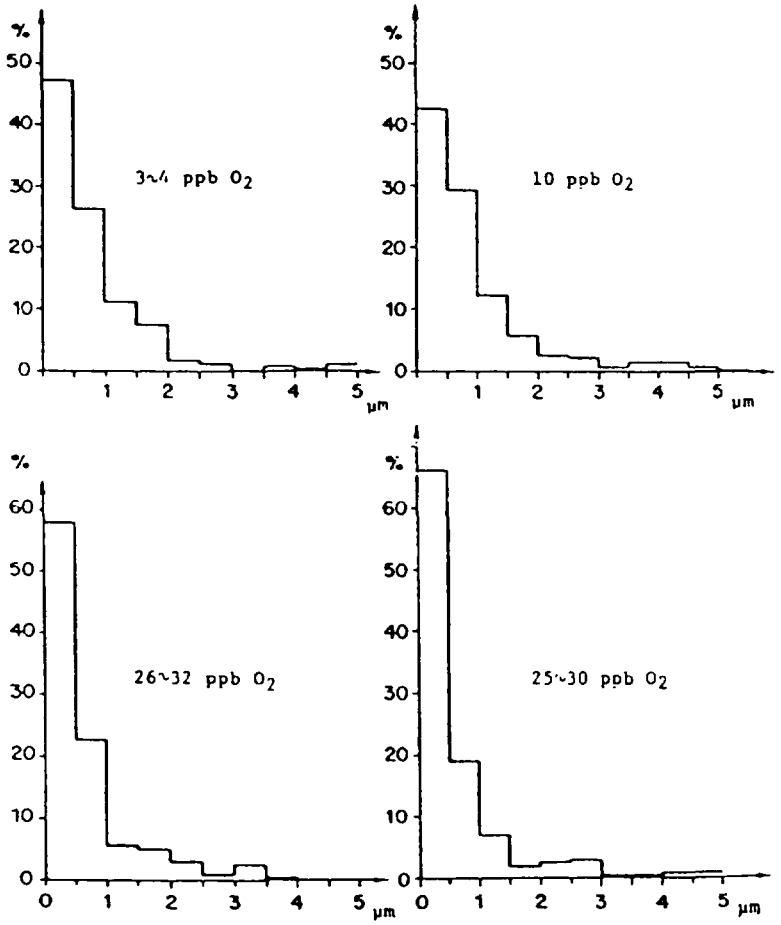

Fig.5. Suspended particle diameter distribution in feed water line of a BWR, before and during an oxygen dose experiment.[21]

The examination of fuel deposits in BWRs shows that the fuel deposits consist of two types of particles, small(0.1～0.3μm) irregular shaped particles and larger particles(0.5~3μm) having sharper egges and faces.[22)]

Nuclepore or millipore filters with nominal pore sizes are sometimes used to descriminate particles of different diameter.[23)] It is to be noted that the mechanism of colloid particle filtration is not simply the bulk filtration with the filters. Double layer interaction between the colloid particle and the filter surface also plays an important role, since both of them have their own surface charges depending on pH of the solution. Thus, the filtration efficiency is sharply dependent on pH of the solution, and particles of 0.15μm diameter are readily collected on a millipore filter with nominal 8μm pores at neutral pH, as shown in Fig.6.[24)]

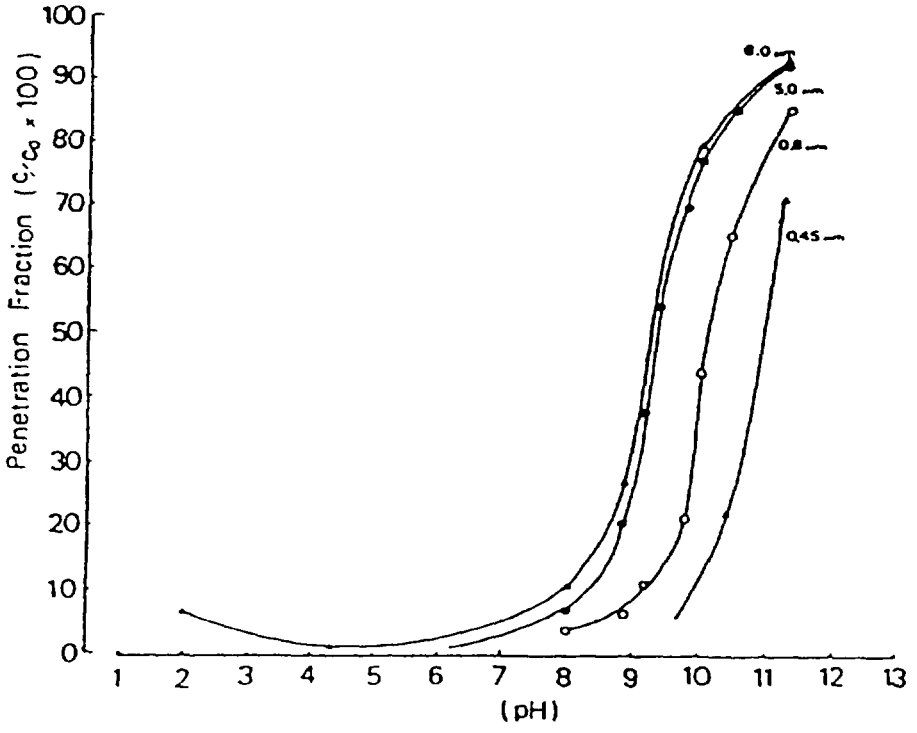

Fig.6. Penetration fractions of hematite particles with millipore filters in model experiment.[24)]

flow rate 0.24cm/sec.

filter pore △ 8μm, ● 5μm

○ 0.8μm, ▲ 0.45μm

hematite particle diameter 0.15μm

(2) Removal of crud particles in purification units.

The majority of the corrosion products in the feed water of BWRs arises from leakage of crud through the condensate treatment systems, and, thus, performance of the condensate demineralizers is a very important factor in controlling the corrosion product levels in the final feed water. Condensate demineralizers,deep bed type ion-exchange resin columns and/or powdered resin filters are normally in use. Whereas powdered resin filters are very effective in removing crud particles from the turbine condensate, the performance of deep bed columns employing bead resins for crud particles is rather variable from plant to plant. Deep bed ion-exchange resins were originally intended to remove ionic impurities arising from leakage of condenser but not crud particles. Some of the crud particles, however, are actually retained at the surface of the beep bed ion-exchange resins. The filtration mechanism of colloidal particles with deep beds is rather complicated and varies in time with increasing amounts of the deposited particles on the collectors. From the practical point of view, it seems that the early stage of the filtration is rather important, since the deep bed resins are routinely regenerated in short cycles in normal plant operation.

A conceptual model was proposed to describe the filtration of suspended particles with packed deep beds.[25] In this model a single spherical collector (resin bead) is considered and it is assumed that this collector is unaffected by its neighbors and fixed in space in the flowing suspension as shown in Fig.7. Three transport processes are considered : interception, sedimentation and diffusion. Interception occurs when a suspended particle following a stream-line of the flow comes in contact with the collectors as case A in Fig.7. A particle having a density greater than that of water will follow a different trajectory affected by the gravitational force field (case B). This is sedimentation. Brownian motion of a suspended particle drives it to the surface of the collector, and this transport process is diffusion.

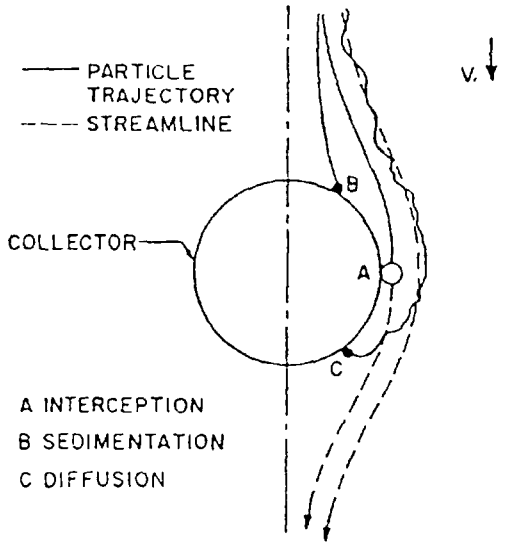

Fig.7. Basic transport mechanism in water filtration.[21]

In this model, performance of a packed bed is represented by Eq.(8).

$$\ln\frac{C_{in}}{C_{eff}} = \frac{3}{2}(1-\varepsilon)\alpha\eta\left(\frac{L}{d}\right) \tag{8}$$

where C_{in} and C_{eff} are the influent and effluent concentrations for a packed bed, respectively, ε the bed porosity, d the diameter of the collector, L the bed length. η is the contact efficiency of a single collector and defined as the rate at which particles strike the collector divided by the rate at which particles flow toward the collector. α is the collision efficiency factor or sticking factor, defined as the number of the contacts which succeed in producing adhesion divided by the number of collisions. The contact efficiency η is related to the transport processes of the suspended particles and evaluated theoretically as follows :

$$\eta_D = 0.9\left(\frac{kT}{\mu d_p v}\right)^{2/3} \tag{9}$$

$$\eta_I = \frac{3}{2}\left(\frac{d_p}{d}\right)^2 \tag{10}$$

$$\eta_G = \frac{(\rho_p-\rho)gd_p^2}{18\mu v} \tag{11}$$

$$\eta = \eta_D + \eta_I + \eta_G \qquad (12)$$

where η_D, η_I and η_G are theoretical single-collector efficiencies, corresponding to diffusion, interception and sedimentation, respectively. μ the water viscosity, d_p the diameter of the suspended particles, v the water velocity, g the gravitational acceleration, ρ and ρ_p are densities of water and the suspended particles.

The sticking factor α is supposed to reflect the chemistry of the system, but is treated as adjusting parameter, since no reliable theoretical evaluation method is available for this parameter. This model seems to explain qualitatively the dependence of the removal efficiency on the diameters of the suspended particles, as shown in Fig.8, but still some discrepancy remains between the theory and the experimental results. It was reported that the double layer interaction plays an important role in the filtration process [26,27], and closely relates to the sticking factor. Optimum adhesion corresponded to systems in which the suspended particles and the collectors were oppositely charged. It was also found that the deposition process of the adhered particles becomes important under special conditions, depending strongly on the pH and the ionic strength of the system.

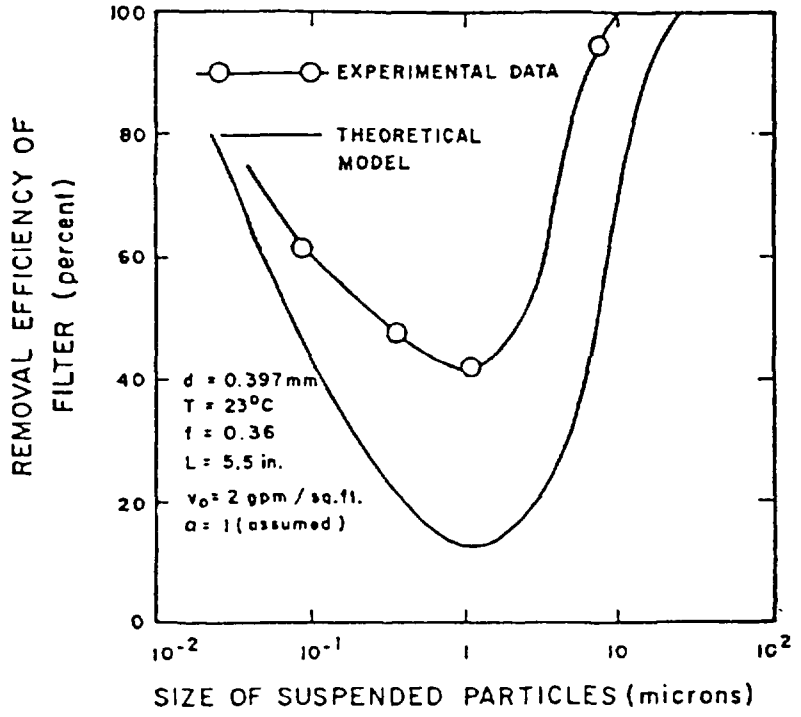

Fig.8. Comparison of theoretical model and experimental data.[25]

In another model[28] the desorption term as well as the deposition of suspended particles is incorporated in the rate equation to explain the rapid reduction of deposition rate with increasing coverage of the collector surface.

In a recent model[29] the filtration process is classified into 4 stages. The first is the early stage during which the resin surfaces are covered with very small amounts of the suspended particles and still available for the adsorption. During this stage direct double layer kinetic interaction between the surface of the collector and the suspended particle affects strongly the adhesion process of the particle. The second is a transient stage where the bead resin surfaces have not been covered completely with particles but the interaction between the resin surface and the approaching particle is attenuated or shielded by the particles already adsorbed. In the third stage when the surface of the resin has been covered completely with particles, the interaction between the particles already adsorbed and those approaching becomes predominant instead of that between the collector surface and the approaching particle. During the final stage decrease in the porosity of the packed bed is no longer negligible, and pressure drop across the deep bed sharply increase with increasing amounts of the adsorbed particles. Finally the bed will become clogged.

The basic conservation equation is expressed as Eq.(13)

$$\varepsilon \frac{\partial C}{\partial t} + \frac{\partial \sigma}{\partial t} + \varepsilon v \frac{\partial C}{\partial z} - D_L \frac{\partial^2 C}{\partial z^2} = 0 \tag{13}$$

$$\sigma = \rho_c A(1-\varepsilon)S \tag{14}$$

where C refers to the concentration of suspended particles in the water phase, σ the concentration of the particles adsorbed on the surfaces of the collectors, z the axial distance, D_L the modified coefficient of axial diffusion and dispersion combined, ρ_c the density of the collector, A the specific surface area available for the particle adsorption, S the adsorption density of the particles per unit surface area.

Usually the last term is negligible in Eq.(13) compared with the convection term. Hence Eq.(13) reduces to Eq.(15).

$$\varepsilon \frac{\partial C}{\partial t} + \frac{\partial \sigma}{\partial t} + \varepsilon v \frac{\partial C}{\partial z} = 0 \tag{15}$$

In the first stage of the filtration, a Langmuir type rate expression is introduced in consideration of the saturation effect of the adsorption as follows.

$$\frac{\partial s}{\partial t} = k_a(S_{sat} - S)C - k_d S \tag{16}$$

Here S_{sat} is the limited value of S, and k_a and k_d are the adsorption and desorption rate coefficients, respectively. Analytical solution of (15) combined with (13) and (16) is possible and the final form is given as follows.

$$\frac{C(\alpha,\beta)}{C_o} = \frac{X(\alpha,\beta)-\delta}{1-\delta} \tag{17}$$

$$\frac{S(\alpha,\beta)}{S_{sat}} = 1 - X(\beta,\alpha) \tag{18}$$

$$X(\alpha,\beta) = \frac{\delta T(\alpha,\beta) + T(\beta,\alpha) + I_o(2\sqrt{\delta\alpha\beta})}{T(\alpha,\beta) + T(\beta,\alpha) + I_o(2\sqrt{\delta\alpha\beta})} \tag{19}$$

$$T(\alpha,\beta) = e^{\alpha} \int_o^{\alpha} e^{-\tau} I_o(2\sqrt{\gamma\beta z})\, d\tau \tag{20}$$

$$\delta = \frac{k_d}{C_{in}k_a + k_d} \tag{21}$$

$$\alpha = \left(\frac{\rho_c A(1-\varepsilon)}{\varepsilon} S_{sat} k_a\right)\frac{z}{v} \tag{22}$$

$$\beta = (C_{in}k_a + k_d) \tag{23}$$

$$\tau = t - \frac{z}{v} \tag{24}$$

where $I_o(x)$ is the modified Bessel function of zero-th order.

This solution is of rather complicated form to use, but is reduced to a simplified formula as shown below when the release rate constant

(k_d) is assumed to be approximately zero as is the case with the early stage filtration of BWR condensate demineralizer.

$$\ln(C_{in}/C_{eff} - 1) = \ln(e^{\alpha_L} - 1) - (\frac{L}{v} C_{in} k_a)\eta \quad (25)$$

$$\alpha_L = \frac{L}{v} \frac{\rho_c A(1-\varepsilon)}{\varepsilon} S_{sat} k_a \quad (26)$$

$$\eta = \frac{L}{v} t - 1 \quad (27)$$

Eq.(25) means that a plot of $\ln(C_{in}/C_{eff} - 1)$ versus η should be linear in this stage of filtration.

On the other hand, in the third stage of the filtration the rate of particle adsorption is controlled by the interaction between the particles already adsorbed and approaching. Therefore, there will be no further adsorption limit at this stage until the bed is clogged. Thus, the rate equation should be changed to (28) instead of (16).

$$\frac{\partial s}{\partial t} = k_a' C - k_d' S \quad (28)$$

If the desorption of the particles is assumed to be neglected as in the first stage, a simple solution is derived from (17) as follows.

$$C_{eff}/C_{in} = e^{-\alpha'} \quad (29)$$

$$S/C_{in} = k_a' (t - \frac{z}{v}) e^{-\alpha'} \quad (30)$$

$$\alpha' = \frac{\rho_c A(1-\varepsilon)}{\varepsilon} k_a' (\frac{L}{v}) \quad (31)$$

Eq.(29) shows that the effluent particle concentration C_{eff} is independent of time t as opposed to the situation in the first stage.

In Fig.9 is shown the plots of $\ln(C_{in}/C_{eff} - 1)$ versus η for the model experiment using hematite. It is seen that the plots change from linear relation in the initial stage to the constant, corresponding to the change from the first to the third stage.

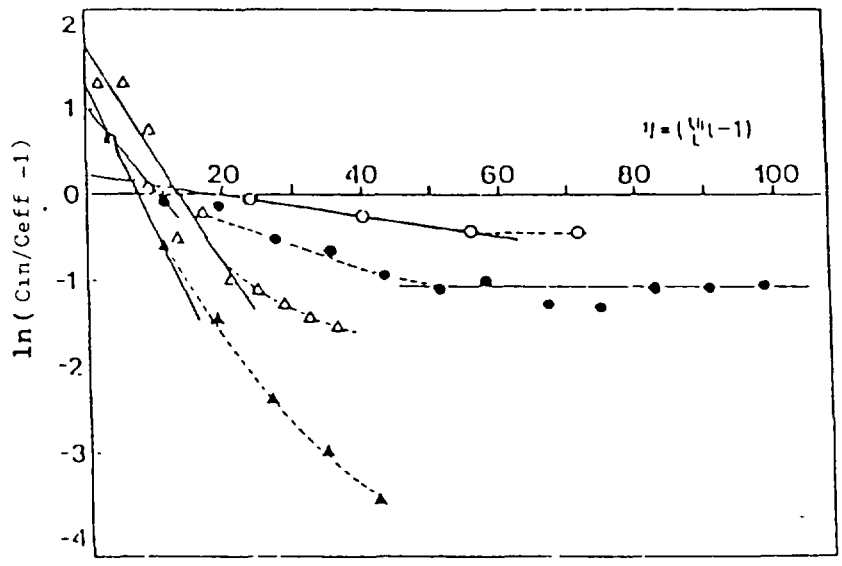

Fig.9. Plots of $\ln(C_{in}/C_{eff} - 1)$ versus n in model experiment using hematite particle (d_p 0.15 m).[29)]

○ Co = 6.73 ppm, L = 4 cm, v = 0.10 cm/sec.
● C_o = 28.9 ppm, L = 9 cm, v = 0.16 cm/sec.
△ C_o = 31.1 ppm, L =19 cm, v = 0.13 cm/sec.
▲ C_o = 52.0 ppm, L = 9 cm, v = 0.14 cm/sec.

(3) Deposition of crud particles on boiling surfaces

The deposition of crud particles on fuel surfaces is one of the most important step in radioactivity build-up in the primary systems. In BWR, the boiling of water in core enhances the deposition process, and high heat flux and radiation dose may also influence the morphology of the deposits on the fuel surfaces. It is known that the deposits on BWR fuels again show a double layer structure, inner and outer layers. The latter is assumed to be transformed into the former[30)] probably owing to the high heat flux and radiation dose.

Model experiments show that there are several factors which have large influence on the deposition rates of crud particles on boiling surfaces. The particle deposition on boiling surfaces is, however, a complicated phenomenon, and the transport process of the particles around boiling bubbles is very difficult to deal with theoretically.

Most of the relevant reports therefore concentrate on finding the factors affecting the deposition process and treat it rather phenomenologically. The phenomenological description is given in the following section.

As already mentioned, boiling of water promotes the deposition of particles on boiling surfaces in comparison with the case without boiling under the same heat flux.[31) - 33)] A model has been proposed[33)] to explain the effect of boiling on the heated surfaces. In this model it is assumed that particle deposition takes place around boiling points. At the boiling sites bubbles grow and evaporation of a microlayer of water formed between the bottom of growing bubble and the heated surface plays an important role as shown in Fig.10. Only the particles present in the dried-out microlayer deposit on the heated surface. On the other hand, it is claimed[34)] that crud particles having lyophobic property are trapped on the interfaces between water and bubble, and are collected preferentially in the boundary area between the bubble and the heated surface.

Almost all the reports agree that the deposition rate of the particles on boiling surfaces is proportional to the concentration of the particles.[33)-32)-37)] On the other hand, there has been some controversy on the dependence of the deposition

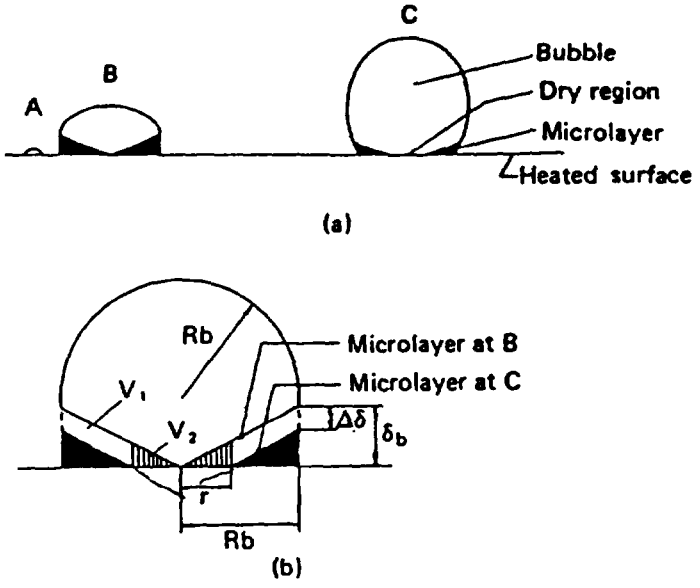

Fig.10. Schematic model of iron oxide deposition : (a) bubble growth (b) microlayer evaporation and dryout.[33)]

rate on the heat flux through the heat transfer surfaces. It is reported in one group of papers[35), 36), 38)] that the deposition rate is proportional to the square of the heat flux, whereas another group[33), 34), 37)] of papers claims that the deposition rate is directly proportional to the heat flux.

The pH of the dispersing solution affects the surface charges on dispersed particles, the heated surface and, consequently, the double layer interaction between them. It was pointed out[40)] that the electrostatic[39)] double layer interaction is very important in the deposition process of the particles, or especially when they are small, even under boiling condition. The effect of pH on the deposition process was investigated under boiling condition to examine the influence of double layer interaction. It was found[34), 37)] that the particle deposition rate decreases near the point of zero charge (PZC) of the particles. This cannot be explained by the simple DLTO theory. It is necessary to include the effects of hydrodynamics and mass transfer in boiling.

It was inferred on the basis of plant data that smaller particles deposit more effectively on boiling surfaces than larger particles.[30)] A model experiment, however, showed[37)] that the above prediction is partly valid, but partly wrong. As shown in Fig. 11, there is an optimum particle diameter for deposition on boiling surfaces. This result is also explained by the assumption of the optimum interaction barrier described above.

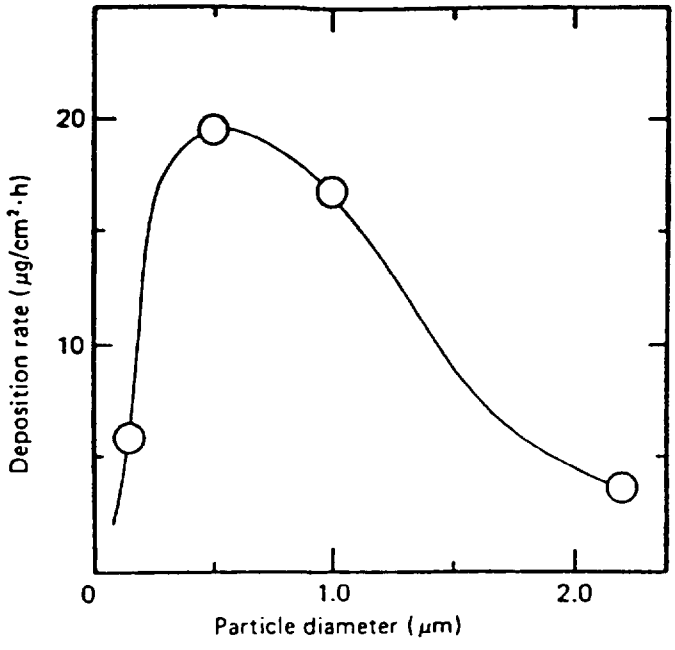

Fig.11. Relation between the deposition rate and particle diameter, with hematite concentration = 1 ppm iron and heat flux = 10 W/cm^2.[37)]

There have been experimental reports on the effect of flow rate of the dispersion solution on the deposition rate of particles. A model experiment showed that the deposition rate decreases with increasing flow rate, which was well explained by the microlayer deposition model cited previously.[33]

At the initial stage of the particle deposition, the release process of deposited particles is usually neglected. This does not hold, however,as the deposition proceeds. As shown in Fig.12, the amounts of the deposits level off at long time, and approach an equilibrium value.[34]

The deposition and release processes are treated by a rather simple equation as given below.[33]

$$\frac{dW}{dt} = k_1 c - k_2 W \tag{32}$$

where W refers to the deposit weight of particles per unit area, k_1 the rate constant of deposition, c the concentration of the particles and k_2 the rate constant of release. As above mentioned, the deposition rate constant (k_1) is known to depend on many factors, but little is known about the release rate constant (k_2).

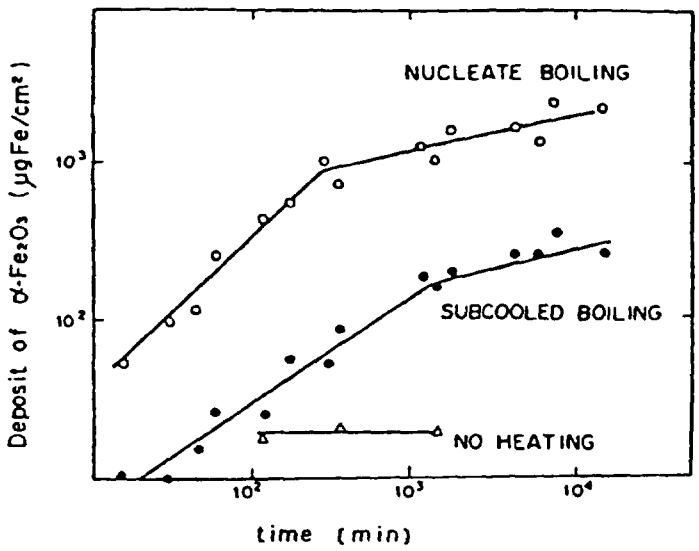

Fig.12. Effect of boiling regimes on deposition.[34]

Plant data show that the deposits on the fuel surfaces take double layer oxide structure, inner and outer layers, but no model experiment has provided the evidence of the double layer formation during deposition, probably due to experimental periods being too short for the transformation of deposits to take place. Therefore, nothing is known about the rate constants of the outer to inner transformations, which are accepted as taking place in actual BWR plants.

4. Behavior of Soluble Species

(1) Interaction of Co ion with crud particles.

The bahavior of cobalt ions is the most important, since cobalt-60 makes the greatest contribution to the surface dose rate of recirculation piping, and the dominant form of Co corrosion products is in soluble ionic form. It is well known that metal cations such as cobalt are readily adsorbed on the surfaces of oxide particles. Therefore, cobalt and cobalt-60 ions in the primary water of BWR are adsorbed on the surfaces of crud particles, fuel deposits and oxide layers on the piping. The adsorption of cobalt ions on the oxide surfaces is strongly dependent on the solution pH, as shown in Fig.13[41]. There has been some controversy on this pH dependence in relation to the mechanism of adsorption. It is generally accepted that metal hydroxide groups such as >FeOH provide the sites for adsorption, and the metal hydroxide groups have amphoteric properties as shown by the following reactions.

$$>FeOH + H^+ \rightleftharpoons FeOH^+ \quad (33)$$

$$>FeOH \rightleftharpoons FeO^- + H^+ \quad (34)$$

It has been shown in the previous part(Fig.3-1 in PWR Review) that ions are subject to hydrolysis reactions, depending on pH of the solution. It was suggested[42] that $CoOH^+$ is predominant species adsorbed on metal oxide surfaces, and the hydrolysis product, $Co(OH)^+$, formed in aqueous phase was claimed to be preferentially adsorbed on the surfaces of oxides[43] because of its much lower desolvation energy.[42]

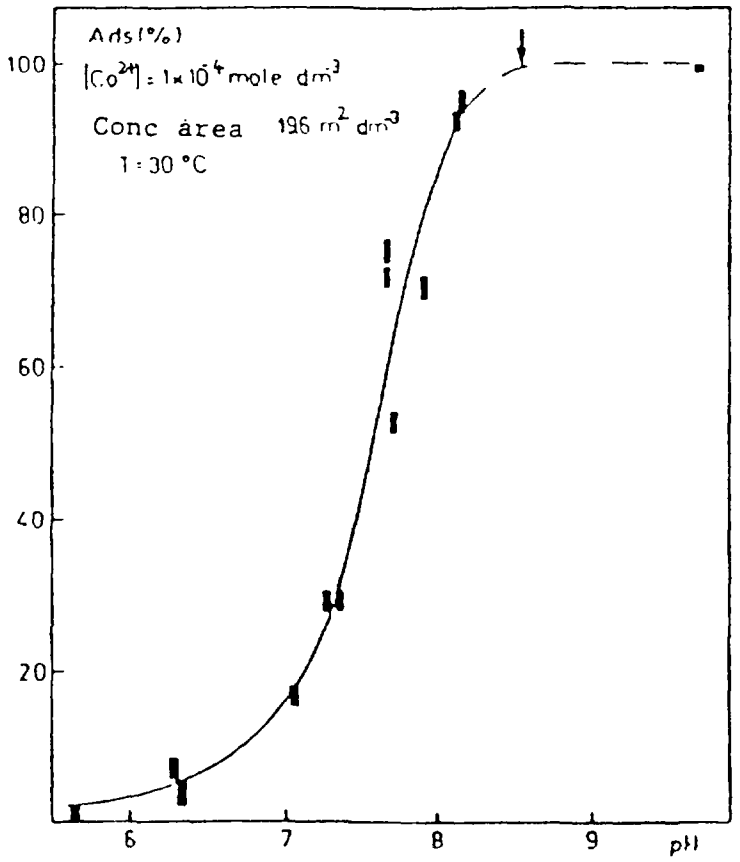

Fig.13. pH dependence of cobalt(II) adsorption at 30°C.[41]

It was proposed, however, that the formation of bidentate surface complexes are necessary to explain the pH dependence of the adsorption.[44), 45)]

$$\text{(FeOH)}_2 + Co^{2+} \rightleftharpoons \begin{matrix} \text{FeO} \\ \diagdown \\ \text{Co} \\ \diagup \\ \text{FeO} \end{matrix} + 2H^+ \qquad (35)$$

On the other hand, it was pointed out[46)] in the case of other metal cations such as Cd and Cu that if the electrical double layers on the surfaces of the particles are considered and the complex formation between hydroxide and metal cation at surfaces is due to electrostatic bonding, then the experimental results are better explained by assuming the presence of two types of the complexes shown below (36) and (37) than by the introduction of the bidentate complexes (35).

$$>FeOH + Co^{2+} \rightleftharpoons Fe\text{-}O^{-} \cdots Co^{2+} \quad (36)$$

$$>FeOH + Co^{2+} + H_2O \rightleftharpoons Fe\text{--}O \quad CoOH \quad (37)$$

In this model the effect of surface potentials on the equilibrium of the complex formation is taken into account as follows.

$$[FeO^{-}\text{-}Co^{2+}] = \frac{[FeOH][Co^{2+}]}{[H^{+}]} \exp[(e\psi_o - 2e\psi_B)/kT] \; K^{int}_{Co^{2+}} \quad (38)$$

where $[Co^{2+}]$ and $[H^{+}]$ refer to the concentrations of cobalt ions and protons in bulk solution, respectively. Surface potentials ψ_o and ψ_B are defined in Fig.14. The cobalt ions are assumed to be placed in σ_B plane, while protons and hydroxide ions are bonded in σ_o plane.

On the contrary, an electron spin resonance (ESR) experiment[47] showed that some divalent metal cations are adsorbed on the surfaces of oxides by the formation of covalent bonds and not only by electrostatic bonds.

Recently, a new model has been proposed[48] in which the covalency of the bond between metal cation and oxide surface is taken into account.

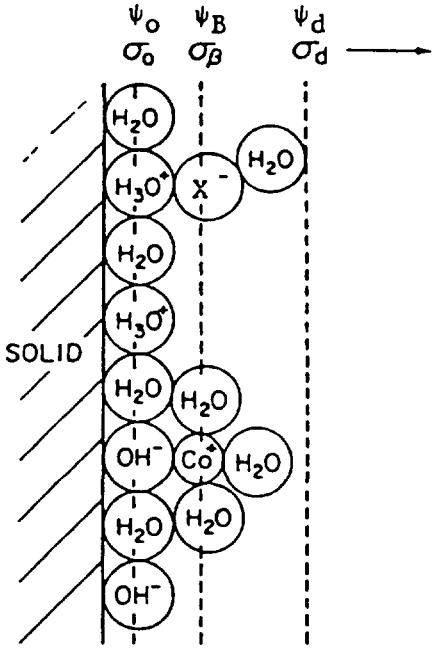

Fig.14. Schematic representation of an oxide interface showing possible location for molecules comprising the places of charge.

Here the metal cations as well as protons and hydroxide ions are arranged in σ_o plane in Fig.14. Therefore, the equilibrium of Eq.(36) is represented by (39) instead of (38). The cobalt ion adsorbed on the

$$[FeOCo^+] = \frac{[FeOH][Co^{2+}]}{[H^+]} \exp[-e\psi_o/kT] \; K^{int}_{Co^{2+}} \qquad (39)$$

oxide surface is considered to hydrolyze the water molecule to release a proton, and, therefore, Eq.(37) is rewritten more explicitly as follows.

$$\rangle FeOCo^+ + H_2O \longrightarrow FeOCoOH + H^+ \qquad (40)$$

This model was reported[48] to account satisfactorily the adsorption isotherms and pH dependence of various metal ions. Any of the proposed models for the adsorption of hydrolysable cations on oxide surfaces accounts for the adsorption isotherms and pH dependence. The model proposed by Regazzoni,[10] where adsorption is not restricted to a monolayer, accounts in addition for the observed electrokinetic behaviour. This idea is supported by the recent adsorption-surface precipitation model.[53]

Most of the adsorption experiments have dealt with the adsorption-desorption equilibria, and very few data are available on the kinetics of the adsorption and desorption processes, which are very important from the view point of modelling corrosion product transport. Pressure jump methods were applied[49] to measure the rate constants of adsorption and desorption, and it was found that the relaxation processes detected by electric conductivity contain both fast and slow steps. The interpretation of the result , however, not straightforward due to the complexity of the mechanism.

High temperature data on the cobalt adsorption and desorption are also very limited. It is recognized [50], [51], [52] that larger amount of cobalt ions are adsorbed on the oxide surfaces at higher temperature as shown in Fig. 15. It was suggested that at high temperature the cobalt ions adsorbed on the surfaces of magnetite and hematite are transformed[50], [53], [54] to a cobalt ferrite phase after diffusing into the inside of the crystal lattices. This is also supported by evidence collected in plant.[41]

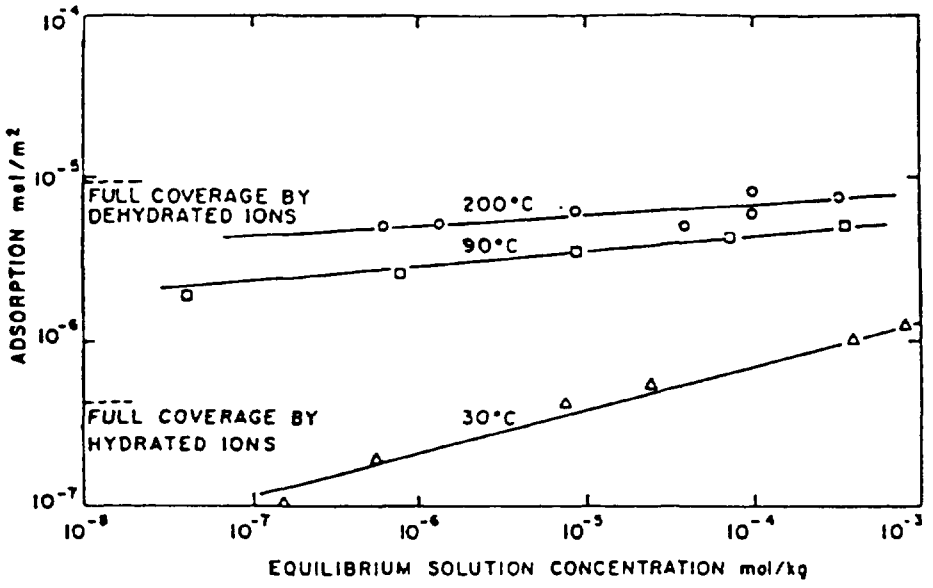

Fig.15. Log Co(II) adsorbed versus log equilibrium Co(II) solution concentration on $NiFe_2O_4$ at different temperatures, pH_{25} 6.5.[50)]

References

1) Y. Koine, Y. Takashima, K. Ohsumi, S. Uchida, M. Izumiya and M. Miki, Proc. of IAEA Symposium on Water Chemistry and Corrosion Problems in Nuclear Power Plants, IAEA-SM-264/1, p. 3, 1983.

2) E.G. Brush and W.L. Pearl, Corrosion-NACE, 28, 129, 1972.

3) M. Izumiya, H. Mizuniwa, K. Ohsumi, T. Kambayashi, Y. Matsushita and K. Tanno, Karyoku Genshiryoku Hatsuden, 27, (15) 419, 1976.

4) M. Matsudaira, N. Suzuki, Y. Sato, M. Hashimoto, M. Okumura and M. Miyazaki, Boshoku Gijutsu, 28, (1), 32, 1979.

5) C. Welty and W. Bilanin, Proc. of EPRI Seminar on BWR Corrosion, Chemistry and Radiation Control, paper 17, 1984.

6) E.C. Potter and G.M.W. Mann, Proc. of 1st Int. Cong. Metallic Corrosion, London, p. 417, 1961.

7) L. Tomlinson, Corrosion-NACE, 37, 591, 1981.

8) A.E. Regazzoni, C.A. Unutic, M.A. Blesa and A.j.G. Maroto, J. Inog. Chem. 43, 1489 (1981).

9) Y. Tanura, K. Ito, T. Katsura, J. Chem. Soc. Daltan Teams 1983 189.

10) A.E. Regazzoni, phD. (1984) Universidad de Tucuman CNEA · Rp-NT 2/84.

11) K. Ishigure, N. Fujita, T. Tamura and K. Oshima, Nucl. Tech., 50, 169, 1980.

12) C.F. Falk, EPRI NP-2263, 1982.

13) C.J. Wood, Proc. of EPRI Seminar on BWR Corrosion, Chemistry and Radiation Control, paper 33, 1984.

14) S. Uchida, M. Kitamura, M. Izumiya, K. Ohsumi and M. Miki, Water Chemistry of Nuclear Reactor Systems II, BNES, 229, 1980.

15) K. Ishigure, C. Matsuura, S. Ono and N. Fujita, unpublished data.

16) T. Iwahori, S. Kato, K. Wada, H. Kanbe and T. Mizuno, Boshoku Gijutsu, 32, 202, 1983.

17) H. Fujiwara, H. Mochizuki, T. Sawa, M. Yamamoto, Y. Hanamoto, Paper presented at Annual Meeting of Atom. Energy Soc. of Japan (1986) Kyoto.

18) S. Uchida, M. Kitamura, Y. Matsushita, K. Yonezawa, K. Ohsumi and M. Miki, Nucl. Sci. Eng., 77, 496, 1981.

19) P.J. Darley and B.J. Macforlane, Water Chemistry of Nuclear Reactor Systems I, BNES, 215, 1977.

20) D.J. Ferrett, E.J. Bird and G.C.W. Comley, Proc. of IAEA Symposium on Water Chemistry and Corrosion Products in Nuclear Power Plants, IAEA-SM-264/39, p 47, 1983.

21) G. Bart, K. Wasserfallen, M. Haller and M. Mokos, ibid., IAEA-SM-264/3, p.35, 1983.

22) L.D. Anstine, J.T. Zimmer and T.L. Wong, EPRI NP-3687, 1984.

23) R. Vandbrabant and P de Reggs, Water Chemistry of Nuclear Reactor Systems II, BNES, 279, 1980.

24) K. Ishigure, C. Matsuura, M. Kawaguchi, N. Fujita and K. Oshima, Corrosion/82, Houston, paper 225, 1982.

25) K. Yao, M. Hajian and c.R. O'Melia, Envron. Sci. Tech., 5, 1105, 1980.

26) R.J. Kuo and E. Matijević, J. Colloid Interface Sci., 78, 407, 1980.

27) E.J. Chayfield, A.J. Smith, Environ. Sci. Techn. 4, 413 (1970).

28) R. Rajagopalan and R.Q. Chu, ibid., 86, 299, 1982.

29) K. Ishigure, M. Takahashi, M. Kawaguchi, Y. Wagoya, N. Fujita and Y. Nabatame, Water Chemistry of Nuclear Reactor Systems III, BNES, 315, 1983.

30) C.C. Lin, C.R. Pao, J.S. Wiley and W.R. Dehollander, Water Chemistry of Nuclear Reactor Systems II, BNES, 311, 1980.

31) F.D. Nicholson and J.V. Sarbutt, corrosion-NACE, 36, 1, 1980.

32) N. Taylor, AERE-R-8164, 1976.

33) Y. Asakura, K. Kikuchi, S. Uchida and H. Yusa, Nucl. Sci. Eng., 67, 1, 1978.

34) T. Iwahori, T. Mizuno and H. Koyama, Corrosion/78, Houston, paper 37, 1978.

35) N.N. Mankina, Teploenergetika, 7, (3), 8, 1960.

36) D. Charlesworth, Chem. Eng. Progress, Sym. Series, 66, 21, 1970.

37) M. Kawaguchi, K. Ishigure, N. Fujita and K. Oshima, Nucl. Tch., 62, 253, 1983.

38) K.A. Burrill, Can. J. Chem. Eng., 56, 79, 1978.

39) R. Gasparini, C.D. Rocci and -E. Ioannilli, Combustion, (NO.11), 12, 1969.

40) A.J.G. Maroto, M.A. Blesa, S.I. Passagio, A.E. Regazzoni "Water Chemistry" II BNES p. 247 (1981).

41) M.A. Blesa, R.M. Larotonda, A.J.G. Marato and A.E. Reyazzoni, Colloid Surface, 5, 197, 1982.

42) R.O. James and J.W. Healy, J. Colloid Interface Sci., 40, 42, 63, 65, 1972.

43) P.H. Tewari, A.B. Campbell and W. Lee, Can. J. Chem., 50, 1642, 1972.

44) P.W. Shindler, B. Furst et al., ibid., 55, 469, 1976.

45) H. Hohl and W.J. Stumm, ibid., 55, 281, 1976.

46) J. A. Davis and J.O. Leckie, ibid., 67, 90, 1978.

47) M.B. McBride, Soil Sci. Soc. Am. J., 42, 27, 1978.

48) K. Hachiya, M. Sasaki, Y. Saruta, N. Mikami and T. Yasunaga, J. Phys. Chem., 88, 23, 1984.

49) K. Hachiya, M. Sasaki, T. Ikeda, N. Mikami and T Yasunaga, J. Phys. Chem., 88, 27, 1984.

50) P.H. Tewari and W. Lee, J. Colloid Interface Sci., 52, 77, 1975.

51) H. Tamura, E. Matijević and J. Meites, ibid., 92, 303, 1983.

52) B. Venkataramani, K.S. Venkateswarlu, J. Shankar, L.H. Baetsle, Proc. Indian Acad. Sci., 87 A (Chem. Sci. 6) 415 (1978).

53) R. Kuwae, Y. Yamashita, J. Takabayashi, M. Hishida and H. Nagao, J. Nucl. Sci. Tech., 21, 484, 1984.

54) D. Briggs and Y.M. Bosworth, J. Colloid Interf. Sci., 59, 194 (1977.

55) K. J. Farley, D.A. Dzombak, F.M.M. Morel, J. Coll. Inf. Sci., 106, 226 (1985).

II. Computer Code Describing the Behavior of Corrosion Products in BWRs.

1. Introduction

There are several computer models or codes reported in the literature to describe the behaviour of products in BWRs and thereby calculate the amount of radioactivity corrosion deposited on the surfaces of recirculation piping and corresponding dose rates at the reactor shut-down. Each plant vendor of BWRs has its own code to simulate and forecast present and future situations of its own plants. In these computer codes, scenarios are described for the overall process of radioactivity build-up, starting from corrosion product release and leading to the deposition of cobalt. Each step comprising the overall process of corrosion product transport is formulated mathematically according to the scenario, then represented by several differential equations, which are solved numerically with plant data provided as input. There are many parameters, such as rate coefficients, included in the models, and these are usually determined by model experiments or fitting to plant data. The mechanism of radioactivity build-up is, however, very complicated as mentioned in the previous section, and is not understood completely. Thus, the computer models are rather semi-empirical and phenomenological, and sometimes oversimplification is introduced to the formulation where the mechanism of the process is not understood well. Therefore, all the models reported are incomplete at present and should be refined as we understand more of the detailed mechanism included in radioactivity transport process.

2. GE model

The basic transport phenomena assumed in this model are shown in a diagram in Fig.1. Some important points are hypothesized here as follows.[1)]

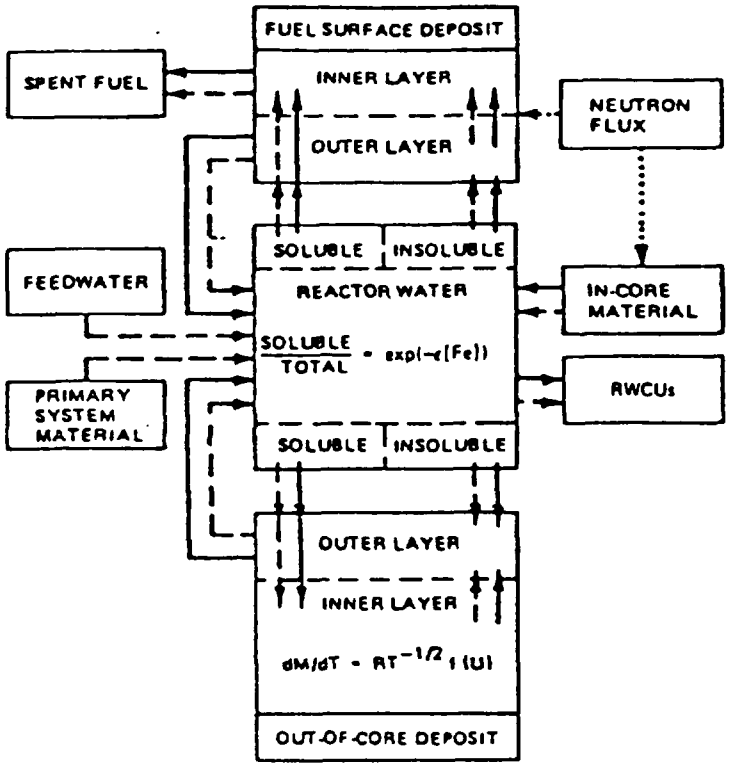

Fig. 1. Block diagram of ^{59}Co/ ^{60}Co transport model [1)]

1) Some interactions are considered to exist between soluble ions and crud particles, which include adsorption of ionic species on crud particles.
2) Both crud and soluble species deposit on the fuel surfaces, crud playing an important role in the deposition of the soluble species.
3) There are two layers, loosely attached and tenacious ones, deposited on fuel surfaces, and some of the former is transformed into the latter.
4) Radioactive species are released from in-core materials and also from the fuel surface deposits. They are distributed between soluble and insoluble species, following Freundlich adsorption isotherms.

5) Soluble and insoluble radioactive species deposit on out-of-core surfaces. Double oxide layers, inner and outer layers, are formed on the surfaces of the out-of-core base metal.

Mathematical equations are developed to describe the corrosion products transport during the steady state operation of BWRs.[2)]

Iron Transport

a) Deposition and release of iron on fuel surfaces.

$$\frac{dM_f^{Fe}(i)}{dt} = \frac{1}{n}\epsilon_f^{Fe} F_{core} C_{RW}^{Fe} - k_f^{Fe} M_f^{Fe}(i)$$

$$\epsilon_f^{Fe} = \delta_1 \epsilon^0 \frac{X}{36}$$

$$k_f^{Fe} = \frac{\delta_2 C_{RW}^{Fe}}{730 + 300\, C_{RW}^{Fe}} .$$

Here both δ_1 and δ_2 are dependent on properties of iron species. See note after the Nomenclature. i in the parentheses is associated with i'th fraction of the fuel bundles.

b) Deposition and release of iron in out-of-core deposits.

Inner layer

$$\frac{dM_{oi}^{Fe}}{dt} = R_s - k_{oi} M_{oi}^{Fe} .$$

$$R_s = \frac{S_o R_{cor}\{1 + \alpha(\mathcal{U} - 0.055)\}}{(TM + t)^{0.5}}$$

Corrosion rate (R_s) is assumed to be a function of water conductivity ($\mathcal{U}$), and TM is a small time period arbitrarily chosen so that R_s does not became infinite as $t \longrightarrow 0$.

Outer layer

$$\frac{dM_o^{Fe}}{dt} = \delta_0 \beta_o^{Fe} S_o C_{RW}^{Fe} + k_{oi} M_{oi}^{Fe} - k_o^{Fe} M_o^{Fe} .$$

c) Iron in reactor water

$$Wd\frac{C_{RW}^{Fe}}{dt} = WT + \sum_1^n k_f^{Fe} M_f^{Fe}(i) + k_o^{Fe} M_o^{Fe}$$

$$- (\epsilon_{cu}^{Fe} F_{cu} + \epsilon_f^{Fe} F_{core} + \delta_0 \beta_o^{Fe} S_o) C_{RW}^{Fe}$$

$$WT = C_{FW}^{Fe} F_{FW} .$$

Cobalt (Co and ^{60}Co) Transport

a) Deposition and release of cobalt on fuel surfaces.

Inner layer

$$\frac{dM_{fi}(i)}{dt} = \frac{1}{n}\epsilon_{fi}C_s^{59}F_{core} + k_{ft}(i)M_{fo}(i) - k_{fi}M_{fi}(i)$$

$$\epsilon_{fi}(i) = \gamma_{fi}\left[nM_f^{Fe}(i)/S_f\right]^{0.5}$$

$$k_{ft}(i) = \delta_3\epsilon_{k1} - \epsilon_{k2}M_f^{Fe}(i)$$

$$k_{fi} = \delta_4 k_f^{Fe} .$$

$$\frac{dA_{fi}(i)}{dt} = \lambda P_f M_{fi}(i) + \frac{1}{n}\epsilon_{fi}(i)C_s^{60}F_{core} + k_{ft}(i)A_{fo}(i) - (\lambda + k_{fi})A_{fi}(i)$$

$$P_f = 1.63 \times 10^{-11}\frac{\sigma}{MW}\cdot\phi_f .$$

where k_{ft} is the rate constant of the transformation of the outer layer to the inner layer and depends on the characteristic of the iron oxide, decreasing as the total iron deposits on the fuel surface increase.

Outer layer

$$\frac{dM_{fo}(i)}{dt} = \frac{1}{n}\epsilon_{fo}C_{IN}^{59}F_{core} + \frac{1}{n}\gamma_{fo}(i)C_S^{59}F_{core} - \left[k_{ft}(i) + k_{fo}\right]M_{fo}(i)$$

$$\epsilon_{fo} = \epsilon_f^{Fe}$$

$$\gamma_{fo}(i) = \delta\epsilon_{fi}(i)$$

$$k_{fo} = \delta_5 k_f^{Fe} .$$

$$\frac{dA_{fo}(i)}{dt} = \lambda P_f M_{fo}(i) + \frac{1}{n}\epsilon_{fo}C_{IN}^{60}F_{core} + \frac{1}{n}\gamma_{fo}(i)C_S^{60}F_{core} - \left[\lambda + k_{ft}(i) + \delta_8 k_{fo}\right]A_{fo}(i) .$$

b) Deposition and release of cobalt in out-of-core surfaces.

Inner layer

$$\frac{dM_{oi}}{dt} = \beta_{oi}C_s^{59}R_s + \epsilon_{oi}M_{oi}^{Fe}C_s^{59} - (k_{oi} + k_{oi})M_{oi}$$

$$\beta_{oi} = \epsilon_{g1} - \epsilon_{g2}M_o^{Fe} .$$

$$\frac{dA_{oi}}{dt} = \beta_{oi}C_s^{60}R_s + \epsilon_{oe}(M_{oi}C_s^{60} - A_{oi}C_s^{59}) - (\lambda + k_{oi} + k_{oi})A_{oi} .$$

The deposition rate constant(β_{oi}) for the inner layer decreases as the outer layer iron deposits(M_o^{Fe}) increase.

Outer layer

$$\frac{dM_{oo}}{dt} = \delta_6 \beta_{oo} C_{IN}^{59} S_o + \epsilon_{oo} M_o^{Fe} C_s^{59} + k_{oi} M_{oi} - k_{oo} M_{oo}$$

$$\frac{dA_{oo}}{dt} = \delta_7 \beta_{oo} C_{IN}^{60} S_o + \epsilon_{oo} M_o^{Fe} C_s^{60} + k_{oi} A_{oi} - (\lambda + k_{oo}) A_{oo} .$$

c) ^{60}Co production in in-core materials.

$$\frac{dA_i}{dt} = \lambda P_i M_i - \lambda A_i$$

$$P_i = 1.63 \times 10^{-11} \frac{\sigma}{MW} \cdot \phi_i .$$

d) Balance of cobalt in reactor water.

$$\frac{W dC_{RW}^{59}}{dt} = MT + \sum_i^n k_{fo} M_{fo}(i) + \sum_i^n k_{fi} M_{fi}(i) + k_{oi} M_{oi} + k_{oo} M_{oo} - \sum_i^n \frac{1}{n} (1 + \delta) \epsilon_{fi}(i) C_s^{59} F_{core} - \epsilon_{fo} C_{IN}^{59} F_{core} - \beta_{oi} C_s^{59} R_s - \epsilon_{oi} M_{oi}^{Fe} C_s^{59} - \epsilon_{oo} M_o^{Fe} C_s^{59} - \delta_6 \beta_{oo} C_{IN}^{59} S_o - \epsilon_{cu} C_{RW}^{59} F_{cu}$$

$$MT = 10^{-3} C_{FW}^{59} F_{FW} + D_i M_i + D_p M_p$$

$$C_s^{59} = C_{RW}^{59} \exp(-\epsilon_{59} C_{RW}^{Fe})$$

$$C_{IN}^{59} = C_{RW}^{59} - C_s^{59}$$

$$\frac{W dC_{RW}^{60}}{dt} = D_i A_i + \sum_i^n \delta_8 k_{fo} A_{fo}(i) + \sum_i^n k_{fi} A_{fi}(i) + k_{oi} A_{oi} + k_{oo} A_{oo} - \sum_i^n \frac{1}{n} (1 + \delta) \times \epsilon_{fi}(i) C_s^{60} F_{core} - \epsilon_{fo} C_{IN}^{60} F_{core} - \beta_{oi} C_s^{60} R_s - \lambda C_{RW}^{60} W - \epsilon_{oo} M_o^{Fe} C_s^{60} - \delta_7 \beta_{oo} C_{IN}^{60} S_o - \epsilon_{cu} C_{RW}^{60} F_{cu} - \epsilon_{or} \times (M_{oi} C_s^{60} - A_{oi} C_s^{59}) .$$

$$C_s^{60} = C_{RW}^{60} \exp(-\epsilon_{60} C_{RW}^{Fe}) .$$

$$C_{IN}^{60} = C_{RW}^{60} - C_s^{60} .$$

e) ^{60}Co concentration on out-of-core surfaces and radiation dose rate.

$$A_s = 10^4 (A_{oi} + A_{oo}) / S_o$$

$$A_{Rs} = K_R (A_s + K_s M_o^{Fe} / S_o)^{\gamma} .$$

Nomenclature

Reactor Parameters

W = reactor water mass (10^6 kg)

F_{cu} = RWCU flow rate (10^6 kg/day)

F_{fw} = feedwater flow rate (10^6 kg/day)

F_{core} = core flow rate (10^6 kg/day)

n = integer number of fractions of fuel replacement per cycle (dimensionless)

S_o = total out-of-core surface area (cm^2)

S_f = total fuel surface area (cm^2)

X = rated core average heat flux on fuel surface (W/cm^2)

Nuclear Data

λ = activity decay constant (day^{-1})

MW = atomic weight of target material (g/mol)

σ = activation cross section (b)

ϕ_f = thermal neutron flux on fuel surface ($n/cm^2 \cdot s^{-1}$)

ϕ_i = thermal neutron flux on in-core material ($n/cm^2 \cdot s^{-1}$)

P_f = activity production rate in fuel deposit (Ci/g)

P_i = activity production rate on in-core material (Ci/g)

Input Parameters

WT = total iron input from feedwater (g/day)

MT = total cobalt input to reactor water (g/day)

D_pM_p = cobalt release from primary system material (g/day)

M_i = cobalt in in-core material exposed to neutron flux and available for release[b] (g)

D_i = release rate constant for M_i[b] (day^{-1})

R_s = primary system surface total corrosion rate (g/day)

R_{cor} = primary system surface corrosion rate constant ($g/cm^2 \cdot day^{-0.5}$)

TM = pre-startup time (day)

$\mho$ = reactor water conductivity (μS/cm)

α = coefficient relating the conductivity with corrosion rate ($cm/\mu S$)

Activity Inventories

A_{fo} = activity in fuel deposit, outer layer (Ci)

A_{fi} = activity in fuel deposit, inner layer (Ci)

A_{oo} = activity in out-of-core deposit, outer layer (Ci)

A_{oi} = activity in out-of-core deposit, inner layer (Ci)

A_o = activity in out-of-core deposit, total (Ci)

A_s = activity concentration on out-of-core surface ($\mu Ci/cm^2$)

A_{re} = contact radiation dose rate on recirculation piping wall (mR/h)

A_i = activity in in-core material available for release (Ci)

A_{cu} = activity removed by RWCU system (Ci)

Concentrations in Water

C_{FW}^{Fe} = iron concentration in feedwater [ppb (10^{-6} g/kg)]

C_{RW}^{Fe} = iron concentration in reactor water (ppb)

C_{RW}^{59} = cobalt concentration in feedwater [ppt (10^{-9} g/kg)]

C_{RW}^{59} = total cobalt concentration in reactor water (ppb)

C_S^{59} = soluble cobalt concentration in reactor water (ppb)

C_{IN}^{59} = insoluble cobalt concentration in reactor water (ppb)

C_{RW}^{60} = total ^{60}Co concentration in reactor water (μCi/kg)

C_S^{60} = soluble ^{60}Co concentration in reactor water (μCi/kg)

C_{IN}^{60} = insoluble ^{60}Co concentration in reactor water (μCi/kg)

Material Inventories

M_{fo} = weight of cobalt in fuel deposit, outer layer (g)

M_{fi} = weight of cobalt in fuel deposit, inner layer (g)

M_{oo} = weight of cobalt in out-of-core deposit, outer layer (g)

M_{oi} = weight of cobalt in out-of-core deposit, inner layer (g)

M_{cu} = weight of cobalt removed by RWCU system (g)

M_f^{Fe} = weight of iron in fuel deposit (g)

M_o^{Fe} = weight of iron in out-of-core deposit, outer layer (g)

M_{oi}^{Fe} = weight of iron in out-of-core deposit, inner layer (g)

M_{cu}^{Fe} = weight of iron removed by RWCU system (g)

Transport Constants

ϵ_{cu} = RWCU system removal efficiency for cobalt (dimensionless)

ϵ_{cu}^{Fe} = RWCU system removal efficiency for iron (dimensionless)

ϵ_0 = fuel deposition constant (dimensionless)

ϵ_f^{Fe} = fuel deposition efficiency for iron (dimensionless)

ϵ_{fi} = fuel deposition efficiency for soluble cobalt, inner layer (dimensionless)

ϵ_{fo} = fuel deposition efficiency for insoluble cobalt, outer layer (dimensionless)

γ_{fi} = fuel deposition efficiency coefficient for soluble cobalt ($cm/g^{0.5}$)

γ_{fo} = fuel deposition efficiency for soluble cobalt, outer laver (dimensionless)

β_o^{Fe} = out-of-core deposition rate constant for iron (kg/cm^2 day^{-1})

β_{oo} = out-of-core deposition rate constant for insoluble cobalt (kg/cm^2 day^{-1})

ϵ_{oo} = out-of-core interaction rate constant for soluble cobalt, outer (kg/g day^{-1})

ϵ_{oi} = out-of-core interaction rate constant for soluble cobalt, inner (kg/g day^{-1})

β_{oi} = out-of-core deposition rate constant for soluble cobalt, inner (kg/g)

ϵ_{oc} = Co/^{60}Co isotopic exchange rate constant (kg/g day^{-1})

$\epsilon_{\beta 1}$ = deposition rate constant coefficient 1 (kg/g)

$\epsilon_{\beta 2}$ = deposition rate constant coefficient 2 (kg)

ϵ_{59} = ^{59}Co soluble/insoluble distribution coefficient (ppb^{-1})

ϵ_{60} = ^{60}Co soluble/insoluble distribution coefficient (ppb^{-1})

K_f^{Fe} = fuel deposit release rate constant for iron (day^{-1})

k_{fi} = fuel deposit release rate constant for cobalt, inner layer (day^{-1})

k_{fo} = fuel deposit release rate constant for cobalt, outer layer (day^{-1})

k_{fi} = fuel deposit transformation rate constant for cobalt (day^{-1})

ϵ_{k1} = fuel deposit transformation rate coefficient 1 (day^{-1})

ϵ_{k2} = fuel deposit transformation rate coefficient 2 (day^{-1} g^{-1})

k_o^{Fe} = out-of-core deposit release rate constant for iron (day^{-1})

k_{oi} = out-of-core deposit release rate constant for cobalt, inner (day^{-1})

k_{oo} = out-of-core deposit release rate constant for cobalt, outer (day^{-1})

k_{oi} = out of-core deposit transformation rate constant for cobalt (day^{-1})

Rel = release constant during shutdown (day^{-1})

Empirical Constants

K_R = empirical constant for the ratio of ^{60}Co dose rate to ^{60}Co surface concentration on recirculating piping [(mR/h)/(μCi/cm^2)]

K_s = empirical constant for activities other than ^{60}Co on piping surface in dose rate calculation (μCi/g cm^{-2})

$\delta_1, \delta_2, \delta_3, \delta_4$ = empirical constants related to the properties on iron species[c] (dimensionless)

δ_4 = empirical constant for Co/^{60}Co release from fuel deposit, inner layer (dimensionless)

δ_5 = empirical constant for Co/^{60}Co release from fuel deposit, outer layer (dimensionless)

δ_7 = empirical correction factor for insoluble ^{60}Co deposition on out-of-core surface (dimensionless).

δ_8 = empirical correct factor for ^{60}Co release from fuel deposit due to activation recoil (dimensionless)

δ_9 = correction for soluble/insoluble distribution due to sampling error (dimensionless)

δ = fraction of soluble cobalt deposition in fuel outer layer (dimensionless)

It should be noted that in this model difference in crud characteristics are throughly emphasized. These are considered to arise from the different type of the condensate demineralizers, Powdex or deep bed. and the option of forward pumped heater drain systems.

This model includes many transport coefficients and empirical constants, which are determined on the basis of laboratory informa-

tion and plant data from three reactors with different type of condensate demineralizers and forward pumping systems. The constants determined are assumed to be constant for all BWRs with the same type of the condensate systems.

Type of Condensate Treatment System	δ_1	δ_2	δ_3	δ_4
Powdex (without FPHD)	1.2	0.75	1.5	1.0
Deep bed (without FPHD)	1.0	1.0	1.0	1.0
Forward pumped heater drain (FPHD)	0.4	1.5	0.75	0.5

3. ASEA-ATOM model

In Sweden a computer model called "CRUD" has been developed to study radioactivity transport and to determine the origin of the measured radioactivity on pipe surfaces.[3] A schematic diagram of the model is shown in Fig.2. In this model all the species are treated as elements or nuclides, and the core is divided into an optional number of fuel bundle batches and seven axial positions. According to plant experience, fuel deposits tend to turn into a more tenacious layer with increasing time. The release rates from fuel deposits are therefore assumed to decrease with time.

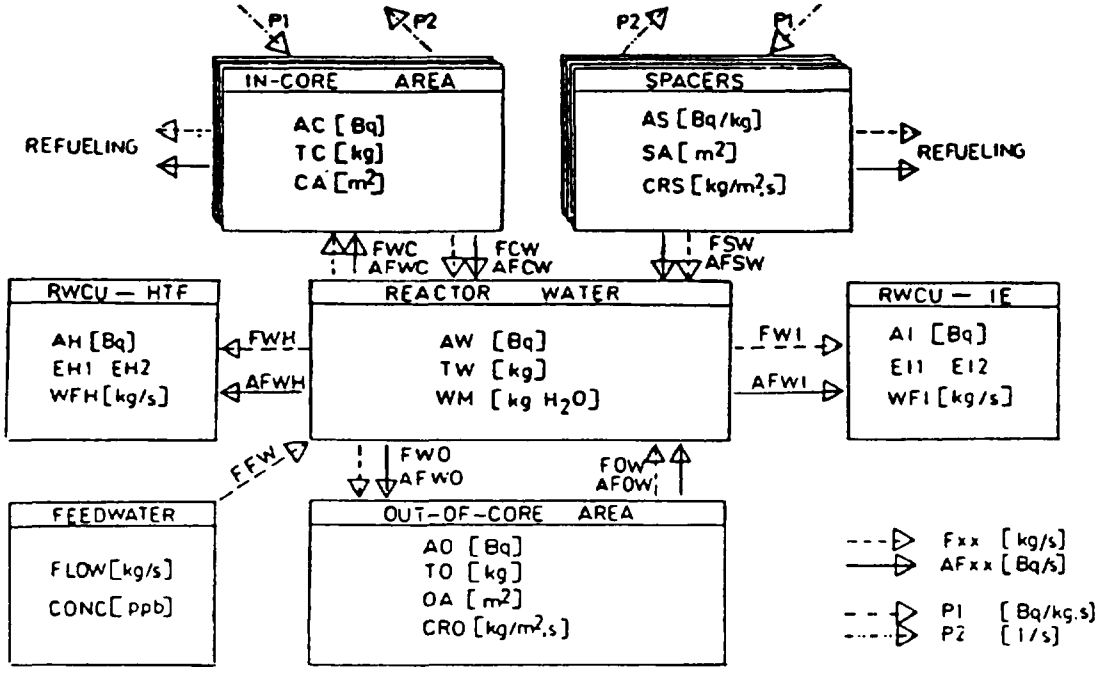

Fig.2. Block diagram of computer code "CRUD".[3]

The mathematical formation is shown below.

Material balance in core

$$\frac{d}{dt} TC_{n,m} = FWC_{n,m} - FCW_{n,m}$$

$$\frac{d}{dt} AC_{n,m} = P1_{n,m} \cdot TC_{n,m} + AFWC_{n,m} - AFCW_{n,m} - (P2_{n,m} + \lambda) \cdot AC_{n,m}$$

$$FCW = \sum_{n,m} FCW_{n,m} = \sum_{n,m} RC1_n \cdot TC_{n,m}$$

$$AFCW = \sum_{n,m} AFCW_{n,m} = \sum_{n,m} RC2_n \cdot AC_{n,m}$$

$$RC1_n = F \cdot RC1$$

$$RC2_n = F \cdot RC2$$

$$F = \ln(1 + \frac{\epsilon_p}{c}) / \frac{\epsilon_p}{c}$$

Here indices n and m refer to differential fuel bundle batches and axial positions, respectively.

The fuel spacers in Swedish BWRs are made of Inconel X-750, containing 0.1% of Co. The corrosion rates of the spacer materials are assumed to follow a parabolic law.

Activation and release from fuel spacers

$$\frac{d}{dt} AS_{n,m} = P1_{n,m} \cdot TPS - (P2_{n,m} + \lambda) \cdot AS_{n,m}$$

$$FSW = \sum_{n,m} FSW_{n,m} = \sum_{n,m} RS_n \cdot TPS$$

$$AFSW = \sum_{n,m} AFSW_{n,m} = \sum_{n,m} RS_n \cdot AS_{n,m}$$

$$RS_n = CRS_n \cdot SA$$

$$CRS_n = CRS_{2000} \cdot (C_0 + C_1 \cdot \epsilon_p)^{-1/2}$$

The rates of corrosion, corrosion product deposition and release are assumed to be identical with respect to all out-of-core surfaces, which take single layer structure. The corrosion rates of base metals are taken to be constant at all time.

Material balance in out-of-core areas

$$\frac{d}{dt} TO = FWO - RO1 \cdot TO$$

$$\frac{d}{dt} AO = AFWO - AFOW - \lambda \cdot AO$$

$$FOW = RO1 \cdot TO + CRO \cdot OA \cdot TPO$$

$$AFOW = RO2 \cdot AO$$

Material balance in reactor water

$$TW = \frac{FFW + FCW + FSW + FOW}{DC1 + DH1 + DI1 + DO1}$$

$$AW = \frac{AFCW + AFSW + AFOW}{DC2 + DH2 + DI2 + DO2 + \lambda}$$

$$FW_z = Dz1 \cdot TW$$

$$AFW_z = Dz2 \cdot AW$$

(z = C, H, I or O)

For Swedish reactors the following reactions are studied using this model.

Fe-54 (n,p) Mn-54

Fe-58 (n,γ) Fe-59

Ni-58 (n,p) Co-58

Co-59 (n,γ) Co-60

Zn-64 (n,γ) Zn-65

Considering the accepted importance of insoluble iron in feed water and reactor water, an extended version of the code, "CRUD-2" is now under development.[4] In the new model, corrosion products in the reactor water are divided into soluble and insoluble species and the out-of-core surfaces take a double layer structure, the outer loose layer and the inner tenacious layer. The release and deposition of soluble corrosion products from and to the in-core area are taken to be a function of the amounts of iron deposited.

t - Time (s)

AC - Activity in-core area (Bq)
AS - Activity spacers (Bq/kg)
AW - Activity reactor water (Bq)
AO - Activity out-of-core area (Bq)
AH - Activity high temperature filters (HTF)(Bq)
AI - Activity ion exchangers (IE)(Bq)

TC - Target in-core area (kg)
TW - Target reactor water (kg)
TO - Target out-of-core area (kg)

AFWC - Activity flow water to in-core area (Bq/s)
AFWH - Activity flow water to HTF (Bq/s)
AFWI - Activity flow water to IE (Bq/s)
AFWO - Activity flow water to out-of-core area (Bq/s)
AFCW - Activity flow in-core area to water (Bq/s)
AFSW - Activity flow spacers to water (Bq/s)
AFOW - Activity flow out-of-core area to water (Bq/s)

FFW - Target flow feedwater to water (kg/s)
FWC - Target flow water to in-core area (kg/s)
FWH - Target flow water to HTF (kg/s)
FWI - Target flow water to IE (kg/s)
FWO - Target flow water to out-of-core area (kg/s)
FCW - Target flow in-core area to water (kg/s)
FSW - Target flow spacers to water (kg/s)
FOW - Target flow out-of-core area to water (kg/s)

CA - In-core area (m^2)
SA - Spacer area (m^2)
WM - Reactor water mass (kg)
OA - Out-of-core area (m^2)
TPS - Target proportion in spacer material
TPO - Target proportion in out-of-core materials
CRS - Corrosion rate spacer material (kg/s, m^2)
CRS_{2000} - CRS after 2000 hours (kg/s,m^2)
C_0.C_1 - Constants
CRO - Corrosion rate out-of-core materials (kg/s, m^2)

DCx - Deposition on in-core area (s^{-1})
DOx - Deposition on out-of-core area (s^{-1})
DHx - Deposition in HTF (s^{-1})
DIx - Deposition in IE (s^{-1})

RCx - Release from in-core area (s^{-1})
RS - Release from spacer material (kg/s)
ROx - Release from out-of-core areas (s^{-1})

x=1 - Target material
x=2 - Activity

F - Operation time dependent function
t_p - Operation time (days)
C - Constant (days)
λ - Decay constant (s^{-1})

P1,P2 - Activation (Bq/kg,s) and burn-up rate (s^{-1})

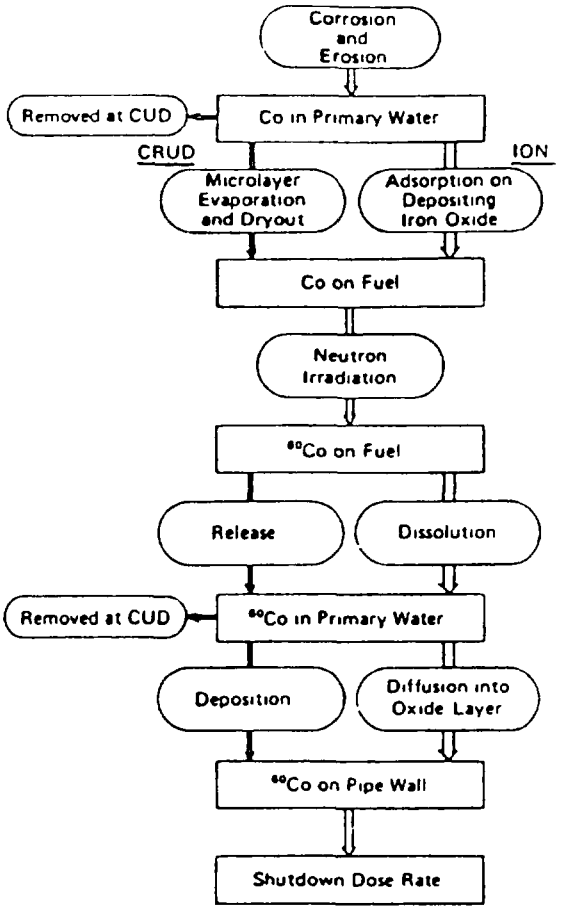

Fig.3. Block diagram of Hitachi model.[5)]

4. Hitachi model

A mathematical model has been developed to predict radioactivity transport in some Japanese BWRs. Basic processes involved in the model are shown in Fig.3. In this model the main concern is focused on the behavior of iron, cobalt-59 and cobalt-60. The cobalt-60 in the reactor water is divided into two kinds, soluble and insoluble. The former is adsorbed by the deposits on the fuel surfaces and the latter is carried by crud particles. The most simple forms of the mathematical formula are given as follows.[5)]

$$V dC_{Fe}/dt = X_{Fe} + \zeta_c M_{Fe} - (\delta_c + B) C_{Fe} V$$

$$dM_{Fe}/dt = \delta_c C_{Fe} V - \zeta_c M_{Fe}$$

$$V dC_{Co}/dt = X_{Co} + \zeta_i M_{Co} - (\delta_i + B) C_{Co} V$$

$$dM_{Co}/dt = \delta_i C_{Co} V - S_i M_{Co}$$

$$\gamma V dR_i/dt = X_i + \zeta_i A - \gamma(\delta_i + B) R_i V$$

$$\gamma V dR_c/dt = \zeta_c A - \gamma(\delta_c + B) R_c V$$

$$dA/dt = kM_{Co} + \gamma\delta_1 R_1 V - (\zeta_1+\zeta_c+\lambda)A$$

$$d\Gamma_1/dt = \delta_{p1} R_1 - (\zeta_{p1}+\lambda)\Gamma_1$$

$$d\Gamma_c/dt = \delta_{pc} R_c - (\zeta_{pc}+\lambda)\Gamma_c$$

$$d\Gamma_x/dt = \delta_{px}\Gamma_c - (\zeta_{p1}+\lambda)\Gamma_x$$

$$D = k_g(\Gamma_1+\Gamma_c+\Gamma_x)$$

where $k = \lambda\sigma N_0 \phi/(3.7\times10^{10})$

$\delta_1 = \delta^* M_{Fe}$

These differential equations can be solved analytically,[6] and used for the calculation of dose rates on recirculation piping.

Recently some modification has been given to the model. For instance, the ^{60}Co deposits on the out-of-core surfaces are divided into two kinds, soft deposits and hard spinel layer.[7] Crud ^{60}Co deposits on the pipe surfaces and forms the soft deposits, while soluble ^{60}Co ions are taken up into the spinel layer. It is also assumed that a quantity of ^{60}Co is released from the soft deposits and transferred to the inner spinel layer. The following modification is added to the mathematical formulation.

$$d\Gamma_1/dt = \delta_1 R_i - (\lambda + \zeta_1 + \zeta_3)\Gamma_1 ,$$

$$d\Gamma_2/dt = \delta_2 R_c - (\lambda + \zeta_2 + \delta_3)\Gamma_2 + \zeta_3(\Gamma_1 + \Gamma_3) ,$$

and

$$d\Gamma_3/dt = \delta_3\Gamma_2 - (\lambda + \zeta_1 + \zeta_3)\Gamma_3 .$$

$$\delta_1 = Sg ,$$

$$\delta_2 = k_2 Re^{0.83}/d ,$$

$$\delta_3 = \zeta^* \delta_1 ,$$

These new differential equations are solved analytically using some simplifications.

Another modification is also added to take into account the effect of crud particle size distribution.[8] The particle diameter is assumed to influence the corrosion product transport in two ways. The deposition of crud particles on fuel surfaces is affected by the particle diameter, and it is inferred that the larger the particles are, the smaller the deposition rate is. The particle diameter also has large influence on the adsorption of Co on the fuel deposits through the specific surface area of the deposits.[59]

Nomenclature

t = time, h
V = total weight of primary cooling water, ton
X_{Fe} = feed rate of iron, mg/h
X_{Co} = feed rate of cobalt, mg/h
X_i = feed rate of ^{60}Co (contribution of RPV internal materials), μCi/h
M_{Fe} = amount of iron deposited on the fuel surface, mg
M_{Co} = amount of cobalt deposited on the fuel surface, mg
A = amount of ^{60}Co deposited on the fuel surface, μCi
C_{Fe} = concentration of iron in the primary cooling water, mg/ton
C_{Co} = concentration of cobalt in the primary cooling water, mg/ton
R_i = concentration of ionic ^{60}Co in water, μCi/ml
R_c = concentration of crud ^{60}Co in water, μCi/ml
β = ion and crud removal efficiency in the cleanup line, h^{-1}
δ = deposition rate of ion on fuel surface, h^{-1}
δ_c = deposition rate of crud on fuel surface, h^{-1}
ζ_i = release rate of ion from fuel surface, h^{-1}
ζ_c = release rate of crud from fuel surface, h^{-1}
δ^* = deposition rate of ion on iron oxide surface, h^{-1}/mg
λ = decay constant of ^{60}Co, h^{-1}
σ = average cross section of cobalt, cm^2
ϕ = average neutron flux in core, n/cm^2s
N_0 = number of atoms of cobalt in unit mass, n/mg
γ = specific volume of coolant, ml/ton
Γ = amount of ^{60}Co deposited on the pipe surface, $\mu Ci/cm^2$
Γ_i = contribution of ionic ^{60}Co to the amount deposited on the pipe surface, $\mu Ci/cm^2$
Γ_c = contribution of crud ^{60}Co to the amount deposited on the pipe surface, $\mu Ci/cm^2$
Γ_x = contribution of ionic ^{60}Co released from the crud to the amount deposited on the pipe surface, $\mu Ci/cm^2$
δ_{pi} = deposition rate of ion on pipe surface, cm/h
δ_{pc} = deposition rate of crud on pipe surface, cm/h
δ_{px} = deposition rate of ion release from the crud on pipe surface, h^{-1}
ζ_{pc} = release rate of crud cobalt-60 from pipe surface, h^{-1}
ζ_{pi} = release rate of ionic cobalt-60 from pipe surface, h^{-1}
D = shutdown dose rate, mR/h
k_g = geometrical factor for calculation of dose rate, mR/h per $\mu Ci/cm^2$
ε_j = removal coefficient of condensate demineralizer, - (j : j th equipment)
x_j = release rate, $mg/(m^2h)$
s_j = wetted surface, m^2
α^j_{Fe} = ion content in material, -
α^j_{Co} = cobalt content in material, -
n_j = number of atoms of cobalt in unit mass, n/mg
τ_j = exposure time, s
Γ_1 = contribution of ^{60}Co ion taken up into spinel to the amount of ^{60}Co deposited on the pipe surface, Ci/m^2
Γ_2 = contribution of crud ^{60}Co deposition to the amount of ^{60}Co deposited on the pipe surface, Ci/m^2
Γ_3 = contribution of ^{60}Co transferred from soft deposits to spinel to the amount of ^{60}Co deposited on the pipe surface, Ci/m^2
δ_1 = deposition rate of ^{60}Co ion uptake into spinel, m/s
δ_2 = deposition rate of crud ^{60}Co, m/s
δ_3 = transfer rate of ^{60}Co ion from soft deposits to spinel, s^{-1}
ζ_1 = release rate of ^{60}Co ion from spinel, s^{-1}
ζ_2 = release rate of crud ^{60}Co, s^{-1}
ζ_3 = transfer rate of spinel to soft deposit by oxidation, s^{-1}
S = site number of spinel structure to be prepared for ion deposition, m^{-2}
g = binding coefficient of ion for a site in the spinel, m^3/s
λ = decay constant, s^{-1}
Re = Reynolds number
d = diameter of pipe, m
ζ^* = release coefficient of ion from crud surface, m^{-1}

5. Toshiba model

Another model developed in Japan uses a rather complicated scenario for corrosion product transport as shown in Figs.4 and 5.[9] The species in the reactor water are divided into four kinds, "crud," large particles, small particles and ions. On fuel surfaces there are four kinds of oxide deposited, tightly adhered hematite, loosely adhered large and small particles, and tightly adhered spinels. The out-of-core surfaces have a double layer structure, loose hematite layer and tenacious spinel layer. According to plant experience in some BWRs a significant contribution to the dose rate is made by radioactive particles sedimented around the bottom of the RPV.

The size of these sedimented particles is relatively large(ca. 10μm). This situation is taken into account in the Toshiba model. Simplified mathematical formulae are given below.[10] These differential equations are solved analytically and used for the calculation of the quantity of radioactive deposit on out-of-core piping surfaces and dose rates.

Mass Balance

a. concentration in reactor water

$$V\frac{dC_{RW}}{dt} = F_{FW}\,C_{FW} + \zeta M_F + \eta M_s - (\delta + \gamma + \beta + \epsilon)C_{RW}\cdot V \ .$$

b fuel surface

$$\frac{dM_F}{dt} = \delta C_{RW}\cdot V - \zeta M_F \ .$$

c. out-of-core surface of primary coolant system

$$\frac{dM_s}{dt} = \gamma C_{RW}\,V - \eta M_s \ .$$

Activity Balance

a. concentration in reactor water

$$V\frac{dA_{RW}}{dt} = R\cdot C_{RW}\cdot v + \zeta A_F + \eta A_s - (\lambda + \delta + \gamma + \beta + \epsilon)A_{RW}\cdot V \ .$$

b. fuel surface

$$\frac{dA_F}{dt} = RM_F + \delta A_{RW}\cdot V - (\lambda + \zeta)A_F \ .$$

c. out-of-core surface of primary coolant system

$$\frac{dA_s}{dt} = \gamma A_{RW}\cdot V - (\lambda + \eta)A_s \ .$$

Nomenclature

A_{RW} = concentration of activated corrosion product in reactor water, MBq/kg coolant

A_F = activated corrosion products on fuel rod surface, GBq

A_s = activated corrosion products on out-of-core surface, GBq

C_{RW} = concentration of corrosion product in reactor water, μg/kg coolant

C_{FW} = concentration of corrosion product in feedwater, μg/kg coolant

F_{FW} = flow rate of feedwater, g/h

M_F = corrosion products on fuel rod surface, g

M_s = corrosion products on out-of-core surface, g

R = rate of activation, GBq/h·g

V = weight of reactor water, g

v = effective weight of reactor (in-core) water, g

t = time, h

β = rate constant of reactor cleanup system, per hour

γ = deposit rate constant on out-of-core surface, per hour

δ = deposit rate constant on fuel rod (in-core) surface, per hour

ζ = release rate constant from fuel rod (in-core) surface, per hour

η = release rate constant from out-of-core surface, per hour

λ = radioactive decay constant, per hour

ϵ = carry-over rate to main steam system

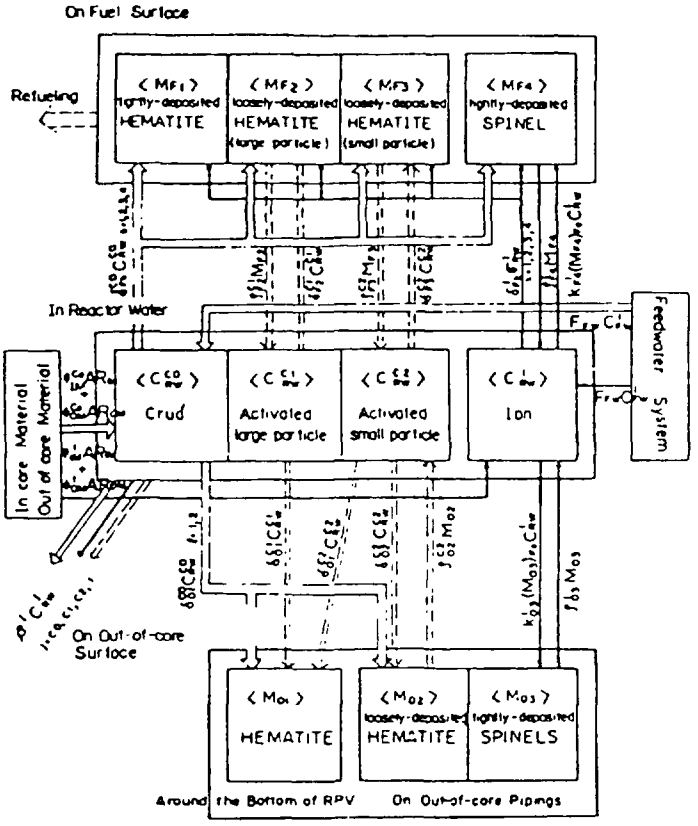

Fig.4. Block diagram of mass transport. (Toshiba model)[9)]

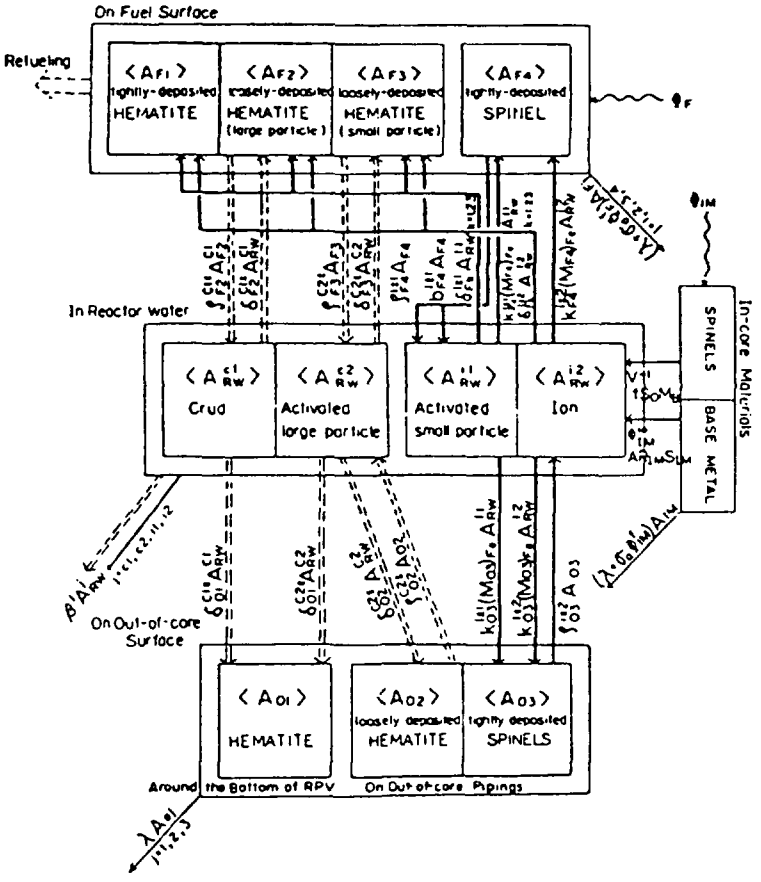

Fig.5. Block diagram of activity transport. (Toshiba model)[9)]

Nomenclature for Figs. 4 and 5.

List of parameters

Symbol	Meaning	Dimension
M	mass	g
A	activity (conc. of activity in RW)	Ci(pCi/g)
C	conc. of metal in RW	ppb
S	specific activity	Ci/g
F	flow of water	t/hr
V	volume of reactor water	t
AR	surface area	m^2
δ	deposition rate	t/hr
ζ	release or dissolution rate	hr^{-1}
k	equilibrium rate	t/hr/gFe
b	release rate by self-diffusion	hr^{-1}
ϕ	release rate by erosion-corrosion	g/hr
β	removal rate by RWCU system	t/hr
DE	D.F. of RWCU system	
DF	D.F. of fuel deposit cleaning	
f	fraction	
a	natural fraction of isotope	%
Φ	flux of neutron	$n/cm^2/sec$
$\sigma(\sigma_a)$	activation (annihilation) cross section	cm^{-2}
w	atomic weight	g
λ	decay constant	hr^{-1}

List of subscripts

Symbol	Meaning	Example
Under subscript		
FW	feedwater	F_{FW}, C_{FW}
RW	reactor water	C_{RW}, A_{RW}
CU	RWCU system	M_{CU}, A_{CU}
F	fuel surface	M_F, A_F
O	out-of-core surface	M_O, A_O
IM	in-core materials	Φ_{IM}, AR_{IM}
OM	out-of-core materials	AR_{OM}
Upper subscript		
C	crud	δ^{CO}
i	ion	δ^{i}
*	active	δ^{i*1}
f	fast neutron	Φ_F^f

6. Comparison of the BWR models.

All the computer models described in the previous sections contain some ambiguity on the mechanism of each process comprising radioactivity build-up on the circuit pipe surfaces. Therefore, they have been refined or improved as more data have been obtained on radioactivity transport from laboratory experiments and plant operation experience and our knowledge of the mechanisms has increased. This refinement continues. In the course of this refinement the models have become more or less similar to each other.

In Table I a comparison of these models are summarized.

Table I. Comparison of BWR models

	GE	ASEA-ATOM	HITACHI	TOSHIBA
Nuclides	Fe, Co	Fe, Co, Ni, Zn	Fe, Co, Ni**	Fe, Co, Ni**
	Co-60 Mn*-54, Fe*-59	Fe-59, Co-60, Co-58 Mn-54, Fe-59, Zn-65	Co-60, Co-58**	Co-60, Co-58** Fe-59, Mn-54
Species considered	ion, crud	originally not distinguished, soluble and insoluble in the new model	ion and crud for ^{60}Co	ion, crud large particles small particles
Corrosion and release rate	corrosion rates depend on electrical conductivity of coolant.	corrosion product release from core spacer is considered. This follows a parabolic law.	constant release rate	constant release rate
Interaction Co/Fe	Co adsorption on crud	not considered	not considered	Co scavenged on crud
In core deposits	oxide double layers	oxide single layer release from fuels decreases with time	oxide single layer saturation limits for deposit	oxide [illegible]
Out-of-core oxide layer and Co deposition	oxide double layers on corroding surfaces parabolic law	oxide double layers on corroding surfaces in the newer model.	three steps of Co up-take 1.crud deposition 2.Lister mechanism 3.outer ⟶ inner	[illegible] corroding surfaces parabolic law
Other remarks	corrosion product behaviour depends strongly on type of demineralizer.	core divided into subsections	effect of particle diameter is taken in into account in a new version.	deposits of large particles around RPV bottom

* empirical estimation
** considered in new version

References

1) C.C. Lin, C.R. Pao, J.S. Wiley and W.R. Dehollander, Water Chemistry of Nuclear Reactor Systems II, BNES, 311, 1980.

2) C.C. Lin, C.R.Pao, J.S. Wiley and W.R. Dehollander, Nucl. Tech., 54, 253, 1980.

3) K. Lundgrum, ibid., p.305, 1980.

4) K. Lundgrum, EPRI NP-3114, 2, A-82, 1983.

5) S. Uchida, M. Kitamura, M. Izumiya, K. Ohsumi and M. Miki, Water Chemistry of Nuclear Reactor Systems II, BNES, 299, 1980.

6) S. Uchida, M. Kikuchi, Y. Asakura and H. Yusa, Nucl. Sci. Eng., 67, 245, 1978.

7) S. Uchida, Y. Ozawa, E. Ibe and Y. Meguro, Nucl.Tech., 59, 498, 1982.

8) S. Uchida, Y. Asakura, M. Kitamura, K. Ohsumi, K. Yonezawa and Y. Matsushita, J. Nucl. Sci. Tech., 20, 414, 1983.

9) Y. Hemmi, T. Kamata, Y. Nakayama, A. Tani, Y. Morikawa, Y. Sato, H. Nagao, S. Sasaki, Y. Sato, M. Kuba and M. Kakefuda, Water chemistry of Nuclear Reactor Systems II, BNES, 319, 1980.

10) K. Yamazaki, S. Fujita, T. Kamata, Y. Morikawa, K. Numata, K. Osamura and Y. Megro, Nucl.Tech. 52, 7, 1981.